Alma Mater Studiorum – Università di Bologna

DOTTORATO DI RICERCA IN

Biologia Molecolare e Cellulare

Ciclo XXX

Settore Concorsuale di afferenza: 05/D1

Settore Scientifico Disciplinare: BIO/09

Oligodendrocyte lineage regulation during development, adult life, inflammatory lesions and

hypoxia/ischemia insults. Focus on Nuclear Receptors.

Presentata da: Vito Antonio Baldassarro

Coordinatore Dottorato	**Supervisore**
Prof. Giovanni Capranico	**Prof.ssa Laura Calzà**

Esame finale anno 2018

Index

Abbreviations

DIV: day in vitro

HI: hypoxia/ischemia

HCS: high content screening

MS: multiple sclerosis

NSCs: neural stem cells

OGD: oxygen-glucose deprivation

OLs: oligodendrocytes

OPCs: oligodendrocyte precursor cells

T3: triiodothyronine

TH: thyroid hormone

ABSTRACT

Oligodendrocyte precursor cells (OPCs) are the main actors involved in developmental myelination and adult myelination dynamic, including remyelination after myelin injury. The *recapitualtion hypothesis* states that remyelination in adulthood is a complete recapitulation of developmental myelination. However, the different nature of foetal and adult OPCs could reflect a different myelination mechanism and different response to demyelinating insults.

The main objective of the present study is the investigation of foetal and adult OPCs vulnerability to the two main components of the demyelinating diseases: inflammation and hypoxia/ischemia (HI). In order to develop the main objective, robust and efficient *in vitro* models and readouts were set up. In particular, a cell-based high content screening approach was used as the elective technique in order to obtain robust and reproducible data.

Moreover, since the differential response of foetal and adult OPCs could come from a different physiological differentiation process, driven by thyroid hormone (TH) and exerted by nuclear receptors (NRs) activity, we first focused on the role of NRs and co-regulator in foetal and adult OPCs differentiation. We found a different expression of NRs in early precursors, a different response to T3-mediated differentiation, the selective importance of PARP activity for foetal OPCs and the fundamental role of RXRγ in both systems.

Differences in physiological differentiation can reflect different responses to noxious stimuli. Thus, we exposed OPCs to inflammatory cytokines mix, in order to mimic the inflammation environment, or to oxygen-glucose deprivation (OGD), in order to mimic HI. OGD was first characterized in primary neuronal cultures and tested for its reliability in disease model studies and pharmacological analysis.

Foetal and adult OPCs show both a cytokines-mediated differentiation block, reflecting what the *in vivo* pathological condition. We thus tested a pharmacological tool in adult cultures, in order to study the mechanism. In particular, we found that the differentiation block was linked

to an increase of deiodinase 3 (D3), the enzyme inactivating T3, the active form of TH and, blocking its activity, it was possible to restore the OPC differentiation process.

On the other hand, only foetal OPCs are sensitive to OGD, showing OPCs/OLs-specific cell death. Since we found an increase in D3 expression after OGD in foetal OPCs, further studies will elucidate the mechanism underlying the foetal-selective OPCs cell death, analysing the role of D3 in the process and glutamate-mediated excitotxicity, the major triggerer of HI-induced cell death.

The better understanding of OPCs biology and mechanisms underlying physiological and pathological conditions, bound to information about differences in foetal and adult OPCs, will open the way to new therapies development, based on differential strategies for demyelinating diseases affecting foetal or adult life.

1 INTRODUCTION

1.1 The oligodendrocyte precursor cell in development and myelin turnover

Oligodendrocytes (OLs) are the glial-subtype myelinating cells of the central nervous system (CNS), generated from oligodendrocytes precursor cells (OPCs), discovered by Robertson in 1899 (Robertson, 1899) and named and classified by Rio Hortega in 1921 (Rio Hortega et al., 1921). During embryonic development, the life of an OL is defined by four distinct phases: i) birth, migration, and proliferation of OPCs; ii) morphological differentiation; iii) axonal contact, and generation of compact myelin and iv) long-term trophic and metabolic support of the encased axon (Michalski et al., 2015). During the adult life, a substantial number of OPCs persist in the CNS. Here, they comprise the largest population of dividing cells, involved in myelin turnover, repair and replacement (Dawson et al., 2003; Hughes et al., 2013).

1.1.1 Development

The development of the oligodendrocyte lineage begins with specification of OPCs from neural stem cells (NSCs) during late embryonic gestation. NSCs initially expand within the ventricular lining of the CNS generated by the neuroepithelial cells along the neuroaxsis. These multipotent stem cells give rise to neurons, radial glia, astrocytes and bipotential astrocyte-oligodendrocyte progenitor cells that colonize the CNS. Neurons and their radial glial guides are the first cell types to be specified while only late in neurogenesis significant gliogenesis and glial progenitor cell production begin (Goldman and Kuypers, 2015).

OPCs are recognized because of the expression of membrane protein, e.g. NG2, a type I membrane glycoprotein expressed by a subpopulation of glial cells and, in the developing brain, also by pericytes. NG2 is a marker for early OPCs overlapping CNPase (2', 3'-cyclic nucleotide 3'-phosphodiesterase), a marker for mature OLs, but absent in myelinating OLs expressing MOG (myelin oligodendrocyte glycoprotein) (Karram et al., 2005; Polito and Reynolds, 2005). NG2-expressing cells are recognized as progenitors of glia, given rise to both OPCs and astrocytes and they are also referred as NG2-glia, in order to distinguish these progenitors from other NG2-expressing cells, like pericytes or macrophages (Dimou and Gallo, 2015). Thus, OPCs are recognized as NG2/PDGFRα (platelet-derived growth factor alpha receptor)-expressing cells with high proliferative and migrating capability. They differentiate through premyelinating stage to become mature and myelinating oligodendrocytes, interacting with neuronal axons in order to organize the nodal, paranodal nad juxtaparanodal regions of myelinated axons (Bercury et al., 2015).

NG2-progenitors are not an homogeneous population and they give rise to different progenies in different brain regions and in different stages of the development (Dimou and Gallo, 2015; Viganò and Dimou, 2016; Figure 1). In the CNS three separate waves (starting at E12.5 in mice and during the second trimester of gestation in humans), define the OLs population. OPCs are first produced ventrally, along the neural tube in the ventral ganglionic eminence, in a process driven by Sonic Hedgehog (Shh). After this first wave, they are completely replaced by a dorsal derived population (from the dorsal cortical subventricular zone) and, at last, within the cortex (Kessaris et al., 2006; Jakovcevski et al., 2009).
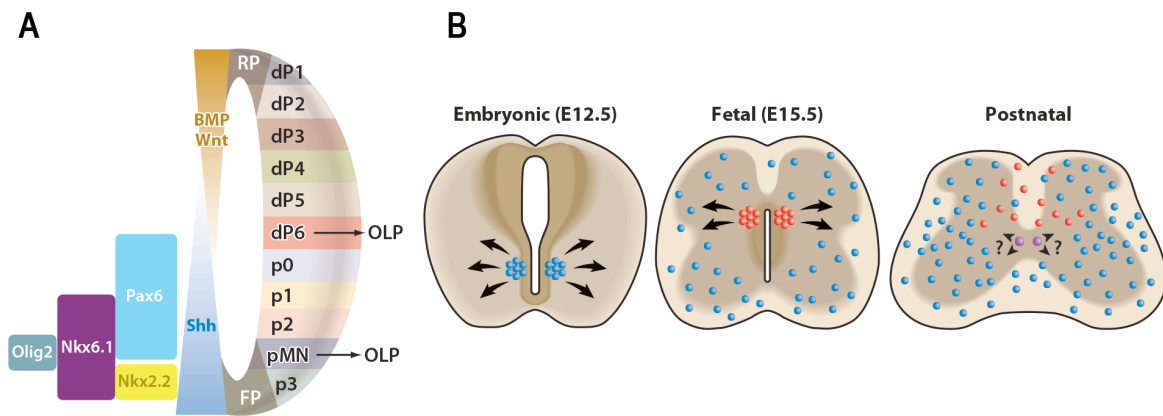
Figure 1. Oligodendrocyte precursor cells generation during development.
(A) Patterning of the embryonic neural tube by organizing signals (Shh, Wnt, BMP) is reflected in the expression of Olig2 and homeodomain (Nkx2.2, Nkx6.1, Pax6) transcription factors in restricted progenitor domains (pMN, p0-p3, dP1-dP6). (B) Embryonic OPCs arise from the ventral domain under control of Shh, replaced by OPC-generating in the dorsal region in foetal stage and within the cortex in postnatal age (Fancy et al., 2011 modified).

The progression of OPCs along the myelination process is tightly regulated in all the stages, by signals including growth factors, protein kinases and extracellular matrix molecules, all of which influence epigenetic modifications, transcriptional and translational regulation, and the actin cytoskeleton (Bercury et al., 2015).

In the mouse forebrain, several transcription factors, such as Znf488 and Znf536, are involved in the early phase of oligodendroglial lineage restriction, a process also mediated by downregulation of Sox2, and upregulation of Sox8 and Sox9. Upregulation of these genes, is correlated to the upregulation of Nkx2.2, Olig1, Olig2 and Sox10, the main mediators of OPCs differentiation, leading to the upregulation of PDGFRα. Moreover, OPCs maturation, can proceed only after cell cycle arrest, repressing E2F1 and c-myc genes, a process requiring p27kip1. At the transition between proliferating to differentiating OPCs, other transcription factors are upregulated. In particular Sox17 repress the Wnt signaling, triggering the cell cycle exit. After OL specification, myelination is triggered by the myelin regulatory factor (MYRF),

activating the expression of myelin basic protein (MBO), proteolipid protein 1 (PLP), myelin-associated glycoprotein (MAG), CNPase and MOG. The retained transcription of Olig2 and Sox10 is necessary for the mantainence of MYRF expression (Goldman and Kuypers, 2015; Figure 2). Thus, gene expression regulation through chromatin remodelling is a key process that regulates OL development, involving histone acetylation/deacetylation and ATP-dependent remodeling by SWI/SNF enzymes (Zuchero and Barres, 2015).

	Early blastocyst (ICM)	Neural stem cell	OPC		Premyelinating oligodendrocyte		Myelinating oligodendrocyte	
Stage-selective surface antigens	SSEA4 TRA-1-60 TRA-1-81	CD133 (PROM1)	A2B5 (ST8SIA1) PDGFRα (CD140a) NG2 (CSPG4) CD9 (TSPAN29)		CD9 (TSPAN29) O4 (sulfatide)		CD9 (TSPAN29) O1 (GALC)	
Stage-specific regulated proteins	LIN28	BMI1 MSI1 NES	CNP GPR17 PTPRZ1		CLDN11 CNP MAG MAL PLP1 SMARCA4 (BRG1) TRF TSPAN27 (CD82)		CLDN11 CNP MAG MBP MOBP MOG MAL PLP1	SMARCA4 (BRG1) TRF TSPAN27 (CD82)
Stage-specific transcription factors	KLF4 MYC NANOG OCT4 (POU5F1) SOX2	ASCL1 SOX3 HES1 PAX6 SOX1 SOX2	ASCL1 NKX2.2 HES1 OLIG1 ID2 OLIG2 ID4 SOX9 MYT1 SOX10		MYT1 SOX10 NKX2.2 SOX17 NKX6.2 ZFP191 OLIG1 ZFP488 OLIG2 ZFP536		MYT1 SOX10 MYRF SOX17 NKX6.2 ZFP191 OLIG1 ZFP488 OLIG2 ZFP536	
Stage-specific miRNAs	miR-290 family miR-302 family Let-7 family	miR-137 miR-195 miR-9	miR-17-92 family miR-214 miR-9/9*		miR-138 miR-219 miR-23a miR-338		miR-219 miR-23a miR-338	

Figure 2. Transcription factors in OPCs differentiation and associated markers.
At the cellular level, pluripotent stem cells progress through serial developmental stages: neuroepithelial stem cell, OPC, premyelinating and ultimately myelinating oligodendroglia. Figure shows all the factors involved in this differentiation process (Goldman and Kuypers, 2015, modified).

The most important factors regulating the differentiation process are thyroid hormones (THs; Calzà et al., 2017). Triiodothyronine (T3), the active form of TH, acts via genomic, epigenetic

and non-genomic mechanisms (Lee and Petratos, 2016), inducing OPCs cell cycle exit and terminal differentiation (Durand and Raff, 2000; Raff, 2006). In particular, after a definite number of cell division, proliferating OPCs start expressing thyroid hormone receptors (TRs) and became sensitive to T3 (Maruvada et al., 2004). T3 mediates its action binding TRs (TRα and TRβ), a class of nuclear receptors (NRs) that migrate into the nucleus and regulate the expression of specific genes controlling OPCs cell cycle exit and regulating the expression of premyelinating genes (Baxi et al., 2014; Casaccia-Bonnefil and Liu, 2003; Dugas et al., 2012).

1.1.2 Adult life

OPCs generated during the development are distributed in the adult brain and spinal cord, in the grey and the white matter. They comprise the largest population of dividing cells in the mature CNS and, each OPC, exists within unique spatial pockets established through inter-repulsive cues with other progenitors (Michalski et al., 2015). These cells are highly exploratory, sampling in search of unoccupied space and are responsible for the myelin turnover and repair in adult life. In response to specific stimuli, they can proliferate, migrate to axons and differentiate in mature oligodendrocytes (Fukushima et al., 2015). New OPCs are also generated from NSCs in the subventricular zone (SVZ) of the lateral ventricle (Urbán and Guillemot, 2014). This neurogenic area of the adult CNS contains the *niche* of multipotent stem cells, composed by three different kind of cells: type B (neural stem precursor cells), type C (transit-amplifying cells) and type A (neuroblasts) (Alvarez-Builla and Garcia-Verdugo, 2002; Figure 3). New OPCs can be generated from type C cells differentiating into NG2-positive glia, migrating and starting the maturation process to became myelinating OLs (Gonzalez-Perez and Alvarez-Buylla, 2011; Menn et al., 2006).
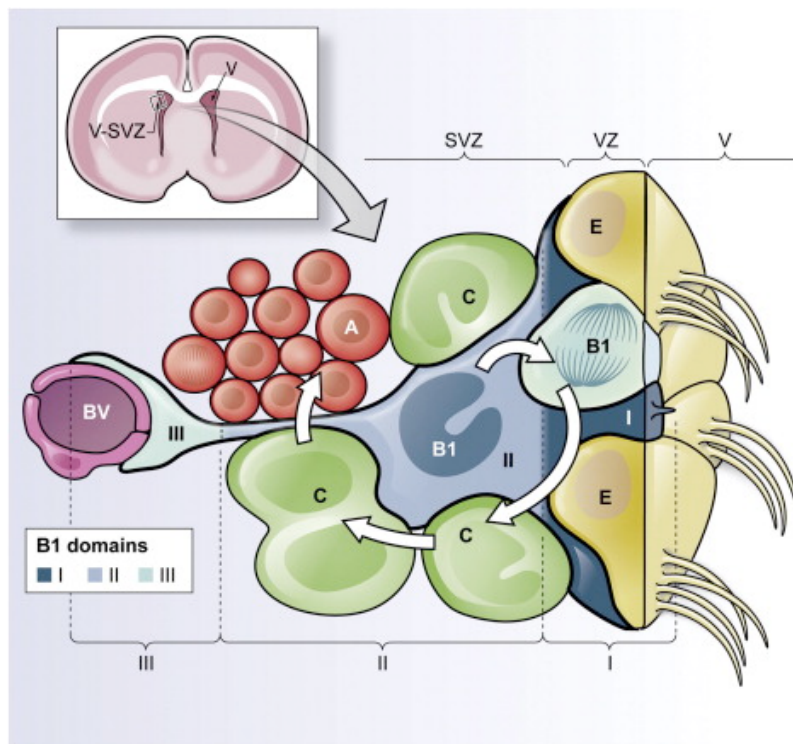
Figure 3. Subventricular zone niche and neural stem cells multipotency.

In the upper panel is showed the cross section of the mouse brain, highlighting the lateral ventricle (V) and the subventricular zone (SVZ).

The lower panel shows cellular composition of the adult SVZ niche: B1 cells are surrounded by multiciliated ependymal cells (E) and contact the lateral ventricle with an apical region (I) containing a primary cilium and, on the opposite side, contacting blood vessels with a long distal process (III). These cells give rise to C cells (transit-amplifying cells) that divide to generate neuroblasts (type A cells). B1 cells domain II (intermediate) is in close proximity to C cells, neuroblasts, neuronal terminals, and other supporting cells (Fuentealba et al., 2012).

In the healthy adult brain, new myelin is continually generated, showing a persisting remodelling (Yeung et al., 2014). Myelin volume in humans is activity-dependent, and can increase producing new cells or new membrane from the already existing cells (Bercury et al., 2015) when practicing new skills (Bengtsson et al., 2005), in learning a language (Schlegel et al., 2012), etc.

Myelination is a conserved process during adult life, showing high plasticity. An effective remyelination can occurs after demyelination insults, also leading to a complete anatomical and functional myelin sheath restoration, thus representing the only true regenerative capability of the CNS (Crawford et al., 2013). Remyelination process is not performed by pre-existing mature OLs, but involves the generation of new mature cells from the quiescent OPC pool distributed throughout the CNS or from the subventricular zone. Factors derived from activated microglia activate local OPCs switch from quiescent state to a regenerative phenotype, migrate to demyelinated areas and generate mature OLs remyelinating axons (Bradl and Lassmann, 2010), in a process that is believed to be similar to the developmental myelination (Franklin and Hinks 1999; Franklin and Ffrench-Constant, 2008).

Different factors are involved in the activation of OPCs cell cycle and their migration, two fundamental processes for an efficient remyelination. Inflammation plays a critical role in the activation of OPCs, through inflammation–associated factors (e.g. IL-1b, TNFa, LIF; see chapter *1.2.1 Inflammation*). Than chemotactic factors induce OPCs proliferation, and attract OPCs to the demyelinated site (e.g. by PDGF, bFGF, CXCL1), than remyelination starts by an upregulation of Olig2 and Nkx2.2 (Miron et al., 2011). It has been shown that Bmp (Bone morphogenic protein) signalling regulates migration of neural crest cells and osteoblasts, but also OPCs into cortical areas, both in development and in adult life (Choe et al., 2014).

As already described for foetal OPCs, T3 is a key player in OPC maturation. The biological activity of TH versus target cells is determined by the intracellular concentration of T4 and T3, which depends on: i) circulating T4 and T3, ii) the presence and activity of transporters on the plasma membrane, and iii) the presence and activity of tissue specific deiodinases. TH cellular action implies that T4, as produced by the thyroid gland, is converted into the active form T3 by deiodinases enzymes in the target

15

organs. T4 is in fact considered the "prohormone" (the most abundant in the blood) and T3 is the active form (Calzà et al., 2015).

A correct tissue THs metabolism is fundamental for an appropriate adult OPCs maturation. The circulating prohormone T4 is converted in T3 *in loco*, by astrocytes throught deiodinase 2 (D2) enzyme (Bianco et al., 2002; Calzà et al., 2015; Morte and Bernal, 2014). Deiodinase 3 (D3) guarantees the THs homeostasis inactivating T4 in reverse-T3 (rT3) and T3 in 3,5-diiodo-l-thyronine (T2).

THs cross the Blood Brain Barrier (BBB) by specific transporters, leading to a concentration of TH in the brain 20% higher than in the blood. The process is also regulated by the highest affinity of TH transporters to T4 than T3. Moreover, T4 in the blood is mostly segregated by its transporter, transthyretin. THs are transported from blood to CNS mainly by monocarboxylate transporter 8 (MCT8) and organic anion transporter protein 1C1 (OATP1C1). This last transporter mediates also the transport of T4 inside astrocytes, where is converted in T3 by D2. Also integrin aVb3 has high affinity to T4, and it is the mediator of the non-genomic effects of TH (Calzà et al., 2015). The importance of TH transporters and, thus of the intracellular T3 concentration, is also demonstrated in humans with MCT8 mutations, leading to the Allan-Herndon-Dudley syndrome, characterized by severe neurodevelopmental defects (Dumitrescu and Refetoff, 2013).

THs metabolism and transport guarantees the appropritate intracellular content of THs mediating the downstream genomic and non-genomic processes (Dentice et al., 2013; Bernal et al., 2015; Lee et al., 2015).

1.1.3 Is remyelination a recapitulation of developmental myelination?

Myelination and remyelination share a common objective: wrap non-myelinating axons, to create the correct cellular and molecular structure for an efficient saltatory axonal conduction. The recapitulation hypothesis of myelin regeneration holds that mechanisms that underlie remyelination after injury are essentially a rerunning of a developmental myelination program (Franklin and Hinks 1999). For example, two of the best studied pathways, identified as crucial players in regulating developmental myelination, have been subsequently found to be also limiting factors for remyelination: Notch signaling pathway and the leucine-rich repeat and Ig-containing Nogo receptor interacting protein-1 (LINGO-1), two strong inhibitors of OPCs differentiation and myelination. Both factors are expressed during development and contribute to the control of differentiation timing and, in different demyelinating conditions, they are highly expressed, contributing to the pathogenesis (Bhatt et al., 2014).

However, in spite of the evidences remarking the recapitulation hypothesis, morphological differences between the two processes lead to the view that these two mechanisms are differentially regulated (Miron, 2011). The OPCs generated by the three different waves during development, produce the adult OPCs pool. Thus, these cells are different spatio-temporally defined OPCs classes, differing from their perinatal forebears for antigenic markers, growth factor responsiveness, basal motility rates and cell cycle (Fancy et al., 2011). Moreover, compared to foetal OPCs, adult progenitors show a longer cell cycle time and a slower rate of migration.

Little is known about transcription factors roles during remyelination, but Olig1 and Olig2 seem to play different roles in the two processes. According to some authors, Olig1 is essential for myelination but not for remyelination (Bradl and Lassmann, 2008), but other authors believe that is essential also for remyelination (Fancy et al., 2011). It is well known, instead, that Olig2 is fundamental for remyelination (Bradl and Lassmann, 2008).

Moreover, even Notch signalling is a limiting factor for remyelination, it seems not to be essential for the process, in a opposite way compared to the developmental myelination. The myelin morphology is also different from the one formed during development or after remyelination, showing thinner and shorter sheath segments in remyelinated axons (Bradl and Lassmann, 2008).

All these morphological and molecular differences could reflect a different response to demyelinating stimuli in foetal and adult OPCs.

1.1.4 The role of Nuclear Receptors in oligodendrocyte precursor cells.

NRs represent a superfamily of intracellular receptors, which upon binding of specific ligands, change conformation to facilitate recruitment to DNA and regulation of gene expression. The NRs superfamily comprises 48 members in human and 49 in mouse.

NRs response elements contain two or more closely spaced core recognition motifs, each of which comes into contact with a single DNA binging domain (DBD). Some responsive elements are bound by NRs homodimer, like the steroid-hormone receptors, while a subset of NRs bind to DNA as heterodimers. These heterodimers act also independently from ligands (Glass et al., 2006). The ligand binding domain (LBD) is connected to the DBD by flexible hinge domain and contains three-layered, antiparallel, helical sandwich in which a central core layer of three helices packed between two additional layers of helices forms the ligand-binding cavity. At C-terminus of LBD is also present an additional helix required for the ligand-dependent transcriptional activation. The LBD is the region conferring the specific ligand-binding properties, but it also contributes to dimerization (Saijo et al., 2010).

Many NRs have the ability to bind to DNA even in the absence of their ligand, but often act as transcriptional repressors in this form rather than activators (Gonzales and Ng, 2013). NRs

harbour a C-terminal ligand-binding and transactivation domain (LBD), a central DNA-binding domain (DBD) and a variable N-terminal disordered transactivation domain. These receptors transduce signals regulating gene expression by recruiting co-regulator proteins that modify chromatin (Kojetin et al., 2015).

NRs play fundamental roles in all the OLs differentiation stages, from NSCs self-renewal and lineage specification, to OLs maturation. Relatively to NSCs biology, key members include the thyroid hormone receptors (TRs), the retinoic acid receptors (RARs), the retinoid X receptors (RXRs), the peroxisome proliferator-activated receptors (PPARs), the liver X receptors (LXRs), the estrogen receptors (ERs), the mineralocorticoid receptor (MR), the glucocorticoid receptor (GR), as well as orphan nuclear receptors, for which no known cognate endogenous ligands have yet been identified (Stergiopoulos, 2013).

As described above, T3, one of the key player in oligodendrocyte differentiation, act through binding TRs. The two TR isoforms, α and β, are NRs acting as ligand-regulated transcription factor trasducing the hormonal signal, physiologically exerting their action within a limited time windows, in a spatially and timely controlled way (Mohácsik et al., 2011).

The biological effect of T3 in a given tissue depends on a number of factors: i) the amount of bioavailable hormone, ii) the levels of different TR isoforms, and post-transcriptional modifications of TRs, iii) the type of their heterodimerization partners, iv) the interaction with co-repressors and co-activators, and v) on the structure of thyroid hormone response elements (TREs) in the promoters of target genes (Puzianowska-Kuznicka et al., 2006).

It is well known that TH regulates the cell cycle of different cells, including OPCs during developmental myelination. In particular, OPCs start showing TH sensitivity at E14 in mice, due to the expression of TRs, giving to them the role of the timer controller of the differentiation (Gao et al., 1998; Billon et al., 2001). T3 directly regulates different proteins involved in cell cycle control. It has been shown that T3-mediated action of TRs decreases the expression of E2F1 and c-myc, molecules involved in the transcriptional activation of

different positive regulators of cell cycle (e.g. cyclin E, cyclin A and cdk2) and reduces the expression of cyclin D1 (Puzianowska-Kuznicka et al., 2006). It has also been demonstrated that T3 is the mediator of Sertoli cells cell cycle exit, during development, by acting to the transcriptional control of the Kip/Cip family member p27 (Holsberger et al., 2003), an important factor also in OPCs proliferation (Gao et al., 1998). Moreover, Runt-related transcription factor 1 (Ranx1), a well known factor controlling the hematopoietic stem cells development, is proven to be directly involved in the T3-mediated cell cycle control of OPCs, regulating the expression of p15/INK4b, the major effector molecule for the TH-dependent cell cycle deceleration in OPCs (Tokumoto et al., 2017).

The regulation of TH sensitivity is also dependent on the cell cycle phase. *In vitro* data suggest that TRs expression varies according to cell cycle. In particular there is no expression in early S phase, but progressive increase during late S and G2 until maximal level at G2/M, showing also an increase in TH binding capability (Maruvada et al., 2004).

The critical role of TH in OPC development and myelination is well supported by the dozens of publication describing the effect of hypothyroidism in experimental and clinical studies (Calzà et al., 2015). For example, TH depletion results in the reduction of OLs in the white matter (Schoonover et al., 2004) and hypothyroidism delays the expression of genes involving in the myelination process (myelin basic protein, MBP; proteolipid protein, PLP; myelin-associated glycoprotein, MAG) and the number of myelinating axons (Ibarrola and Rodríguez-Pe˜na, 1997). TRα1 mediates the differentiating effect of TH on OPCs, in fact TRα1-/- P7 OPCs in mice are unable to exit cell cycle and differentiate, while overexpression of TRα1 accelerate OPCs differentiation *in vitro* (Billon et al., 2002).

Apart of TRs, other NRs are involved in the gene expression regulation in OPCs and OLs and, moreover, TRs can act as homodimer or as heterodimer producing different effects on gene expression regulation (Zhuang S et al., 2013). For example, PPARγ agonists promote OL

differentiation of mouse NSCs by modulating the expression of different genes involved in stemness and differentiation (Kanakasabai et al., 2012).

Other fundamental NRs are retinoic acid receptors and, in particular RXRs (Retinoid X Receptors). RXRγ has been described as upregulated during the regenerative phase of remyelination, in fact its expression was detected in OLs in remyelinating lesions in rat CNS and in tissue from individuals with multiple sclerosis (MS), a disease characterized by extensive demyelination and remyelination attempts. The activation of RXR by pharmaco-logical and genetic manipulation, stimulates oligodendrocyte differentiation, enhancing remyelination (Huang et al., 2011). Moreover, TR/RXR heterodimer, is proposed to be the primary mediators of the target gene regulation by T3 (Lee and Privalsky, 2005; Figure 4).

NRs action is also mediated by binding coactivator (e.g. steroid receptor coactivator, SRC) or corepressor (e.g. nucler receptor corepressor, NCoR; silencing mediator of retinoic acid and thyroid hormone receptor, SMRT) molecules. The ligand-dependent transcriptional activation involves an allosteric change in the LBD that decreases its affinity for corepressors, increasing affinity for coactivators (Saijo et al., 2010). TRs and RARs (Retinoic Acid Receptors) heterodimers typically recruit corepressors and repress gene expression in the absence of hormone. When the lingand binds the heterodimer, the conformational changes allow it to interact with coactivators, thus activating gene expression. In the presence of T3, corepressor complexes are released from TRs, and coactivator complexes are recruited, leading to increased local histone acetylation and transcriptional activation (Maruvada et al., 2004).
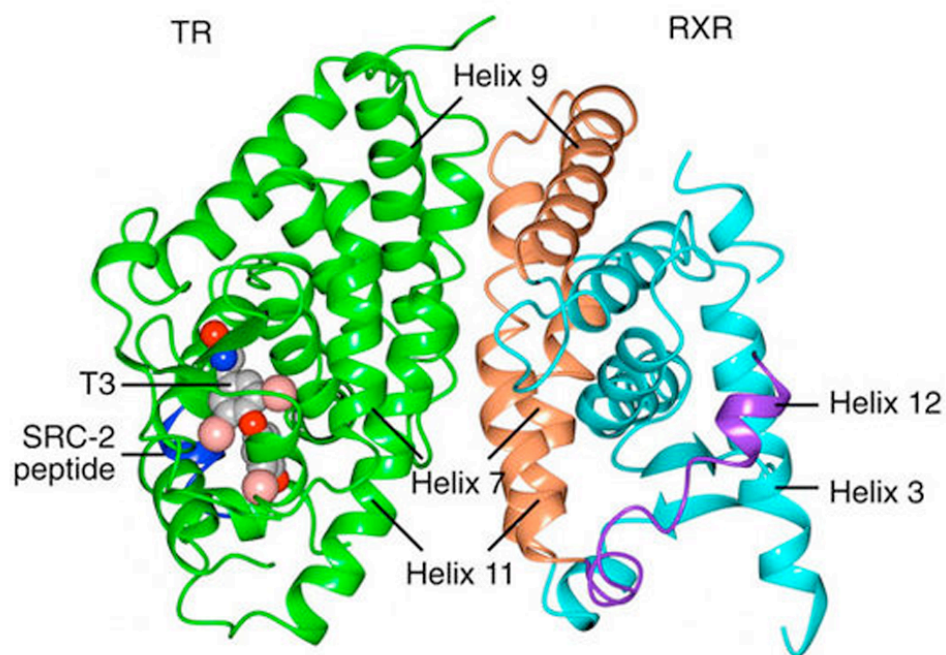
Figure 4. Structure of the TR/RXR heterodimer.

The figure shows the structure of the TRβ (green)/RXRα (light blue) heterodimer and the ligand position of T3 and SRC-2 peptide (Steroid Receptor co-activator 2) (Kojetin et al., 2015 - modified).

Molecules involved in the regulation of NRs expression and activity are also key players in the transcription regulation process. Poly (ADP-ribose) polymerase 1 (PARP-1) is a well known factor involved in DNA repair and cell death induction. It also acts as a transcription regulator, probably interacting with NRs (Ko and Ren, 2012), regulating Olig2 gene expression. PARP-1 inhibition results in decreased myelination in specific areas (corpus callosum, SVZ; Plane et al., 2012).

1.2 The oligodendrocyte precursor cell in acute lesions of foetal and adult brain

Myelin damages can be efficiently and correctly repaired and functions restored (Crawford et al., 2013) thanks to OPCs, which proliferate, migrate to the unmyelinated axons and differentiate in mature OLs after lesion (Trotter et al., 2010). Two main pathological mechanisms are involved in myelin injury and demyelination, both in foetal (e.g. neonatal hypoxia/ischemia) and adult lesions (e.g. MS, spinal cord and brain trauma, stroke): inflammation and hypoxia/ischemia (Calzà et al., 2017; Figure 5).

1.2.1 Inflammation

Inflammation has a dual role on myelin and OPC pathobiology, being a promoter of myelin repair in some conditions, and a severe inhibitor in other conditions (Tognatta and Miller, 2016). The establishment of an inflammation environment is essential to activate quiescent OPCs and for a successful proliferation, migration and remyelination, and cytokines and chemokines promote OPCs proliferation. In particular, cytokines mediate inflammatory response promoting pathogen clearance and preventing excessive tissue damage, playing a critical role in repair mechanisms in CNS. Some cytokines seem also to be involved in the physiological OLs maturation process, as through the activation of TNFR2. Chemokines, also, induce direct chemotaxis of immune cells and migration and maturation of NSCs, playing a fundamental role in CNS repair process. On the other hand, depending on the severity of the inflammation, an overproduction of cytokines/chemokines may lead to excessive inflammation and cell death, thus interfering with the repair process (Patel and Klein, 2011). In fact, for unknown reasons, the remyelination process fails in several conditions, usually characterized by the establishment of severe (and chronic) inflammatory environment. This remyelination failure is a pathological landmark in different neurological conditions

characterized by intense inflammation, and it is a major cause in related chronic sensory, motor, and cognitive disabilities. For example, acute demyelination after spinal cord injury is caused by an oligodendrocyte loss (Myers et al., 2016) and impaired OPC differentiation (Franklin & Ffrench-Constant, 2008; Mekhail et al., 2012) both in experimental animals and humans. Also in stroke models local OPCs in the white matter proliferate and part of them differentiates into astrocytes, while the remaining cells are mainly blocked in a progenitor phenotype (Sozmen et al., 2016).

The most important example of the strong implication of inflammation in remyelination failure is MS, the most diffuse inflammatory/demyelinating disease in humans (Goodin, 2014). In the acute focal phase of the disease, remyelination is efficient (Rodgers et al., 2013), however this process progressively fails (Boyd et al., 2013; Lassmann et al., 2012), and the most accredited hypothesis for remyelination failure is the block of OPCs maturation (Kuhlmann et al., 2008; Miller and Mi, 2007). In fact, the blocking of this process does not guarantee anymore the OPCs differentiation in mature OLs, leading to an inefficient myelin repair (Zhang et al., 2015).

Numerous *in vitro* and *in vivo* studies have indicated that inflammatory cytokines are involved in OPCs differentiation block, affecting cell cycle exit and the expression of genes encoding for proteins regulating and determining remyelination (Chew et al., 2005; Falahati et al., 2013; Kang et al., 2013; Su et al., 2011; Tanner et al., 2011; Fernandez et al., 2016).

In vivo experiments in our lab have demonstrated that a complex dysregulation of the TH tissue signalling is present in acute phase of EAE (experimental allergic encephalomyelitis), the rodents and primate animal model of MS (Dell'Acqua et al., 2012; D'Intino et al., 2011; Fernandez et al., 2016), which correlates with the rise of inflammatory cytokines released by peripheral cells and resident microglia (Borjini et al., 2016). Cytokines and chemokines play a key role in the MS pathogenesis, by regulating cell migration, proliferation, and activation of resident and infiltrating cells (Dendrou et al., 2015). In EAE model, it has been demonstrated

that a strong modulation of cytokines/chemokines expression occurs during all the phases of the disease progression, from the very early stages (Borjini et al., 2016). Moreover, a direct correlation between the onset of the inflammatory microenvironment and an increase of D3 enzyme expression has been described *in vivo* and *in vitro* (Dell'Acqua et al., 2012; Fernandez et al., 2016), possibly resulting in a local disregulation of TH metabolism leading to a depletion of T3 and down-regulation of TRs, supporting the view that a local hypothyroidism induced by inflammatory cytokines is a co-factor in remyelination failure (Calzà et al., 2015). An increase in D3 activity and mRNA expression level has been described in other neurological conditions characterized by inflammation and demyelination, e.g., ischemia-induced hypoxic brain damage (Jo et al., 2012) and nerve lesion (Li et al., 2001). This hypothesis has been confirmed by *in vitro* studies in our lab, where we demonstrated that the inhibition of the T3 inactivating enzyme D3 restores the OPC differentiation during exposure to an inflammatory cytokine cocktail (Fernandez et al., 2016**).**
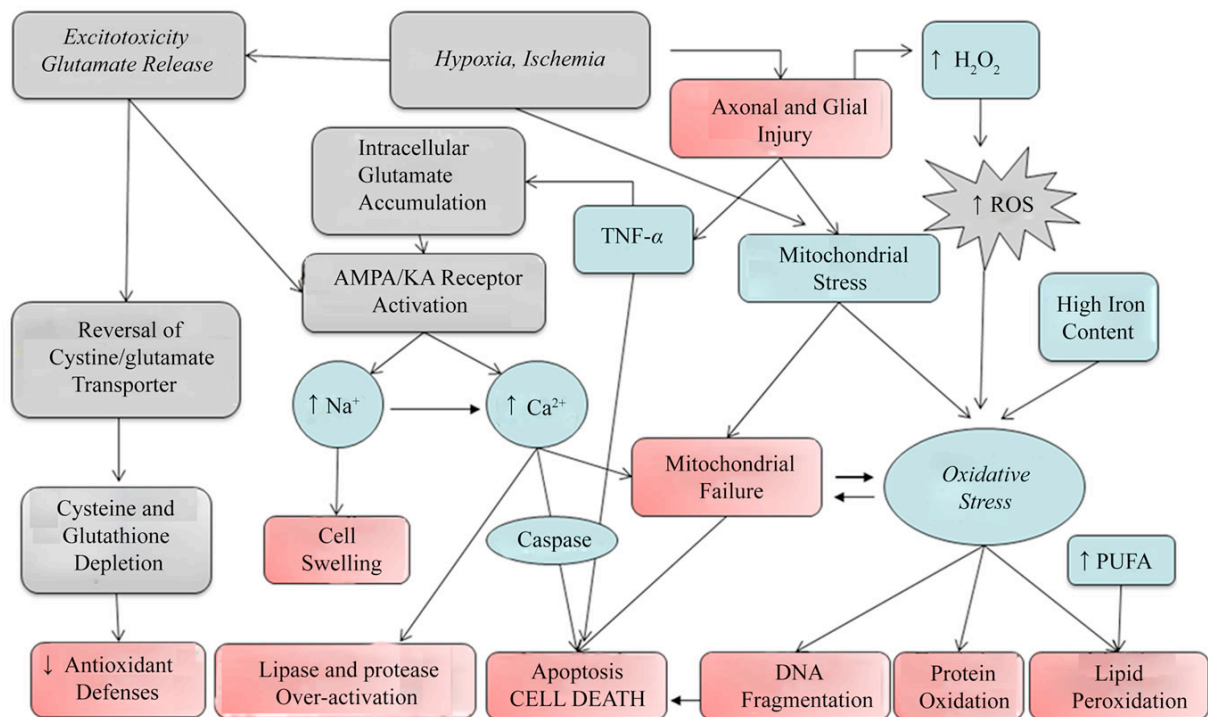
Figure 5. Injury mechanisms in Oligodendrocytes.
Schematic representation of the principal mechanisms involved in oligodendrocytes vulnerability: glutamate excitotoxicity, hypoxia/ischemia, oxidative stress and cytokines (Liao and Mani, 2011).

Thus, an altered TH tissue metabolism induced by inflammatory cytokines could be one of the most relevant factors involved in the OPCs differentiation block, extending to the CNS the evidence described in peripheral tissues on the relationship between inflammatory cytokines and TH tissue metabolism (Boelen et al., 2011; de Vries et al., 2015). In fact, in peripheral tissues, T3 level drops during starvation and illness, without affecting the thyroid function, as indicated by TSH and THs serum levels (De Groot, 2015). This condition has been defined "*nonthyroidal illness syndrome* (NTIS)" because it does not involve alteration in thyroid function but a tissue dysregulation of TH metabolism, played mostly by tissue-specific deyodinases enzymes, transporters and TH receptors (Warner and Beckett, 2010).

Since the role of TH in developmental myelination and the OPC differentiation block in the presence of inflammatory cytokines, our lab proposed the TH supplementation as a possible therapeutic strategy to overcome OPC differentiation block in MS (Calzà et al, 2002; Fernandez et al., 2004; D'Intino et al., 2011; Dell'Acqua et al., 2012). Afterwards, several other laboratories indicated that TH supplementation favours myelin protection/repair in different demyelination models characterized by intense tissue inflammation (reviewed in Calzà et al., 2005, Calzà et al. 2010, Calzà et al. 2015, Calzà et al., 2017), thus suggesting the possibility of including TH as adjuvant therapy during the acute inflammatory phase of disease and injuries characterized by demyelination. TH may be the ideal compound that can promote remyelination and impede MS progression. TH treatment activate OPCs, probably by stimulating KLF9 transcription, a key factor in the maturation process, related with CXCL12/CXCR4 signal axis (Zhang et al., 2016).

1.2.2 Hypoxia/ischemia

As described above, demyelination and white matter lesion also occurs in acute injuries, like trauma and stroke. Most of white matter infarcts are believed to be secondary to vascular occlusion and endothelial cell dysfunction (El Waly et al., 2014). In fact, three hours after hypoxia/ischemia (HI), OLs show swelling and vacuolization, followed by retraction and cell death after 24 hours (Pantoni et al., 2006; McIver et al., 2010).

Oxygen deprivation in perinatal period often results in HI-induced brain damage, which remains a common cause of neonatal brain injury and affects 1 to 3 per 1000 live births in developed countries and up to 26 per 1000 live births in the developing world. The pattern of injury depends on the level of the development of the brain and on the severity of the insult (Rocha-Ferreira and Hristoya, 2016). In particular, demyelination following brain damage is a typical event at neonatal stages, correlating with susceptibility of late OPCs (Back et al.,

2002), and leading to apoptosis, delayed maturation of OLs and activation of the Cdk2 pathway, inducing proliferation of OPCs (Jablonska et al., 2012).

The mechanism and mode of HI-induced cell death depends on: severity of the insult, glutamate receptor stimulation, degree of calcium overload, cellular energy depletion and mitochondrial dysfunction (Rocha-Ferreira and Hristoya, 2016). Moreover, OLs vulnerability to HI is maturation-dependent: the most susceptible stage is PreOLs (late OPCs), followed by early OPCs and mature OLs, which implies death of PreOLs and subsequent failure of myelination (Back et al., 2002). *In vitro* experiments demonstrated that oxygen-glucose deprivation (OGD) in primary OPCs, induces intracellular Ca^{2+} overload, mitochondrial damage and ROS generation (via ERK1/2 pathway), resulting in PreOLs death (Cai et al., 2016). Calcium overload leads also to lipases, endonucleases and proteases activation, leading to the cytoskeleton disaggregation (Rocha-Ferreira and Hristoya, 2016).

HI injury is also characterized by an early excitotoxic-oxidative cascade, caused by the reduction of the high-energy phosphate metabolism, the consequent increase in lactic acid, and cell membrane ionic transport failure. This, combined with cytoskeleton destruction, causes depolarization and excessive presynaptic release of glutamate, worsen by the depleted glutamate reuptake caused by the reduced glucose availability (Rocha-Ferreira and Hristoya, 2016).

The excitatory neurotransmitter glutamate is a major player in CNS cell death. Excessive glutamate release causes excitotoxicity and can trigger OLs apoptosis, depending on the developmental stage (Butts et al., 2008). HI-mediated glutamate excitotoxicity have been also demonstrated in *in vitro* models in which OGD causes a local glutamate accumulation leading to cell death, enhanced by mitochondrial dysfunction (Deng et al., 2006).
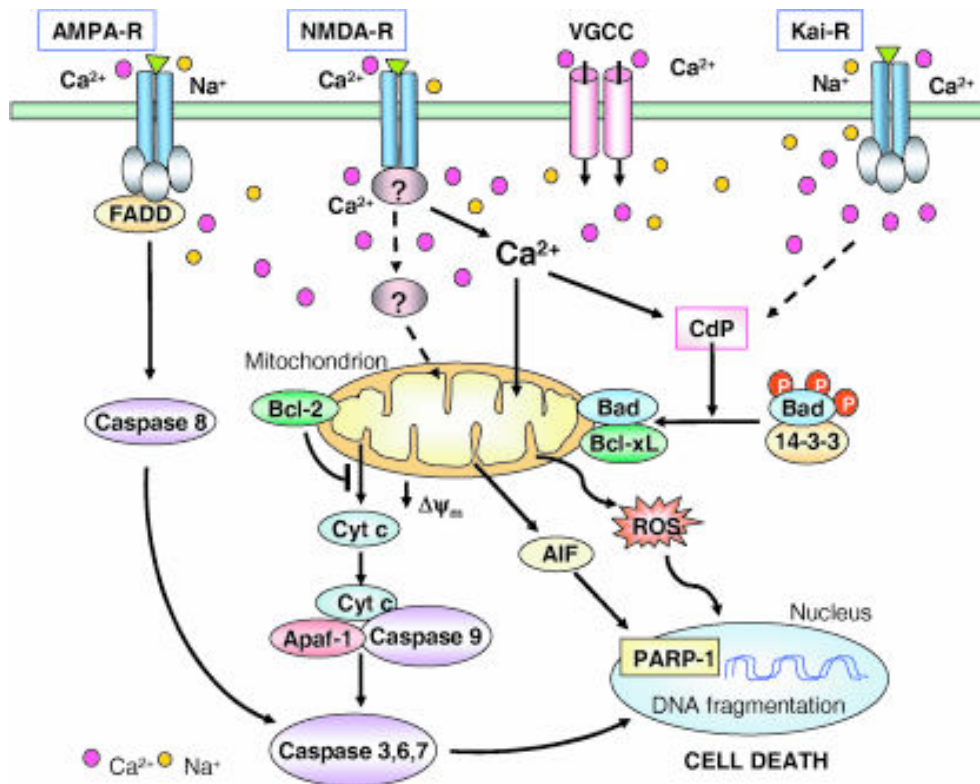
Figure 6 – Glutamate excitotoxicity in oligodendrocyte.

AMPA and kainite receptors activation leads to Na^+ and Ca^{2+} influx and consequent depolarization, contributing to the Ca^{2+} concentration increasing by the activation of VGCC channels. Calcium influx in mitochondria results in depolarization, increase in ROS production and finally in Cyt-c release, which interacts with Apaf-1 and activate caspases. AIF also contribute to apoptosis induction by activating PARP-1. Moreover, AMPA-R activates CdP, which dephosphorylates Bad and facilitates apoptosis. *Abbreviations: AIF, apoptosis-inducing factor; Apaf-1, apoptotic protease-activating factor 1; Cdp, calcineurin; Cyt-c, cytochrome c; FADD, Fas-associated death domain; 14-3-3, phosphoserine-binding protein 14-3-3; PARP-1, poly(ADP-ribose)polymerase-1; ROS, reactive oxygen species; VGCC, voltage-gated Ca^{2+} channels* (Matute et al., 2007; based on Sánchez-Gómez et al., 2003).

For many years, AMPA/kainite, but not NMDA receptors, have been considered the mediator of glutamate excitotoxicity in glial cells (Tekkök and Goldberg, 2001) and, in particular, the HI-induced cell death glutamate-mediated in pre OLs (Deng et al., 2003). These data are supported by the *in vitro* demonstration that OLs glutamate-induced cell death is prevented by

AMPA/KA receptors block. However, more recently it has been demonstrated that NMDA receptors play a role during development myelination (Káradóttir and Attwell, 2007; Figure 7) and are partners in the OL myelinating processes. Moreover, neurodegenerative disorders and MS, usually involve a small, but prolonged rise in extracellular glutamate concentration. Thus, the higher glutamate affinity of NMDA receptors, compared to AMPA receptors, makes them more likely to be activated (Káradóttir et al., 2005). A different expression of these receptors during the differentiation process, could also explain the different sensitivity to glutamate in different stages. In particular OPCs show higher expression of AMPA/kainite receptor, mGluR while, postmitotic OLs have higher NMDA receptor expression (Butts et al., 2008).

Excitotoxic cell death in OLs can be mediated in different ways (Matute et al., 2007). For instance, a calcium influx and accumulation in mitochondria is generated by AMPA/kainite receptor, leading to mitochondria depolarization, cytochrome c release into the cytosol and production of reactive oxygen species (ROS). Cytochrome c release into the cytosol triggers the intrinsic caspase activation pathway, thus causing apoptosis, while the maximal AMPA receptor stimulation can trigger necrosis. Moreover, in pro-OLs, glutamate mediates also the pro-apoptotic Bax translocation into mitochondria. Additionally, OPC vulnerability to excitotoxicity mediated by calcium influx is also influenced by the fact that i) the particular GluR subunits expressed in OPCs are those that confer high calcium permeability; and ii) OPCs, unlike neurons, do not express calcium-binding proteins for maintenance of intracellular calcium homeostasis (Butts et al., 2008).
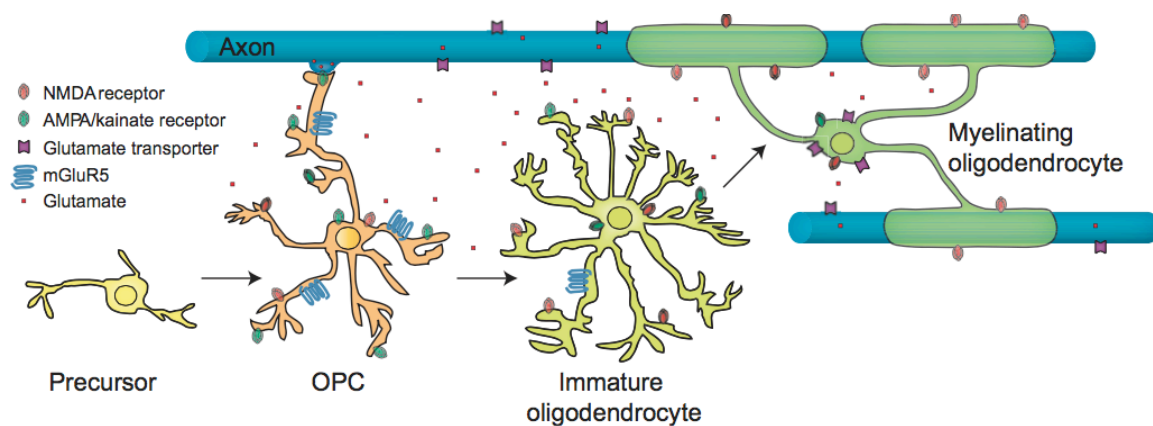
Figure 7. Role of Glutamate receptors in OPCs differentiation

OPCs, immature OLs and mature OLs express glutamate receptors. Glutamatergic stimulation of OPCs regulates their differentiation while, in conditions of energy deprivation (e.g. stroke or ischemia following spinal cord injury) axonal and OLs glutamate transporters cause a non-vesicular glutamate release (Kolodziejczyk et al., 2010).

HI also induces an inflammatory response that has the positive role to remove damaged cells, debris and lipids, followed by a switch from pro- to anti-inflammatory profile that stimulates repair processes (Rocha-Ferreira et al., 2016). Several cell types are involved in these complex events, which is quite different in neonatal and adult life. After HI in adult CNS, leukocytes are activated and migrate into the brain/spinal cord injured site, where cytokines are produced in large amounts. This process takes place within hours in adult. On the contrary, HI induces an immediate (minutes) innate immune response in new-borns. Age differences in HI-response mechanisms include also the cross-talk between excitotoxic, oxidative and inflammatory injury, creating "windows of susceptibility" to HI-injury during embryonic and early postnatal brain in development (Liu et al., 2013).

Different responses to THs treatments have been described in neonatal inflammatory-demyelinating lesions and diseases. TH treatment has been suggested to overcome myelin

damages of neonatal encephalopathy, a combined insult of infection/inflammation and HI, leading to OPCs injury and death and also to failure of proper OLs maturation (La Gamma and Paneth, 2012; Schang et al., 2014). However, conflicting results have been obtained by TH treatment in experimental perinatal inflammation-induced white matter injury and HI, probably because of substantial differences in the models tested (Calzà et al., 2017).

1.2.3 Nuclear Receptors and neuroinflammation

It is well known the role of some NRs in inflammation, including glucocorticoid receptor (GR), PPARs, LXRs and NR4A (Huang and Glass, 2010). It has been widely investigated the action of different NRs to inhibit inflammation by different mechanisms, including ligand-dependent inhibition of inflammatory gene expression and enhancing expression of genes that encode inhibitory proteins. In this context, the most extensively studied receptor is the GR, exerting its action throughout glucocorticoids binding activation and subsequent DNA binding and expression regulation of target genes involved in inflammatory response. However, the main interaction between NRs action and inflammation, called *transrepression*, is a mechanism in which NRs interfere with activation of inflammatory response through protein-protein interactions with coregulatory proteins and transcription factors, rather than directly interacting with DNA (Pascual and Glass, 2006). Moreover, receptor-specific mechanisms for repression indicate that each nuclear receptor has a distinct impact on the development of the inflammatory response (Glass et and Ogawa, 2006).

The different mechanisms involved in NRs-mediated inflammatory response include i) ligand-dependent inhibition of inflammatory gene expression by sequence-specific binding of NRs to negative regulatory elements, ii) positive regulation of genes that encode inhibitory proteins, and iii) ligand-dependent transrepression. NRs require an overlapping set of coactivator proteins, some of which already present in cells at functionally limiting levels.

Moreover, evidence for a coactivator competition model of transrepression involving cAMP response element-binding protein (CREB)-binding protein (CBP) was first provided for RXR and GR transrepression of AP-1 target genes. In addition, many NRs have been suggested to exert inhibitory effects on inflammatory response genes through direct interactions with NF-kB and AP-1 factors (Pascual and Glass, 2006).

Interestingly, several NRs positively and negatively regulate T cells and myeloid-mediated immune responses in MS, including RORs, oestrogen receptors, GR, VDR, RAR, and PPARγ. T cell receptor stimulation in the presence of IL-6 and TGFβ skews naïve T cell differentiation and all-trans retinoic acid (at-RA), a ligand for RAR, strongly inhibits this process (Mucida et al., 2007). Moreover, in *in vivo* model of demyelination RXRs-ligand mediated activation accelerates CNS remyelination, also modulating the inflammatory response (Huang and Glass, 2010).

NRs and cytokines influence each other by a complex crosstalk. Inflammation mediators are substantially regulated by AP-1, C/EBP and NF-kB transcriptional factors and their expression can be repressed by NRs. Glucocorticoids and oestrogens are immunosuppressive NRs, suppressing proinflammatory cytokines expression, while RA induces IFN-α synthesis. PPARγ also shows anti-inflammatory properties, inhibiting the secretion of IL-6, TNFα and IL-1b (Wang et al., 2004).

The role of NRs in regulation of inflammation response in macrophages and T cells is widely described (reviewed in Glass and Saijo, 2010) however, little is known about their interaction in demyelinating diseases.

Proinflammatory cytokines have been associated with *non-thyroidal illness syndrome* in view of their capability to decrease D1 and TRβ mRNA expression in the liver. In particular, Il1b is able to decrease TRβ1 expression in the liver and TRα1 and TRα2 mRNA level in hepatoma cells, in an NFkB-dependent way (Kwakkel et al., 2007). IL1b and IL6 also downregulate

TRβ1 and TR cofactor DOR/TP53INP2, in cultured hepatocytes and, moreover, the TRα1, TRα2 and TRβ1 T3-mediated upregulation is blocked by IL-6 exposure (Malik et al., 2010).

1.3 *In vitro* models for OPC: methodological remarks

In vitro models are simple and widely applicable systems that provide information about OLs development and their vulnerability at different noxious stimuli, also for drug discovery purposes. These models are useful to study physiologic and pathological conditions at cellular and molecular level, recreating some cellular interactions and microenvironment complexity. Obviously, *in vitro* models lack the *in vivo* complexity, being also difficult to recreate the spatial and temporal signalling of OLs development and the complexity of multifactorial diseases (Barateiro and Fernandes, 2014).

However, several key aspects of *in vitro* modelling should be carefully considered in order to compare published data, and to try to address specific experimental question using the most appropriate approach, i.e. cell source and experiment readout.

1.3.1 Cell sources

In vitro OPCs models include cell lines, stem cells-derived OPCs (from embryonic stem cells or foetal/adult neurospheres) and primary OPCs isolated from both developing and adult CNS.

Few cell lines are available for OLs. Oligodendrocyte-type 2 astrocyte (O-2A) precursors were spontaneously generated from cultures of neonatal rat cerebral cortex and give rise to bipotential cell line (CG4) able to generate both oligodendrocytes and astrocytes (Franklin et al., 1995). Also the OLN93 line, derived from primary rat brain cultures, resembles the O2A-

progenitor cells and can be differentiated into immature OLs when cultured in the presence of serum (Richter-Landsberg and Heinrich, 1996).

Mice immortalized cell lines were also produced. In 1993 (Jensen et al., 1993) 6E12 line were derived from MBP-SV40 large T-antigen transgenic mouse spinal cord. These cells express O4 and GalC lightly and they need activation with forskolin or dibutyryl cyclic AMP to increase the expression of these markers and turn on PLP mRNA expression. However, this cell line is unable to express MBP (Merrill, 2009). Oli-neu is a mouse OPC line containing replication-defective retroviruses expressing the t-neu oncogene. These cells are useful in co-culture studies, because of their ability to interact with neurons, in order to analyse neuron-glia interactions (Kipp et al., 2012).

Human OLs cell lines were also generated, to overcome the difficulty to obtain human culture of OLs. HOG, MO3.13 and KG-1C lines express immature OL markers, (CNPase and GalC), and do not express GFAP. HOG and MO3.13 can be differentiated to express MBP and MOG, while KG-1C remains mostly undifferentiated (Buntnix et al., 2003).

Cell lines show considerable variability, largely depending on the origin, isolation method and growth conditions. They usually maintain proliferative status, due to their tumorigenic potential, and differentiation is difficult and often incomplete (Lin et al., 2006; Pringproa et al., 2008).

The most widely used OLs cultures are primary OPCs, isolated from P1-P2 rodents brain, and purified by the shake-off technique, that prifits by the different cell adhesion capability of the different cell types (Chen et al., 2007). Cells can be purified also by using the magnetic activated cell sorting (MACS), just after the brain dissociation, using magnetic beads linked to specific antibodies. These cultures usually show 4.3% of early nestin-expressing precursors, 84.5% of NG2-positive OPCs and 10.6% of pre-OLs A2B5-positive, with only 0.6% of GFAP-positive cells (Barateiro and Fernandes, 2014).

Human foetal OPCs can also be obtained from post-mortem foetal spinal cord and brain (18-23 weeks of gestation), reaching 90% of purity by using immunomagnetic microbeads separation (Merrill, 2009). These cells show less variability and are more genetically stable compared to OPCs derived from stem cells, and they are as similar as possible to the *in vivo* counterparts. However, in comparison with cell lines and NSCs-derived OPCs, there are limitations of this *in vitro* model. Passages and freezing/thawing of these cells cause their differentiation in astrocytes, due to the capability of O4-positive OPCs to retain the capacity to differentiate in GFAP-positive cells. Moreover, additional factors are necessary to accompany T3 for high yield of differentiation (Dincman et al., 2012).

OPCs can be differentiated from NSCs isolated from foetal or adult brain. As described above, NSCs are a mixed population of uni- and multipotent cells that, driven by specific signals, which can differentiate in OPCs.

NSCs can be isolated from foetal forebrain and from adult hippocampal sub-granular zone (SGZ) and SVZ, and maintained *in vitro* as spheroids called neurospheres (Alhenius and Kokaia, 2010). SVZ-derived neurospheres are widely used as a NSCs *in vitro* model and, even if physiological *in vivo* differences of the two neurogenic niches are widely explored (Fuentealba et al., 2012), little is known about differences in their *in vitro* derivatives. Moreover, even regional differences in the same niche are emerging. For example it has been demonstrated that the rostral side of the SVZ shows the major activity in generating OPCs after demyelinating stimuli (Brousse et al., 2015).

Spheroids can be passed several times under the exposure to two specific growth factors, i.e. basic fibroblast growth factor (bFGF) and epidermal growth factor (EGF). In order to drive the OPC differentiation, after the first splitting, bFGF/EGF mix should be replaced by bFGF/PDGF growth factors, generating the so-called oligospheres. Once splitted and seeded as single cell culture they can differentiate in mature OLs, removing growth factors and

adding T3 (Chen et al., 2007). OPCs can be generated also from foetal human neurospheres expressing O4, NG2 and Sox10 markers and very low expression of GFAP and Tuj1, showing capability to respond to OLs differentiation induction (Lu et al., 2015).

OPC cultures derived from neurospheres show phenotypic variability (Chen et al., 2007) and, subtle cellular changes can occur with culture passages, often resulting in a cell type having molecular properties different from the original cells (Lin et al., 2006). However, NSCs-based *in vitro* differentiation model allows the study of the whole process, from early progenitors to mature OLs. Moreover, these cells are highly sensitive to T3-mediated differentiation induction, a necessary condition to induce mature OLs. This allows the analysis of the whole mechanism of T3 action and the pathological interferences on the molecular machinery involved in the process (Castelo-Branco et al., 2014; Baldassarro et al., unpublished-a).

In particular, NSCs derived from foetal or adult rodent brain show phenotypic and genotypic differences, such as OPCs derived at different developmental stages, but properties of these two cell systems are not yet fully characterized. For example, foetal NSCs need bFGF for self-renewal and are less sensitive to PDGF, while adult cells could generate neurospheres driven by PDGF and NT-3 but they do not need bFGF, even if they need more time to generate spheroids. Moreover, the capacity of foetal NSCs-derived OPCs to generate OLs decreases through passages and with the increase of the foetal brain tissue age (Chojnacki et al., 2008).

In order to mimic *in vivo* myelination process, the co-culture is the most suitable and informative technique. This model preserves the physiological relevance of the neurons-OLs interaction maintaining the accessibility of *in vitro* cultures, without the interference of other glial cells. However, although *in vitro* cultures and co-cultures are very useful and accessible models, their main disadvantage resides in the loss of the three-dimensional structure. To

overcome this issue, it is possible to study diverse neurobiological processes using *ex vivo* brain slice cultures, which preserve the three-dimensional architectural organization that supports all tissue circuits and interactions. Slices are thick brain sections (250–400 μm) grown on semi-porous membranes and kept at an air–liquid interface, which causes less tissue thinning and allow much simple maintenance and processing (Barateiro and Fernandes, 2014).

Another 3D model is the isolation of CNS spheroids from telencephalon or embryonic whole brain, both from rodents or humans fetus. When cultured under continual rotation, cells gradually reassemble into clusters. In these 3D structures, myelin is multilayered, resembling myelin in CNS and responds to demyelination stimuli, as antibody anti-MOG or IFNg (Kipp et al., 2012).

As described above, foetal and adult OPCs share common myelination mechanisms, but also show quite different cellular and molecular aspects, not yet well characterized. Several *in vivo* and *in vitro* studies indicate that OPCs have substantially different properties according to their chronological age. For example, human foetal OPCs from different gestational stages exhibit differences in the myelination profile (Cui et al., 2012), such as human OPCs derived from foetal brain during the period of maximum oligoneogenesis or from adult subcortical white matter (Windrem et al., 2004). Even if the mechanisms behind the different age-related OPC biological properties are not known, these could reflect differences in OPCs *in vitro* models when isolated at different stages of the development.

Three different subsets of OPCs were identified in adult human CNS, expressing different miRNAs compared to foetal OPCs and mature OLs. Moreover, two subsets of OPCs were isolated from early and mid second trimester foetal brains. Both in adult and foetal brains, the different OPCs subsets, have been identified by the different O4 expression level, leading to

different expression of the different genes involved in OLs maturation (Olig2, Nkx2.2 and PDGFαR; Leong et al., 2014).

Adult OPCs isolated from grey and white matter shows also differences. Transplanted OPCs isolated from white matter are able to differentiate into mature myelinating OLs both in white and gray matter, while gray matter-OPCs are less efficient. This difference could derive from the surrounding environment where cells reside from the CNS development (Viganò et al., 2013). This variability is also proven in cuprizone-induced demyelination mouse model, where the remyelination in the corpus callosum is faster than in the cerebral cortex (Gudi et al., 2009), as also confirmed in humans MS patients (Albert et al., 2007).

As discussed above, it is well known that O-2A-expressing OPCs isolated from animals at different ages have different properties (Gao and Raff, 1997; Wolswijk and Noble, 1989; Wolswijk et al., 1990; 1991). Moreover, in rats at P7, when myelination is ongoing in different brain regions, different O-2A-expressing OPCs population where identified, characterized by cell-intrinsic differences in self-renewing, maturation-induction responses and intracellular redox state (Power et al., 2002).

1.3.2 Robust readouts for OPC/OL in vitro models

Depending on the experimental question, different *in vitro* models have been set up in order to study proliferation, differentiation, maturation, myelination and vulnerability of the OPCs/OLs cell systems.

While proliferation in cultured OPCs is usually analysed by standard *in vitro* assays (e.g. MTT, cell counting and Ki67 staining), differentiation and maturation analysis need specific OPCs/OLs lineage markers.

As described above, in absence of axons, neurospheres-derived or primary OPCs are able to proliferate and, under specific stimuli, to differentiate in mature OLs. Using these models, it is possible to evaluate if any compound added during proliferation or differentiation stages is able to delay or reduce OLs differentiation, analysing the number of OPCs (e.g. NG2- or PDGFαR-positive cells) and OLs (e.g. MBP-positive cells) in the culture.

Different challenges could also affect OLs maturation, by affecting cell morphology. This is possible to analyse by dividing mature OLs in different categories by the complexity of the cell structure: i) poorly branched OLs, ii) complex branched OLs, and iii) complex branched OLs forming membrane (Barateiro and Fernandes, 2014).

Although cultured MBP-positive OLs are considered myelinating OLs, the lack of axons do not preserves the OL-neuron interaction. A co-culture model comprising dorsal root ganglion neurons, growing on 3D Matrigel and primary OLs, allows the study of axon myelination in vitro (Wang et al., 2007). However, new methods involving engineered artificial fibers mimicking axonos, has been developed in order to co-cultures limitations on time, costs and reproducibility (Lee et al., 2013).

Using the described above models to study proliferation, differentiation/maturation and myelination, it is possible to analyse noxious stimuli mimicking pathological mechanisms. OPCs/OLs are highly sensitive to inflammatory mediators and HI. However, mechanisms underlying OPCs vulnerability or perturbations in the maturation and myelination process are still not well defined.

As described above, OPCs and mature OLs are sensitive to glutamate excitotoxicity, depending on their developmental stage and glutamate is the main triggerer of the HI-induced cell death. In order to mimic the HI condition *in vitro*, the *oxygen-glucose deprivation* (OGD) model has been set up, resembling the fundamental aspects of the *in vivo* damage: low oxygen

pressure, low nutrient levels and reperfusion. This system was initially used in oncology to mimic necrosis (Hlatky et al., 1988), than applied to both pure or mixed neuronal/astrocytes cultures (Goldberg et al., 1993) and finally transferred to brain and spinal cord slices (Berger et al., 1998). The OGD model is particularly interesting in the study of neonatal hypoxic-ischemic encephalopathy (HIE), a syndrome determined by asphyxia occurring during the perinatal period (Kurinczuk et al., 2010), and to screen potential neuroprotective drugs. Moreover, this model is also useful to study the extreme form of metabolic stress resulting from oxygen and glucose deprivation, such as in cerebral ischemia (stroke) that most commonly occurs when the blood supply to a part of the brain is suddenly interrupted by occlusion of a vessel. Because *in vivo* cerebral ischemia often consists of both reversible ischemia and blood flow re-perfusion, the cultures in the OGD model are first exposed to *in vitro* HI, then returned to a normal medium in an oxygen atmosphere environment to simulate the *in vivo* blood flow reperfusion period (Goldberg et al., 1993).

OGD model in neuronal cultures is used in a wide range of conditions and timing and the contribution of oxygen or glucose deprivation is not well characterized. Due to the different sensitivity of OPCs and OLs to this noxious stimulus and the different possible cell sources, it is also not well defined the contribution of HI on OPCs vulnerability in demyelinating diseases affecting different stages of the development.

Different *in vitro* models have been also set up in order to mimic the inflammation environment in the CNS. Inflammation is a very complex condition, involving different type of cells and molecules, leading to the difficulty of modelling it *in vitro*. However, these models are useful to study the contribution of specific molecules and specific cells to inflammation-mediated effects and vulnerability.

Lipopolysaccharide (LPS) treatment is the most used inflammation-inducing factor in culture. LPS in MO3.13 cell line leads to increased expression and activity of nNOS, leading to the activation of reactive nitrogen species decreasing cell survival (Yao SY et al., 2010; Yao S et al., 2010). However, inflammation is usually mediated by other glial cells. In this context had been proven that preOLs are selective vulnerable to LPS-induced cell death in primary mixed glial cultures and that the effect is mediated mainly by microglia activation, but not by astrocytes and, in particular, by the cytokines secretion (Li et al., 2009).

In order to study the interaction between the different cells involved in the inflammation, co-cultures are useful tools to retain the cell-cell contact between the specific cells. Treatment of OPCs cultures with conditioned medium obtained from activated microglia or mixed glia cultures allow also the focus on glia-secreted molecules effect on OPCs differentiation and survival.

In a more specific way, it is possible to treat OPCs with specific molecules identified in activated glial cultures, in animal models of demyelinating diseases or in human patients. Moreover, this model allows studying the role of specific molecule, or molecules mix, identified in specific phases of the diseases, on specific developmental/maturational OPCs stages (Fernandez et al., 2016). Also in this context, due to the different cell sources, contrasting results are reported using different OPCs *in vitro* models. IFN-c either inhibits (postnatal rat purified OPCs primary cultures and adult mice SVZ derived OPCs, Chew et al., 2005; Pluchino et al., 2008, respectively) or induces (7-days postnatal O/2A OPC primary cultures from the corpus callosum, Tanner et al., 2011) cell cycle exit in OPCs, also abrogating the T3-induced differentiation (Tanner et al., 2011). TNF-a is cytotoxic and inhibits OPCs differentiation (primary OPCs, Su et al., 2011) while IL-17 prevents OPCs maturation (OPCs-enriched primary culture from foetal mice NPCs, Kang et al., 2013). IL-1b, IL-6, TGF-b1, and TNF-a produced as a result of ischemia shifted OPCs toward the more immature form (1-day postnatal rat ischemia, Falahati et al., 2013).

All the described *in vitro* assays and models involve primary cultures in combination complex systems of molecules and environmental challenges, used in a wide range of conditions and timing. These models thus require protocol standardization and robust and reliable readouts. In fact, the high variability of results could come also from the different readouts and human-biased techniques. Automated morphometric analyses for image-based high-content screening (HCS) is based on determining shapes of cells, distinguishing increased branching, and quantitating secondary and tertiary process numbers and lengths. HCS algorithms compatible with automated digital cell micro-imagers, data acquisition systems and counting software can be used for analysis of single or multiple imaging channels. These hardware/software systems remove the subjectivity and time-consuming component of visualization and manual evaluation (Merrill, 2009).

2. AIM OF THE STUDY

Mechanisms underlying OPCs vulnerability and differentiation block, linked to remyelination failure, in different demyelinating diseases are still unknown. Foetal and adult OPCs, can be both affected by demyelinating insults and, due to their different nature, could differentially respond to noxious stimuli.

The main objective of the present study is the investigation of foetal and adult NSCs-derived vulnerability to demyelinating diseases. In order to pursue the main objective the study was aimed to establish reliable *in vitro* systems and studying differences in T3-mediated physiological differentiation of foetal and adult OPCs.

In particular, in order to obtain robust *in vitro* models, the following objectives were carried out: i) cell-based HCS viability and lineage analysis set up; ii) OGD model set up and characterization; and iii) OGD translation on disease model and drug testing.

Since physiological OPCs differentiation is mediated by T3, exerting its action throughout NRs, the following objectives were investigated: i) NRs expression in early progenitors, ii) gene and protein expression of OPCs/OLs specific markers, iii) RXRγ role in OPCs differentiation and, iv) role of PARP in OPCs viability and differentiation.

Once set up robust *in vitro* models and readouts and clarified physiological similarity and differences in differentiation process, OPCs were challenged with the two main component of demyelinating diseases: inflammation and HI.

The analysis of differences between these two cell populations in physiological and pathological environment, will allow the deep understanding of their biology, carrying the possibility to develop differential therapies between foetal and adult demyelinating diseases.

3. MATERIAL AND METHODS

3.1 Neural stem cells and oligodendrocytes precursor cells cultures

All animal protocols described herein were carried out according to the European Community Council Directives (86/609/EEC), and comply with the guidelines published in the NIH Guide for the Care and Use of Laboratory Animals.

Mouse foetal and mouse/rat adult NSCs were isolated from E.13-14 foetal forebrain or striatum or 2.5 month old mice sub-ventricular zone (SVZ), following the Ahlenius and Kokaia protocol (Ahlenius and Kokaia, 2010). Oligodendrocyte differentiation was performed following the Chen protocol (Chen et al., 2007) with some modifications (Figure 8). In another set of experiments the same protocol was used to differentiate OPCs from neurospheres isolated from foetal brain (whole forebrain or striatum) and adult SVZ of RXRγ+/+ and RXRγ -/- mice (Krezel et al., 1996).

Tissues were enzymatically dissociated using trypsin (SIGMA), hyaluronidase (SIGMA) and DNase (SIGMA), than mechanically dissociated by piepetting. The solution was filtered, centrifuged and the resulting pellet was washed twice in HBSS. After 7 minutes centrifugation at $400 \times g$, the cellular pellet was resuspended in serum-free medium (DMEM/F12 GlutaMAX 1 x; 8 mmol/L HEPES; 100 U/100 μg Penicillin/Streptomycin; 0.1 x B27; 1 x N-2; 20 ng/mL bFGF; 20 ng/mL EGF) and, after cell count, cells were plated in suspension at a density of 10 cells/μl in a final volume of 3 mL in low-attachment 6-well plates (NUNC). Half medium was changed every three days, centrifuging the cell suspension at $300 \times g$ for 5 minutes and gently resuspending the cellular pellet in fresh medium. Neurospheres were allowed to proliferate until they attained a diameter of about 100μm.

To obtain secondary neurospheres, primary neurospheres were centrifuged, mechanically dissociated in single cell suspension and replated in the NSCs medium

containing bFGF and EGF. While, in order to obtain oligospheres, single cells were plated at a density of 10 cells/μl in a final volume of 3 mL of OPCs medium (DMEM/F12 GlutaMAX 1 x; 8 mmol/L HEPES; 100 U/100 μg Penicillin/Streptomycin; 0.1 × B27; 1 × N-2; 20 ng/mL bFGF; 20 ng/mL PDGF) in low-attachment 6-well plates (NUNC). Oligospheres were centrifuged and the pellet was mechanically dissociated to obtain a single cell suspension. After cell count, cells were plated at a density of 3000 cells/cm2 on poly-D,L-ornithine (50μg/ml)/laminin (5μg/ml) coating, in OPC medium.

In order to induce oligodendrocyte differentiation and maturation, after 3 DIVs OPC medium was replaced with the OL differentiation medium (DMEM/F12 GlutaMAX 1 x; 8 mmol/L HEPES; 100 U/100 μ g Penicillin/Streptomycin; 0.1 x B27; 1 x N-2; 50 nM T3; 10 ng/ml CNTF; 1x N-acetyl-L-cysteine -NAC-).

3.2 PCR array

The RNeasy Micro Kit (QIAGEN) was used for total RNA extraction and 300 ng were retrotranscribed using the RT2 First Strand Kit (QIAGEN) following the manufacturer's instructions.

For the study of NSCs gene expression, the 96-well QIAGEN PCR array for nuclear receptors and co-regulators was used in combination with the RT2 SYBR Green qPCR Mastermix (QIAGEN), using 10 ng of cDNA per well.

Using the web-software STRING [http://string-db.org/], proteins derived from the genes of interest were connected in clusters according to their interactions and involvement in biological processes. The software allows the identification of net of interactions including other proteins closely linked to the one analysed to be extended, in order to obtain a better understanding of the possible pathways involved in the differentially expressed genes.

3.3 Cell-based High Content Screening set up for NSCs lineage analysis

NSCs were isolated from mice foetal (E13.5) forebrains described above. Secondary neurospheres were dissociated and plated at a density of 1 x 10^4 cells/cm^2 in the same culture medium without mitogens. To achieve full lineage commitment and cell differentiation, seeded cells were cultured for 15 days.

Cells were seeded on different substrates: Cultrex (Trevigen)-coated glass, laminin (Sigma)-coated glass, laminin-coated or not PLLA- FILM, laminin-coated or not random and aligned electrospun PLLA scaffold.

In order to study cell viability and lineage specification, cell-based HCS was used. The HCS software allow the identification of the nucleus, by nuclear staining, and the study of its morphology. Condensed nuclei (smaller and brighter) are recognized as dead cells. Moreover, the software allow the identification of the cytoplasmatic fluorescence around the nucleus, identified as single cell.

HCS viability results were than compared with the standard MTT viability assay, in order to validate the HCS technique.

HCS was thus used for the analysis of cell viability and lineage specification markers (see section 3.16).
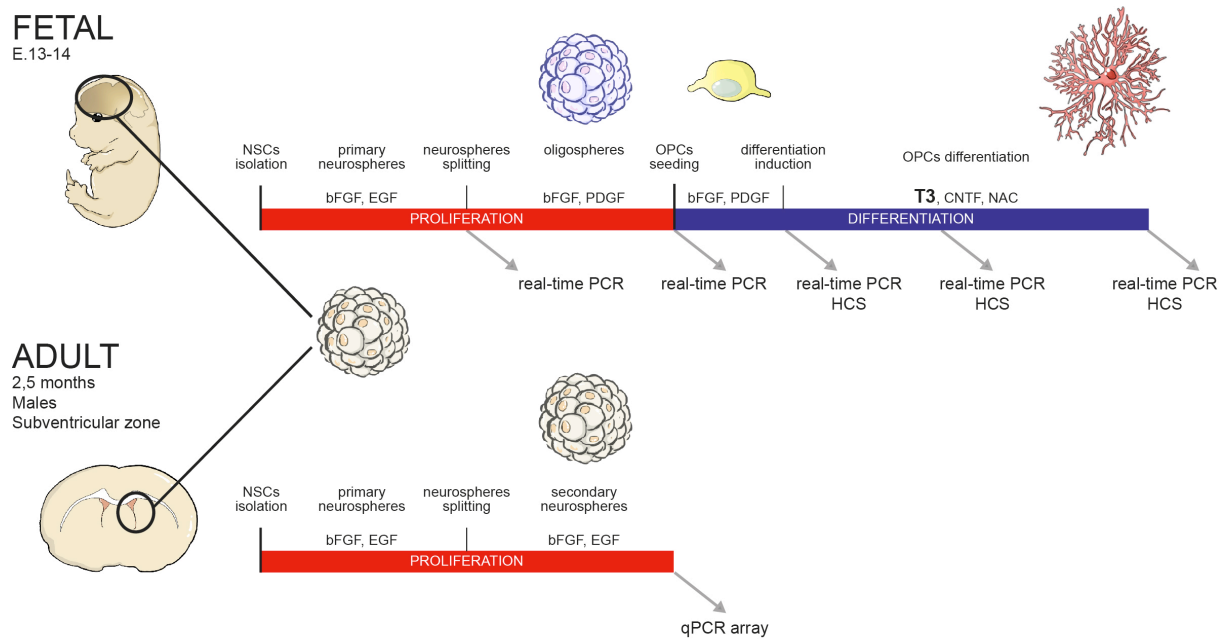
Figure 8. Neural stem cells- derived oligodendrocyte precursor cells culture protocol.

Foetal NSCs cultures were obtained from E13-14 forebrain or striatum, while adult cultures were obtained from SVZ of 2.5 months old male mice. Cells divide in suspension generating primary neurospheres. After the first splitting, depending on the growth factors added, secondary neurospheres (bFGF/EGF) or oligospheres (bFGF/PDGF) were produced. Secondary neurospheres were used for the qPCR array analysis. Oligospheres were seeded as single cells and, after 3 days, exposed to the differentiation medium, containing T3, for 12 days.

Abbreviations: bFGF, basic fibroblast growth factor; CNTF, ciliary neurotrophic factor; DIV, day in vitro; EGF, epidermal growth factor; HCS, high content screening; NSCs, neural stem cells; OPCs, oligodendrocyte precursor cells; SVZ, sub-ventricular zone; T3, triiodothyronine.

3.4 PARP inhibitor treatments in mouse OPCs cultures

The following PARPi (PARP inhibitors) were used in this study: TIQ-A (IC50 140-450 nM), PJ34 (IC50 20nM) and Olaparib (IC50 5nM; Ferraris, 2010; Hans et al., 2011). First, neurospheres and oligospheres PARPi treatment was tested (Figure 9A). Than, OPCs were treated 24 h before the T3-mediated differentiation induction (-1 DIV), and cell viability was analysed at DIV 12 of differentiation. In order to study effects of PARPi on foetal and adult cultures, different treatment were performed: i) in order to study PARP1-2 expression and PARP activity, cells were analysed 24 hours after treatment (DIV 0); ii) a dose-response curve of PARPi were performed, treating cultures with a series of 7 concentrations (0-10μM). PARPi treatments were maintained after the oligodendrocyte differentiation medium change, until DIV 12; iii) foetal cultures were also treated with PJ34 10μM and analysed for cell number and cell death at DIV 0, 6 and 12; iv) both foetal and adult cultures were treated with lower dose of PARPi (1μM and 10μM) and analysed for mature oligodendrocytes at DIV 12; v) foetal cultures were treated with PJ34 1μM and analysed for mRNA quantification at DIV 12 (Figure 9B).

3.5 PARP-1 activity assay

PARP-1 activity was analysed in primary rats neuronal cultures exposed to OGD and foetal/adult mice OPCs cultures (0 DIV and 24 h after PARPi treatments).
Proteins from cell lysates were quantified by Lowry assay (BioRad) following the manufacturer's instructions. The same amount of proteins were used for all the samples (400 ng). PARP enzymatic activity was measured using HT Colorimetric PARP Apoptosis Assay Kit (Trevingen), following the manufacturer's instructions.
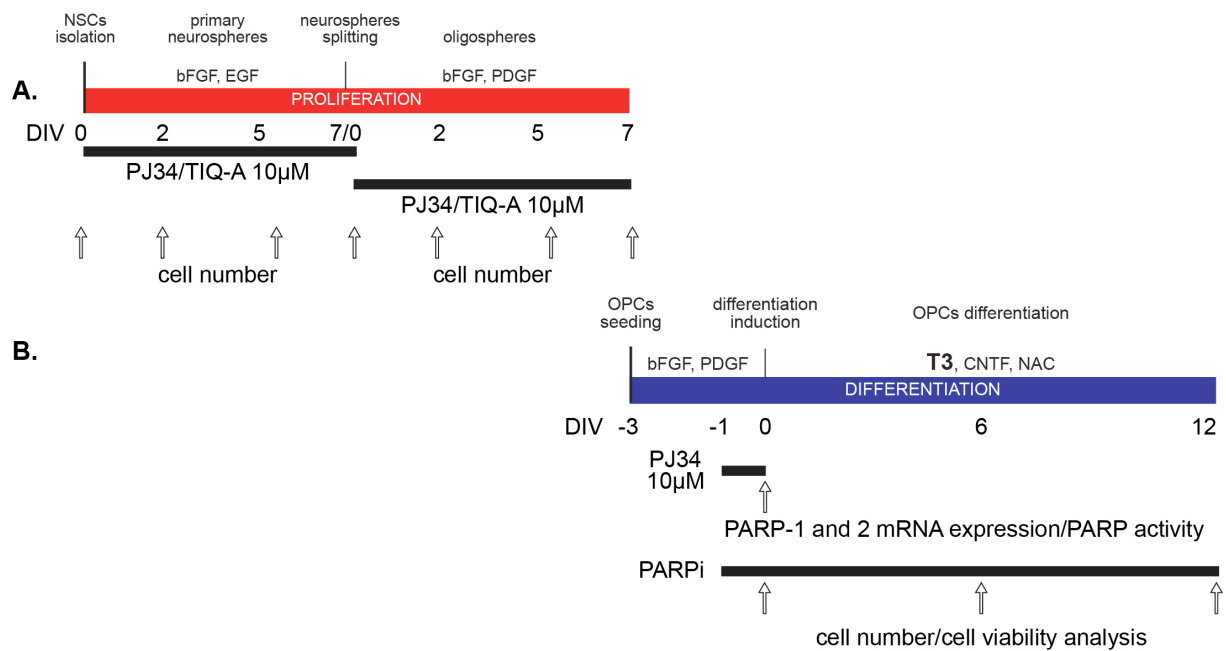
Figure 9. OPCs cultures PARP inhibitors treatment.

(A) Primary neurospheres or oligospheres were treated with PJ34, TIQ-A or vehicle and cell number was measured during the whole period (arrows).

(B) In another set of experiments cells were exposed to PJ34 before the adding of T3 to the medium, for 24 hours, and than lysed in order to study mRNA expression. Cells were also treated from the same time point for all the differentiation period and cell viability was measured at DIV 0, 6 and 12 (arrows).

Abbreviations: bFGF, basic fibroblast growth factor; CNTF, ciliary neurotrophic factor; DIV, day in vitro; EGF, epidermal growth factor; HCS, high content screening; NSCs, neural stem cells; OPCs, oligodendrocyte precursor cells; SVZ, sub-ventricular zone; T3, triiodothyronine.

3.6 Primary cortical pure neurons and mixed neurons/astrocytes cultures

Cultures of primary cortical neurons were isolated from neonatal (within 24 hours from birth) Wistar rats, pooling tissues from different pups, or from single Wt or Tg2576 (Taconic, Hudson, NY, USA) mice, according to the standard protocol (Fernandez et al., 2005; Del Vecchio et al., 2009; Figure 10A). Briefly, brains were removed, and cortical tissue dissected, freed from the meninges, and minced into small pieces. Cells were dispersed in Kreb's buffer (0.12 MNaCl, 4.8mMKCl, 1.2mM KH2PO3, 25.4 mM NaHCO3, 14.2 mM glucose, 0.01 mg/ml phenol red, 1.5 mM MgSO4) containing BSA 0.3% and 0.025% trypsin (Sigma-Aldrich) for 15 min at 37 °C, followed by mechanical trituration with a Pasteur pipette in Kreb's buffer containing 0.004% deoxyribonuclease I (DNaseI), and 0.052% soybean trypsin inhibitor (SBTI; Sigma-Aldrich). After centrifugation (500 x g, 5 min), cells were resuspended in Neurobasal culture medium supplemented with 2% B27 (Gibco), 2 mM glutamine (Sigma-Aldrich), 100 U/ml penicillin, and 100 μg/ml streptomycin (Gibco) and plated onto Cultrex 2D substrate (0.25 mg/ml, Trevingen)-coated plates or coverslips. Cells were maintained in a humidified incubator at 37 °C with 5% CO2. To obtain pure neuronal culture (99% neurons) cells were treated after 24 h with cytosine arabinofuranoside (Sigma-Aldrich) 10 μM for rats and 5 μM for mouse cultures. For mixed cultures no mitotic inhibitor was used. At 4 DIV, half of the medium was changed in both cultures.

Neurons isolated from Tg2576 mice are denoted as APPswe primary neurons.

3.7 Genotyping

Mouse tails were used for genotyping analysis. The mouse genomic DNA was extracted using the GenElute Mammalian Genomic DNA MiniPrep Kit (Sigma-Aldrich) according to the manufacturer's instructions and eluted in 100 μl of elution solution. DNA concentration was determined using a spectrophotometer and Tg2576 mice were identified by the presence of the mutated human APP gene (FW: 5′-GATGAGGATGGTGATGAGGTA-3'; REV: 5′-ACTGGCTGCTGTTGTAGG-3′) using the Real Time PCR technique and the SYBR Green qPCR master mix (Bio-Rad) and 0.4 μM forward and reverse primers. The amount of DNA used for each sample was 10 ng and PCR amplification conditions were: 60°C for 30 s.

3.8 Glutamate excitotoxicity on pure neurons and mixed neurons/astrocytes.

At 7 DIV neuronal cultures were treated with glutamate (0.5 mM for rat and 42 μM for mouse cultures; Figure 10B). Medium was removed and cells were exposed to Krebs buffer containing or not glutamate, for 10 min. After glutamate treatment, Krebs buffer was replaced with the former conditioned medium. One group of cells were treated with MK801 (10 μM) from 1 h before the treatment to the end of the glutamate exposure (Fernandez et al., 2005).

3.9 Oxygen-glucose deprivation

OGD was performed using an air-tight hypoxia chamber (Billups-Rothenberg Inc., Del Mar., CA) saturated with 95% N2- 5% CO2 (Goldberg and Choi, 1993) on rat primary pure neuronal cultures and mixed cultures, Wt and APPswe mice pure neurons (Figure 10C) and mice foetal/adult neurospheres-derived OPCs (Figure 11B).

Glucose deprivation was achieved using a glucose-free complete medium. Oxygen was removed by flushing the hypoxia chamber with N2-CO2 mixture for 6-8 min at 25 l/min. The flushing was repeated after half the incubation time. The OGD condition was maintained for 3 h, after which plates were re-oxygenated for 24 h in the old medium in a cell incubator.

Pure neurons and mixed neurons/astrocytes cultures were exposed at OGD at 7 DIV while OPCs at 2 DIVs after plating, 24 h before the T3-differentiation induction.

In another set of experiments, Wt and APPswe primary cortical neurons, were treated from 2 DIV to the end of the experiment (8 DIV) with 10 μM LY450139 (Figure 10D).
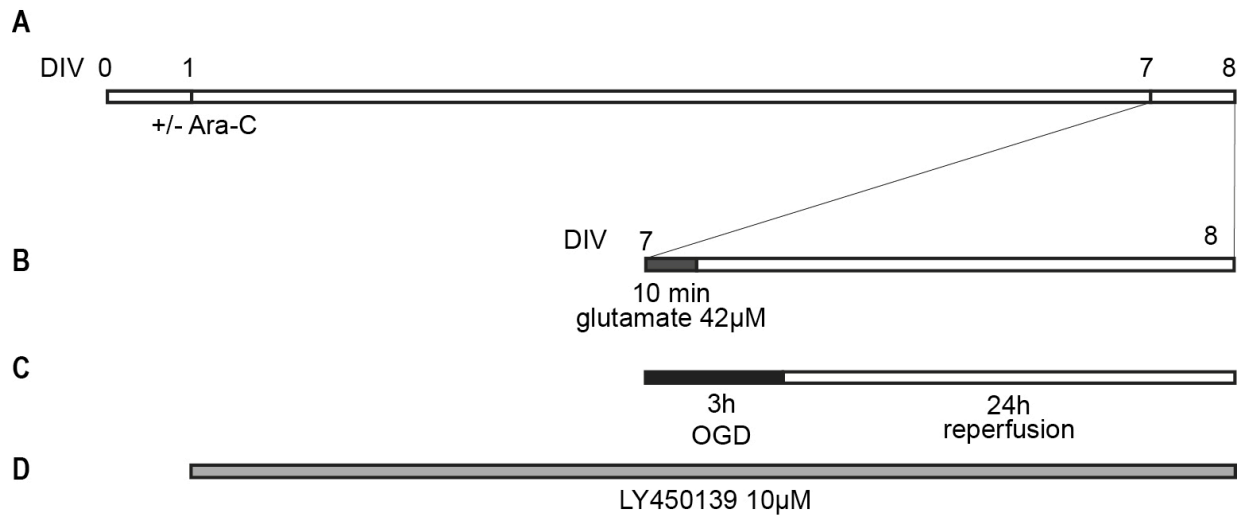
Figure 10. Primary pure neuronal and mixed neurons/astrocytes cultures protocol.

(A) Primary neuronal cultures were treated or not with Ara-C in order to obtain pure neurons (99%) or mixed neurons (50%) /astrocytes (50%) cultures.

(B) In one set of experiments, pure neuronal cultures were treated for 10 minutes with glutamate. Cell viability was analysed after 24 hours.

(C) In another set of experiments, pure and mixed cultures were exposed for 3 hours at OGD. After 24 hours of reoxygenation, cell viability was assessed.

(D) In the APPswe pure neuronal cultures, LY450139 drug treatment was used in order to block the APP cleaving. Cells were also exposed to OGD/reoxygenation during the drug treatment.

Abbreviations: Ara-C, Cytosine arabinoside ; DIV, day in vitro; OGD, oxygen-glucose deprivation.

3.10 Cytokines exposure

Foetal and adult cultures from rats and mice were exposed to cytokines at different steps of the OPCs differentiation. For adult rats/mice and foetal mice cultures, after primary neurospheres splitting, cells were divided into two groups: one treated with a mix of six different cytokines (TGF-b1, TNF-a, IL-1b, IL-6, IL-17 and IFN-c; 20 ng/mL each) and the other treated with vehicle (0.04% of the cytokines solvent: 10% glycerol/100 nM glycine/25 nM Tris, pH 7.3; Figure 11C). Images of oligospheres were taken at 3, 5 and 7 DIV. Oligospheres were centrifuged at 300g for 5 min and the pellet was mechanically dissociated to obtain a single cell suspension. After cell count, cells were plated at a density of 3,000 cells/cm2 on poly-D,L-ornithine (50 mg/mL)/laminin (5 mg/mL) coating, in OPCs medium, containing 20 ng/mL bFGF and 20 ng/mL PDGF.

After 3 DIV, OPCs medium was replaced with the oligodendrocyte differentiation medium [DMEM/F12 GlutaMAX 13; 8 mmol/L HEPES; 100 U/100 lg penicillin/streptomycin; 0.13 B27; 13 N-2; 50 nM T3; 10 ng/mL CNTF; 13 N-acetyl-L-cysteine (NAC)]. For adult rats OPCs cultures, the cytokine treated group was then divided into two subgroups: one treated with vehicle and the other treated with IOP (10 mM; Figure 11D). Another vehicle-exposed experimental group was treated with the cytokine mix during the differentiation phase, while the control group was treated with vehicle (Figure 11E). Oligodendrocyte differentiating factors (T3, CNTF and NAC) were refreshed every two days.
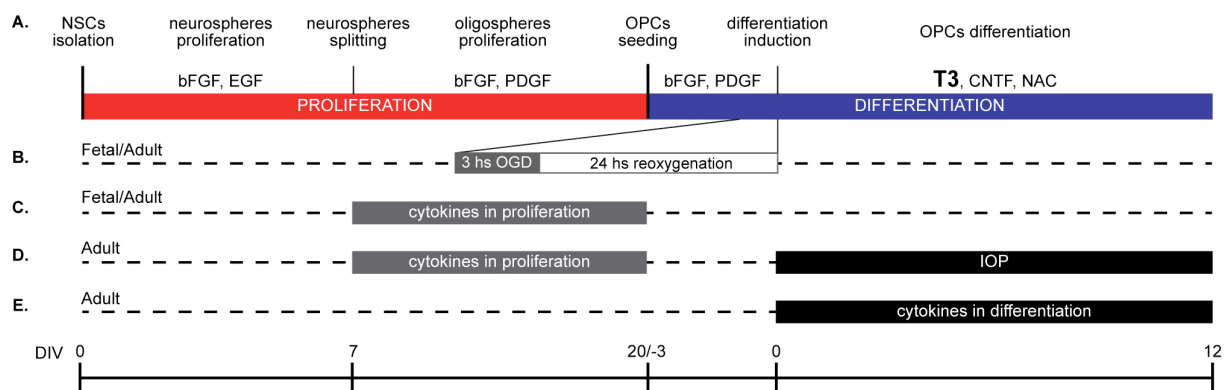
Figure 11. OPCs cultures vulnerability studies protocol.

(A) Experimental design of the standard NSCs-derived OPCs cultures.

(B) Foetal and adult cultures were exposed at 3 hours OGD and 24 hours of reoxygenation, before the T3-mediated differentiation induction.

(C) Foetal and adult cultures were exposed to a cytokines mix (…) during the oligospheres stage.

(D) Adult cultures were exposed to the cytokines mix also during the whole differentiation phase, from the adding of T3, for 12 DIVs.

(E) In another set of experiments, proliferation cytokines-exposed adult cultures were exposed to IOP during the whole differentiation stage.

Abbreviations: bFGF, basic fibroblast growth factor; CNTF, ciliary neurotrophic factor; DIV, day in vitro; EGF, epidermal growth factor; HCS, high content screening; IOP, iopanoic acid; NSCs, neural stem cells; OGD, oxygen-glucose deprivation; OPCs, oligodendrocyte precursor cells; SVZ, sub-ventricular zone; T3, triiodothyronine.

3.11 Population doubling

Oligospheres images were analyzed using Image Proplus software (Media Cybernetics, Bethesda, MD). Counting procedure was performed as already described (Baldassarro et al., 2013) calculating the cell number based on spheres and single cell area. Population doubling was calculated using the following formula: PD= log10 (N/ N0) x 3.33, where PD is the Population Doubling, N and N0 are the final and initial number of cells, respectively.

3.12 MTT viability assay

Rat pure neuronal and mixed cultures were tested for cell viability by MTT colorimetric assay. Thiazolyl Blue Tetrazolium Bromide (Sigma-Aldrich) was dissolved 6.5 mg/ml in PBS and diluted 0.5 mg/ml in OptiMem (Gibco).Medium was removed and cells incubated for 3 h in incubator with the MTT solution. Formazan salts were solubilized by adding solubilisation solution (80% v/v isopropyl alcohol, 10% v/v HCl 1 N, 10% v/v Triton-X) and shaking the plates for 1 h at room temperature (RT). Absorbance wasmeasured with a microplate reader (BioRad) at 570 nm.

3.13 LDH activity assay

In order to compare the two colorimetric methods, rat neuronal cultures were also tested for LDH activity. Measurement was performed with PIERCE LDH Cytotoxicity Assay Kit, following the manufacturer's instructions. Both neuronal and mixed cultures were grown in a 96well plate (100,000 cells/ well); after the re-oxygenation period, medium was collected and the activity of LDH enzyme in the medium was measured.

3.14 MitoTracker staining

Cells were stained with MitoTracker Orange (Thermo Scientific, Waltham, MA, USA) following the manufacturer's instructions. Briefly, cells were treated for 30 min at 37°C with 150 nM MitoTracker. After two washes with PBS, cells were fixed and used in the immunocytochemistry procedure.

3.15 Immunocytochemistry

Indirect immunocytochemistry (ICC) was used to identify and quantify specific markers. Cells were fixed with ice-cold 4% paraformaldehyde for 20 min at RT. After a fast wash in PBS, cells were incubated for 1 h with BSA 1% and 1% of the specific serum depending on the secondary antibody used (Donkey or Goat), in PBS- 0.3% Triton-X 100, then incubated overnight at 4°C with primary antibodies. Cells were than washed with PBS and incubated with secondary antibodies for 30 min at 37 °C. After immunofluorescence staining, cells were incubated with the nuclear dye Hoechst 33258 (1 μg/ml in PBS, 0.3% Triton-X 100) for 20 min at RT and finally washed in PBS. For 96 well plates, cells were left in PBS (see *3.16 Cell-based High content screening* section) while for microscopy glasses, were coverslipped in glycerol and PBS (3:1, v/v) as mounting medium containing 0.1% paraphenylenediamine.

Primary rat pure neuronal and mixed cultures were seeded onto Cultrex 2D substrate (0.25 mg/ml, Trevingen)-coated coverslips and fixed after treatment. The following primary antibodies: anti-β-III-tubulin (mouse, R&D, 1:1000), anti-GFAP (rabbit, Dako, 1:1000), anti-Iba-1 (rabbit, Wako, 1:250), anti active caspase 3 (rabbit, BD Pharmingen 1:200) diluted in PBS-0.3% Triton-X 100; and the following secondary antibodies: goat Alexa 488-conjugated anti mouse and/or goat Alexa 568-conjugated anti-rabbit (Invitrogen), were used.

58

Mouse Wt and APPswe primary neuronal cultures were fixed at 8 DIVs. The following primary antibodies: anti-6E10 (mouse; Covance, SIG-39320, batch no. D11AF00145; 1:1000), anti-β-III-tubulin (mouse; R&D Systems, MAB-1195, batch. no. HGQ0113121; 1:1000), anti-GFAP (rabbit; Dako, Z0334, batch no. 20005461; 1:1000) and the following secondary antibodies: goat Alexa 488-conjugated antimouse, goat Alexa 568-conjugated anti-rabbit, goat Alexa 658-conjugated anti-mouse (Invitrogen) were used.

Mouse foetal/adult OPCs in the PARP inhibition and differentiation studies were stained at different DIV to identify OPCs (NG2- and PDGFαR-positive cells), mature (CNPase- and APC-positive cells) and myelinating (MBP-positive cells) OLs, neurons (β-IIItubulin-positive cells) and astrocytes (GFAP-positive cells). OPCs in the different stages of differentiation were analysed by the triple staining APC/Olig1/Olig2. The following primary antisera were used: mouse anti-β-III-tubulin (R&D system, Trento, Italy) 1:3000; rabbit anti-GFAP (Glial Fibrillary Acidic Protein, Dako) 1:1000; rabbit anti-NG2 (chondroitin sulphate proteoglycan, neural/glial antigen 2, Millipore, Merck S.p.a., Milan, Italy) 1:350; rabbit anti-PDGFαR (Platelet derived frowth factor alpha receptor, Santa Cruz Biotechnology) 1:300; mouse anti-CNPase (2', 3'-cyclic nucleotide 3'-phosphodiesterase, Millipore) 1:500; mouse IgG2b anti-APC (anti-adenomatous polyposis coli, clone CC1, Calbiochem) 1:100; mouse IgG1 anti-Olig1 (Oligodendrocyte transcription factor 1; NeuroMab) 1:500 and mouse IgG1a anti-Olig2 (Oligodendrocyte transcription factor 2; Neuromab) 1:500; rabbit anti-MBP (Myelin Basic Protein, Dako) 1:500. Donkey Alexa Fluor 488-conjugated anti mouse, goat Alexa Fluor 555-conjugated anti- mouse IgG1, goat Alexa Fluor 488-conjugated anti- mouse IgG2a, goat Alexa Fluor 647-conjugated anti- mouse IgG2b and donkey Alexa 568-conjugated anti-rabbit (1:500; ThermoFisher Scientific) were used as secondary antisera.

59

Adult rat OPCs in the cytokine exposure experiment, were fixed and stained at 12 DIV after the differentiation induction, Primary antibodies and dilutions used were: mouse anti beta-III-tubulin (R&D system, Trento, Italy) 1:3000; rabbit anti PDGFαR (platelet derived growth factor alpha receptor, Santa Cruz Biotechnology) 1:300; mouse anti NG2 (membrane-spanning chondroitin sulphate proteoglycan, Millipore), 1:300; mouse anti CNPase (20,30-cyclic nucleotide 30-phosphodiesterase, Millipore) 1:500; rabbit anti MBP (Myelin Basic Protein, Dako) 1:500; rabbit anti GFAP (Glial Fibrillary Acidic Protein, Dako) 1:1,000; goat anti D3 (Deiodinase type 3, Santa Cruz Biotechnology), 1:100. Secondary antisera and dilutions used were: Alexa488-coniugated affinity-pure Donkey anti-Mouse IgG (Life Technologies, Eugene, OR) 1:500, Alexa568-conjugated affinity-pure Donkey anti-Mouse IgG (Molecular Probe, Eugene, OR) 1:500, DyLight488-conjugated affinity-pure Donkey anti-Goat IgG (Jackson Immunoresearch) 1:100, Alexa568- conjugated affinity-pure Donkey anti-Rabbit IgG (Life Technologies) 1: 500, and RRX-conjugated Donkey anti-rabbit IgG (Jackson Immunoresearch) 1:500, all diluted in PBS/0.3% Triton X-100.

3.16 Cell-based High content screening

For HCS analysis cells were grown in 96 flat-bottom well HCS plates (NUNC; 100,000 cells/well). Analysis were performed with Cell Insight™ CX5 High Content Screening (HCS; ThermoFisher Scientific).

For rat pure neuronal and mixed cultures, Mitotracker was used to stain mitochondria of living cells and GFAP staining to identify GFAP-positive or –negative cells. Analysis of the MitoTraker fluorescence was performed on GFAP-negative cells only, identified as neurons.

Cells showing a low MitoTracker fluorescence are considered with depolarized mitochondria. The software is able to detect nuclei as "object" considering each nucleus a single cell and it also detect the fluorescence in the cytoplasm belonging to the identified nucleus. This allows to clearly associate positive cells to a specific markers. In the same cultures, the software is used to analyse the nuclear morphology based on the fluorescence intensity of the Hoechst 33258 staining and the nuclear size, using GFAP staining to differentiate neurons and astrocytes. Nuclei showing high fluorescence intensity and small size are identified as condensed/fragmented.

Based on nuclear staining, the software is able to recognise nuclei and calculate the percentage of high intensity/small sized condensed nuclei. Moreover, based on nuclei identification, the software is able to detect the presence of the marker-specific stain in the cell body, calculating the percentage of immunoreactive cells and fluorescence intensity. For the MitoTracker analysis, the software is able to recognize every single cell by its nuclear staining and quantifies the fluorescence intensity inside the cell body. The operator can select a fluorescence threshold that allows the software to discriminate between 'high-intensity staining' and 'low-intensity staining'. Using the same parameters and the same threshold it is possible to perform an automatic, statistically robust and objective analysis. This technique avoids also the bias of the analysis of randomly chosen fields, because the analysis is performed in all cells.

Between 60,000 and 100,000 cells/well were analysed.

3.17 Fluorescence microscopy

Coverslips were observed using a Nikon eclipse E600 (Nikon, Italy) equipped with digital CCD camera Qimaging Retiga 20002V (Q Imaging, Surry, BC, Canada). All images were taken at a magnification of 20× objective, 5 fields per coverslip were considered and at least 2

coverslips per condition were analysed from two independent observators. Controls using the secondary antibodies, alone,were performed and resulted negatives.

In order to study the effect of the OGD on caspase-3 activation and the effect of the drugs on pure neuronal and mixed cultures we used a fluorescence microscopy approach to analyse the nuclear morphology. Immunocytochemistry was performed as described above to identify neurons and astrocytes. Percentage of condensed nuclei and active caspase-3 positive cells was calculated.

For adult rat OPCs cultures, Hoechst staining was used to identify the total cell number and condensed nuclei, while the different markers were used to identify specific lineage (beta-III-tubulin for neurons, GFAP for astrocytes, NG2 for OPCs, CNPase for mature oligodendrocytes and MBP for myelinating oligodendrocytes). The lineage analysis was performed on cells presenting intact, non-condensed nucleus.

3.18 RNA isolation and reverse transcription

Total RNA isolation was performed with the RNeasy Micro kit (Qiagen) following the manufacturer's instructions. Total RNAwas eluted in RNasefree water and concentration estimated through absorbance values at 260, 280 and 320 (Nanodrop 2000 spectrophotometer, Thermo Scientific). Firststrand cDNAs were obtained using the iScript cDNA Synthesis Kit (Bio-Rad), incubating at 42°C for 30 min. An RNA sample with no reverse transcriptase enzyme in the reaction mix was processed as a no-reverse transcription control sample.

3.19 Semi-quantitative real-time PCR

Semi-quantitative real-time PCR was performed using the CFX96 real-time PCR system (Bio-Rad). The reactions were performed in a final volume of 20 µl consisting of 1× SYBR

Green qPCR master mix (Bio-Rad) and 0.4 μM forward and reverse primers. In order to avoid possible contamination of genomic DNA in isolated RNA, the sample with no reverse transcriptase enzyme was processed in parallel with the others and tested by real-time PCR for every pair of primers used. All primers used were designed using Primer Blast software (NCBI) and synthesized by IDT (Coralville).

All primers sequences are listed in Table 1.

Gene	Specie	Forward (5'-3')	Reverse (5'-3')
VEGFA	mouse	AAGAGAAGGAAGAGGAGAG	ACCCAAGAGAGCAGAAAG
FLT1	mouse	CGTGCAAGGAACCTCAGACA	ATCATAGGGCAGCCGTTCAC
KDR	mouse	ATGTCCTTGGCTGTGCAAGA	CCTTCATTGGCCCGCTTAAC
PARP-1	mouse	GCCACACATCTCAGGGAGAC	CCCAAACCTTTGACACTGTGC
PARP-2	mouse	GAAGGACGCAGACAGGACAA	ACATGAGCCTTTCCCAGCTT
Olig1	mouse	CCGCCCCAGATGTACTATGC	AACCCACCAGCTCATACAGC
Olig2	mouse	GCTTAGATCATCCCTGGGGC	AGATCATCGGGTTCTGGGGA
TRa	mouse	GCAAACACAACATTCCGC	TCCTGATCCTCAAAGACCTC
TRβ	mouse	GCAAACACAACATTCCGC	CACCAAACTGCTGCTCAA
Klf9	mouse/rat	AGTGGCTTCGAAGGGGAAAC	TCCGAGCGCGAGAACTTTTT
GAPDH	mouse/rat	GGCAAGTTCAATGGCACAGTCAAG	ACATACTCAGCACCAGCATCACC

Table 1. Primers sequences
Detailed information about primers forward (F) and reverse (R) sequences.
Abbreviations: FLT1, vascular endothelial growth factor receptor 1; GAPDH, glyceraldehyde-3-phosphate dehydrogenase; KDR, vascular endothelial growth factor receptor 2; KLF9, kruppel-like factor 9; Olig1 and 2, oligodendrocyte transcription factor 1 and 2; PARP1 and 2, Poli (ADP-ribose) polymerases 1 and 2; TRα and b, thyroid hormone receptor a and b; VEGFA, vascular endothelial growth factor.

GAPDH was used as a housekeeping gene to normalize the amount of reverse-transcribed RNA used for PCR. Thermal profile of PCR reactions consisted first of a denaturation step (95°C, 2 min) and 40 cycles of amplification (95°C for 15 s and 60°C for 60 s). At the end of the amplification cycles, the melting curve of amplified products was performed according to the following temperature/time scheme: heating from 55°C to 95°C with a temperature increase of 0.5°C/s. Primer efficiency values for all primers were 95-102%. The $2^{(-\Delta\Delta CT)}$ method was used for the calculation of gene expression.

3.20 Statistical Analysis

All data derive from at least three independent experiments. The number of technical replicates included in each experiment is indicated in the result. Prism software (GraphPad Software) was used for statistical analyses and the preparation of graphs. Data in histograms are reported as mean ± SEM or SD as specified in the figure legend. Student's t-test, one-way ANOVA or two-way ANOVA and Dunnett's multiple comparison post-hoc test were used to analyse data. Results were considered significant when the probability of their occurrence as a result of chance alone was less than 5% (P b 0.05).

Exclusion criteria in data analysis were pre-established for each assay as follows. mRNA analysis: samples in which curves not fitting the melting temperature or in which a double peak was observed were excluded from the analysis; HCS analysis: wells in which the software was unable to automatically identify the nuclei were excluded from the analysis. The final number of data per group is reported in the figure legends.

4. RESULTS

4.1 Summary

The main objective of the present study was the investigation of the vulnerability of foetal and adult NSCs-derived OPCs to demyelinating diseases. Similarity and differences in response to noxious stimuli will enhance the knowledge of the biology of these cells, throughout the whole differentiation process and will elucidate the pathological basis of demyelinating diseases in foetal and adult life.

As *in vitro* model NSCs-derived OPCs, isolated from foetal and adult brain, were used and their physiological T3-mediated differentiation and response to noxious stimuli was tested.

First, a reliable *in vitro* readout was set up, in order to obtain robust data from a complex and mixed cell system, as OPCs differentiated from NSCs. Cell-based HCS was set up in order to study cell viability and lineage specification for cultured NSCs, on 2D and semi-3D cell growth surfaces and materials. In this study we compared also the standard procedure to test cell viability, the MTT assay, with the HCS assay based on nuclear morphology, finding the same readouts but a strong statistically significance of the HCS-based assay (Baldassarro et al., 2016). HCS was thus chosen as the elective assay for testing *in vitro* systems used in the present study.

In order to pursue the main objective, the study was first focused on investigating differences in T3-mediated physiological differentiation of the two cellular systems. In particular, since T3 acts mainly by NRs activation, the physiological differentiation was analysed at different levels: i) gene expression of NRs and co-regulators in early progenitors (neurospheres), ii) T3-driven OPCs differentiation and maturation (gene expression and OLs-lineage markers detection), iii) role of RXRγ in the differentiation process, and iv) role of PARP activity on OPCs viability and differentiation.

We found that adult NSCs show an higher expression of TRβ and a lower expression of RXRγ, two main NRs involved in the OLs development. Moreover we analysed the expression of Olig1, Olig2, TRβ, TRα and Klf9, key genes regulating the differentiation process, throughout all the stages of *in vitro* cultures, from NSCs to mature OLs. We found a more mature phenotype of adult OPCs in early stages, while foetal OPCs are more responsive to T3-induced differentiation. These data were also confirmed by the detection of OPCs (PDGFαR and NG2) and OLs (CNPase and MBP) markers, where adult cultures showing less myelinating OLs at the end of the differentiation phase.

T3 exert its action by NRs and the two differentially regulated genes in early precursors (TRβ and RXRγ) can form eterodymers in response to T3 binding. In order to study the role of RXRγ in OPCs differentiation, we replicate the protocol on cells isolated from RXRγ-/- foetal and adult mice. In both cultures this NRs is necessary to reach the T3-mediated maturation of OLs. However, RXRγ seems not to directly regulate the differentiation machinery. In fact, differentiated OLs present in the RXRγ-/- cultures show the same population pattern of the RXRγ+/+. Moreover, analysing the expression of the key genes involved in the differentiation 24 hours after the T3 exposure, no differences in expression were detected. However, we found an increase in OPCs percentage in RXRγ-/- cultures at the end of the differentiation phase, suggesting that RXRγ-/- cells are not responsive to the T3-mediated cell cycle exit. This was proved analysing the percentage of replicating OPCs by using the double staining PDGFαR/Ki67. RXRγ-/- cells show higher percentage of replicating OPCs compared to RXRγ+/+. Moreover replicating OPCs are not affected by T3 exposure, while in RXRγ+/+ T3 treatment decreased the replicating OPCs percentage already 24 hours after the T3 exposure (Baldassarro et al., unpublished - a).

No differences were found between foetal and adult cultures in RXRγ-/- cells. However, the two systems show totally different responsiveness to PARP inactivation, a factor involved in

the regulation of different NRs, including TRβ and also the dymerization between TRβ and RXRγ. We showed that PARP1 and PARP2 mRNA expression and PARP activity are much higher in foetal than in adult-derived OPCs, suggesting a different role in the two cell systems. In fact, PARP inhibition produces substantially different effects in OPCs derived from foetal and adult brain. In particular: i) the culture treatment with PARP inhibitors is cytotoxic for OPCs derived from foetal, but not from adult, brain; (ii) PARP inhibition reduces cell number in proportion to the inhibitory potency of the compounds; (iii) the PARP inhibition effect in foetal OPCs is a slow process (iv) PARP inhibition impairs OPC maturation into myelinating OL in foetal, but not in adult OPCs, according to the inhibitory potency of the compounds.

Overall, these results suggest that a different PARP signalling in foetal and adult OPCs might be part in the biological properties of OPCs at different chronological ages (Baldassarro et al., 2017 a).

Differences in physiological differentiation may reflect a different response to demyelinating challenges. Demeylinating diseases have two major components: inflammation ad HI. As inflammation *in vitro* model we used the exposure to a defined inflammatory cytokines mix, while for HI we used the OGD model.

We first analyse the response of foetal and adult OPCs to cytokine exposure, finding that in both cultures cytokines are mediating the OPCs differentiation block. In fact, cells exposed to inflammatory cytokines during the proliferation phase, show a severe impairment in the differentiation, with a strong decrease in mature/myelinating OLs at the end of the differentiation phase (Baldassarro et al., unpublished b).

Since inflammation is recognized as the main cause of the OPCs differentiation block in MS, leading to remyelination failure, we than focused on the effect of inflammation in adult OPCs. We found that cytokines exposure is linked to an increase of D3 expressing OPCs. D3 is the

enzyme that inactivates T3, thus blocking the OPCs differentiation. This was also confirmed by the restoring of differentiation mediated by D3 pharmacological inhibition (Fernandez et al, 2016).

Even if no differences between foetal and adult OPCs were found in inflammation exposure, they respond in a totally different way to HI. In literature, OGD is a common *in vitro* HI model, however, the model is not well characterized and numbers of variables (cell system, percentage of oxygen, timing, readout, ecc.) are not well described or controlled. For this purpose, we first set up the OGD system on neuronal cultures, the most widely used cultures in HI studies. OGD was tested on both pure neuronal (99% neurons) and astrocyte/neurons (50% astrocytes, 50% neurons) cultures derived from neonatal rat cerebral cortex. Different assays were used to study cell viability, including standard cell viability-assays (MTT and LDH) and cell-based HCS (nuclear morphology, mitochondrial depolarization).

We first investigated the contribution of glucose- or oxygen-deprivation, alone or in combination, to cell viability/death. Both MTT and LDH assay indicated that glucose deprivation is the major trigger of cell death in both pure and mixed cultures, while the contribution of oxygen deprivation appears to be negligible.

Since these biochemical assays do not allow any discrimination between the different cell types (neurons vs. glia) present in the culture, we also used a morphological approach based on cell-specific antigen recognition and coupled to HCS imaging and analysis to distinguish the OGD-affected population in mixed cultures (Baldassarro et al. 2018).

In order to test the reliability of the system, we translate the OGD model on a disease/drug study. We used pure cortical neurons primary cultures isolated from wild type or APPswe mice. These are transgenic animals expressing the human APP gene carrying the Swedish mutation, a model for the familial Alzheimer disease, accumulating Aβ fragments, linked to

the perturbation of the brain vascular system and consequent HI. We showed that APPswe neurons are more susceptible to OGD and that a drug treatment blocking the Ab accumulation is able to rescue APPswe neurons from OGD-induced cell death (Baldassarro et al., 2017 b).

Once the OGD model was set up and characterized, we exposed foetal and adult OPCs to this insult during the OPCs proliferation phase, 24 hours before adding the T3 to the cultures. We showed that foetal cells are sensitive to OGD, with a severe increase of cell death and consequent strong reduction in cell number. The OGD-mediated cell death is a slow process, showing cell death only at the end of the differentiation phase and not soon after OGD exposure. In an opposite way, adult OPCs viability is not influenced by OGD exposure. Moreover, adult cultures show an increase of cell number and on OPCs percentage in response to OGD. On the other end, foetal cultures show a decrease of OPCs and mature/myelinating OLs markers in live cells and an OGD-mediated selective OPCs/OLs lineage cell death.

Future studies will elucidate the mechanisms underlying the selective foetal-OPCs/OLs death, investigating the differences between foetal and adult cells in systems involved in metabolism and HI response. We found an increase in D3 expression soon after OGD exposure, suggesting a possible role of T3 inactivation in the pathological mechanism (Baldassarro et al., unpublished - b). Deeper investigations on D3 and glutamate excitotoxicity involvement in the process will elucidate the OGD-induced cell death mechanism.

4.2 Nuclear receptors and foetal vs. adult oligodendrocyte precursor cells differentiation (Baldassarro et al., unpublished – a).

Nuclear receptors and foetal vs. adult oligodendrocyte precursor cells differentiation.

Vito Antonio Baldassarro[1,2], Wojciech Krężel[3], Luciana Giardino[1,4,5], Laura Calzà[1,2,4]

[1]Health Science and Technologies Interdepartmental Center for Industrial Research (HST-ICIR), University of Bologna, Italy; [2]Department of Pharmacy and Biotechnology, University of Bologna, Italy; [3]Institut de Génétique et de Biologie Moléculaire et Cellulaire, Illkirch, France; [4]IRET Foundation, Ozzano Emilia, Italy; [5]Department of Veterinary Medical Sciences, University of Bologna, Italy.

Correspondence:

Laura Calzà

CIRI-SDV, University of Bologna

Via Tolara di Sopra 41/E

40064 Ozzano Emilia (Bologna)

ITALY

laura.calza@unibo.it

Abstract

Nuclear receptors (NRs) play key roles in the oligodendrocytes (OLs) differentiation, from NSCs self-renewal and lineage specification, to OLs maturation. Foetal and adult oligodendrocyte precursor cells (OPCs) share the same objective: to wrap and functionally myelinate axons, in a process mediated by thyroid hormone (TH), and acting throughout NRs-signals. In particular, thyroid hormone receptors (TRs) are the main NRs involved in the process, acting as homodimer or heterodimer with others NRs, expecially RXRs. Here we showed that neural stem cells (NSCs), the progenitors of OPCs, isolated from foetal and adult brain, differentially express two fundamental NRs involved in the differentiation process: TRβ and RXRγ. We showed that both systems need TH to differentiate in mature OLs. However, even if adult cells show a more mature profile in early stages, they are less responsive to TH differentiating signal. Moreover, we demonstrated that RXRγ is fundamental in both systems to achieve differentiation, showing a severe reduction in mature/myelinating OLs in cultures isolated from RXRγ-/- mice. However, RXRγ-/- cultures show the same gene expression regulation in response to T3-differentiation induction, compares to RXRγ+/+ cultures, suggesting that it is not directly involved in the molecular machinery of the maturation process. RXRγ-/- cultures show an higher percentage of replicating OPCs and do not show reduction of proliferation in response to T3, indicating a role of RXRγ in the control of cell cycle exit. Differences and similarity in T3-mediated OPCs differentiation will open new strategies in understanding their biology and developing new therapies in demyelinating disease, differentially affecting foetal or adult OPCs.

Keywords

1. *Introduction*

Oligodendrocytes (OLs) are the glial-subtype myelinating cells of the central nervous system (CNS) that derives from oligodendrocytes precursor cells (OPCs; Robertson, 1899; Rio Hortega et al., 1921). During embryonic development, the life of an OL is defined by four distinct phases: i) birth, migration, and proliferation of OPCs; ii) phenotypic differentiation of OPC into myelinating OL; iii) axonal contact, and generation of compact myelin and iv) long-term trophic and metabolic support of the encased axon (Michalski et al., 2015). During the adult life, a substantial number of OPCs persist in the CNS, being responsible for myelin turnover, replacement and repair (Dawson et al., 2003; Hughes et al., 2013).

The oligodendrocyte lineage begins with specification of OPCs from neural stem cells (NSCs) during late embryonic life. These multipotent stem cells give rise to neurons, radial glia, astrocytes and bipotential astrocyte-oligodendrocyte progenitor cells that colonize the CNS (Goldman and Kuypers, 2015). OPCs, recognized as replicating NG2-positive progenitors, are not a homogeneous population and they give rise to different progenies in different brain regions and in different stages of the development (Viganò and Dimou, 2016), during three separate waves, finally defining the whole OLs populations (Kessaris et al., 2006; Jakovcevski et al., 2009).

OPCs generated during the development are distributed in the adult brain and spinal cord, in the grey and the white matter, comprising the largest population of dividing cells in the mature CNS (Michalski et al., 2015). After lesion, they can proliferate, migrate to axons and differentiate in mature oligodendrocytes (Fukushima et al., 2015). In the adult life, new OPCs are also generated by proliferation and asymmetric division from NSCs in the subventricular zone (SVZ) of the lateral ventricle (Urbán and Guillemot, 2014).

In the healthy adult brain, new myelin is continually generated, showing a persisting remodelling (Yeung et al., 2014). Myelin volume in humans is activity-dependent, and can

increase producing new cells or new membrane from the already existing cells (Bercury et al., 2015), for example when practicing new skills (Bengtsson et al., 2005) or in learning a language (Schlegel et al., 2012). In fact, myelination is a conserved process during adult life, showing high plasticity. Moreover, an effective remyelination can occurs also after demyelination insults, leading to a complete anatomical and functional myelin sheath restoration, thus representing a true regenerative capability of the CNS (Crawford et al., 2013).

Remyelination process is not performed by pre-existing mature OLs, but involves the generation of new cells from the quiescent OPC pool distributed throughout the CNS or from the SVZ. Different soluble factors, also produced from activated microglia, stimulate local OPCs to switch from quiescent state to a regenerative phenotype, to migrate to demyelinated areas and generate mature OLs (Bradl and Lassmann, 2010), in a process that is believed to be similar to the developmental myelination (Franklin & Hinks 1999).

The progression of OPCs along the myelination process is tightly regulated in all the stages, by signals including growth factors, protein kinases and extracellular matrix molecules, all of which influence epigenetic modifications, transcriptional and translational regulation, and the actin cytoskeleton arrangement (Bercury et al., 2015).

One of the most important factors regulating the OPCs differentiation process is thyroid hormone (TH; Billon et al., 2002, 2004; Calzà et al., 2017). Triiodothyronine (T3), the active form of TH, acts via genomic, epigenetic and non-genomic mechanisms (Lee and Petratos, 2016), inducing OPCs cell cycle exit and terminal differentiation (Durand & Raff, 2000). T3 mediates its action by binding thyroid hormone receptors (TRs; TRα and TRβ), a class of nuclear receptors (NRs) that migrate into the nucleus and regulate the expression of specific genes controlling OPCs cell cycle exit and regulating the expression of premyelinating genes (Baxi et al., 2014; Casaccia-Bonnefil and Liu, 2003; Dugas, et al., 2012). Other nuclear receptors are also involved in OPC differentiation. In particular, RXRγ (Retinoic X Receptors

gamma) has been shown to be a positive regulator of the differentiation process (de la Fuente et al., 2015) also acting as TR/RXR heterodimer (Lee and Privalsky, 2005).

In order to dissect the respective contribution of TRs and RXR in foetal and adult OPC differentiation, in this study we explored the T3-mediated differentiation of OPC derived from foetal and adult NSCs. In particular, in these cell preparations we analysed (i) the differential expression level of NR, related co-represser and coactivators, and target genes; (ii) T3-mediated differentiation; (iii) OPC generation from RXRγ -/- mice.

2. *Materials and methods*

2.1 *Cell Cultures*

All animal protocols described herein were carried out according to the European Community Council Directives (86/609/EEC), and comply with the guidelines published in the *NIH Guide for the Care and Use of Laboratory Animals*.

Foetal and adult NSCs were isolated from E.13-14 foetal forebrain or 2.5 month old adult SVZ, following the Ahlenius and Kokaia protocol (Ahlenius and Kokaia, 2010). Oligodendrocyte differentiation was performed following the Chen protocol (Chen et al., 2007) with some modifications.

Ion another set of experiments the same protocol was used to differentiate OPCs from neurospheres isolated from foetal brain (whole forebrain or striatum) and adult SVZ of RXRγ+/+ and RXRγ -/- mice (Krezel et al., 1996).

Tissues were enzymatically dissociated using trypsin (Sigma-Aldrich), hyaluronidase (Sigma-Aldrich) and DNase (Sigma-Aldrich), than mechanically dissociated by piepetting. The solution was filtered, centrifuged and the resulting pellet was washed twice in HBSS. After 7 minutes centrifugation at $400 \times g$, the cellular pellet was resuspended in serum-free medium (DMEM/F12 GlutaMAX 1 x; 8 mmol/L HEPES; 100 U/100 μg Penicillin/Streptomycin; 0.1 x B27; 1 x N-2; 20 ng/mL bFGF; 20 ng/mL EGF) and, after cell count, cells were plated in suspension at a density of 10 cells/μl in a final volume of 3 mL in low-attachment 6-well plates (NUNC). Half medium was changed every three days, centrifuging the cell suspension at $300 \times g$ for 5 minutes and gently resuspending the cellular pellet in fresh medium. Neurospheres were allowed to proliferate until they attained a diameter of about 100μm.

To obtain secondary neurospheres, primary neurospheres were centrifuged at $300 \times g$ for 5 minutes. The pellet was mechanically dissociated by pipetting and cells were counted and

plated again at a density of 10 cells/µl under the same condition. While, to obtain oligospheres, the single cell culture were plated in a final volume of 3 mL of OPCs medium (DMEM/F12 GlutaMAX 1 x; 8 mmol/L HEPES; 100 U/100 µg Penicillin/Streptomycin; 0.1 × B27; 1 × N-2; 20 ng/mL bFGF; 20 ng/mL PDGF) in low-attachment 6-well plates (NUNC). Oligospheres were centrifuged and the pellet was mechanically dissociated to obtain a single cell suspension. After cell count, cells were plated at a density of 3000 cells/cm^2 on poly-D,L-ornithine (50µg/ml)/laminin (5µg/ml) coating, in OPC medium.

In order to induce oligodendrocyte differentiation and maturation, after 3 DIVs OPC medium was replaced with the oligodendrocyte differentiation medium (DMEM/F12 GlutaMAX 1 x; 8 mmol/L HEPES; 100 U/100 µg Penicillin/Streptomycin; 0.1 x B27; 1 x N-2; 50 nM T3; 10 ng/ml CNTF; 1x *N*-acetyl-L-cysteine -NAC-).

2.2 *RNA isolation and reverse transcription*

Total RNA isolation was performed with the RNeasy Mini kit (Qiagen, Milan, Italy) following manufacturer's instructions. Total RNA was eluted in RNase Free Water and concentration estimated through absorbance values at 260, 280 and 320 (Nanodrop 2000 spectrophotometer, Thermo Scientific). First strand cDNAs were obtained using the iScript™ cDNA Synthesis Kit (BioRad), incubating at 42°C for 30 min. An RNA sample with no reverse transcriptase enzyme in the reaction mix was processed as a no-reverse transcription control sample.

2.3 *PCR array*

The RNeasy Micro Kit (Qiagen) was used for total RNA extraction and 300 ng were retrotranscribed using the RT² First Strand Kit (Qiagen) following the manufacturer's instructions.

For the study of NSC gene expression, the 96-well Qiagen PCR array for nuclear receptors and co-regulators was used in combination with the RT2 SYBR Green qPCR Mastermix (Qiagen), using 10 ng of cDNA per well.

STRING software (version 10.0; European Molecular Biology Laboratory, Heidelberg, Germany; https://string-db.org/) was used to analyse the protein-protein interaction (PPI) of proteins derived from the genes differentially expressed between fetal and adult NSCs (fold of difference < 2). The STRING database provides interaction information from different panels, including protein and PubMed queries, connecting proteins in clusters according to their interactions and involvement in biological processes. In order to fit the strength of protein interactions the default options were used (minimum confidence, 0.400). The proteins were processed by the undirected edges method. STRING software allows the identification of net of interactions including other proteins closely linked to the one analysed, in order to obtain a better understanding of the possible pathways involved in the differentially expressed genes.

2.4 *Semi-quantitative real-time PCR*

Semi-quantitative real-time PCR was performed using the CFX96 real-time PCR system (BioRad, CA, USA). The reactions were performed in a final volume of 20 µl consisting of 1x SYBR Green qPCR master mix (BioRad) and 0.4 µM forward and reverse primers. In order

to avoid possible contamination of genomic DNA in isolated RNA, the sample with no reverse transcriptase enzyme was processed in parallel with the others and tested by real-time PCR for every pair of primers used. All primers used were designed using Primer Blast software (NCBI, MD, USA) and synthesised by IDT (Coralville, IA, USA). The following primer sequences were used: Olig1 (FW: 5'- CCGCCCCAGATGTACTATGC -3'; REV: 5'- AACCCACCAGCTCATACAGC -3'), Olig2 (FW: 5'- GCTTAGATCATCCCTGGGGC -3'; REV: 5'- AGATCATCGGGTTCTGGGGA -3'), TRα (FW: 5'- GCAAACACAACATTCCGC -3'; REV: 5'- TCCTGATCCTCAAAGACCTC -3'),TRβ(FW: 5'- GCAAACACAACATTCCGC -3'; REV: 5'- CACCAAACTGCTGCTCAA -3'), Klf9 (FW: 5'- AGTGGCTTCGAAGGGGAAAC -3'; REV: 5'- TCCGAGCGCGAGAACTTTTT -3'). GAPDH (FW: 5'- GGCAAGTTCAATGGCACAGTCAAG -3'; REV: 5'- ACATACTCAGCACCAGCATCACC -3') was used as housekeeping gene to normalize the amount of reverse-transcribed RNA used for PCR. Thermal profile of PCR reactions consisted first of a denaturation step (95°C, 2 min) and 40 cycles of amplification (95°C for 15 sec and 60°C for 60 sec). At the end of the amplification cycles the melting curve of amplified products was performed according to the following temperature/time scheme: heating from 55°C to 95°C with a temperature increase of 0.5°C/sec.

Primers efficiency values for all primers were 95-102%. The $2^{(-\Delta\Delta CT)}$ method was used for the calculation of gene expression.

2.5 *Immunocytochemistry*

Indirect immunofluorescence was used to identify OPCs (NG2- and PDGFαR-positive cells), mature (CNPase- and APC-positive cells) and myelinating (MBP-positive cells) OLs, neurons (β-III-tubulin-positive cells), astrocytes (GFAP-positive cells), replicating cells (Ki67-positive

cells) and Olig1 and Olig2 expressing cells. The following primary antisera were used: mouse anti-β-III-tubulin (R&D system, Trento, Italy) 1:3000; rabbit anti-GFAP (Glial Fibrillary Acidic Protein, Dako) 1:1000; rabbit anti-NG2 (chondroitin sulphate proteoglycan, neural/glial antigen 2, Millipore, Merck S.p.a., Milan, Italy) 1:350; rabbit anti-PDGFαR (Platelet derived frowth factor alpha receptor, Santa Cruz Biotechnology) 1:300; mouse anti-CNPase (2', 3'-cyclic nucleotide 3'-phosphodiesterase, Millipore) 1:500; mouse IgG2b anti-APC (anti-adenomatous polyposis coli, clone CC1, Calbiochem) 1:100; rabbit anti-MBP (Myelin Basic Protein, Dako) 1:500; anti-Ki67 (Calbiochem) 1:250; mouse IgG1 anti-Olig1 (Oligodendrocyte transcription factor 1; NeuroMab) 1:500 and mouse IgG1a anti-Olig2 (Oligodendrocyte transcription factor 2; Millipore) 1:500. Donkey Alexa Fluor 488-conjugated anti mouse, goat Alexa Fluor 555-conjugated anti- mouse IgG1, goat Alexa Fluor 488-conjugated anti- mouse IgG2a, goat Alexa Fluor 647-conjugated anti- mouse IgG2b and donkey Alexa 568-conjugated anti-rabbit (1:500; ThermoFisher Scientific) were used as secondary antisera. After immunofluorescence staining, cells were incubated with the nuclear dye Hoechst 33258 (1 μg/mL in PBS, 0.3% Triton-X 100) for 20 min at RT. Cells were finally washed in PBS and mounted in glycerol and PBS (3:1, v/v) containing 0.1% paraphenylendiamine.

2.6 *Confocal microscopy*

Confocal microscopy was used to study the culture lineage composition of RXRγ+/+ and RXRγ-/- cultures. Galsses were scanned with a Nikon Ti-E fluorescence microscope coupled to an A1R confocal system (Nikon). A diode laser system with 405 wavelength output, air-cooled Argon-Ion laser system with 488 wavelength output and Yellow diode-pumped solid state laser system with 561 wavelength output were used. Images were acquired with 20x objective with an optical resolution of 0.18 micron, using Nis-Elements AR 3.2 software. All

the z-stacks were collected in compliance with optical section separation (z-interval) values suggested by Nis-Elements AR 3.2 software (1µm). Major intensity projections were used for the image analysis

The percentage of APC-, MBP- and NG2-positive cells were quantified, based on the total number of cells identified by the nuclear staining. Using the triple staining APC/Olig1/Olig2, the OPCs/OLs populations were identified, according to their positivity to these three different markers (Nakatani et al., 2013). Moreover, the effect of the RXRγ gene knock out on the cell cycle was analysed by using the double staining PDGFαR/Ki67. The percentage of the double positive PDGFαR+/Ki67+ were calculated on the total number of PDGFαR-positive cells. Double positive cells represent the percentage of replicating OPCs. Five random fields per glass (duplicate per sample) were used for the analysis.

2.7 *High Content Screening*

For HCS analysis cells were grown in 96 flat-bottom well HCS plates (NUNC). Analysis of condensed nuclei, cell number and lineage/differentiation markers were performed with Cell Insight™ CX5 High Content Screening (HCS; Thermo Scientific), using the *Compartmental analysis* BioApplication. Based on nuclear staining, the software is able to recognise nuclei and calculate the percentage of high intensity/small sized condensed nuclei. Moreover, based on the nuclei identification, the software is able to detect the presence of the marker-specific stain in the cell body, calculating the percentage of the immunoreactive cells. Lineage/differentiation markers analysis was performed only on cells showing intact nuclei, excluding condensed nuclei from the percentage calculation.

2.8 Statistical Analysis

Data are reported as mean ± SEM. Prism software (GraphPad) was used for statistical analyses and graph generation. Student's t test, one-way ANOVA or two-way ANOVA and Dunnett's multiple comparison post-hoc were used to analyse data. Results were considered significant when the probability of their occurrence as a result of chance alone was less than 5% ($P < 0.05$).

3. *Results*

3.1. TRβ and RXRγ are differentially expressed in foetal and adult neurospheres

In order to study possible roles of NRs in OPCs lineage and differentiation, we first analysed the NRs and co-regulators mRNA expression in very early precursors. For this purpose we lysate secondary foetal and adult neurospheres, extracted the RNA and analysed the expression of all NRs and co-regulators by using the PCR array technology (Fig 1 A). The list of all the analysed gene is presented in supplementary material (Table 1).

Results we analysed by comparing adult- to foetal-derived NSC gene expression, and expressed as fold of increase. Adult NSCs show a general up-regulated profile compared to foetal cells (Figure 1 B). Genes showing a difference in expression equal or higher than 2 folds were considered as significantly differentially expressed. In particular, 28 NRs and co-regulators are more expressed and 3 genes are less expressed in the adult compared to foetal NSCs (Figure 1 C). The list of all differentially regulated genes is included in the figure (Figure 1 D).

Different genes related to androgens (Ar, Med12, Med13 and Nr1i3), estrogen (Ncoa6), glucocorticoids (Ncoa6 and Nr3c1), vitamin D (Med12 and Med13), steroid hormones (Nr1d1, Nr1h3, Nr2c1, Nr2f2, Nr3c2, Ppara, Rarg, Rora, Rxra, Thrb), retinoic acid receptors (Ncoa6, Rarg, Rxra and Rxrg) and, in particular to THs (Med12, Med13, Ncoa4, Nr1d1, Nr1h3, Nr1i3, Trip4 and Thrb) are differentially regulated.

In particular, two key genes involved in OPCs differentiation were differentially expressed in adult compared to foetal OPC: TRβ (Trhb) and RXRγ (Rxrg). TRβ is 12.52 folds more expressed, while RXRγ is 9.27 folds less expressed in adult compared to foetal NSCs.

The net of the proteins encoded by differentially regulated genes were analysed by the STRING software. The software uses the interactions between proteins in order to build a network, where nodes are represented by interconnected proteins encoded by the selected genes. The analysis of the interactions shows that all the proteins encoded by the differentially regulated genes are functionally interconnected. TRβ is in the core, indicating its central role in the net (red arrow, Fig 1 E). Protein encoded by genes involved in retinoic acid metabolism (Rorb, Rxrg and Rora) show also a central position, and a strong interaction with TRβ.

3.2 *Foetal and adult NSCs-derived OPCs need T3 to differentiate in mature OLs*

We then confirmed the role of T3 as key agent in the OPC differentiation process from NSC. Both foetal and adult NSCs cultures were used for the differentiation protocol described in figure 2 A. The lineage progression was analysed by counting the number of differentiated cells, using CNPase as marker for pre-myelinating PL, and MBP as marker for myelinating OL. Both cultures need T3 to differentiate in mature/myelinating

CNPase-/MBP- positive OLs. In fact, in the absence of T3 very few CNPase (foetal: 12%; adult: 9%) and MBP (foetal: 5%: adult: 8%)-positive cells are observed compared to T3 exposed cultures (*data not shown*). Representative images of vehicle- or T3-treated cultures at the end of the differentiation process are showed in Figure 2 B-I.

3.3 Adult NSCs-derived OPCs have the same expression pattern of OLs markers compared to foetal, but different yield of maturation

In order to dissect the molecular steps involved in the differentiation process in adult and foetal-derived OPC, we analysed the expression of five key genes in the differentiation process (Olig1, Olig2, TRα, TRβ and Klf9) in all the differentiation step of NSCs-derived OPCs, from neurospheres to myelinating OLs (Fig 3 A). These genes are regulators of the cell cycle exit and of the maturation of OLs and are tightly functionally connected (Fig 3 B).

Olig1, Olig2, TRα, TRβ and Klf9 mRNA expression level is regulated by time and differentially expressed between the two cultures (Two-way ANOVA: Olig1, time, $p < 0.0001$, age, $p = 0.0021$ interaction, $p < 0.0001$; Olig2 time, $p < 0.0001$, age, $p = 0.0035$, interaction, $p < 0.0001$; TRα, time, $p = 0.0143$, age, $p < 0.0001$ interaction, $p = 0.0002$; TRβ, time, $p < 0.0001$, age, $p = 0.0127$ interaction, $p = 0.0006$; Klf9, time, $p < 0.0001$, age, $p < 0.0001$ interaction, $p < 0.0001$). In particular, adult cultures show higher expression of Olig1, Olig2, TRβ and Klf9 at neurospheres and oligospheres stages (Olig1, neurospheres $p < 0.0001$, oligospheres $p < 0.0001$; Olig2, neurospheres $p < 0.0001$, oligospheres $p < 0.0001$; TRβ, neurospheres $p < 0.0001$, oligospheres $p = 0.0229$ and Klf9, neurospheres $p < 0.0001$, oligospheres $p < 0.0001$).

However, in later stages of differentiation, at OPCs level (0 DIV) and after T3-induced differentiation (6 and 12 DIVs), foetal cells are more responsive to differentiation stimuli, showing an higher expression of Olig1 at 6 DIV ($p < 0.0001$) and Olig2 and TRα at all the differentiation time points studied (Olig2, 0 DIV, $p = 0.0001$, 6 DIV, $p < 0.0001$, 12 DIV, $p = 0.0248$; TRa, 0 DIV, $p = 0.001$; 6 DIV, $p < 0.0001$, 12 DIV, $p = 0.0128$).

Notably, even if Klf9 expression is retained in adult cells at early stages (0DIV, $p < 0.0001$), Klf9 expression is higher in the foetal cultures in later stages (6 DIV, $p = 0.0111$; 12 DIV, $p = 0.0007$; Fig. 3 C-F), after T3 exposure.

We then analysed how this gene expression profiles correlate with the OLs maturation by analysing different markers during the differentiation process (0, 6 and 12 DIV; Figure 4 A), e.g. PDGFαR and NG2 for OPCs, CNPase for mature OLs, MBP for myelinating OLs, GFAP for astrocytes and beta-III-tubulin for neurons.

Results were analysed by two-way ANOVA for each lineage marker. The percentage of PDGFαR- positive cells varies according to the culture time in both foetal and adult OPC (time, $p = 0.0108$, $F_{(2,24)} = 5.499$; interaction, $p < 0.0001$), with a decrease in foetal cultures at 6 DIV (0 vs. 6 DIV, $p = 0.0006$) and an increase at the same time point in the adult (0 vs. 6 DIV, $p = 0.0007$), but reaching the same percentage at the end of differentiation (12 DIV; Fig 4 B-D). However, NG2-positive cells percentage is affected by both time and age (time, $p = 0.0029$, $F_{(2,24)} = 7.516$; age, $p = 0.0058$, $F_{(2,24)} = 9.159$; Fig 4E-G). Mature, CNPase-positive OLs, show no age (foetal vs. adult) or time differences, but the two parameters are significantly interacting (interaction, $p = 0.001$; Fig 4 H-J). However, MBP-positive cells percentage is significantly affected by the age parameter (age, $p < 0.0001$; $F_{(2,24)} = 32.66$; interaction, $p = 0.0007$; $F_{(2,24)} = 9.987$), with a significant low percentage in adult-derived cultures at the end of the differentiation process, compared to foetal-derived cells (12 DIV, $p = 0.0020$; Fig 4 K-M).

In term of morphological phenotype, cells derived from foetal NSCs show a more mature phenotype compared to cells derived from adult NSCs, as illustrated by MBP-IR (Fig 4 L and M).

Moreover, since NSCs-derived cultures are mixed culture including also astrocytes and neurons, we also evaluated these cell population: GFAP-positive cells are around 40% of the cultures in both cell cultures, at the end of the differentiation phase, and a little percentage of neurons (foetal, 5%; adult, 1%; *data not shown*) was also detected throughout the whole culture.

3.4 *Foetal and adult NSCs-derived OPCs need RXRγ to differentiate in mature OLs*

In order to study the role of RXRγ, a NR differentially expressed in foetal and adult early precursors, we isolated NSCs from foetal and adult brain of RXRγ+/+ and RXRγ-/- mice. For foetal cultures, cells were isolated both from the whole forebrain or selectively from the striatum, the region where RXRγ is more expressed in the brain; while for adult NSCs were isolated from the SVZ. The same differentiation protocol was used (Fig 5 A).

Cells isolated from RXRγ-/- animals show a reduced percentage of mature OLs at the end of the differentiation process, (Student's t test: APC-positive cells; E13.5, RXRγ-/- p = 0.0001; RXRγ-/- p = 0.0007; adult RXRγ-/- p < 0.0001; Fig 5B) and myelinating (MBP-positive cells; E13.5, RXRγ-/- p < 0.0001; RXRγ-/- p < 0.0001; adult RXRγ-/- p < 0.0001; Fig 5C). Panel in figure 5 D-K shows representative images of the cultures. Results were similar for foetal cells isolated either from the whole forebrain or from the striatum (*data not shown*).

Using the anti-APC antibody, in combination with the detection of Olig1 and Olig2, it is possible to discriminate between the different populations of OPCs and OLs at different

stages of maturation. Progenitors (OPCs) are APC- and Olig1- negative, but positive for Olig2. APC-positive cells can be divided in a crescent level of maturation in Olig1-/Olig2+, Olig1+/Olig2+ and Olig1-/Olig2+ (Nakatani e al., 2013). Both in foetal and adult cultures, the cells reaching APC-positivity display the same pattern of distribution of the different population. However, foetal cells isolated from the whole forebrain, compared to RXRγ+/+, show a higher percentage of APC-negative cells (black column, p = 0.0246) and less APC+/Olig1-/Olig2+ cells (p = 0.0473), corresponding to the most mature OLs population (Fig 5 L).

3.5 RXRγ is involved in T3-mediated cell cycle exit

In order to investigate the possible role of RXRγ receptors in the expression regulation of key genes involved in OLs maturation and in cell cycle exit, we isolated foetal cells from the whole forebrain of RXRγ-/- and RXRγ+/+ mice (Fig 6A). Foetal cultures of NSCs-derived OPCs were lysed before adding T3 (0 h), and after 6 and 24 h after the T3-differentiation induction. No differences in expression levels were detected in TRα1, TRβ, Olig1, Olig2 and Klf9 expression (Fig 6 B).

T3 is the best-known differentiating agent in OPCs being the key regulator of the cell cycle from undifferentiated precursors (Billon et al., 2001). Thus, in order to analyse the effect of RXRγ gene KO in the cell cycle regulation, were measured the percentage of OPCs generated from cells isolated from the whole foetal forebrain of RXRγ-/- and RXRγ+/+ mice, after 24 h of the T3-mediated differentiation, compared with cultures that were not treated with T3. RXRγ-/- cultures show an higher number of NG2-positive cells at the end of the differentiation phase, compared to RXRγ+/+ cultures (p < 0.0001; Fig 6 C-E), suggesting a possible dysregulation of the T3-induced cell cycle exit.

Cells were then stained for PDGFαR, in order to identify OPCs, and for Ki67, in order to identify replicating cells. T3 induces a reduction in Ki67-positive OPCs, compared to RXRγ+/+ cultures treated with vehicle (p = 0.0486). RXRγ-/- cultures show an higher percentage in replicating-OPCs compared to RXRγ+/+ (p = 0.0315). Moreover, the percentage of Ki67-positive OPCs is not affected by T3 treatment and the level remains higher, compared to RXRγ+/+ cells treated with T3 (p < 0.0001; Fig 6 F-J).

4. *Discussion*

OPCs are the key cells for myelin formation and repair in the CNS. Thus, understanding the molecular mechanisms underlying their maturation from the precursor until the myelinating stage would provide fundamental information also in view of therapeutic opportunities for demyelinating diseases and lesions (Hydleburg abd D'Aversa, 2014). In spite of the fact that most of OPCs populating the mature CNS are developmentally derived, the foetal and mature OPCs show substantial differences in molecular and biological properties. For instance, we demonstrated that the enzymatic activity of Poly (ADP-ribose) polymerase (PARP) family members is much higher in foetal than in adult- OPCs derived from NSCs, and that PARP inhibition is cytotoxic for OPCs derived from foetal, but not from adult brain (Baldassarro et al., 2017). Moreover, in vivo and in vitro studies indicate that OPCs have substantially different properties according to their chronological age (Cui et al., 2012); the sensitivity of OL lineage to apoptosis is maturation-dependent (Butts et al., 2008); and adult OPC have a longer cell cycle than perinatal OPC (Tang et al., 2000). In view of the key role of several members of NRs superfamily in OPC biology, in this study we investigated the differentiation process of OPCs obtained from NSCs derived from foetal (E13.5) and adult brain (SVZ), focusing on the role of NRs. This cell system was preferred to primary and purified OPCs to better mimic developmental biology of OPC, including lineage specification,

proliferation/survival and differentiation. This culture contains also astrocytes, fundamental players in the THs metabolism and signalling, expressing also TRs and affected by T3 exposure (see Trentin, 2006 for a review).

We showed that (i) the mRNA expression level of several NR and co-regulators is different in foetal and adult OPCs at comparable differentiation stages; (ii) adult NSCs-derived OPCs have a different yield of maturation compared to foetal-derived OPC; (iii) both foetal and adult NSCs-derived OPCs need RXRγ to complete the T3-dependent maturation, and this effects is probably related to the cell cycle exit.

4.1. NR signalling in foetal vs adult OPC.

NRs play fundamental roles in all the differentiation stages of OLs, from NSCs self-renewal and lineage specification, to OPCs cell cycle exit and OLs maturation. NRs members include the thyroid hormone receptors (TRs), the retinoic acid receptors (RARs), the retinoid X receptors (RXRs), the peroxisome proliferator-activated receptors (PPARs), the liver X receptors (LXRs), the estrogen receptors (ERs), the mineralocorticoid receptor (MR), the glucocorticoid receptor (GR), as well as orphan nuclear receptors, for which no known cognate endogenous ligands have yet been identified (Stergiopoulos, 2013). According to the classical view, most of these receptors act at genomic level either in the presence or absence of the endogenous ligand, modulating expression or repression of the target genes, respectively (Mendoza and Hollenberg, 2017).

Here we showed that foetal and adult NSCs show a different expression level of two key NRs involved in OLs lineage and differentiation. In particular, NSCs derived from the SVZ of the adult brain has much higher TRβ and a much lower RXRγ mRNA expression level than NSCs derived from foetal brain. Moreover, differentiated cultures obtained from adult animals also show an higher expression of Olig1, Olig2 and Klf9 mRNAs expression level in early stages

of the differentiation (until oligospheres for Olig1 and 2 and until OPCs, 0 DIV, for Klf9), compared to foetal brains. Olig1 and Olig2 are closely related transcription factors playing critical roles in OLs specification and differentiation. They are structurally similar but only partially functionally redundant in OPCs differentiation, whit a major role of Olig2. The main target of Olig2 are Sox10 and Sip1, factors enhancing the OPCs differentiation, inhibiting neuronal differentiation of multipotent precursors. The expression of the two Oligs is temporally regulated, with a later expression of Olig1, inducing the expression of mature OLs genes (Mbp and Plp1; see Maijer et al., 2012 for a Review). Klf9 is a T3-target gene, which is critically involved in OPC maturation and directly induced by T3 (Dugas et al., 2012). In embryonic NSCs, TRβ participates in the regulation of neuronal differentiation and oligodendrogenesis, while in adult NSCs acts inhibiting the proliferation and regulating the gliogenesis (Gkikas et al., 2017). RXRγ induces gliogenesis in foetal NSCs (Takouda et al., 2017), while no data are available in adult-derived NSCs. Primary OPC cell cultures need T3 to differentiate into myelinating OL, and here we confirmed that also OPC derived from foetal and adult NSC also need T3. T3 acts as TRs ligand (Billon et al., 2002), being the α and β TR isoforms, ligand-regulated transcription factor for target genes. We showed that foetal cells are more responsive to T3-induced differentiation, reaching higher level of the T3-target gene Klf9. The higher T3-responsiveness in foetal cultures is also showed by the analysis of OLs markers during the differentiation process, proving that foetal differentiated cultures are more enriched of MBP-positive OLs compared to adult at the end of the in vitro differentiation process, according also to the higher expression of mRNA encoding for differentiation factors (Olig1, Olig2 and Klf9) in the late stages of the differentiation. Moreover, the morphological phenotype of CNPase and MBP-positive cells is more mature in foetal than adult cultures, suggesting a possible delay in the differentiation of adult cultures.

These results support the general view that T3 action on differentiation process of different cell precursors is spatially and timely controlled. In fact, T3-dependent gene expression

regulation is spatially and temporally regulated. The same gene can be differentially regulated according to the developmental stage and according to the cell type, possibly according to a differential expression of co-regulators (Mohácsik et al., 2011). In particular, it is now clear that TRs can regulate negatively or positively gene target transcription, through mechanisms involving co-repressor and co-activators. These proteins interact with either ligand-bound or unliganded NRs, acting as a bridge between receptors and the transcription machinery (see Astapova, 2016 for a review).

4.2. RXRγ involvement in T3-mediated OPC cell cycle exit

It is well known that T3 regulates the cell cycle of different cells, including OPCs. According to the classical experiments by Raff and collaborators (Billon et al., 2001), T3 drives the OPC out from the cell cycle after a defined number of cell replication (or corresponding time), possibly acting through p27 protein, directly enhancing the expression of the gene (Perez-Juste and Aranda, 1999). T3 is also needed to start differentiation, proven by the fact that the accumulation of p27 protein in OPCs is enough to block cell cycle, but cells fail to differentiate in absence of T3. Infact, in absence of T3, and in the presence of mitogens, OPCs keep proliferating with no chances to differentiate (Tokumoto et al., 2002).

During development, OPCs start showing TH sensitivity at E14 in mice, due to the expression of TRs, giving to them the role of the timer controller of the differentiation (Gao et al., 1998; Billon et al., 2001). T3 directly regulates different proteins involved in cell cycle control. For example, T3-mediated action of TRs decreases the expression of E2F1 and c-myc, molecules involved in the transcriptional activation of different positive regulators of cell cycle (e.g. cyclin E, cyclin A and cdk2) and reduces the expression of cyclin D1 (Puzianowska-Kuznicka et al., 2006). The regulation of TH sensitivity is also dependent on the cell cycle phase, as suggested by *in vitro* data. In particular there is no TRs expression in early S phase, but TRs

expression progressive increase during late S and G2 until maximal level at G2/M, showing also an increase in TH binding capability (Maruvada et al., 2004).

Apart from TRs, other NRs are involved in the gene expression regulation in OPCs, acting as homodimers or heterdimers also with TRs (Zhuang et al., 2013; Kanakasabai et al., 2012). In this context, the retinoic acid receptors RXRs are of particular interest, namely RXRγ. The activation of RXR by pharmacological and genetic manipulation stimulates oligodendrocyte, differentiation enhancing remyelination (Huang et al., 2011; de la Fuente et al., 2015), and the TR/RXR heterodimer is proposed to be the primary mediators of the target gene regulation by T3 (vedi geni indagati) (Lee and Privalsky, 2005). Moreover, an upregulation of RXRγ mRNA expression level has been described during remyelination, being expressed in OLs in remyelinating lesions in rat CNS (ref) and in tissue from individuals with multiple sclerosis (MS), a disease characterized by extensive demyelination and remyelination attempts (ref).

Here we showed that the lack of RXRγ severly impairs OLs maturation both in foetal and adult cultures. We showed that the percentage of mature and myelinating OLs at the end of the T3-differentiation mediated phase is much lower in cell isolated from RXRγ-/- than from WT animals, indicating a substantial impairment in OPC differentiation in the absence of RXRγ. However, the small number of the mature OLs present in RXRγ-/- cultures shows the same maturation pattern of the RXRγ+/+ cells, and no differences in key genes mRNA expression level (Olig1, Olig2, Klf9) involved in the differentiation process were detected after 6 and 24 hours from the T3-mediated differentiation induction. These results support a major role of RXRγ in the T3-mediated OPCs differentiation, and suggest that this effect is not mediated by the molecular machinery at the base of the differentiation process.

An alternative possibility is that RXRγ is involved in the T3-mediated cell cycle exit. In fact, foetal cultures of NSCs-derived OPCs isolated from RXRγ-/- mice, show an higher number of OPCs compared to OPCs isolated from RXRγ+/+ mice, suggesting that T3 failed to induce cell cycle exit and OPCs do not stop proliferating. This hypothesis was confirmed by the

PDGFαR/Ki67 double staining experiments, allowing the quantification of replicating OPCs. RXRγ-/- OPCs show an higher number of replicating OPCs in the absence of differentiation stimuli and also 24 hours after the T3- differentiation induction, as indicated by the unchanged number of Ki67-positive OPCs.

In conclusion, we showed that foetal and adult NSCs-derived OPCs differentially respond to T3-mediated differentiation. This process needs T3 in both cultures. Moreover, in both cultures RXRγ is fundamental to trigger the differentiation, probably acting as heterodimer with TRs. RXRγ is directly affecting OPCs differentiation, probably by affecting the T3-mediated OPCs cell cycle exit. Further studies will elucidate the interactions between TRs and RXRγ in this process.

Acknowledgements

References

Alhenius H and Kokaia Z. Isolation and generation of neurosphere cultures from embryonic and adult mouse brain. Methods Mol Biol, 2010; 633: 241-252.

Astapova I. Role of co-regulators in metabolic and transcriptional actions of thyroid hormone. J Mol Endocrinol, 2016. 56: 73-97.

Baxi EG, Schott JT, Fairchild AN, Kirby LA, Karani R, Uapinyoying P, et al. A selective thyroid hormone β receptor agonist enhances human and rodent oligodendrocyte differentiation. Glia, 2014; 62: 1513–1529.

Bengtsson SL, Nagy Z, Skare S, Forsman L, Forssberg H and Ulleʹn F. Extensive piano practicing has regionally specific effects on white matter development. Nat. Neurosci. 2005; 8: 1148–1150.

Bercury KK and Macklin WB. Dynamics and Mechanisms of CNS myelination. Developmental Cell. 2015; 32: 447-458.

Billon N, Tokumoto Y, Forrest D and Raff M. Role of thyroid hormone receptors in timing oligodendrocyte differentiation. Dev Biol, 2001. 235: 110-120.

Billon N, Jolicoeur C, Tokumoto Y, Vennstr€om B, Raff M. Normal timing of oligodendrocyte development depends on thyroid hormone receptor alpha 1 (TRalpha1). EMBO J. 2002; 21: 6452–6460.

Billon N, Terrinoni A, Jolicoeur C, McCarthy A, Richardson WD, Melino G and Raff M. Roles for p53 and p73 during oligodendrocyte development. Development, 2004. 131:1211-1220.

Bradl M and Lassmann H. Oligodendrocytes: biology and pathology. Acta Neuropathol. 2010; 119: 37-53.

Calzà L, Baldassarro VA, Fernandez M, Giuliani A, Lorenzini L and Giardino L. Thyroid hormone and the white matter of the central nervous system: from development to repair. Vit and Horm, 2017. 106: 253-280.

Casaccia-Bonnefil P and Liu A. Relationship between cell cycle molecules and onset of oligodendrocyte differentiation. Journal of Neuroscience Research, 2003. 72: 1–11.

Chen Y, Balasubramaniyan V, Peng J, Hurlock EC, Tallquist M, Li J and Lu QR. Isolation and culture of rat and mouse oligodendrocyte precursor cells. Nat Proc, 2007; 2: 1044-1051.

Crawford AH, Chambers C and Franklin RJ. Remyelination: The true regeneration of the central nervous system. Journal of Comparative Pathology, 2013. 149: 242–254.

Dawson MR, Polito A, Levine JM and Reynolds R. Therapeutic applications of PARP inhibitors: anticancer therapy and beyond. Mol Aspects Med, 2003. 34: 1217-1256.

de la Fuente AG, Errea O, van Wijngaarden P, Gonzales GA, Kerninon C, Jarjour AA, Lewis HJ, Jones CA, Nait-Oumesmar B, Zhao C, Huang JK, ffrench-Constant C and Franklin RJ. Vitamin D receptor-retinoid X receptor heterodimer signaling regulates oligodendrocyte progenitor cell differentiation. J Cell Biol, 2015. 211: 975-985.

Dugas JC, Ibrahim A and Barres BA. The T3-induced gene KLF9 regulates oligodendrocytes differentiation and myelin regeneration. Mol Cell Neurosci, 2012. 50: 45-57.

Durand B and Raff M. A cell-intrinsic timer that operates during oligodendrocyte development. Bioessays, 2000. 22: 64–71.

Franklin RJM and Hinks GL. 1999. Understanding CNS remyelination: Clues from developmental and regeneration biology. J Neurosci Res 58:207–213.

Fukushima S, Nishikawa K, Furube E, Muneoka S, Ono K, Takebayashi H and Miyata S. Oligodendrogenesis in the fornix of adult mouse brain; the effect of LPS-induced inflammatory stimulation. Brain Res, 2015. 1627: 52-69.

Gao FB, Apperly J and Raff M. Cell-intrinsic timers and thyroid hormone regulate the probability of cell -cycle withdrawal and differentiation of oligodendrocyte precursor cells. Dev Biol. 1998. 197: 54-66.

Gkikas D, Tsampoula M and Politis PK. Nuclear receptors in neural stem/progenitor cell homeostasis. Cell Mol Life Sci, 2017. 74: 4097-4120.

Goldman SA and Kuyoers NJ. How to make an oligodendrocyte. Development, 2015. 142: 3983-3995.

Huang MP, Rodgers KA, O'Mara R, Mehta M, Abuzahra HS, Tannenbaum AD, Persons K, Holick MF and Safer JD. The thyroid hormone degrading type 3 deiodinase is the primary deiodinase active in murine epidermis. Thyroid, 2011 21:1263–1268.

Hughes EG, Kang SH, Fukaya M and Bergles DE. Oligodendrocyte progenitors balance growth with self-repulsion to achieve homeostasis in the adult brain. Nat Neurosci. 2013. 16: 668–676.

Hydleburg M and D'Aversa TG. Current therapies for Multiple Sclerosis: A brief review. Austin J Scler & Neuroimmunol, 2014. 1: 4.

Jakovcevski I, Filipovic R, Mo Z, Rakic S and Zecevic N. Oligodendrocyte development and the onset of myelination in the human foetal brain. Frontiers in Neuroanatomy, 2009. 3: 1-15.

Kanakasabai S, Pestereva E, Chearwae W, Gupta SK, Ansari S and Bright JJ. PPARg agonists promote oligodendrocyte differentiation of neural stem cells by modulating stemness and differentiation genes. PlosONE, 2012. 7: e50500.

Kessaris N, Fogarty M, Iannarelli P, Grist M, Wegner M and Richardson WD. Competing waves of oligodendrocytes in the forebrain and postnatal elimination of an embryonic lineage. Nat. Neurosci, 2006. 9:173–79.

Krezel W, Dupé V, Mark M, Dierich A, Kastner P and Chambon P. RXR gamma null mice are apparently normal and compound RXR alpha +/-/RXR beta -/-/RXR gamma -/- mutant mice are viable. Proc Natl Acad Sci USA, 1996. 93: 9010-9014.

Lee, JY and Petratos S. Thyroid hormone signaling in oligodendrocytes: From extracellular transport to intracellular signal. Molecular Neurobiology, 2016. 53: 6568–6583.

Lee S and Privalsky ML. Heterodimers of retinoic acid receptors and thyroid hormone receptors display unique combinatorial regulatory properties. Mol Endocrinol, 2005. 19: 863-878.

Maijer DM, Kane MF, Mehta S, Liu H, Harrington E, Taylor CM, Stiles CD and Rowitch. Separated at birth? The functional and molecular divergence of OLIG1 and OLIG2. Nat Rev Neurosci, 2012. 13: 819-831.

Maruvada P, Dimitrieva NI, East-Palmer J and Yen PM. Cell cycle-dependent expression of thyroid hormone receptor-beta is a mechanism for variable hormone sensitivity. Molecular Biology of the Cell, 2004. 15: 1895-1903.

Mendoza A and Hollenberg AN. New insights into thyroid hormone action. Pharmacol Ther, 2017. 173: 135-145.

Michalski JP and Kothary R. Oligodendrocytes in a nutshell. Frontiers in Cellular Neuroscience, 2015. 9: 1-11.

Mohácsik P, Zeöld A, Bianco AC and Gereben B. Thyroid hormone and the neuroglia: both source and target. J Thyroid Res, 2011. 2011: 215718.

Nakatani H, Martin E, Hassani H, Clavairoly A, Maire CL, Viadieu A, Kerninon C, Delmasure A, Frah M, Weber M, Nakafuku M, Zalc B, Thomas JL, Guillemot F, Nait-Oumesmar B and Parras C. Ascl1/Mash1 promotes brain oligodendrogenesis during myelination and remyelination. J Neurosci, 2013. 33: 9752-9768.

Perez-Juste G and Aranda A. The cyclin-dependent kinase inhibitor p27(Kip1) is involved in thyroid hormone-mediated neuronal differentiation. J Biol Chem, 1999. 274: 5026-5031.

Puzianowska-Kuznicka M, Pietrzak M, Turowska O and Nauman A. Thyroid hormones and their receptors in the regulation of cell proliferation. Acta Biochim Pol, 2006. 53: 641-650.

Rio Hortega DP. Histogenesis y evolucion normal; exodo y distribucion regional de la microglia. Memor. Real. Soc. Esp. Hist. Nat, 1921 11, 213–268.

Schlegel AA, Rudelson JJ, and Tse PU. White matter structure changes as adults learn a second language. J. Cogn. Neurosci, 2012. 24: 1664–1670.

Takouda J, Katada S and Nakashima K. Emerging mechanisms underlying astrogenesis in the developing mammalian brain. Proc Jpn Acad Ser B Phys Biol Sci, 2017. 93: 386-398.

Trentin AG. Thyroid hormone and astrocyte morphogenesis. J Endocrinol, 2006. 189: 189-197.

Tokumoto YM, Apperly JA, Gao FB and Raff MC. Posttranscriptional regulation of p18 and p27 Cdk inhibitor proteins and the timing of oligodendrocyte differentiation. Dev Biol, 2002. 245: 224-234.

Urbán N and Guillemot F. Neurogenesis in the embryonic and adult brain: same regulators, different roles. Front Cell Neurosci, 2014. 8: 396.

Viganò F and Dimou L. The heterogeneous nature of NG2-glia. Brain Res, 2016. 1638: 129-137

Yeung MS, Zdunek S, Bergmann O, Bernard S, Salehpour M, Alkass K, Perl S, Tisdale J, Possnert G, Brundin L, et al. Dynamics of oligodendrocyte generation and myelination in the human brain. Cell, 2014. 159: 766–774.

Zhuang S, Bao L, Linhananta A and Liu W. Molecular modeling revealed that ligand dissociation from thyroid hormone receptors is affected by receptor heterodimerization. J Mol Graph Model, 2013. 44: 155-160.

Figure captions

Figure 1. Nuclear receptors and coregulators in adult vs. foetal neurospheres

(A) Experimental design: in order to study nuclear receptors and co-regulators expression in foetal and adult early precursors, secondary neurospheres were lysed and mRNA expression was analysed using the PCRarray technology.

(B) Heat Plot representation of the whole array, showing expression of adult vs. foetal neurospheres. Fold of change is expressed in colours code from green (down-regulated) to red (up-regulated).

(C) Gene list of the differentially expressed genes (fold of change > 2).

(D) Graphic elaboration of the STRING software interaction analysis. Proteins encoded by the differentially expressed genes were analysed by the STRING software in order to study the interaction net. In the centre of the net, the TRβ is highlighted by the red arrow.

Figure 2. T3-driven foetal and adult NSCs-derived OPCs differenitation in mature OLs

(A) Experimental design: 3 DIV after OPC seeding, cells were exposed to vehicle (DMSO) or T3 (50nM). At the end of the differentiation phase (12 DIV) cells were stained for mature OLs markers.

(B-E) Images show the vehicle treated groups, stained for CNPase (B, C) and MBP (D, E) markers, in foetal (B, D) and adult (C, E) cultures.

(F-I) Images show the T3 treated groups, stained for CNPase (F, G) and MBP (H, I) markers, in foetal (F, H) and adult (G, I) cultures.

Abbreviations: CNPase, 2',3'-cyclic nucleotide 3'-phosphodiesterase; MBP, myelin basic protein.

Figure 3. Gene expression in foetal and adult NSCs-derived OPCs

(A) Experimental design: gene expression was analysed during the whole differentiation process, from early progenitors to mature OLs. Arrows show the time point of the analysis: neurospheres, oligospheres, 0 DIV (before the T3 differentiation induction), 6 DIV, 12 DIV.

(B) The active form of the thyroid hormone (T3) exert its action throughout nuclear receptors (NRs), including thyroid hormone nuclear receptors alpha and beta. In this way, T3 actives the molecular machinery, involving Olig1 and Olig2 expression dynamics and Klf9 activation, allowing the OPC cell cycle exit and maturation process.

(C-G) Gene expression analysis of five key genes involved in the differentiation process: Olig1 (C), Olig2 (D), TRα (E), TRβ (F) and Klf9 (G). Results are showed as fold of changes of all foetal and adult time points normalized on foetal neurospheres.

Statistical analysis: Two-way ANOVA followed by Tukey's post-hoc. Asteriscs represent differences in the expression at the same time point between foetal and adult cultures (* P < 0.5; ** P < 0.1; *** P < 0.01; **** P < 0.001).

Bars represent mean value + SEM. Statistical analysis: Two-way ANOVA followed by Tukey's post-hoc; * p < 0.05, ** p < 0.01, *** p < 0.001, **** p < 0.0001.

Abbreviations: Klf9, kruppel-like factor 9; Olig1, Oligodendrocyte transcription factor 1; Olig2, Oligodendrocyte transcription factor 2; TRα, Thyroid hormone receptor alpha; TRb, thyroid hormone receptor beta.

Figure 4. OLs differentiation markers in foetal and adult NSCs-derived OPCs

(A) Experimental design: cell morphology and OPCs/OLs markers expression were analysed during the differentiation process. Arrows show the time point of the analysis: 0 DIV (before the T3 differentiation induction), 6 DIV, 12 DIV.

(B-D) Graph shows the percentage of the PDGFαR-positive cells during the three analysed time point in foetal (red line) and adult (blue line) cultures (B). Images represent foetal (C) and adult (D) cultures at the end of the differentiation process (12 DIV).

(E-G) Graph shows the percentage of the NG2-positive cells during the three analysed time point in foetal (red line) and adult (blue line) cultures (E). Images represent foetal (F) and adult (G) cultures at the end of the differentiation process (12 DIV).

(H-J) Graph shows the percentage of the CNPase-positive cells during the three analysed time point in foetal (red line) and adult (blue line) cultures (H). Images represent foetal (I) and adult (J) cultures at the end of the differentiation process (12 DIV).

(K-M) Graph shows the percentage of the MBP-positive cells during the three analysed time point in foetal (red line) and adult (blue line) cultures (K). Images represent foetal (N) and adult (M) cultures at the end of the differentiation process (12 DIV).

Statistical analysis: Two-way ANOVA followed by Tukey's post-hoc. Asteriscs represent differences in the expression at the same time point between foetal and adult cultures (* P < 0.5; ** P < 0.1; *** P < 0.01; **** P < 0.001).

Bars represent mean value + SEM. Statistical analysis: Two-way ANOVA followed by Tukey's post-hoc; * p < 0.05, ** p < 0.01, *** p < 0.001, **** p < 0.0001.

Abbreviations: CNPase, 2',3'-cyclic nucleotide 3'-phosphodiesterase; MBP, myelin basic protein; NG2, chondroitin sulphate proteoglycan, neural/glial antigen 2; PDGFαR, platelet derived growth factor alpha receptor.

Figure 5. Effect of RXRγ gene knock out in NSCs-derived OPCs differentiation

(A) Experimental design: cell morphology and OLs markers expression were analysed in RXR+/+ and RXRγ-/- NSCs-derived OPCs cultures at the end of the differentiation process. Arrow show the time point of the analysis: 12 DIV.

(B-C) Graphs show the percentage of APC-positive (B) and MBP-positive (C) cells in RXRγ+/+ (white column) and RXRγ-/- (grey column), foetal and adult cultures.

(D-K)) Images show APC- (D, E, H, I) and MBP- (F, G, J, K) stained cells in RXRγ+/+ (D-G) and RXRγ -/- (H-K), in foetal (D, H, F, J) and adult (E, I, G, K) cultures.

(L) Graph shows the OPCs/OLs population analysis, based on the APC/Olig1/Olig2 staining. Cells are divided in four different population, with crescent degree of maturation: APC-/Olig1-/Olig2+; APC+/Olig1-/Olig2+; APC+/Olig1+/Olig2+ and APC+/Olig1+/Olig2-.

Statistical analysis: One-way ANOVA followed by Dunnet's post-hoc, on the RXRγ+/+ groups. Asteriscs represent differences between RXRγ-/- and RXRγ+/+ groups (* P < 0.5; ** P < 0.1; *** P < 0.01; **** P < 0.001).

Bars represent mean value + SEM. Statistical analysis: Student's t test (B, C), One-way ANOVA followed by Tukey's post-hoc (L); * p < 0.05, *** p < 0.001, **** p < 0.0001.

Abbreviations. APC, anti-adenomatous polyposis coli; MBP, Myelin basic protein; O1 (Olig1), Oligodendrocyte transcription factor 1; O2 (Olig2), Oligodendrocyte transcription factor 2; OLs, oligodendrocytes.

Figure 6. RXRγ role in differentiation and cell cycle

(A) Experimental design. Foetal RXRγ+/+ and RXRγ-/- cultures gene expression was analysed 0, 6 and 24 (red arrow) hours after T3-induced differentiation. At the last time point

(red arrow) cells were also fixed and stained for PDGFαR and Ki67 in order to analyse the percentage of replicating OPCs. At the end of the differentiation process, cells were fixed and analysed for the percentage of NG2-positive cells in the culture (black arrow).

(B) Gene expression analysis of five key genes involved in the differentiation process: TRa, TRb, Olig1, Olig2, Klf9.
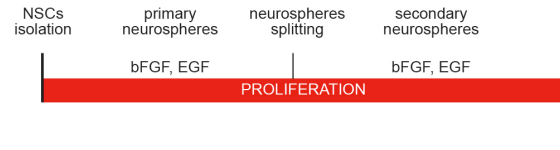
(C-E) Graph shows the percentage of the NG2-positive cells at the end of the differentiation process (12 DIV) in foetal RXRγ+/+ and RXRγ-/- cultures (C). Images represent RXRγ+/+ (D) and RXRγ-/- (E) NG2-stained cultures.

(F-J) Graph shows the percentage of double positive PDGFαR/Ki67 cells on the total number of PDGFαR-positive cells, in vehicle- and T3-treated, RXRγ+/+ and RXRγ-/- cultures (F). Imges show vehicle- (G, H) and T3- (I, J) treated, RXRγ+/+ (G, I) and RXRγ-/- (H, J) cultures.
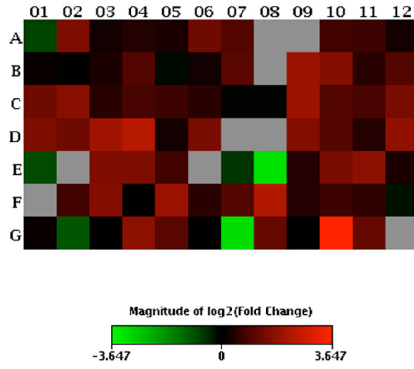
Bars represent mean value + SEM. Statistical analysis: Two-way ANOVA followed by Tukey's post-hoc (B), Student's t test (C), One-way ANOVA followed by Tukey's post-hoc (F); * $p < 0.05$, **** $p < 0.0001$.

Abbrevaitions: *Klf9, kruppel-like factor 9; NG2, chondroitin sulphate proteoglycan, neural/glial antigen 2; Olig1, Oligodendrocyte transcription factor 1; Olig2, Oligodendrocyte transcription factor 2PDGFαR, platelet derived growth factor alpha receptor; TRa, Thyroid hormone receptor alpha; TRb, thyroid hormone receptor beta.*

A

NSCs isolation | primary neurospheres | neurospheres splitting | secondary neurospheres

bFGF, EGF   bFGF, EGF

PROLIFERATION

B

Magnitude of log2(Fold Change)

−3.647   0   3.647

C

Layout	01	02	03	04	05	06	07	08	09	10	11	12
A	Ahr −1.72	Ar 2.88	Arnt 1.18	Brd8 1.33	Cops2 1.27	Crebbp 2.56	Ddx5 1.93	Esr1 −1.34	Esr2 −1.34	Esrra 1.69	Esrrb 1.57	Esrrg 1.19
B	Hdac1 1.13	Hdac2 1.08	Hdac3 1.25	Hdac4 1.94	Hdac5 −1.13	Hdac6 1.18	Hdac7 2.02	Hnf4a −1.34	Itgb3bp 3.91	Kat2b 3.05	Kat5 1.39	Med1 1.94
C	Med12 2.49	Med13 3.20	Med14 1.37	Med16 1.75	Med17 1.60	Med24 1.41	Med4 −1.07	Mta1 −1.08	Ncoa1 3.91	Ncoa2 1.94	Ncoa3 1.77	Ncoa4 2.78
D	Ncoa6 2.94	Ncor1 2.46	Ncor2 4.13	Nfkb2 5.27	Nono 1.19	Notch2 2.82	Nr0b1 −1.34	Nr0b2 −1.34	Nr1d1 3.96	Nr1d2 1.98	Nr1h2 1.33	Nr1h3 3.50
E	Nr1h4 −1.84	Nr1i2 −1.34	Nr1i3 2.86	Nr2c1 2.86	Nr2c2 1.63	Nr2e3 −1.34	Nr2f1 −1.48	Nr2f2 −9.40	Nr2f6 1.31	Nr3c1 2.67	Nr3c2 3.45	Nr4a1 1.22
F	Nr5a1 −1.34	Nr6a1 1.67	Nrip1 3.11	Pgr 1.06	Ppara 3.85	Ppard 1.40	Pparg 1.91	Ppargc1a 5.05	Ppargc1b 1.31	Psmc3 1.57	Psmc5 1.43	Rara −1.18
G	Rarb 1.11	Rarg −2.08	Rbpj −1.00	Rora 3.29	Rxra 2.07	Rxrb 1.03	Rxrg −9.27	Tgs1 2.28	Thra 1.03	Thrb 12.52	Trip4 2.28	Vdr −1.34

DOWN-REGULATED GENES
UP-REGULATED GENES

D

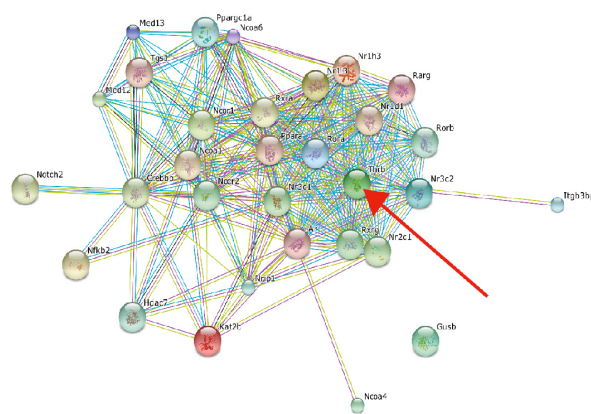| Symbol	Description
Ar	Androgen receptor
Crebbp	CREB binding protein
Hdac7	Histone deacetylase 7
Itgb3bp	Integrin beta 3 binding protein (beta3-endonexin)
Kat2b	K(lysine) acetyltransferase 2B
Med12	Mediator of RNA polymerase II transcription, subunit 12 homolog (yeast)
Med13	Mediator complex subunit 13
Ncoa1	Nuclear receptor coactivator 1
Ncoa4	Nuclear receptor coactivator 4
Ncoa6	Nuclear receptor coactivator 6
Ncor1	Nuclear receptor co-repressor 1
Notch2	Notch gene homolog 2 (Drosophila)
Nr1d1	Nuclear receptor subfamily 1, group D, member 1
Nr1h3	Nuclear receptor subfamily 1, group H, member 3
Nr1i3	Nuclear receptor subfamily 1, group I, member 3
Nr2c1	Nuclear receptor subfamily 2, group C, member 1
Nr2f2	Nuclear receptor subfamily 2, group F, member 2
Nr3c1	Nuclear receptor subfamily 3, group C, member 1
Nr3c2	Nuclear receptor subfamily 3, group C, member 2
Nrip1	Nuclear receptor interacting protein 1
Ncor2	Nuclear receptor co-repressor 2
Nfkb2	Nuclear factor of kappa light polypeptide gene enhancer in B-cells 2, p49/p100
Ppara	Peroxisome proliferator activated receptor alpha
Ppargc1a	Peroxisome proliferative activated receptor, gamma, coactivator 1 alpha
Rarg	Retinoic acid receptor, gamma
Rora	RAR-related orphan receptor alpha
Rxra	Retinoid X receptor alpha
Rxrg	Retinoid X receptor gamma
Tgs1	Trimethylguanosine synthase homolog (S. cerevisiae)
Thrb	Thyroid hormone receptor beta
Trip4	Thyroid hormone receptor interactor 4
Gusb	Glucuronidase, beta

E

Figure 1

104

A

NSCs isolation — primary neurospheres — neurospheres splitting — secondary neurospheres — OPCs seeding — differentiation induction — OPCs differentiation

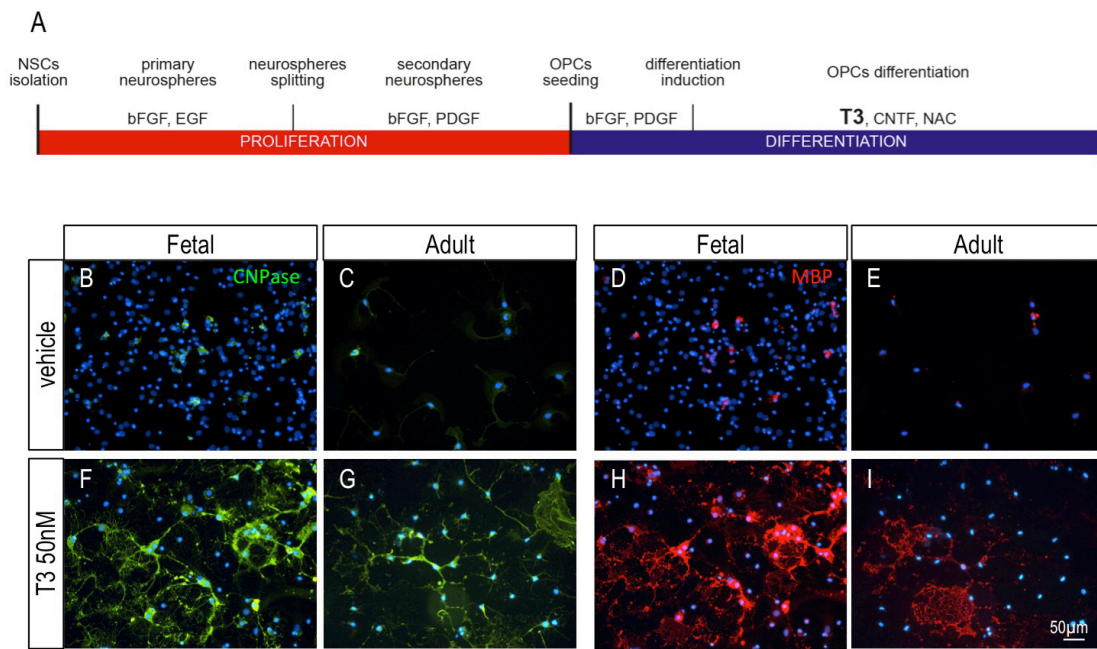bFGF, EGF | bFGF, PDGF | bFGF, PDGF | T3, CNTF, NAC
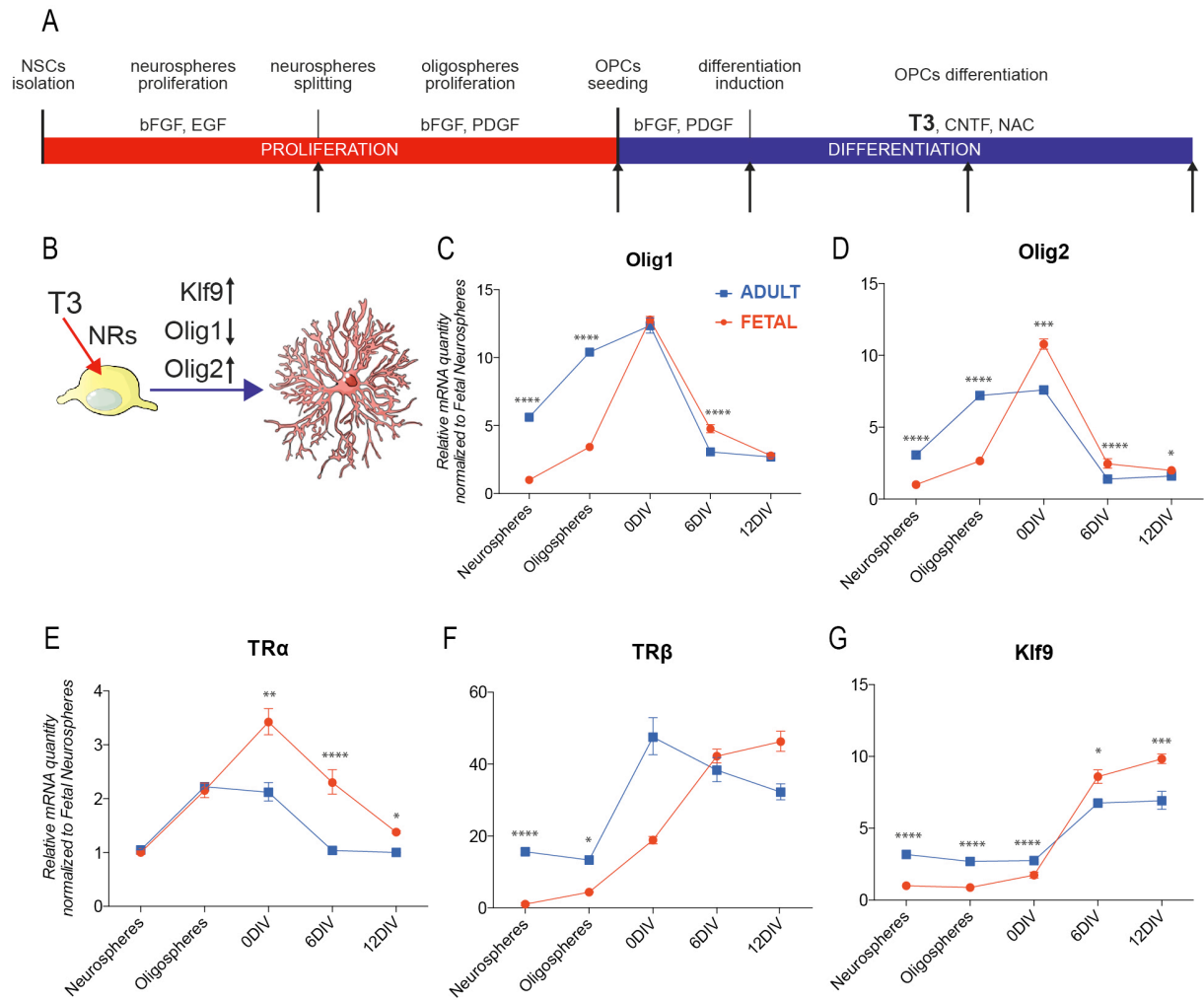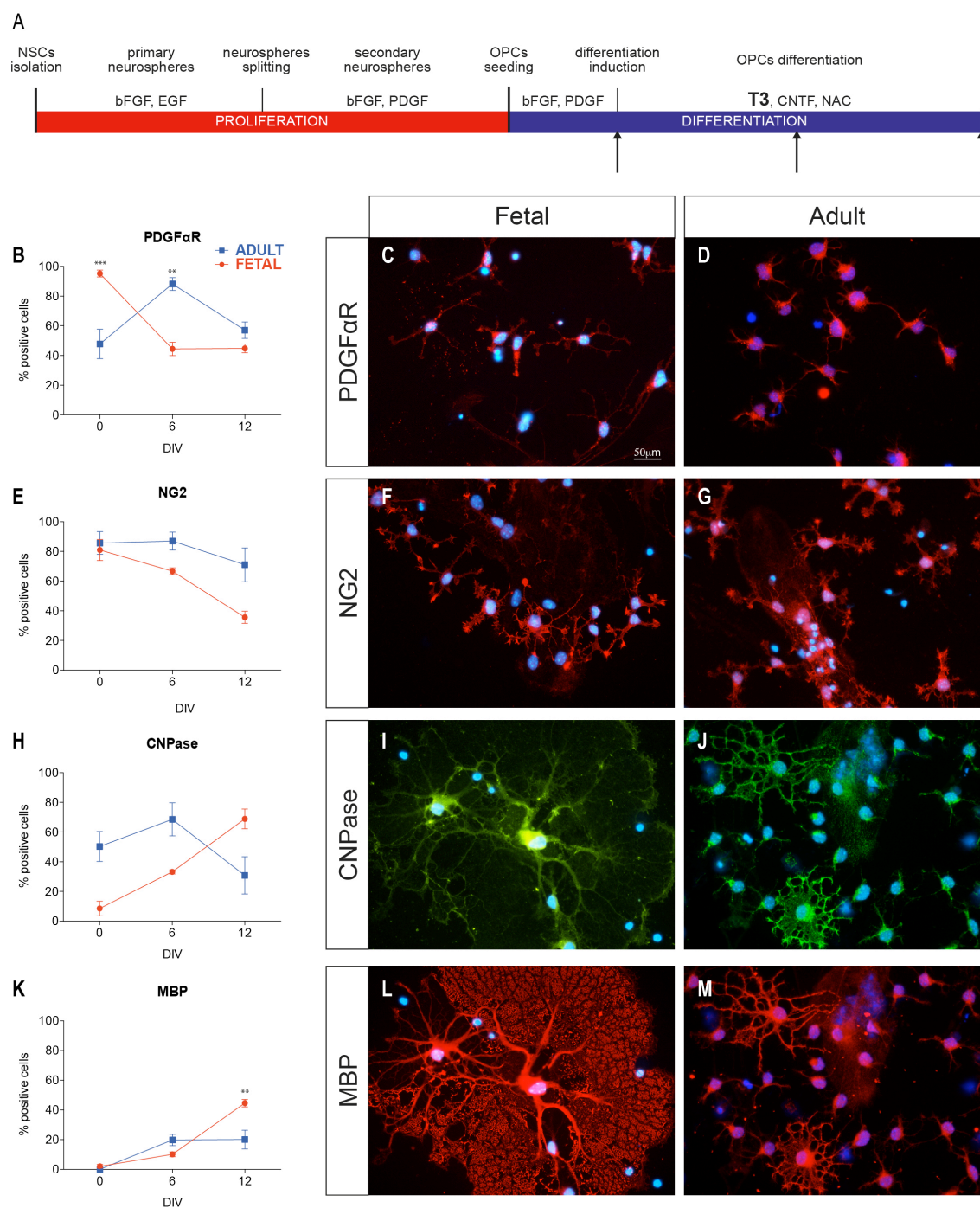
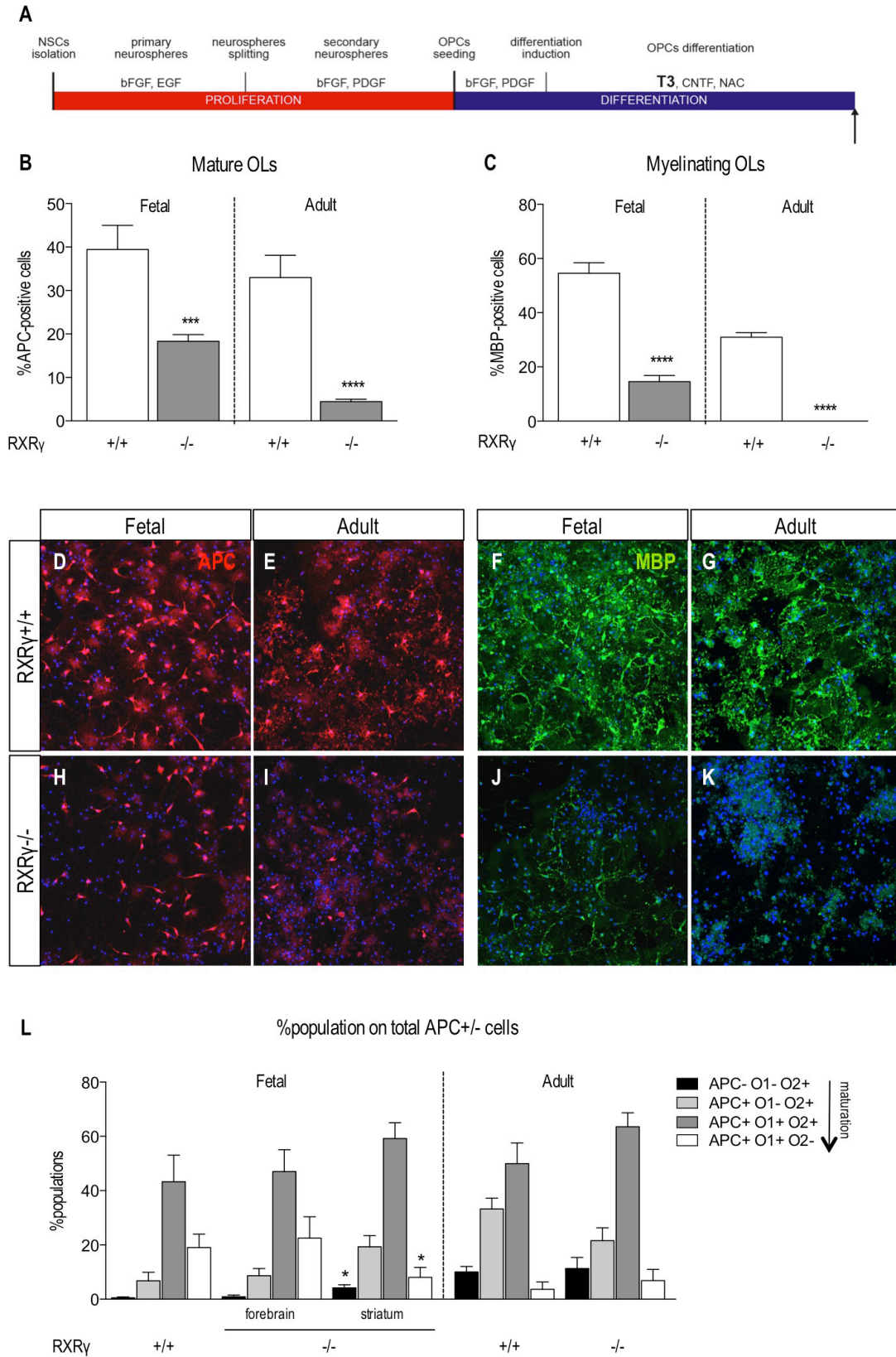PROLIFERATION | DIFFERENTIATION

Figure 2

Figure 3

Figure 4

Figure 5

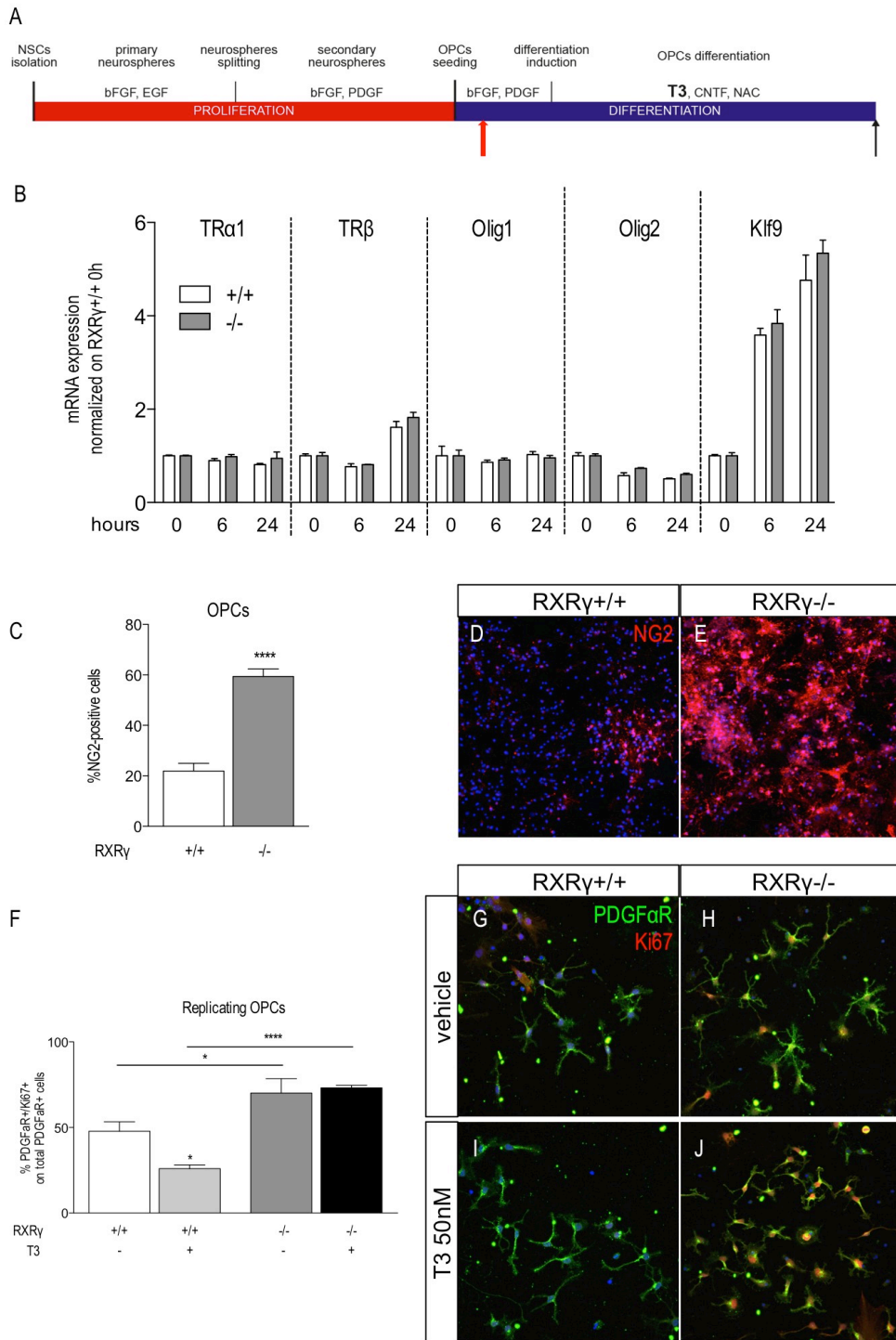*Figure 6*

Supplementary material

GenBank	Symbol	Description
NM_013464	Ahr	Aryl-hydrocarbon receptor
NM_013476	Ar	Androgen receptor
NM_009709	Arnt	Aryl hydrocarbon receptor nuclear translocator
NM_030147	Brd8	Bromodomain containing 8
NM_009939	Cops2	COP9 (constitutive photomorphogenic) homolog, subunit 2 (Arabidopsis thaliana)
NM_001025432	Crebbp	CREB binding protein
NM_007840	Ddx5	DEAD (Asp-Glu-Ala-Asp) box polypeptide 5
NM_007956	Esr1	Estrogen receptor 1 (alpha)
NM_010157	Esr2	Estrogen receptor 2 (beta)
NM_007953	Esrra	Estrogen related receptor, alpha
NM_011934	Esrrb	Estrogen related receptor, beta
NM_011935	Esrrg	Estrogen-related receptor gamma
NM_008228	Hdac1	Histone deacetylase 1
NM_008229	Hdac2	Histone deacetylase 2
NM_010411	Hdac3	Histone deacetylase 3
NM_207225	Hdac4	Histone deacetylase 4
NM_010412	Hdac5	Histone deacetylase 5
NM_010413	Hdac6	Histone deacetylase 6
NM_019572	Hdac7	Histone deacetylase 7
NM_008261	Hnf4a	Hepatic nuclear factor 4, alpha
NM_026348	Itgb3bp	Integrin beta 3 binding protein (beta3-endonexin)
NM_020005	Kat2b	K(lysine) acetyltransferase 2B
NM_178637	Kat5	K(lysine) acetyltransferase 5
NM_013634	Med1	Mediator complex subunit 1
NM_021521	Med12	Mediator of RNA polymerase II transcription, subunit 12 homolog (yeast)
NM_001080931	Med13	Mediator complex subunit 13
NM_012005	Med14	Mediator complex subunit 14
NM_198107	Med16	Mediator complex subunit 16
NM_144933	Med17	Mediator complex subunit 17
NM_011869	Med24	Mediator complex subunit 24
NM_026119	Med4	Mediator of RNA polymerase II transcription, subunit 4 homolog (yeast)
NM_054081	Mta1	Metastasis associated 1
NM_010881	Ncoa1	Nuclear receptor coactivator 1
NM_008678	Ncoa2	Nuclear receptor coactivator 2
NM_008679	Ncoa3	Nuclear receptor coactivator 3
NM_019744	Ncoa4	Nuclear receptor coactivator 4
NM_019825	Ncoa6	Nuclear receptor coactivator 6
NM_011308	Ncor1	Nuclear receptor co-repressor 1
NM_011424	Ncor2	Nuclear receptor co-repressor 2
NM_019408	Nfkb2	Nuclear factor of kappa light polypeptide gene enhancer in B-cells 2, p49/p100
NM_023144	Nono	Non-POU-domain-containing, octamer binding protein
NM_010928	Notch2	Notch gene homolog 2 (Drosophila)
NM_007430	Nr0b1	Nuclear receptor subfamily 0, group B, member 1

NM_011850	Nr0b2	Nuclear receptor subfamily 0, group B, member 2
NM_145434	Nr1d1	Nuclear receptor subfamily 1, group D, member 1
NM_011584	Nr1d2	Nuclear receptor subfamily 1, group D, member 2
NM_009473	Nr1h2	Nuclear receptor subfamily 1, group H, member 2
NM_013839	Nr1h3	Nuclear receptor subfamily 1, group H, member 3
NM_009108	Nr1h4	Nuclear receptor subfamily 1, group H, member 4
NM_010936	Nr1i2	Nuclear receptor subfamily 1, group I, member 2
NM_009803	Nr1i3	Nuclear receptor subfamily 1, group I, member 3
NM_011629	Nr2c1	Nuclear receptor subfamily 2, group C, member 1
NM_011630	Nr2c2	Nuclear receptor subfamily 2, group C, member 2
NM_013708	Nr2e3	Nuclear receptor subfamily 2, group E, member 3
NM_010151	Nr2f1	Nuclear receptor subfamily 2, group F, member 1
NM_009697	Nr2f2	Nuclear receptor subfamily 2, group F, member 2
NM_010150	Nr2f6	Nuclear receptor subfamily 2, group F, member 6
NM_008173	Nr3c1	Nuclear receptor subfamily 3, group C, member 1
NM_001083906	Nr3c2	Nuclear receptor subfamily 3, group C, member 2
NM_010444	Nr4a1	Nuclear receptor subfamily 4, group A, member 1
NM_139051	Nr5a1	Nuclear receptor subfamily 5, group A, member 1
NM_010264	Nr6a1	Nuclear receptor subfamily 6, group A, member 1
NM_173440	Nrip1	Nuclear receptor interacting protein 1
NM_008829	Pgr	Progesterone receptor
NM_011144	Ppara	Peroxisome proliferator activated receptor alpha
NM_011145	Ppard	Peroxisome proliferator activator receptor delta
NM_011146	Pparg	Peroxisome proliferator activated receptor gamma
NM_008904	Ppargc1a	Peroxisome proliferative activated receptor, gamma, coactivator 1 alpha
NM_133249	Ppargc1b	Peroxisome proliferative activated receptor, gamma, coactivator 1 beta
NM_008948	Psmc3	Proteasome (prosome, macropain) 26S subunit, ATPase 3
NM_008950	Psmc5	Protease (prosome, macropain) 26S subunit, ATPase 5
NM_009024	Rara	Retinoic acid receptor, alpha
NM_011243	Rarb	Retinoic acid receptor, beta
NM_011244	Rarg	Retinoic acid receptor, gamma
NM_009035	Rbpj	Recombination signal binding protein for immunoglobulin kappa J region
NM_013646	Rora	RAR-related orphan receptor alpha

NM_011305	Rxra	Retinoid X receptor alpha
NM_011306	Rxrb	Retinoid X receptor beta
NM_009107	Rxrg	Retinoid X receptor gamma
NM_054089	Tgs1	Trimethylguanosine synthase homolog (S. cerevisiae)
NM_178060	Thra	Thyroid hormone receptor alpha
NM_009380	Thrb	Thyroid hormone receptor beta
NM_019797	Trip4	Thyroid hormone receptor interactor 4
NM_009504	Vdr	Vitamin D receptor
NM_007393	Actb	Actin, beta
NM_009735	B2m	Beta-2 microglobulin
NM_008084	Gapdh	Glyceraldehyde-3-phosphate dehydrogenase
NM_010368	Gusb	Glucuronidase, beta
NM_008302	Hsp90ab1	Heat shock protein 90 alpha (cytosolic), class B member 1

Table 1 Gene list of the PCRarray for Nuclear Receptors and co-regulators

GenBank codes, genes symbol and descriptionof gene analysed by PCR array for Nuclear Receptors and co-regulators (Figure 1) are listed in the table.

4.3 In Vitro Testing of Biomaterials for Neural Repair: Focus on Cellular Systems and High-

Content Analysis (Baldassarro et al., 2016).

ORIGINAL RESEARCH ARTICLE   **Open Access**

In Vitro Testing of Biomaterials for Neural Repair: Focus on Cellular Systems and High-Content Analysis

Vito Antonio Baldassarro,[1,2] Luisa Stella Dolci,[1,2] Chiara Mangano,[1] Luciana Giardino,[1,3] Chiara Gualandi,[4] Maria Letizia Focarete,[1,4] and Laura Calzà[1,2,*]

Abstract

Biomimetic materials are designed to stimulate specific cellular responses at the molecular level. To improve the soundness of *in vitro* testing of the biological impact of new materials, appropriate cell systems and technologies must be standardized also taking regulatory issues into consideration. In this study, the biological and molecular effects of different scaffolds on three neural systems, that is, the neural cell line SH-SY5Y, primary cortical neurons, and neural stem cells, were compared. The effect of poly(L-lactic acid) scaffolds having different surface geometry (conventional two-dimensional seeding flat surface, random or aligned fibers as semi3D structure) and chemical functionalization (laminin or ECM extract) were studied. The endpoints were defined for efficacy (i.e., neural differentiation and neurite elongation) and for safety (i.e., cell death/survival) using high-content analysis. It is demonstrated that (i) the definition of the biological properties of biomaterials is profoundly influenced by the test system used; (ii) the definition of the *in vitro* safety profile of biomaterials for neural repair is also influenced by the test system; (iii) cell-based high-content screening may well be successfully used to characterize both the efficacy and safety of novel biomaterials, thus speeding up and improving the soundness of this critical step in material science having medical applications.

Keywords: Good Laboratory Practice guidelines; neural cell lines; neural primary culture; neural stem cells high-content analysis; poly(lactic acid)

Introduction

The potential applications of tissue engineering products for regenerative medicine in acute and chronic diseases of the nervous system are quite wide. There is an extensive literature aimed to compare the biological impact of different scaffolds for neural repair, considering the chemical composition of the materials, architecture, functionalization, etc.[1] However, these studies often brought to contradictory results when translated in animals, and this could be at least partially due to the different cell systems and readout technologies used.[2] In fact, key biological differences in the cellular test systems (i.e., cellular composition, maturation time, culture media composition, growth factor pro-

duction, etc.) make it very hard to compare results and judge the "biomaterial effect on neural cells".[3,4]

Therefore, in this work we compared the biological and molecular effects of different materials on three cell systems commonly used for these purposes, that is, the neural cell line SH-SY5Y, primary cortical neurons, and neural stem/precursor cells (NSC). We investigated glass substrates and poly(L-lactic acid) (PLLA) scaffolds having different surface geometry (conventional two-dimensional seeding [2D] flat surface, random or aligned fibers as semi3D structure) and chemical functionalization (laminin or ECM extract).

We investigated defined endpoints for efficacy (i.e., neural differentiation and neurite elongation) and

[1]Health Sciences and Technologies—Interdepartmental Center for Industrial Research (HST-ICIR), University of Bologna, Bologna, Italy.
Departments of [2]Pharmacy and Biotechnology (FaBit), [3]Veterinary Medical Science, University of Bologna, Bologna, Italy.
[4]Department of Chemistry "G. Ciamician" and National Consortium of Materials, Science, and Technology (INSTM, Bologna RU), University of Bologna, Bologna, Italy.

*Address correspondence to: Laura Calzà, MD, Health Sciences and Technologies—Interdepartmental Center for Industrial Research (HST-ICIR), University of Bologna, Via Tolara di Sopra 41/E, Ozzano Emilia I-40064, Italy, E-mail: laura.calza@unibo.it

safety (i.e., cell death/survival). We also introduced high-content analysis compared with conventional biochemical and morphological readout methods, and the international guidelines for the "mutual acceptance of data" for safety/toxicology tests (Organization for Economic Co-operation and Development–OECD-).[5,6]

Materials and Methods
Detailed methods are provided in the Supplementary Data, Materials and Methods section.

Materials
PLLA (Lacea H.100-E) ($M_w = 8.4 \times 10^4$ g/mol, PDI = 1.7) was supplied by Mitsui Fine Chemicals. Dichloromethane (DCM), dimethylformamide, dimethyl sulfoxide, bovine serum albumin, laminin 1 mg/mL, Triton, paraformaldehyde, retinoic acid (RA), penicillin, and streptomycin were purchased from Sigma-Aldrich and were used without any further purification. Hoechst 33258, Cultrex® basement membrane extract (Trevigen®), DMEM-F12, 1X Minimum Essential Medium/Non Essential Aminoacids, and 1X Penicillin–Streptomycin purchased from Gibco-Invitrogen, fetal bovine serum (Euroclone), and NaOH 10 mM (Carlo Erba) were used.

Cell substrates fabrication, characterization, and chemical functionalization
PLLA films were prepared by the solvent cast method, from a 10% w/v polymer solution in DCM at room temperature. Electrospun scaffolds were fabricated by using a commercial electrospinning machine equipped with a temperature and humidity control system (Spinbow S.r.l.). The electrospun scaffolds were characterized by means of scanning electron microscopy (SEM) and static water contact angle (WCA) measurements.

Electrospun PLLA random and aligned scaffolds, and PLLA-film were cut and assembled by means of CellCrown supports (Scaffdex) in a 24-well. Cover glasses and electrospun were sterilized and functionalized with laminin and Cultrex BME.

Cell cultures
Human neuroblastoma SH-SY5Y cells were differentiated on different surfaces (Cultrex-coated glass, laminin-coated glass, laminin-coated or not PLLA-FILM, laminin-coated or not random and aligned electrospun PLLA scaffold) using 10 μM RA and cultured for 7 days.

Primary neurons were isolated from newborn mice cortex and cytosine-arabinofuranoside (10 μM; Sigma) was added to the culture medium, to inhibit proliferation of the glial cells,[7] and cultured for 15 days.

NSCs were obtained from embryos forebrain and secondary neurospheres were dissociated and plated at a density of 1×10^4 cells/cm^2 in the same culture medium without mitogens.[8,9] To achieve full lineage commitment and cell differentiation, seeded cells were cultured for 15 days.

Animal care and treatment were in accordance with the EU Directive 2010/63/EU and approved by the Ethics Committee of Animal Experimentation, University of Bologna.

Viability assays
Cell viability was determined by high-content analysis (HCS) as the percentage of pyknotic nuclei calculated by Cellomics® Compartmental Analysis BioApplication, using "population characterization" parameter. MTT assay was performed on primary cortical neurons seeded on 2D Cultrex-coated surface and semi3D-aligned uncoated scaffolds. Absorbance was measured at 570 nm.

Immunocytochemistry
Cells were fixed with 4% paraformaldehyde. Cell-specific proteins were identified by indirect immunofluorescence using mouse anti-β-III-tubulin (1:2000; R&D Systems); rabbit anti-GFAP (1:500; Dako) and rabbit anti-MBP (1:250; Dako) antisera. The anti-rabbit DyLight 568- and anti-mouse AlexaFluor 488-labeled (1:500; Invitrogen) were used as secondary antisera. For nuclear staining, cells were incubated with 1 μg/mL Hoechst 33258.

Fluorescence microscopy, image analysis, and HCS
Fluorescence images were taken with 10X objective (10X/0.45 N.A. Plan Fluor Nikon) using NIKON Eclipse E600 (Nikon) equipped with digital CCD camera QImaging Retiga 20002V (QImaging), and analyzed using Imaging NIS Elements software (Nikon). To analyze neurites outgrowth of SH-SY5Y cells, the length of individual neurites in each acquired images was measured. Each sample was repeated twice and data were expressed as mean length ± SEM.

HCS was performed using CellInsight NXT (Thermo Scientific) equipped with digital CCD camera Photometric X1. All images were taken with 10X objective (10X/0.30 N.A. Plan Fluor Olympus) using 4×4 binning (552×552) and analyzed using Cellomics Scan Version 6.4.4 (Thermo Scientific). For each well

examined, multiple fields were sampled. Within each field, matched fluorescent images of Hoechst-labeled nuclei, β-III-tubulin/AlexaFluor 488-labeled cells were acquired using 386/23 (Channel1), 485/20 (Channel2) filters, respectively. Neurite analysis was performed with Cellomics Neuronal Profiling BioApplication. Identification of nuclei, cell bodies, and neurites was optimized using 10 representative images for each condition tested.

Lineage analysis was performed by Cellomics Compartmental Analysis BioApplication, using "population characterization." After the nuclei identification, the user chooses the area around the nucleus and the fluorescence intensity threshold.

Statistical analysis

The study design included at least three independent experiments and data reported in graphs are the mean $\pm$ standard deviation (SD) of the different experiments. Statistical testing was performed with ANOVA followed by appropriate *post-hoc* multiple comparisons test (see legend to the figures for details). Student's *t*-test was also used. A probability level of $p < 0.05$ was considered to be statistically significant.

Results

The following variables were included in the study: (A) *materials and topography of cell substrates*: conventional glass/plastic 2D, semi three-dimensional random electrospun PLLA scaffolds (semi3D, random) and semi three- dimensional aligned electrospun PLLA scaffolds (semi3D, aligned); (B) *substrate chemical functionalization*: no-coating, laminin coating of the above materials and whole ECM extract coating of the above materials; (C) *neural cell type*: SH-SY5Y neural differentiated cell line, primary cortical neurons, and neural stem cells; (D) *assay and technologies for toxicology testing*: conventional low-throughput and cell-based high throughput screening.

Scaffold fabrication and chemical functionalization

PLLA films and electrospun fibrous scaffolds were fabricated to study the influence of substrate topography on neuron viability and differentiation. Scaffolds made of random and aligned fibers were compared (Fig. 1A,B). PLLA fibers without bead defects were obtained with comparable micrometric mean diameters (semi3D-random: $1.8 \pm 0.4 \, \mu$m; semi3D-aligned: $1.8 \pm 0.6 \, \mu$m). To improve wettability and, thus, biocompatibility of the polymer, electrospun scaffolds

were coated with ECM proteins, that is, laminin (Fig. 1C), and the ECM extract Cultrex containing laminin, collagen IV, entactin, and heparin sulfate proteoglycan (Fig. 1D).

In both cases, the morphology of the coated fibers did not appear to be significantly altered by the ECM proteins, and the coating was found to cover quite homogeneously the fiber surface (Fig. 1K,N), without modifying the porous structure of the scaffold.

To investigate the surface hydrophilicity of the scaffolds, WCA measurements were performed and results are shown in Figure 2A,B, where the mean WCA values are reported for all investigated samples, together with the representative behavior of the WCA versus time for selected samples and the water drop images corresponding to a highly hydrophobic (top), intermediate (middle), and hydrophilic (bottom) scaffold. As expected, the semi3D-random and the semi3D-aligned electrospun scaffolds show a similar hydrophobic behavior with a WCA higher than that of the corresponding PLLA film (Fig. 2A), due to their high porosity and air entrapment into pores. Laminin and ECM treatment dramatically lowered the WCA of the electrospun scaffolds (Fig. 2A,B), whereas the laminin coating of the PLLA film increased only slightly the hydrophilicity (Fig. 2A). In the semi3D-laminin-coated scaffold and semi3D-Cultrex-coated scaffold the water drop was spread out instantaneously and immediately penetrated into the scaffold, resulting in a change of the WCA from about 120° to about 20° (or lower) in less than 10 sec.

Figure 1E–P illustrates cell deposition (SH-SY5Y) on the semi3D-uncoated (E–J) and laminin-coated (K–P) PLLA scaffolds, having random (E–G; H–J) and aligned (K–M; N–P) topography, as visualized by conventional microscopy (E, H, K, N) and HCS (F, G, I, J, L, M, O, P).

Scaffolds and neural differentiation

The biological properties of the three different neural systems included in the study were compared on the different 2D/ semi3D substrates and functionalization, in the same experimental assay and using high-throughput analysis. Neurite elongation was taken as primary endpoint for morphological maturation using the cytoskeleton marker β-III-tubulin.

The use of HCS automatic procedure versus conventional computerized morphometry was first validated on semi3D cell systems using SH-SY5Y grown on laminin-coated and uncoated random electrospun scaffolds (Fig. 3A). For conventional morphometry,
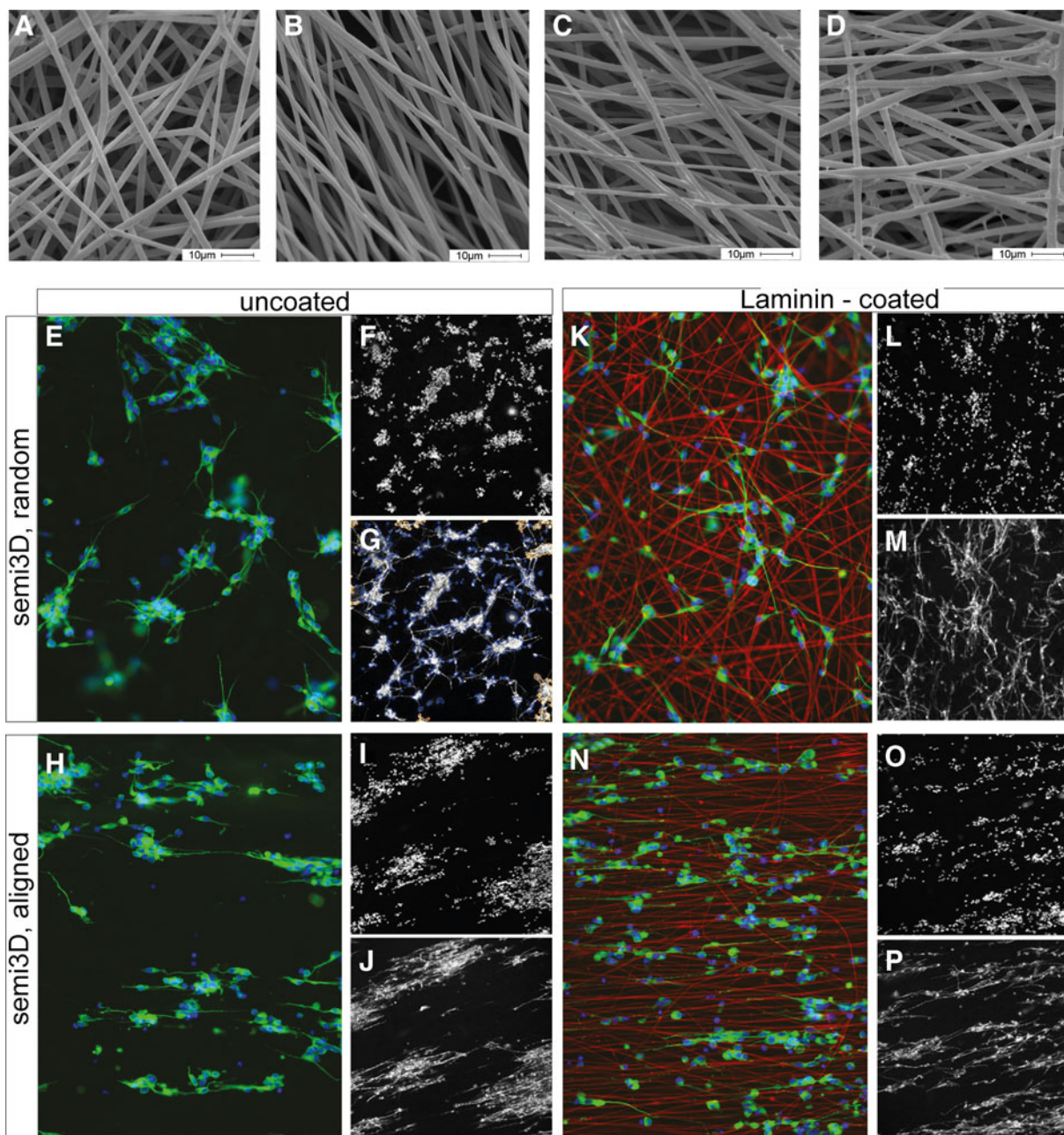
FIG. 1. Scaffold characterization: morphology and cell seeding. SEM micrographs of **(A)** semi3D-random scaffold; **(B)** semi3D-aligned scaffold; **(C)** semi3D-random scaffold coated with laminin; **(D)** semi3D-random scaffold coated with Cultrex. Scale bar: 10 μm. **(E–P)** Conventional fluorescence micrographs showing the SH-SY5Y cell deposition (labeled by β-III-tubulin) on the semi3D uncoated **(E–J)** and laminin-coated **(K–P**; laminin is in red**)** PLLA scaffolds, having random **(E–G; K–M)** and aligned **(H–J; N–P)** topography **(E, H, K, N)**; HCS visualization of the same cell preparations (semi3D, uncoated, random: **F,G**; semi3D, uncoated, aligned: **I,J**; semi3D, laminin-coated, random: **L,M**; semi3D, laminin-coated, aligned: **O,P**). HCS, high-content analysis; PLLA, poly(L-lactic acid); SEM, scanning electron microscopy.
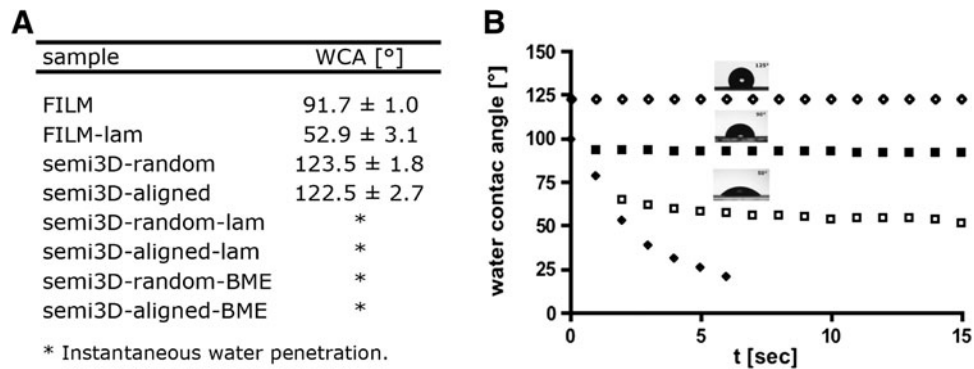
FIG. 2. Scaffold characterization: wettability. **(A)** mean WCA values; **(B)** representative WCA behavior for semi3D-random scaffold (white diamonds), semi3D-random scaffold laminin coated (black diamonds), PLLA-FILM (black squares) and PLLA-FILM laminin coated (white squares); representative images of the water drop are also reported. WCA, water contact angle.
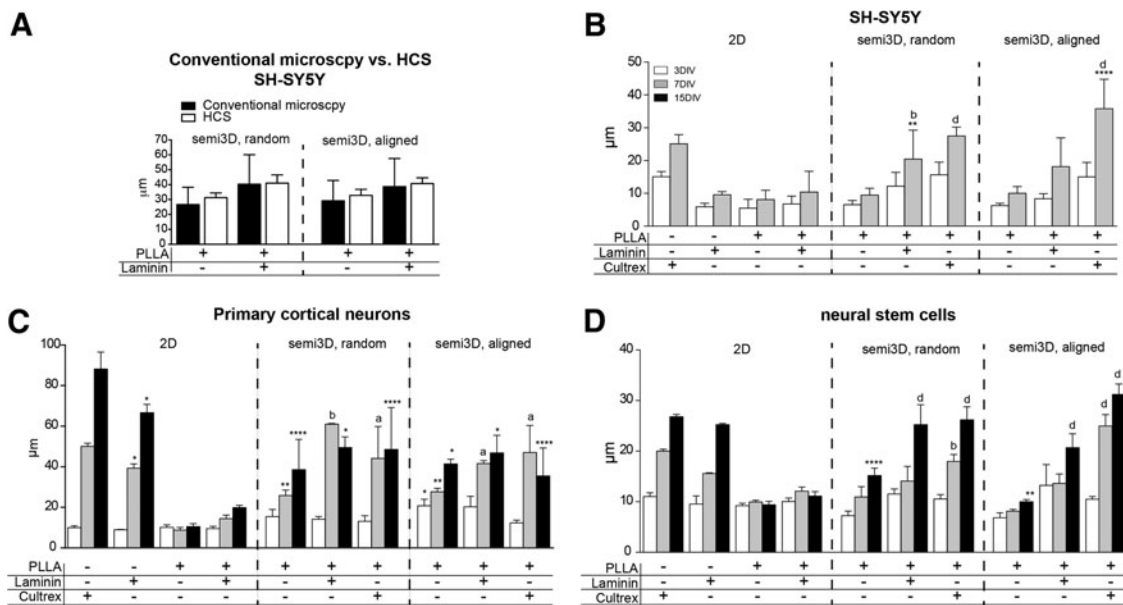

FIG. 3. Effect of different scaffolds on neural differentiation. **(A)** Neurite length of SH-SY5Y cells grown on different scaffolds, as measured by conventional quantitative microscopy and HCS. **(B)** Neurite length of SH-SY5Y cell line, as measured by HCS; **(C)** Neurite length of primary cortical neurons, as measured by HCS; **(D)** Neurite length of neurons derived from NSCs, as measured by HCS. In all cell systems, conventional 2D, semi3D-random and semi3D-aligned scaffolds having different coatings are compared. Data are expressed as mean $\pm$ SD, and represent the mean of three independent experiments. Statistical analysis: two-way ANOVA (SH-SY5Y F[9, 100] = 5.165; primary cortical neurons F[14,45] = 6.317; NSCs F[18,60] = 15.40) followed by Tukey's *post hoc* test. Asterisks represent the difference between the semi3D group versus the relative 2D control group within the same DIV (*$p < 0.05$; **$p < 0.01$; ***$p < 0.001$; ****$p < 0.0001$), letters indicate the difference between coated semi3D groups versus the relative uncoated semi3D control group (a = $p < 0.05$; b = $p < 0.01$; d = $p < 0.0001$). 2D, two-dimensional seeding; SD, standard deviation.

at least nine different fields were taken to obtain a minimum number of 300 neurites (200 cells), whereas for HCS analysis all the cells (a mean of 100,000 cells) were analyzed. The mean length of neurites obtained with the two techniques was equivalent and, as expected in view of the larger number of cells analyzed, the SD derived from HCS analysis was four times smaller compared with conventional morphometry.

We then compared the neurite elongation of the three different neural cells by using HCS. Results are presented in Figure 3, where panel B refers to SH-SY5Y, panel C to primary neurons, and panel D to neural stem cells. In each graph, results are grouped according to the topographic conditions (2D, semi3D random, semi3D aligned), chemical functionalization (PLLA alone, laminin, Cultrex, as indicated in the graphs), and maturation times (3, 7, 15DIV). The statistical analysis is reported in the figure legend.

In all topographic conditions PLLA alone impairs neurite elongation in all cell systems, whereas chemical functionalization with ECM extract favors neurite elongation of both SH-SY5Y and NCSs, an effect that is maximized by alignment. Conversely and regardless of the chemical coating of the PLLA scaffold, semi3D topography impairs maturation of primary cortical neurons. Actually, while SH-SY5Y cells attach to 2D PLLA and then survive, primary neurons and NSC do not attach to 2D PLLA. Notably, semi3D topography seems to overcome this problem even in the absence of chemical coating with ECM extracts or proteins. Moreover, aligned PLLA clearly directs the neurite elongation in a fashion parallel to the fibers.

Scaffolds and glial/neuronal lineage

The capability of PLLA to influence cell lineage in primary cultures (Supplementary Fig. S1) and NSCs (Fig. 4) was then investigated, both as a chemical entity and as regards the topographic arrangement. In both cell systems, the semi3D PLLA arrangement strongly increases the percentage of astrocyte (GFAP-positive cells) in the culture, both at early (3DIV) and late (7DIV) time in culture. Chemical functionalization does not substantially modify the astroglial fate from NSC, whereas it decreases the PLLA effect in primary neurons. In the same experimental conditions, also the oligodendroglial lineage and maturation was analyzed by evaluating the percentage of cells expressing MBP, which is a protein expressed in terminally differentiated oligodendrocytes (Fig. 5). First of all, it was observed

that the PLLA coating of 2D substrate completely prevents adhesion of oligodendrocyte precursors, and so no mature cells are observed. Semi3D topography allows a better adhesion, and Cultrex coating maximizes the effect of topography. However, it should be mentioned that the culture conditions were optimized for neural differentiation, and so chemical agents known to improve oligodendroglial lineage and maturation were not included in the culture medium.

Effect of scaffolds on cell viability

Safety and toxicology testing is a critical step in the biomaterials development as required by the regulatory agencies. We first evaluated the possibility of applying HCS to semi3D cell systems to determine cell viability compared with conventional biochemical methods. Both MTT and HCS-based nuclear morphology indicate that the semi3D-aligned fibers strongly reduce cell survival (Supplementary Fig. S2). HCS was then used to study the toxicity of materials on SH-SY5Y, primary neurons, and neural stem cells, by evaluating the percentage of pyknotic nuclei over all seeded cells. Results are presented in Figure 6, grouped according to the effect of different scaffolds and substrates on SH-SY5Y (A), primary cortical neurons (B), and neural stem/progenitor cells (C). A mean of 300,000 cells/wells, three wells/condition were included in the analysis (mean cell number in each analysis was 900,000 cells/group). In 2D conventional culture conditions, cells from the different systems display substantial differences in viability. Viability of SH-SY5Y cells is not affected by any of the investigated experimental conditions (Fig. 6A), whereas primary cortical neurons show a higher spontaneous cell death even when grown in ideal culture conditions (Cultrex) (percentage of pyknotic nuclei on 2D Cultrex-coated glass: SH-SY5Y 0.26 ± 0.07; primary cortical neurons 9.10 ± 0.59; $p < 0.0001$). The impact of semi3D topography on cell viability was then examined by comparing the semi3D (e.g., PLLA scaffolds) versus the relative 2D (e.g., conventional glass/plastic seeding) control group at the same DIV (asterisks), whereas the effect of the coating was analyzed by comparing the semi3D-coated versus the related uncoated semi3D control group (letters), by one-way ANOVA followed by the Tukey's test. When using NSCs as cell system, a dramatic effect of semi3D PLLA scaffold on cell viability is observed in fully differentiated cells, when PLLA random and aligned fiber distribution causes 20% and 40% cell death, respectively (Fig. 6C). Notably, both laminin
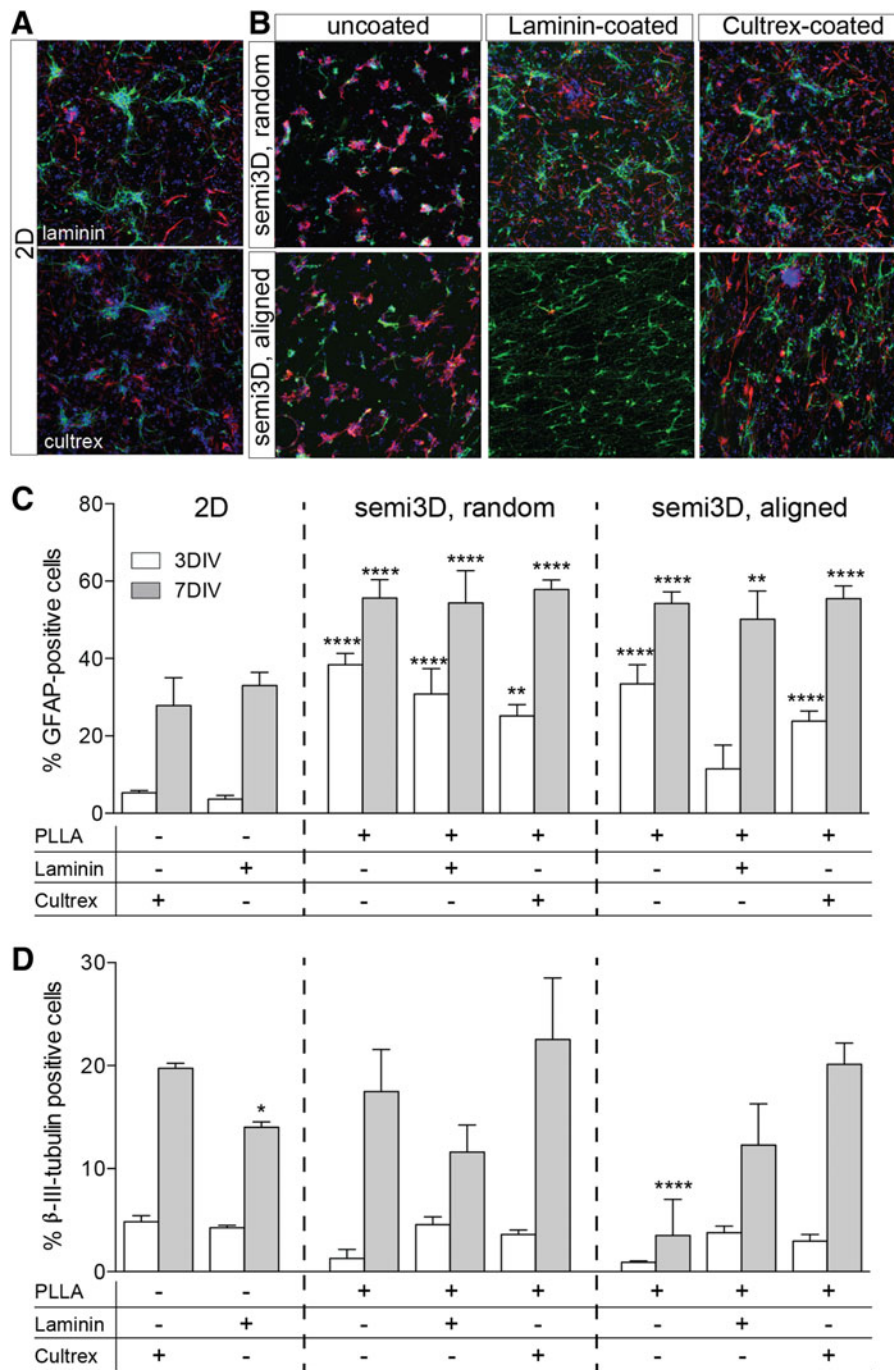
FIG. 4. Effect of different scaffolds in the neural and astroglial specification of NSCs. **(A, B)** Representative images of plated NSCs at 7DIV grown on 2D **(A)** and semi3D scaffolds **(B)**, stained with β-III-tubulin (green), GFAP (red) and Hoechst (blue). **(C, D)** The graphs indicate the percentage of GFAP **(C)** and β-III-tubulin **(D)**-positive cell, according to the PLLA topography and coating. Data are expressed as mean $\pm$ SD, and represent the mean of three independent experiments. Statistical analysis: two-way ANOVA (GFAP $F[7, 32] = 3.404$; β-III-tubulin $F[7, 30] = 7.136$) followed by Tukey's post test. Asterisks represent the difference between the semi3D group versus the relative 2D control group within the same DIV (*$p < 0.05$; **$p < 0.01$; ***$p < 0.001$; ****$p < 0.0001$).
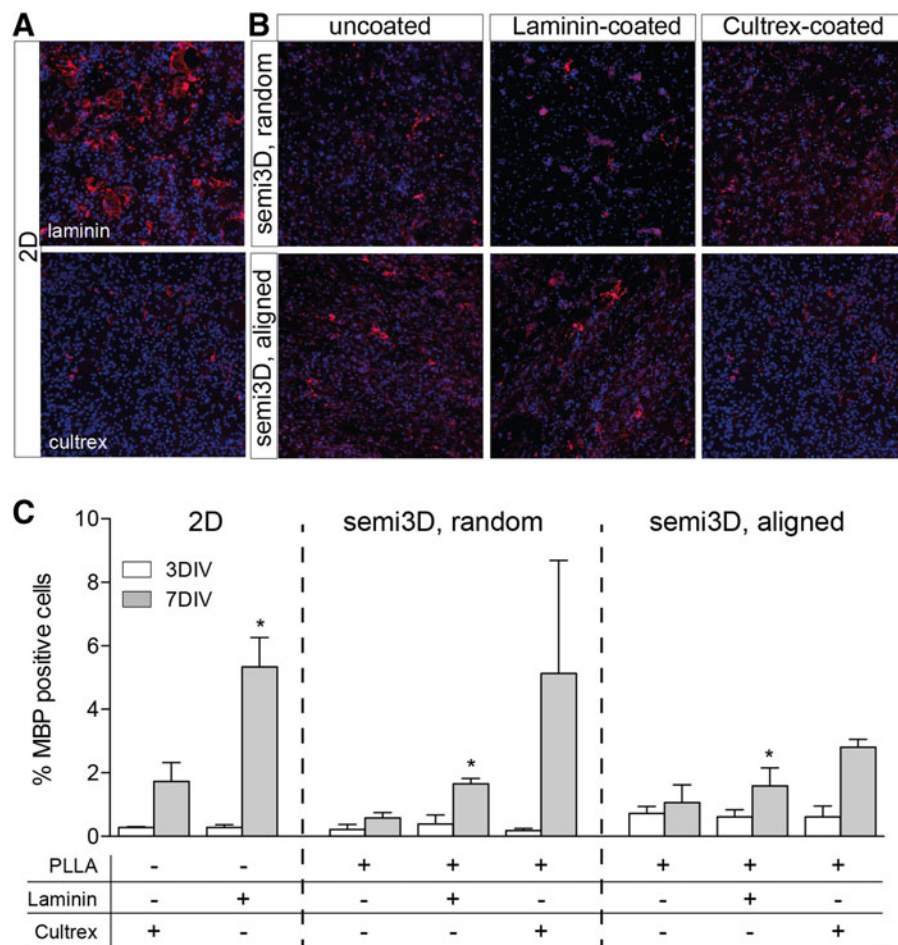
FIG. 5. Effect of different scaffolds on oligodendroglial specification of NSCs. **(A, B)** Representative images of plated NSCs at 7DIV grown on 2D **(A)** and semi3D scaffolds **(B)**, stained with MBP (red) and Hoechst (blue). **(C)** The graph represents the percentage of MBP positive cells. Data are expressed as mean $\pm$ SD, and represent the mean of three independent experiments. Statistical analysis: two-way ANOVA (F[7, 28] = 4.739) followed by Tukey's post test. Asterisks represent the difference between the semi3D group versus the relative 2D control group within the same DIV (*$p < 0.05$; **$p < 0.01$; ***$p < 0.001$; ****$p < 0.0001$).

and Cultrex functionalization protects cell viability almost completely.

Discussion

In this study, we showed that the effect of biomaterials on both neuron viability and differentiation is strongly influenced by the cellular system used for the test. We also showed that cell-based HCS technology can be applied to biomaterial *in vitro* testing, thus improving robustness and statistical consistency of the results.

The right cell-culture has actually been recognized as one of the six most important technical determinants of project success and pipeline quality by the pharmaceutical industry.[10] We then tested the effect of PLLA scaffold on viability and differentiation using three cell systems widely used in the field, that is, the SH-SY5Y cell line, cortical primary neurons, and neural stem cells. The SH-SY5Y neuroblastoma cell line is derived from human tissue, can be easily differentiated toward a neuronal-like cell line, and is a widely available, easy-to-handle, and highly reproducible system.[11] However, its sensitivity to a wide range of toxic stimuli is lower compared with primary neurons,[12] and neurite outgrowth may be different from that occurring in primary neurons.[13,14] Primary neurons and neural stem cells are more physiologically significant and the possibility of
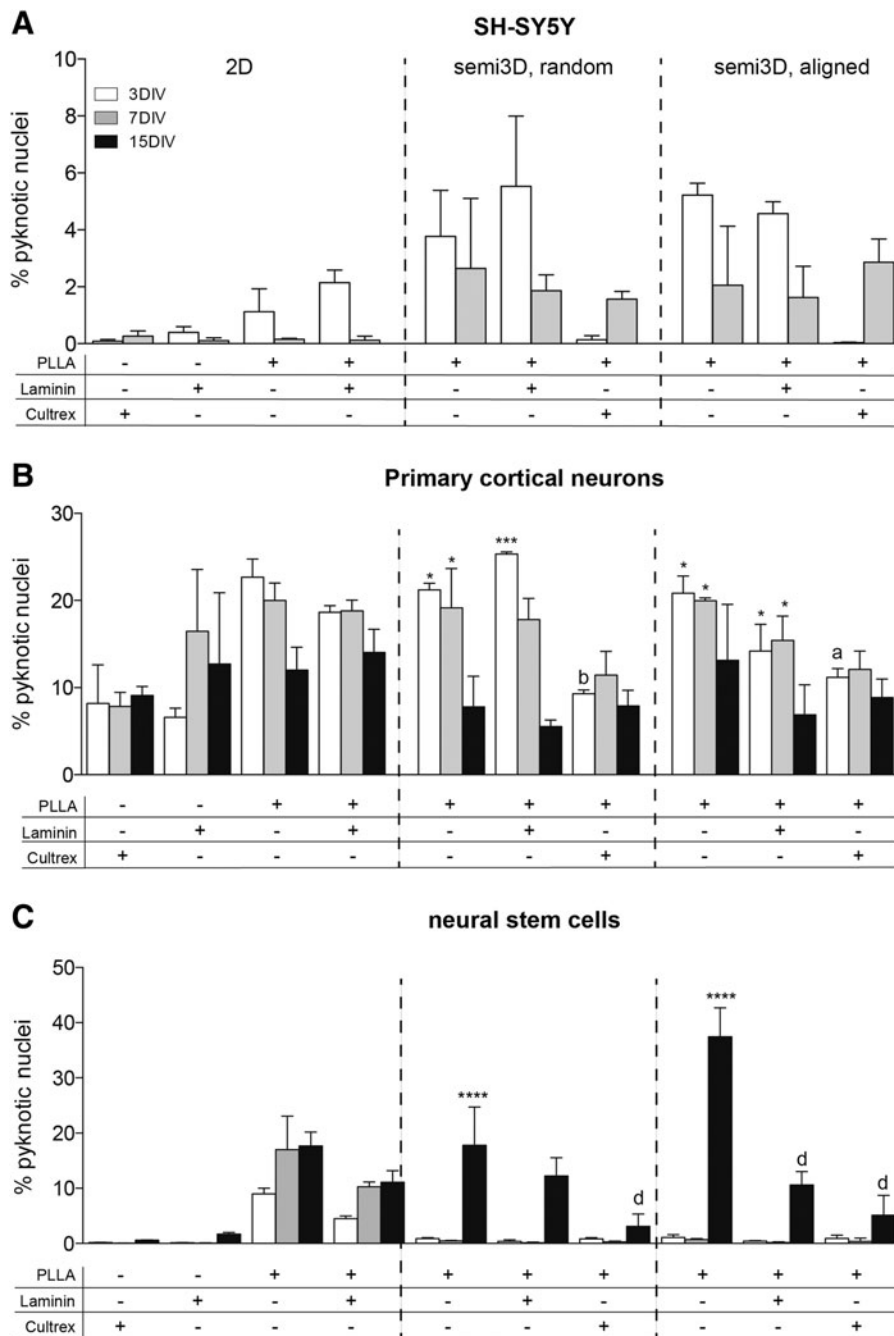
FIG. 6. Effect of different scaffolds on cell viability of SH-SY5H cell line **(A)**, primary cortical neurons **(B),** and NSCs **(C)**. The graphs represent the percentage of pyknotic nuclei measured using HCS technology. Data are expressed as mean ± SD, and represent the mean of three independent experiments. Statistical analysis: two-way ANOVA ($n = 3$; SH-SY5Y $F[9, 60] = 5.682$; primary cortical neurons $F[14, 40] = 4.164$; NSCs $F[18, 60] = 23.57$) followed by Tukey's post test. Asterisks represent the difference between the semi3D group versus the relative 2D control group within the same DIV (*$p < 0.05$; ***$p < 0.001$; ****$p < 0.0001$), letters indicate the difference between coated semi3D groups versus the relative uncoated semi3D control group (a = $p < 0.05$; b = $p < 0.01$; d = $p < 0.0001$).

false positives and negatives is smaller compared with cell lines, thus meeting the basic requirement for *in vitro* safety testing, that is, to represent the *in vivo* situation as closely as possible. However, both require selective skills for handling and result interpretation.[15,16]

The most relevant result from this study is the different safety profiles of the same biomaterial obtained using different neural systems. While viability of SH-SY5Y cells is not modified by the substrates, either primary neurons and neurons derived from stem cell showed a very high degree of mortality on PLLA, that is almost completely prevented by chemical coating with ECM proteins. This result also has implications to establish the appropriate guidelines to test the safety-profile of the materials and fabrication for regulatory decision makers.[3,17]

On the contrary, the effect of PLLA scaffold on differentiation, as established by neurite elongation and branching, is quite similar in all neural cell types. In particular, it was demonstrated that all three cell systems are negatively affected by the PLLA uncoated scaffolds in terms of neurite length, but that ECM protein coating differentially affects the neuron maturation process. Cultrex coating strongly favors neurite elongation of SH-SY5Y cells on semi3D scaffolds, whereas semi3D surfaces, whether coated or not, negatively affect the neurite elongation of primary cortical neurons. Conversely, PLLA scaffolds impair the neurite elongation of neurons derived from NSCs, but this effect is exceeded by Cultrex coating. As already reported,[18–20] aligned fibers display the best ability to guide cell orientation. Our results confirm that the incorporation of ECM molecules favors biological processes, such as cell adhesion, neurite elongation, and cell differentiation.[21–27]

However, the different cell compositions in primary cultures and NSC might also be considered. Primary neurons and NSC-derived neurons contain a different percentage of astrocytes, also according to the chemistry and topography of the substrate. In the same conditions in which we observed an increased percentage of astroglial fate from NSC, also an increase in neurite length was observed, thus raising the question of whether this is because of a direct effect of the topography and chemistry of the culture substrate, or to an indirect effect due to the supporting action of astrocytes on neurons. Astroglial cells actually attach more strongly to microfabricated pillars than to smooth substrates,[28] and the presence of more astrocytes in the test system could itself affect neuronal maturation, neurite elongation, and branching.

Conclusions

Improving the standards for basic and preclinical research is a recognized need to overcome the weakness that pervades the current system of basic and preclinical research, and to increase reproducibility in science.[4,29–31] The statistical consistency of the *in vitro* data could be improved by the extensive use of high-throughput techniques compared with low-throughput conventional analysis. Cell-based high-throughput technology combining cellular imaging with high-throughput data analysis,[14] is successfully applied to drug screening,[32,33] and it was also used to set up standard procedures according to the ECVAM Good Cellular Culture Practice guidelines.[34] In this study we used HCS, combining in the same assay the safety profile (i.e., nuclear morphology) with the efficacy profile (i.e., neurite elongation). We confirmed that HCS is a quite robust technological platform for *in vitro* testing for materials[35] that can truly improve the pipeline of "third-generation biomaterials" development.[36]

Acknowledgments

Author Disclosure Statement

No competing financial interests exist.

References

1. Cao H, Liu T, Chew SY. The application of nanofibrous scaffolds in neural tissue engineering. Adv Drug Deliv Rev. 2009;61:1055–1064.
2. Krishna V, Konakondla S, Nicholas J, et al. Biomaterial-based interventions for neuronal regeneration and functional recovery in rodent model of spinal cord injury: a systematic review. J Spinal Cord Med. 2013;36: 174–190.
3. Nel AE, Nasser E, Godwin H, et al. A multi-stakeholder perspective on the use of alternative test strategies for nanomaterial safety assessment. ACS Nano. 2013;7:6422–6433.
4. Russell AJ. Standardized experimental procedures in tissue engineering: cure or curse. Tissue Eng. 2005;11:vii–ix.
5. Amato S, Ezzell B. *Regulatory Affairs for Biomaterials and Medical Devices.* WP Woodhead Publising, Sawston, Cambridge, 2015.
6. Kühnel D, Nickel C. The OECD expert meeting on ecotoxicology and environmental fate—towards the development of improved OECD

guidelines for the testing of nanomaterials. Sci Total Environ. 2014; 472:347–353.

7. Del Vecchio G, Giuliani A, Fernandez M, et al. Continuous exposure to 900 MHz GSM-modulated EMF alters morphological maturation of neural cells. Neurosci Lett 2009;455:173–177.

8. Ahlenius H, Kokaia Z. Isolation and generation of neurosphere cultures from embryonic and adult mouse brain. Methods Mol Biol. 2010;633: 241–252.

9. Baldassarro VA, Lizzo G, Paradisi M, et al. Neural stem cells isolated from amyloid precursor protein-mutated mice for drug discovery. World J Stem Cells. 2013;5:229–237.

10. Cook D, Brown D, Alexander R, et al. Lessons learned from the fate of AstraZeneca's drug pipeline: a five-dimensional framework. Nat Rev Drug Discov. 2014;13:419–431.

11. Brunetti V, Maiorano G, Rizzello L, et al. Neurons sense nanoscale roughness with nanometer sensitivity. Proc Natl Acad Sci U S A. 2014;107:6264–6269.

12. Wilson MS, Graham JR, Ball AJ. Multiparametric high content analysis for assessment of neurotoxicity in differentiated neuronal cell lines and human embryonic stem cell-derived neurons. Neurotoxicology. 2014;42:33–48.

13. Banker G, Goslin K. *Culturing Nerve Cells*. MIT Press, Cambrige: Massachusetts, 1998.

14. Radio NM, Mundy WR. Developmental neurotoxicity testing in vitro: models for assessing chemical effects on neurite outgrowth. Neurotoxicol. 2008;29:361–376.

15. Malik N., Efthymiou AG, Mather K, et al. Compounds with species and cell type specific toxicity identified in a 2000 compound drug screen of neural stem cells and rat mixed cortical neurons. Neurotoxicol. 2014; 45:192–200.

16. Breier JM, Gassmann K, Kayser R, et al. Neural progenitor cells as models for high-throughput screens of developmental neurotoxicity: state of the science. Neurotoxicol Teratol. 2010;1:4–15.

17. Godwin H, Nameth C, Avery D, et al. Nanomaterial categorization for assessing risk potential to facilitate regulatory decision-making. ACS Nano. 2015;9:3409–3417.

18. Lee YS, Collins G, Arinzeh TL. Neurite extension of primary neurons on electrospun piezoelectric scaffolds. Acta Biomater. 2011;7:3877–3886.

19. Corey JM, Lin DY, Mycek KB, et al. Aligned electrospun nanofibers specify the direction of dorsal root ganglia neurite growth. J Biomed Mater Res A. 2007;83:636–645.

20. Han D, Cheung KC. Biodegradable cell-seeded nanofiber scaffolds for neural repair. Polymers. 2011;3:1684–1733.

21. Koh HS, Yong T, Chan CK, et al. Enhancement of neurite outgrowth using nano-structured scaffolds coupled with laminin. Biomaterials. 2008;29:3574–3582.

22. He L, Shi Y, Han Q, et al. Surface modification of electrospun nanofibrous scaffolds via polysaccharide–protein assembly multilayer for neurite outgrowth. J Mater Chem. 2012;22:13187–13196.

23. Rao SS, Winter JO. Adhesion molecule-modified biomaterials for neural tissue engineering. Front. Neuroeng. 2009;2:6.

24. Ai J, Kiasat-Dolatabadi A, Ebrahimi-Barough S, et al. Polymeric scaffolds in neural tissue engineering: a review. Arch Neurosci. 2014;1:15–20.

25. Dolci LS, Quiroga SD, Gherardi M, et al. Carboxyl surface functionalization of Poly(L-lactic acid) electrospun nanofibers through atmospheric non-thermal plasma affects fibroblast morphology. Plasma Process Polym. 2013;11:203–213.

26. Alessandri M, Lizzo G, Gualandi C, et al. Influence of biological matrix and artificial electrospun scaffolds on proliferation, differentiation and trophic factor synthesis of rat embryonic stem cells. Matrix Biol. 2014;33:68–76.

27. Giuliani A, Lorenzini L, Alessandri M, et al. In vitro exposure to very low-level laser modifies expression level of extracellular matrix protein RNAs and mitochondria dynamics in mouse embryonic fibroblasts. BMC Complement Altern Med. 2015;15:78–85.

28. Turner AM, Dowell N, Turner SW, et al. Attachment of astroglial cells to microfabricated pillar arrays of different geometries. J Biomed Mater Res. 2000;51:430–441.

29. Begley CG, Ioannidis JP. Reproducibility in science: improving the standard for basic and preclinical research. Circ Res. 2015;116:116–126.

30. Begley CG, Ellis LM. Drug development: raise standards for preclinical cancer research. Nature. 2012;483:531–533.

31. Peers IS, Ceuppens PR, Harbron C. In search of preclinical robustness. Nat Rev Drug Discov. 2012;11:733–734.

32. O'Brien PJ. High-content analysis in toxicology: screening substances for human toxicity potential, elucidating subcellular mechanisms and in vivo use as translational safety biomarkers. Basic Clin Pharmacol Toxicol. 2014;115:4–17.

33. Wang HB, Mullins ME, Cregg JM, et al. Varying the diameter of aligned electrospun fibers alters neurite outgrowth and Schwann cell migration. Acta Biomater. 2010;6:2970–2978.

34. Coecke S, Balls M, Bowe G, et al. Guidance on good cell culture practice. A report of the second ECVAM task force on good laboratory practice. Altern Lab Anim. 2005;33:261–287.

35. Zanella F, Lorens JB, Link W. High content screening: seeing is believing. Trends Biotechnol. 2010;28:237–245.

36. Damoiseaux R, George S, Li M, et al. No time to lose—high through-put screening to assess nanomaterial safety. Nanoscale. 2011;4:1345–1360.

Abbreviations Used

2D	= two-dimensional seeding
DCM	= Dichloromethane
HCS	= high-content analysis
NSC	= neural stem/precursor cells
PLLA	= poly(L-lactic acid)
RA	= retinoic acid
SD	= standard deviation
SEM	= scanning electron microscopy
WCA	= water contact angle

4.4 PARP activity and inhibition in fetal and adult oligodendrocyte precursor cells: Effect on

cell survival and differentiation (Baldassarro et al., 2017a).

CrossMark

PARP activity and inhibition in fetal and adult oligodendrocyte precursor cells: Effect on cell survival and differentiation

Vito A. Baldassarro [a,b], Alessandra Marchesini [c], Luciana Giardino [a,c,d], Laura Calzà [a,b,c,*]

[a] Health Science and Technologies Interdepartmental Center for Industrial Research (HST-ICIR), University of Bologna, Italy
[b] Department of Pharmacy and Biotechnology, University of Bologna, Italy
[c] IRET Foundation, Ozzano Emilia, Italy
[d] Department of Veterinary Medical Sciences, University of Bologna, Italy

A B S T R A C T

Poly (ADP-ribose) polymerase (PARP) family members are ubiquitously expressed and play a key role in cellular processes, including DNA repair and cell death/survival balance. Accordingly, PARP inhibition is an emerging pharmacological strategy for cancer and neurodegenerative diseases. Consistent evidences support the critical involvement of PARP family members in cell differentiation and phenotype maturation. In this study we used an oligodendrocyte precursor cells (OPCs) enriched system derived from fetal and adult brain to investigate the role of PARP in OPCs proliferation, survival, and differentiation. The PARP inhibitors PJ34, TIQ-A and Olaparib were used as pharmacological tools. The main results of the study are: (i) PARP mRNA expression and PARP activity are much higher in fetal than in adult-derived OPCs; (ii) the culture treatment with PARP inhibitors is cytotoxic for OPCs derived from fetal, but not from adult, brain; (iii) PARP inhibition reduces cell number, according to the inhibitory potency of the compounds; (iv) PARP inhibition effect on fetal OPCs is a slow process; (v) PARP inhibition impairs OPCs maturation into myelinating OL in fetal, but not in adult cultures, according to the inhibitory potency of the compounds. These results have implications for PARP-inhibition therapies for diseases and lesions of the central nervous system, in particular for neonatal hypoxic/ischemic encephalopathy.

1. Introduction

Oligodendrocytes, the cells wrapping the axons of the central nervous system (CNS) with the myelin sheath, derive from the oligodendrocyte precursor cells (OPCs) generated during development from multipotent neuroectodermal derivatives in the cortex and spinal cord (Bergles and Richardson, 2015). These cells proliferate and migrate to populate the entire adult CNS, where they account for approximately 5–8% of the entire cell population (Dawson et al., 2003). New OPCs can be also generated in the adult CNS from neural stem cells (NSCs; Agathou et al., 2013) and by mitosis, as OPCs are the major proliferating population of the CNS under appropriate stimuli (Fernandez-Castaneda and Gaultier, 2016). These cells are responsible for myelin formation during development (Bergles and Richardson, 2015), and for myelin turnover and repair during adulthood (Young et al., 2013).

The process of myelin formation is highly orchestrated in time and space, involves different cell types, and a key step of this process is the OPC maturation toward myelinating oligodendrocyte (Zuchero and Barres, 2013). Internal and external cues targeting genetic, epigenetic

and cytoplasmic mechanisms provide the appropriate microenvironment that regulates the molecular machinery triggering OPCs out of the cell cycle to terminal differentiation (Zuchero and Barres, 2013; Liu et al., 2016; Fernández et al., 2016).

It has been suggested that remyelination after lesions in the adult CNS recapitulates developmental myelination (Franklin and Hinks, 1999). However, substantial differences could well be expected between a normal turnover process and a repair process (Fancy et al., 2011) triggered by pathological events like inflammation and hypoxic/ ischemic damage. These events actually mobilize a large number of inhibitory factors leading to a differentiation block of OPC (Gaesser and Fyffe-Maricich, 2016). Thus, there is an urgent need to more clearly elucidate the molecular bases of the relationship between OPCs proliferation and differentiation, carefully dissecting developmental myelination vs. myelin turnover in adulthood, and physiological vs. pathological conditions.

In the present study, we investigated the role of poly(ADP-ribose) polymerases (PARPs) in OPCs survival, proliferation and differentiation. PARPs are members of nuclear enzyme family that catalyse the formation of $(ADP-ribose)_n$ chains from NAD^+ on acceptor proteins after DNA double strands breaks (Amé et al., 2004). Because of the PARPs well described role in DNA repair and apoptosis induction (Heeres and Hergenrother, 2007), PARPs inhibition is currently considered a

* Corresponding author at: CIRI-SDV, University of Bologna, Via Tolara di Sopra 41/E, 40064 Bologna, Ozzano Emilia, Italy.
E-mail address: laura.calza@unibo.it (L. Calzà).

therapeutic option for cancer, including glioblastoma (Curtin and Szabo, 2013). Moreover, PARPs inhibition was proposed as a neuroprotective strategy for neonatal asphyxia and hypoxia/ischemia encephalopathy (Neira-Peña et al., 2015), a CNS injury that occurs during a critical period of developmental myelination (Dimou and Götz, 2014). In order to study the effect of PARP inhibition in all stages of differentiation, from NSCs to mature oligodendrocytes, we used OPCs-enriched cultures obtained from the fetal forebrain- and the adult sub-ventricular zone of the mouse to study the different role of PARPs in adult and fetal OPCs differentiation and maturation. We used PARP inhibitors having a different inhibitory concentration as pharmacological toll, including the clinically approved Olaparib (LYNPARZA™).

2. Materials and methods

2.1. Cell cultures

All animal protocols described herein were carried out according to the European Community Council Directives (86/609/EEC), and comply with the guidelines published in the *NIH Guide for the Care and Use of Laboratory Animals*.

Fetal and adult NSCs were isolated from E.13–14 fetal mouse forebrain or 2.5 month old mice sub-ventricular zone (SVZ), following the Ahlenius and Kokaia protocol (Ahlenius and Kokaia, 2010). Oligodendrocyte differentiation was performed following the Chen protocol (Chen et al., 2007) with some modifications. Tissues were enzymatically dissociated using trypsin (SIGMA), hyaluronidase (SIGMA) and DNase (SIGMA), than mechanically dissociated by piepetting. The solution was filtered, centrifuged and the resulting pellet was washed twice in HBSS. After 7 min centrifugation at $400 \times g$, the cellular pellet was resuspended in serum-free medium (DMEM/F12 GlutaMAX $1 \times$; 8 mmol/L HEPES; 100 U/100 μg Penicillin/Streptomycin; $0.1 \times$ B27; $1 \times$ N-2; 20 ng/ml bFGF; 20 ng/ml EGF) and, after cell count, cells were plated in suspension at a density of 10 cells/μl in a final volume of 3 ml in low-attachment 6-well plates (NUNC). Half medium was changed every three days, centrifuging the cell suspension at $300 \times g$ for 5 min and gently resuspending the cellular pellet in fresh medium. Neurospheres were allowed to proliferate until they attained a diameter of about 100 μm.

To obtain oligospheres, primary neurospheres were centrifuged at $300 \times g$ for 5 min. The pellet was mechanically dissociated by pipetting and cells were counted and plated again at a density of 10 cells/μl in a final volume of 3 ml of OPCs medium (DMEM/F12 GlutaMAX $1 \times$; 8 mmol/L HEPES; 100 U/100 μg Penicillin/Streptomycin; $0.1 \times$ B27; $1 \times$ N-2; 20 ng/ml bFGF; 20 ng/ml PDGF) in low-attachment 6-well plates (NUNC). Oligospheres were centrifuged and the pellet was mechanically dissociated to obtain a single cell suspension. After cell count, cells were plated at a density of 3000 cells/cm^2 on poly-D,L-ornithine (50 μg/ml)/laminin (5 μg/ml) coating, in OPC medium.

In order to induce oligodendrocyte differentiation and maturation, after 3 DIVs OPC medium was replaced with the oligodendrocyte differentiation medium (DMEM/F12 GlutaMAX $1 \times$; 8 mmol/L HEPES; 100 U/100 μg Penicillin/Streptomycin; $0.1 \times$ B27; $1 \times$ N-2; 50 nM T3; 10 ng/ml CNTF; $1 \times$ N-acetyl-L-cysteine-NAC-).

2.2. PARP inhibitor treatments

The following PARPi (PARP inhibitors) were used in this study: TIQ-A (IC50 140–450 nM), PJ34 (IC50 20 nM) and Olaparib (IC50 5 nM; Ferraris, 2010; Hans et al., 2011). OPCs were treated 24 h before the T3-mediated differentiation induction (-1 DIV), and cell viability was analysed at DIV 12 of differentiation (Fig. 1A). In order to study effects of PARPi on fetal and adult cultures, different treatment were performed: i) in order to study PARP1–2 expression and PARP activity, cells were analysed 24 h after treatment (DIV 0; Fig. 1A); ii) a dose-

response curve of PARPi were performed, treating cultures with a series of 7 concentrations (0–10 μM). PARPi treatments were maintained after the oligodendrocyte differentiation medium change, until DIV 12 (Fig. 2A); iii) fetal cultures were also treated with PJ34 10 μM and analysed for cell number and cell death at DIV 0, 6 and 12 (Fig. 3A); iv) both fetal and adult cultures were treated with lower dose of PARPi (1 μM and 10 μM) and analysed for mature oligodendrocytes at DIV 12 (Fig. 4A).

2.3. Immunocytochemistry

Indirect immunofluorescence was used to identify OPCs (NG2-positive cells), mature (CNPase-positive cells) and myelinating (MBP-positive cells) OLs, neurons (β-III-tubulin-positive cells) and astrocytes (GFAP-positive cells). The following primary antisera were used: mouse anti-β-III-tubulin (R&D system, Trento, Italy) 1:3000; rabbit anti-GFAP (Glial Fibrillary Acidic Protein, Dako) 1:1000; rabbit anti-NG2 (chondroitin sulphate proteoglycan, neural/glial antigen 2, Millipore, Merck S.p.a., Milan, Italy) 1:350; mouse anti-CNPase (2′, 3′-cyclic nucleotide 3′-phosphodiesterase, Millipore) 1:500; rabbit anti-MBP (Myelin Basic Protein, Dako) 1:500. Donkey Alexa 488-conjugated anti mouse and donkey Alexa 568-conjugated anti-rabbit (Invitrogen) were used as secondary antisera. After immunofluorescence staining, cells were incubated with the nuclear dye Hoechst 33,258 (1 μg/ml in PBS, 0.3% Triton-X 100) for 20 min at RT. Cells were finally washed in PBS and mounted in glycerol and PBS (3:1, v/v) containing 0.1% paraphenylendiamine.

2.4. High content screening

For HCS analysis cells were grown in 96 flat-bottom well HCS plates (NUNC). Analysis of condensed nuclei, cell number and lineage/differentiation markers were performed with Cell Insight™ CX5 High Content Screening (HCS; Thermo Scientific), using the *Compartmental analysis* BioApplication. Based on nuclear staining, the software is able to recognise nuclei and calculate the percentage of high intensity/small sized condensed nuclei. Moreover, based on the nuclei identification, the software is able to detect the presence of the marker-specific stain in the cell body, calculating the percentage of the immunoreactive cells. Lineage/differentiation markers analysis was performed only on cells showing intact nuclei, excluding condensed nuclei from the percentage calculation.

2.5. RNA isolation and reverse transcription

Total RNA isolation was performed by using the RNeasy Mini kit (Qiagen, Milan, Italy) following manufacturer's instructions. Total RNA was eluted in RNase Free Water and concentration estimated through absorbance values at 260, 280 and 320 (Nanodrop 2000 spectrophotometer, Thermo Scientific). First strand cDNAs were obtained using the iScript™ cDNA Synthesis Kit (BioRad), incubating samples at 42 °C for 30 min. An RNA sample with no reverse transcriptase enzyme in the reaction mix was processed as a no-reverse transcription control sample.

2.6. Semi-quantitative real-time PCR

Semi-quantitative real-time PCR was performed using the CFX96 real-time PCR system (BioRad, CA, USA). The reactions were performed in a final volume of 20 μl consisting of $1 \times$ SYBR Green qPCR master mix (BioRad) and 0.4 μM forward and reverse primers. In order to avoid possible contamination of genomic DNA in isolated RNA, the no-reverse transcriptase sample was processed in parallel with the others and tested by real-time PCR for every pair of primers used. All primers used were designed using Primer Blast software (NCBI, MD, USA) and synthesised by IDT (Coralville, IA, USA). The following primer

sequences were used: PARP-1 (FW: 5′-GCCACACATCTCAGGGAGAC-3′; REV: 5′-CCCAAACCTTTGACACTGTGC-3′), PARP-2 (FW: 5′-GAAGGACGCAGACAGGACAA-3′; REV: 5′-ACATGAGCCTTTCCCAGCTT-3′). GAPDH (FW: 5′-GGCAAGTTCAATGGCACAGTCAAG-3′; REV: 5′-ACATACTCAGCACCAGCATCACC-3′) was used as housekeeping gene to normalize the amount of reverse-transcribed RNA used for PCR. Thermal profile of PCR reactions consisted first of a denaturation step (95 °C, 2 min) and 40 cycles of amplification (95 °C for 15 s and 60 °C for 60 s). At the end of the amplification cycles the melting curve of amplified products was performed according to the following temperature/time scheme: heating from 55 °C to 95 °C with a temperature increase of 0.5 °C/s.

Primers efficiency values for all primers were 95–102%. The $2^{(-\Delta\Delta CT)}$ method was used for the calculation of gene expression.

2.7. PARP activity assay

Fetal and adult OPCs at DIV 0, after 24 h of PARPi treatment, were lysed and proteins were quantified using the Lowry method (BioRad) following the manufacturer's instruction. PARP enzymatic activity was measured using HT Colorimetric PARP Apoptosis Assay Kit (Trevingen), following manufacturer's instructions.

2.8. Statistical analysis

Data are reported as mean ± SD. Prism software (GraphPad) was used for statistical analyses and graph generation. Student's t-test or one-way ANOVA and Dunnett's multiple comparison post-hoc were used to analyse data. Results were considered significant when the probability of their occurrence as a result of chance alone was <5% ($P < 0.05$).

3. Results

3.1. PARP expression and activity in fetal and adult OPCs

The cell systems used in this study are presented in Fig. 1. After cell expansion as neurospheres and oligospheres, cells were seeded for 3 DIVs in OPC medium, and then differentiated for 12 days in the presence of T3 (Fig. 1A). Lineage progression from NG2-positive OPC (DIV0) through CNPase-mature OL as far as myelinating MBP-positive OL is illustrated in Fig. 1C–E (representative images). The culture composition changes during the 12 DIV differentiation period, starting from DIV0, where the majority of cells are NG2 positive (NG2-positive cells 80%; CNPase-positive cells 5%), passing thorough DIV 6, where CNPase cells are growing in number (NG2-positive cells 60%; CNPase-positive cells
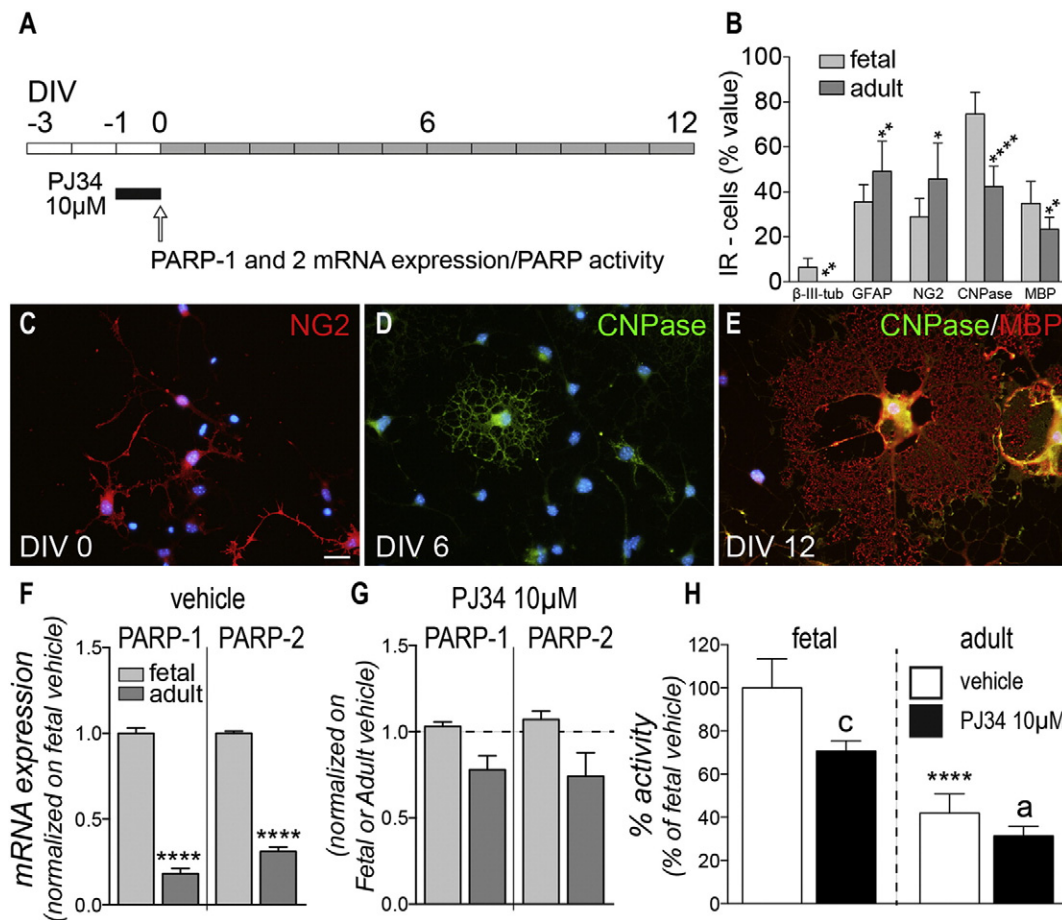

Fig. 1. PARP activity and expression in OPCs-enriched cultures. (A) Experimental design: in order to study PARP mRNA expression and activity, cells were treated for 24 h, form DIV −1 to DIV 0, with PJ34 10 μM. Arrow shows the time point of the represented analysis. Vehicle treated cells were also cultured for 12 DIV after T3-differentiation induction. Gray rectangles represent T3 exposure phase. (B) Fetal and adult OPC culture composition at 12 DIV. Specific markers were used in order to visualize neurons (beta-III-tubulin), astrocytes (GFAP; Glial Fibrillary Acidic Protein), OPCs (NG2; chondroitin sulphate proteoglycan, neural/glial antigen 2), Mature oligodendrocytes (CNPase; 2′,3′-cyclic nucleotide 3′-phosphodiesterase) and myelinating oligodendrocytes (MBP; myelin basic protein). (C–E) Representative images of oligodendrocyte maturation at 0, 6 and 12 DIV. Bar: 40 μm. (F–G) PARP1 and 2 mRNA level quantification in vehicle-treated cells (F) and in cells exposed for 24 h to PJ34 10 μM (G; dashed line represents the level of expression in vehicle-treated cells). (H) PARP activity assay, performed on fetal and adult OPCs at DIV 0, treated or untreated with PJ34 for 24 h. Data are represented as mean ± SD. Statistical analysis: Student's t-test. Asterisks indicate differences between adult and fetal (*$P < 0.05$; **$P < 0.01$; ***$P < 0.001$; ****$P < 0.0001$), letters represent differences between treated and non-treated cultures (a = $P < 0.05$; c = $P < 0.001$).

30%), reaching the end of the differentiation with CNPase/MBP positive cells representing the majority of cells. Culture composition at 12 DIV is presented in Fig. 1B. Adult cultures after 12 DIVs of differentiation show a less mature cell composition, with a high percentage of NG2-positive cells ($P = 0.016$) and less CNPase ($P < 0.0001$) and MBP ($P = 0.008$) positive cells. Fetal cultures show less astrocytes (GFAP-positive cells; $P = 0.0023$) and around 6% of neurons (β-III-tubulin positive cells) that are not detected in adult cultures ($P = 0.002$).

In order to characterize the effect of PARP inhibition in fetal and adult OPCs on oligodendrocyte differentiation and maturation, cells were exposed to PARPi 24 h before differentiation induction (Fig. 1A). We first investigated the gene expression of the two major and more extensively studied PARPs, PARP-1 and 2 (Fig. 1F–G), and PARP activity (Fig. 1H), before the induction of differentiation, 24 h after PARPi treatment (DIV 0). Both genes are expressed in fetal ($\Delta Cq = 3.28 \pm 0.08$) and adult ($\Delta Cq = 5.79 \pm 0.4$) OPCs; gene expression is significantly

higher in fetal compared to adult OPCs (PARP-1, $P < 0.0001$; PARP-2, $P = 0.0002$; Fig. 1F), and PJ34 treatment did not influence the mRNA expression levels (Fig. 1G). PARP activity analysis was based on the capability of PARP to parrylate histons in an ELISA-based assay. PARP activity was significantly higher in fetal OPCs compared to adult ($P < 0.0001$), and PJ34 treatment was able to decrease the activity in both cultures (fetal, $P = 0.0005$; adult $P = 0.0284$), thus confirming that the enzyme is active in both cell systems (Fig. 1H).

3.2. Effect of PARP inhibition on fetal and adult OPCs viability

In order to establish the cytostatic/toxic profile of PARPs inhibition on OPCs, we first constructed a dose-response curve on the cell culture which displayed the higher activity and expression of PARPs, i.e. fetal OPCs, using two standard PARPi, i.e. PJ34 and TIQ-A. The cytostatic effect is evaluated by the cell number (Fig. 2B), the cytotoxic effect by the

Fig. 2. Effect of PARP inhibition on fetal and adult OPC viability. (A) Experimental design: in order to study PARP inhibition effect on cell number and cell viability, cells were treated with PARPi form DIV −1 to DIV 12. Gray rectangles represent T3 exposure phase; arrow shows the time point of the represented analysis. (B–C) Dose-response curves of PJ34 and TIQ-A treatment of fetal OPCs cultures. Results are shown as number of cells (B; total number of nuclei detected by the HCS software) and percentage of condensed nuclei (C) obtained at 12 DIV. (D–E) Comparison between percentage of number of cells (D) and condensed nuclei (E) at 12 DIV (day in vitro) in fetal and adult cultures treated with PJ34 and TIQ-A at 10 μM. (F–G) Dose-response curves of Olaparib treated fetal and adult OPCs. Results are shown as number of cells (F) and percentage of condensed nuclei (G) at 12 DIV. Data are represented as mean ± SD. Statistical analysis: One-way ANOVA followed by Dunnet's post hoc. Asterisks represent difference between treated and untreated groups ($*P < 0.05$; $**P < 0.01$; $***P < 0.001$; $****P < 0.0001$).

percentage of condensed nuclei (Fig. 2C), as established by HCS in three independent experiments. The cytostatic effect was observed at 1 μM and 10 μM using TIQ-A ($P < 0.0001$); at 10 μM using PJ34 ($P < 0.0001$). Both molecules induced an increase in the percentage of condensed nuclei at the highest concentration (10 μM) according to the respective potency (TIQ-A, $P < 0.0001$; PJ34, $P = 0.0362$).

We then investigated the effect of PJ34 and TIQ-A on adult OPCs using the toxic concentration for fetal OPCs (10 μM) finding that PJ34, but not TIQ-A, reduced the cell number in adult cultures (Fig. 2D; $P = 0.0004$) without affecting the percentage of condensed nuclei (Fig. 2E).

We also tested the Olaparib, a clinically approved PARPi, showing the highest PARP inhibitory activity. Olaparib treatment caused a reduction in cell number in both fetal and adult cultures at low concentrations (Fig. 2F; 10^{-1} nM; $P < 0.0001$) but is cytotoxic only for fetal OPCs (Fig. 2G; 10^1 nM; $P < 0.0001$).

In order to better elucidate the timing of the PARP inhibition effect, we performed a time course analysis of cell number and cell death, by using PJ34 at a 10 μM toxic dose, (Fig. 3A). We found that after 24 h from the treatment there were no effects on cell number (Fig. 3B) and cell death (Fig. 3C). In vehicle treated cells, cell number increases over time, while in PARPi-treated cells remain at the same level for the whole differentiation period (Two Ways ANOVA, time $F_{(2, 90)} = 20.37$, $P < 0.0001$; treatment $F_{(1, 90)} = 63.13$, $P < 0.0001$; interaction $F_{(2, 90)} = 15.28$, $P < 0.0001$), leading to a strong difference between the two groups at DIV 6 ($P < 0.0001$) and DIV 12 ($P < 0.0001$; Fig. 3B). In the opposite way, the percentage of condensed nuclei remain constant in the vehicle-treated, while increasing over time in the PARPi-treated group (Two Ways ANOVA, time $F_{(2, 86)} = 12.49$, $P < 0.0001$; treatment $F_{(1, 86)} = 46.65$, $P < 0.0001$; interaction $F_{(2, 86)} = 15.60$, $P < 0.0001$), starting from DIV6 ($P = 0.0003$) and reaching >30% at DIV 12 ($P < 0.0001$; Fig. 3C).

3.3. Effect of PARP inhibition on fetal and adult OLs maturation

We finally investigated the effect of PARP inhibition on the differentiation of remaining OPCs using the two highest concentrations, being either toxic or non-toxic. Fetal OPCs were treated with TIQ-A, PJ34 and Olaparib at 1 μM (non-toxic concentration of TIQ-A and PJ34, toxic concentration of Olaparib) and 10 μM (toxic concentration of all PARPi). Adult OPCs were treated with all 10 μM and 1 μM (both non-toxic concentration of all PARPi). Representative HCS images of CNPase/MBP-

positive cells in the different treatments of both fetal and adult OPCs are presented in Fig. 4B; results of the quantitative HCS analysis in Fig. 4C (fetal) and Fig. 4D (adult). The number of cells included in this analysis ranged from 1199 to 7152/well. Three wells were included in each experiment. PARP inhibition impairs OPCs maturation in fetal, but not in adult, cultures. In cell preparations derived from fetal brain, TIQ-A, the less potent PARPi, does not affect OPC maturation, as indicated by the percentage of MBP-IR cells. On the contrary, PJ34 treatment, already at non-toxic concentrations (1 μM) resulted in a reduction of mature OPCs ($P = 0.0013$), as when used in a toxic dose (10 μM) ($P < 0.0001$). Olaparib treatment at both concentrations resulted in a strong reduction of the percentage of mature and myelinating OPCs ($P < 0.0001$). Notably, all PARPi had no effect on adult OPC differentiation (1 μM treatment, data not shown).

4. Discussion

Several in vivo and in vitro studies indicate that OPCs have substantially different properties according to their chronological age. For example, human fetal OPCs from different gestational stages exhibit differences in the myelination profile (Cui et al., 2012), such as human OPCs derived from fetal brain during the period of maximum oligoneogenesis or from adult subcortical white matter (Windrem et al., 2004). However, the mechanisms behind the different age-related OPC biological properties are not known. The aim of this study was to investigate if PARP is involved in determining the age-related OPCs properties. Thus, we compared OPCs derived from NSCs obtained from fetal and adult brains. This cell system was preferred to primary and purified OPCs to better mimic developmental biology of OPC, including lineage specification, proliferation/survival and differentiation. PARP is a family of enzymes comprising 17 homologues involved in multiple cell functions (Jubin et al., 2016a). Apart from the role in DNA repair, PARP-1 and 2 participate in cell homeostasis maintenance (Bai, 2015), intracellular transports (Abd Elmageed et al., 2012), cell cycle (Madison et al., 2011) inflammation and immunity (Bai and Virág, 2012) and gene expression regulation (Bock et al., 2015) through >100 substrates (Hottiger, 2015). Moreover, PARPs are critically involved in inflammation and in the tissue damage caused by ischemia/reperfusion conditions (Li et al., 2015).

We first showed that PARP mRNA expression and PARP activity are much higher in fetal- than in adult-derived OPCs. Due to the role of

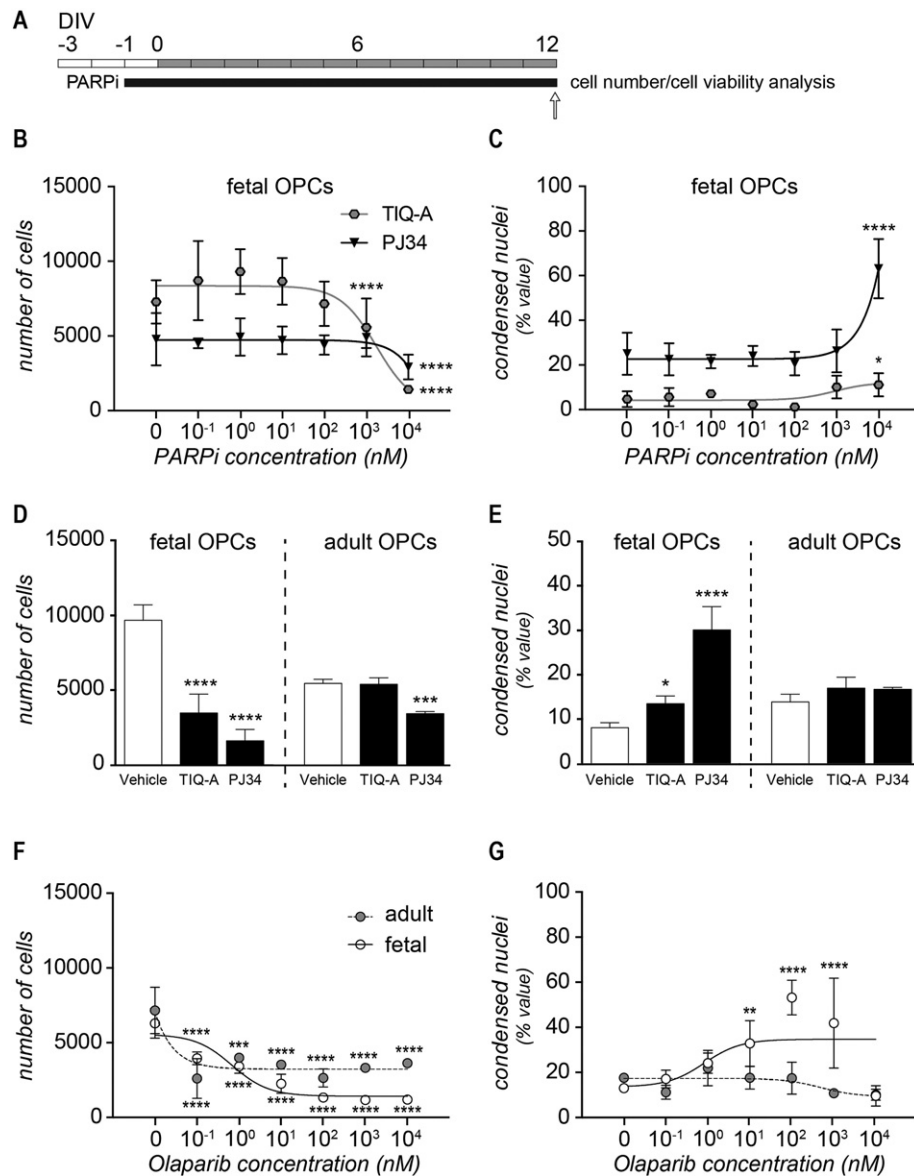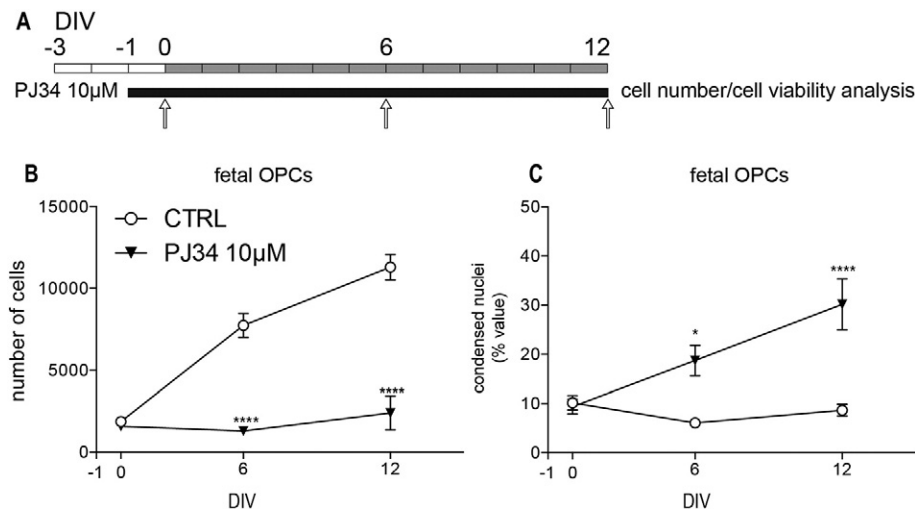**Fig. 3.** Time course of PARP inhibition effect on fetal OPCs. (A) Experimental design: in order to study PARP inhibition effect on cell number and cell viability, cells were treated with PARPi form DIV −1 to DIV 12. Gray rectangles represent T3 exposure phase; arrows show the time points of the represented analysis. (B–C) Time course analysis of number of cells (B) and percentage of condensed nuclei (C) in fetal OPCs treated with vehicle or PJ34 10 μM. Data are represented as mean ± SD. Statistical analysis: Two-way ANOVA followed by Tukey's post hoc. Asterisks represent difference between treated and untreated groups at the same time point (*$P < 0.05$; ****$P < 0.0001$).
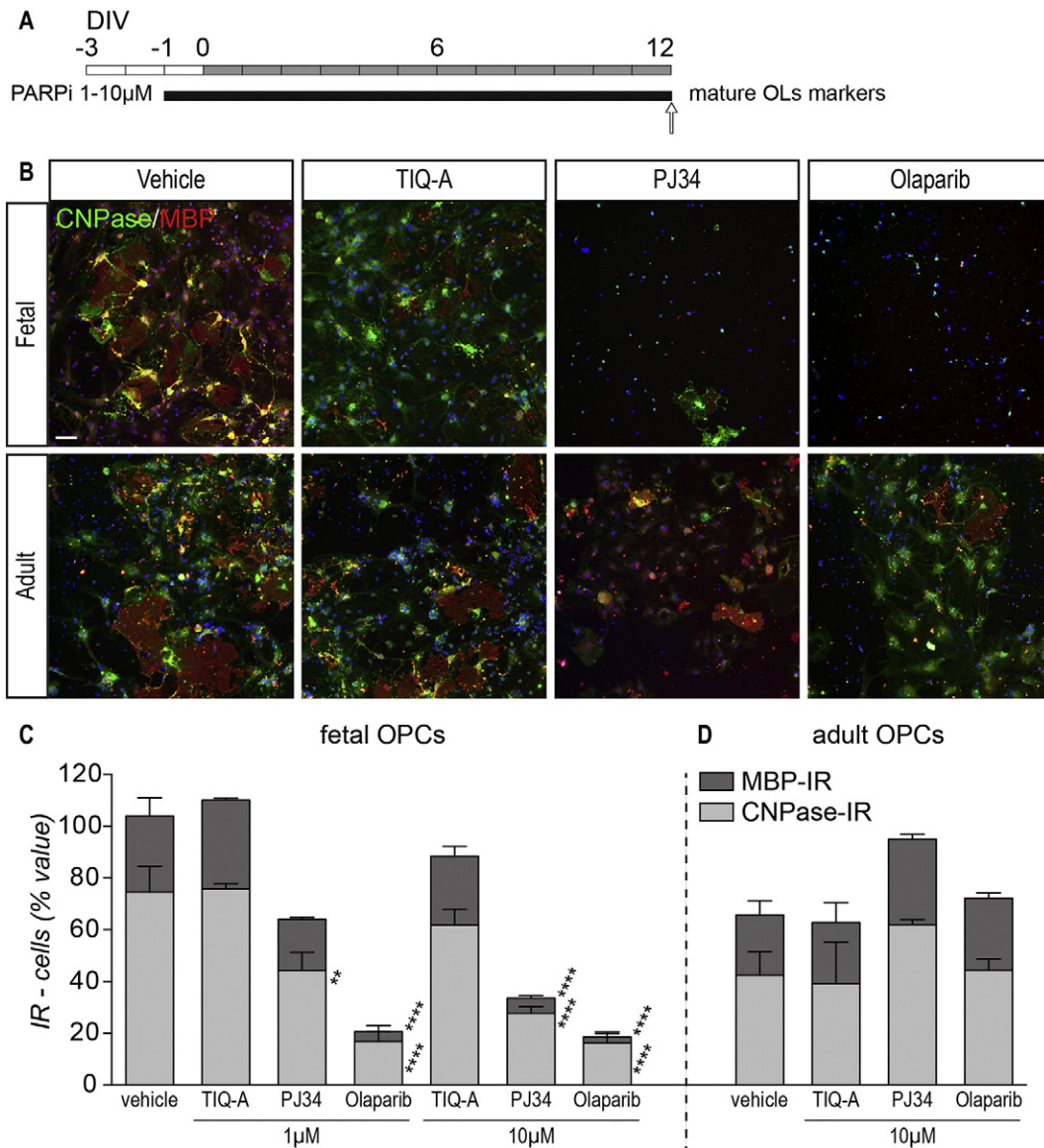
Fig. 4. Effect of PARP inhibition on oligodendrocyte maturation. (A) Experimental design: in order to study PARP inhibition effect on OLs maturation, cells were treated with PARPi form DIV −1 to DIV 12. Gray rectangles represent T3 exposure phase; arrow shows the time point of the represented analysis. (B) Representative HCS images of fetal and adult cultures at 12 DIV. Specific markers were used in order to visualize mature (CNPase; 2′,3′-cyclic nucleotide 3′-phosphodiesterase) and myelinating (MBP; myelin basic protein) oligodendrocytes. Bar: 100 μm. (C–D) Percentage of CNPase- and MBP-positive cells at 12 DIV in fetal (C) or adult (D) cultures. Data are represented as mean ± SD. Statistical analysis: One-way ANOVA followed by Dunnet's post hoc. Asterisks represent difference between treated and untreated groups (**$P < 0.01$; ***$P < 0.001$; ****$P < 0.0001$).

PARPs in DNA repair and apoptosis induction (Heeres and Hergenrother, 2007), the reduction in PARP mRNA expression level and activity observed in adult compared to fetal-derived OPC might reflect the age-related decrease of DNA repair capability (Bürkle et al., 2015). In fact, PARP activity also varies according to the age in different brain regions (Strosznajder et al., 2000), and PARylation is developmentally regulated (Jubin et al., 2016b).

We then showed that PARP inhibition produces substantially different effects in OPCs derived from fetal and adult brain. In particular: (i) the culture treatment with PARP inhibitors is cytotoxic for OPCs derived from fetal, but not from adult, brain; (ii) PARP inhibition reduces cell number in proportion to the inhibitory potency of the compounds; (iii) the PARP inhibition effect in fetal OPCs is a slow process (iv) PARP inhibition impairs OPC maturation into myelinating OL in fetal, but not in adult OPCs, according to the inhibitory potency of the compounds. A primary role of PARP in the differentiation process of different cell types was recently recognized, possibly though chromatin plasticity and epigenetic regulation (Li et al., 2015). In embryonic stem cells,

PARP interacts with the Wnt pathway, Sonic Hedgehog and Pax6 signalling (Hemberger et al., 2003; Yoo et al., 2011). PARP-1 has also a role in neuroectoderm differentiation (Yoo et al., 2011) and favours the transit of NSCs toward a glial fate (Plane et al., 2012). Here we confirmed and further extend this latter observation, showing that PARP inhibition reduced proliferation in fetal-derived neurospheres and oligospheres (see supplemental material), and reduces OPCs differentiation into mature OLs. Notably, key transcription factors involved in OPC maturation, i.e. retinoic acid receptors, thyroid hormone receptors and their hetero-dimerization, such as PDGF signalling, a critical pathway for OPC biology, are targets of PARP regulation (Pavri et al., 2005; Allen, 2008). Overall, these results suggest that a different PARP signalling in fetal and adult OPCs might be part in the biological properties of OPCs at different chronological ages.

These results have also therapeutic implications. In fact, PARP inhibition has even been proposed as a pharmacological strategy in a number of acquired inflammation/demyelinating disorders in which OPCs play a key pathogenic role, occurring both in perinatal/neonatal (e.g. neonatal

hypoxia/ischemia encephalopathy) and adult age (e.g. spinal cord injury and multiple sclerosis; Komjáti et al., 2005; Moroni, 2008; Cavone and Chiarugi, 2012). Contradictory results have been obtained in mice models of inflammatory/demyelinating diseases (Selvaraj et al., 2009; Veto et al., 2010; Casaccia, 2011; Kamboj et al., 2013). PARP-2 deletion in conventional transgenic mice results in a protection from experimental allergic encephalomyelitis (EAE), the most widely used animal model for multiple sclerosis (Kamboj et al., 2013). Conversely, knockout of PARP-1 gene leads to an exacerbated EAE and an increase in the mortality rate (Selvaraj et al., 2009). Pharmacological PARP inhibition in EAE mice has a protective effect, preventing OL death and attenuating inflammation (Veto et al., 2010), although this effect is attributed to the reduction of CNS inflammation and immunomodulation (Scott et al., 2004).

Our data, showing that PARP inhibition is cytotoxic in OPCs derived from the fetal brain, suggest that the OPCs chronological age should be taken into account in considering PARP inhibition as a neuroprotective strategy. In particular, PARP inhibition in ischemic damage should distinguish perinatal/neonatal from adult conditions, considering that the time-window for the treatment of neonatal hypoxia/ischemia encephalopathy is the key period for OPCs proliferation, maturation and developmental myelination.

Acknowledgements

Appendix A. Supplementary data

Supplementary data to this article can be found online at http://dx.doi.org/10.1016/j.scr.2017.05.011.

References

Abd Elmageed, Z.Y., Naura, A.S., Errami, Y., Zerfaoui, M., 2012. The poly(ADP-ribose) polymerases (PARPs): new roles in intracellular transport. Cell. Signal. 24, 1–8.
Agathou, S., Káradóttir, R.T., Kazanis, I., 2013. Niche derived oligodendrocyte progenitors: a source of rejuvenation or complementation for local oligodendrogenesis? Front. Cell. Neurosci. 7, 188.
Ahlenius, H., Kokaia, Z., 2010. Isolation and generation of neurosphere cultures from embryonic and adult mouse brain. Methods Mol. Biol. 633, 241–252.
Allen, N.D., 2008. Temporal and epigenetic regulation of neurodevelopmental plasticity. Philos. Trans. R. Soc. B 363, 23–38.
Amé, J.C., Spenlehauer, C., de Murcia, G., 2004. The PARP superfamily. BioEssays 26, 882–893.
Bai, P., 2015. Biology of poly(ADP-ribose) polymerases: the factotums of cell maintenance. Mol. Cell 58, 947–958.
Bai, P., Virág, L., 2012. Role of poly(ADP-ribose) polymerases in the regulation of inflammatory processes. FEBS Lett. 586, 3771–3777.
Bergles, D.E., Richardson, W.D., 2015. Oligodendrocyte development and plasticity. Cold Spring Harb. Perspect. Biol. 8, a020453.
Bock, F.J., Todorova, T.T., Chang, P., 2015. RNA regulation by poly(ADP-ribose) polymerases. Mol. Cell 58, 959–969.
Bürkle, A., et al., 2015. MARK-AGE biomarkers of ageing. Mech. Ageing Dev. 151, 2–12.
Casaccia, P., 2011. Anti-TANKyrase weapons promote myelination. Nat. Neurosci. 14, 945–947.
Cavone, L., Chiarugi, A., 2012. Targeting poly(ADP-ribose) polymerase-1 as a promising approach for immunomodulation in multiple sclerosis? Trends Mol. Med. 18, 92–100.
Chen, Y., et al., 2007. Isolation and culture of rat and mouse oligodendrocyte precursor cells. Nat. Protoc. 2, 1044–1051.
Cui, Q.L., et al., 2012. Human fetal oligodendrocyte progenitor cells from different gestational stages exhibit substantially different potential to myelinate. Stem Cells Dev. 21, 1831–1837.
Curtin, N.J., Szabo, C., 2013. Therapeutic applications of PARP inhibitors: anticancer therapy and beyond. Mol. Asp. Med. 34, 1217–1256.

Dawson, M.R., Polito, A., Levine, J.M., Reynolds, R., 2003. NG2-expressing glial progenitor cells: an abundant and widespread population of cycling cells in the adult rat CNS. Mol. Cell. Neurosci. 24, 476–488.
Dimou, L., Götz, M., 2014. Glial cells as progenitors and stem cells: new roles in the healthy and diseased brain. Physiol. Rev. 94, 709–737.
Fancy, S.P., Chan, J.R., Baranzini, S.E., Franklin, R.J., Rowitch, D.H., 2011. Myelin regeneration: a recapitulation of development? Annu. Rev. Neurosci. 34, 21–43.
Fernández, M., Baldassarro, V.A., Sivilia, S., Giardino, L., Calzà, L., 2016. Inflammation severely alters thyroid hormone signaling in the central nervous system during experimental allergic encephalomyelitis in rat: direct impact on OPCs differentiation failure. Glia 64, 1573–1589.
Ferraris, D.V., 2010. Evolution of poly(ADP-ribose) polymerase-1 (PARP-1) inhibitors. From Concept to Clinic. J. Med. Chem. 53, 4561–4584.
Fernandez-Castaneda, A., Gaultier, A., 2016. Adult oligodendrocyte progenitor cells - multifaceted regulators of the CNS in health and disease. Brain Behav. Immun. (E-pub ahead of print 12 January). 10.1016/j.bbi.2016.01.005.
Franklin, R.J.M., Hinks, G.L., 1999. Understanding CNS remyelination: clues from developmental and regeneration biology. J. Neurosci. Res. 58, 207–213.
Gaesser, J., Fyffe-Maricich, S.L., 2016. Intracellular signaling pathway regulation of myelination and remyelination in the CNS. Exp. Neurol. (E-pub ahead of print 5 March 2016). 10.1016/j.expneurol.2016.03.008.
Heeres, J.T., Hergenrother, P.J., 2007. Poly(ADP-ribose) makes a date with death. Curr. Opin. Chem. Biol. 11, 644–653.
Hans, C.P., et al., 2011. Opposing roles of PARP-1 in MMP-9 and TIMP-2 expression and mast cell degranulation in dyslipidemic dilated cardiomyopathy. Cardiovasc. Pathol. 20, e68.
Hemberger, M., et al., 2003. Parp1-deficiency induces differentiation of ES cells into trophoblast derivatives. Dev. Biol. 257, 371–381.
Hottiger, M.O., 2015. Nuclear ADP-ribosylation and its role in chromatin plasticity. Cell differentiation, and epigenetics. Annu. Rev. Biochem. 84, 227–263.
Jubin, T., et al., 2016a. The PARP family: insights into functional aspects of poly (ADP-ribose)polymerase-1 in cell growth and survival. Cell Prolif. 49, 421–437.
Jubin, T., et al., 2016b. Poly ADP-ribose polymerase-1: beyond transcription and towards differentiation. Semin. Cell Dev. Biol. (E-pub ahead of print 28 July 2016). 10.1016/j.semcdb.2016.07.027.
Kamboj, A., et al., 2013. Poly(ADP-ribose) polymerase 2 contributes to neuroinflammation and neurological dysfunction in mouse experimental autoimmune encephalomyelitis. J. Neuroinflammation 10, 49.
Komjáti, K., Besson, V.C., Szabó, C., 2005. Poly (adp-ribose) polymerase inhibitors as potential therapeutic agents in stroke and neurotrauma. Curr. Drug Targets CNS Neurol. Disord. 4, 179–194.
Moroni, F., 2008. Poly(ADP-ribose)polymerase 1 (PARP-1) and postischemic brain damage. Curr. Opin. Pharmacol. 8, 96–103.
Li, H., et al., 2015. The role of PARP-1 in host-pathogen interaction and cellular stress responses. Crit. Rev. Eukaryot. Gene Expr. 25, 175–190.
Liu, J., Moyon, S., Hernandez, M., Casaccia, P., 2016. Epigenetic control of oligodendrocyte development: adding new players to old keepers. Curr. Opin. Neurobiol. 39, 133–138.
Madison, D.L., Stauffer, D., Lundblad, J.R., 2011. The PARP inhibitor PJ34 causes a PARP1-independent, p21dependent mitotic arrest. DNA Repair (Amst) 10, 1003–1013.
Neira-Peña, T., et al., 2015. Perinatal asphyxia leads to PARP-1 overactivity, p65 translocation, IL-1β and TNF-α overexpression, and apoptotic-like cell death in mesencephalon of neonatal rats: prevention by systemic neonatal nicotinamide administration. Neurotox. Res. 27, 453–465.
Pavri, R., et al., 2005. PARP-1 determines specificity in a retinoid signaling pathway via direct modulation of mediator. Mol. Cell 18, 83–96.
Plane, J.M., Grossenbacher, S.K., Deng, W., 2012. PARP-1 deletion promotes subventricular zone neural stem cells toward a glial fate. J. Neurosci. Res. 90, 1489–1506.
Scott, G.S., et al., 2004. The therapeutic effects of PJ34 [N-(6-oxo-5,6-dihydrophenanthridin-2-yl)-N,N-dimethylacetamide.HCl], a selective inhibitor of poly(ADP-ribose) polymerase, in experimental allergic encephalomyelitis are associated with immunomodulation. J. Pharmacol. Exp. Ther. 310, 1053–1061.
Selvaraj, V., et al., 2009. PAFotoRP-1 deficiency increases the severity of disease in a mouse model of multiple sclerosis. J. Biol. Chem. 284, 26070–26084.
Strosznajder, J.B., Jesko, H., Strosznajder, P., 2000. Age-related alteration of poly(ADP-ribose) polymerase activity in different parts of the brain. Acta Biochim. Pol. 47, 331–337.
Veto, S., et al., 2010. Inhibiting poly(ADP-ribose) polymerase: a potential therapy against oligodendrocyte death. Brain 133, 822–834.
Windrem, M.S., et al., 2004. Fetal and adult human oligodendrocyte progenitor cell isolates myelinate the congenitally dysmyelinated brain. Nat. Med. 10, 93–97.
Yoo, Y.D., Huang, C.T., Zhang, X., Lavaute, T.M., Zhang, S.C., 2011. Fibroblast growth factor regulates human neuroectoderm specification through ERK1/2-PARP-1 pathway. Stem Cells 29, 1975–1982.
Young, K.M., et al., 2013. Oligodendrocyte dynamics in the healthy adult CNS: evidence for myelin remodelling. Neuron 77, 873–885.
Zuchero, J.B., Barres, B.A., 2013. Intrinsic and extrinsic control of oligodendrocyte development. Curr. Opin. Neurobiol. 23, 914–920.

4.5 Cell death in pure-neuronal and neuron-astrocyte mixed primary culture subjected to oxygen-glucose deprivation: The contribution of poly(ADP-ribose) polymerases and caspases (Baldassarro et al., 2018).

Cell death in pure-neuronal and neuron-astrocyte mixed primary culture subjected to oxygen-glucose deprivation: The contribution of poly(ADP-ribose) polymerases and caspases

Vito A. Baldassarro [a,b,1], Alessandra Marchesini [c,1], Fabrizio Facchinetti [d], Gino Villetti [d], Laura Calzà [a,b,c,*], Luciana Giardino [a,c,e]

[a] Health Science and Technologies Interdepartmental Center for Industrial Research (HST-ICIR), University of Bologna, Italy
[b] Department of Pharmacy and Biotechnology, University of Bologna, Italy
[c] IRET Foundation, Ozzano Emilia, Italy
[d] Chiesi Farmaceutici, Parma, Italy
[e] Department of Veterinary Medical Sciences, University of Bologna, Italy

ARTICLE INFO

ABSTRACT

Primary cortical neurons subjected oxygen-glucose deprivation (OGD) is an *in vitro* model that mimics fundamental aspects of neonatal hypoxic-ischemic encephalopathy (HIE) and is widely used to test neuroprotective treatments. However, controversial results characterize the existing literature on the OGD model. To shed some light on the initial cell death triggers in OGD, we first investigated the contribution of glucose- or oxygen-deprivation, alone or in combination, to cell viability/death in two cell systems, i.e. pure neuronal: 98% neurons; 2% astrocytes- vs. mixed neuron/astrocytes: 50% neurons; 50% astrocytes- culture. Cell viability was evaluated biochemically (MTT, and LDH release) and morphologically by high-content screening. We first found that neuronal death triggered by OGD (3 h OGD + 24 h re-oxygenation) was mainly driven by glucose rather than oxygen deprivation. Astrocytes survival was not substantially affected. Caspase-3 activation was found both in neuronal and mixed neuron/astrocytes cultures, whereas PARP activation was evident only in pure neuronal cultures. To pharmacologically dissect the contribution of these pathways, we measured the effect of TIQ-A (PARP 1 inhibitor) and ZVAD-fmk (pan-caspase inhibitor), individually or in combination, on culture viability after 3 h OGD. We found that only the combination treatment exerts a significant neuroprotective effect particularly evident in pure neuronal cultures. In sum, glucose deprivation is the major cell death trigger in OGD and neurons are more sensitive to OGD than astrocytes. Both PARP and caspases are concurrently activated in pure neuronal cultures and both contribute to neuronal cell death suggesting that neuroprotective strategies may require the simultaneous inhibition of multiple death pathways to be effective.

© 2016 Elsevier B.V. All rights reserved.

1. Introduction

To better comprehend the molecular pathways associated with brain ischemia, *in vitro* models have been used increasingly in recent years. Oxygen-glucose deprivation (OGD) is an *in vitro* organotypic or cellular model that mimics fundamental aspects of hypoxia/ischemia (HI) damage: low oxygen pressure, low nutrient levels and reperfusion. This system was initially used in oncology to mimic necrosis [1], then applied to either pure neuronal or mixed neuron/astrocytes cultures [2] and finally transferred to brain and spinal cord slices [3]. From that moment, OGD model was widely used to study brain ischemia and a variety of other pathologies and lesions involving HI in the central nervous system (CNS), such as stroke-like conditions and trauma [4].

The OGD model has been extensively characterized for its ability to mimic energy failure, recapitulating the *in vivo* situation better than other challenges, such as excitotoxicity exerted by direct exposure to glutamate agonists [5]. This model is particularly interesting in the study of neonatal hypoxic-ischemic encephalopathy (HIE), a syndrome determined by asphyxia occurring during the perinatal period [6], and to screen potential neuroprotective drugs. Moreover, this model is also useful for extreme form of metabolic stress resulting from oxygen and glucose deprivation, such as in cerebral ischemia (stroke) that most commonly occurs when the blood supply to a part of the brain is

suddenly interrupted by occlusion of a vessel. Because *in vivo* cerebral ischemia often consists of both reversible ischemia and blood flow reperfusion, the cultures in the OGD model are first exposed to *in vitro* ischemia, then returned to a normal medium in an oxygen atmosphere environment to simulate the *in vivo* blood flow reperfusion period. Although OGD is a combination of two metabolic insults, there is not a clear picture on what is the individual contribution of glucose and oxygen deprivation to cell death.

Two main molecular players have captured the attention as potential therapeutic targets for HIE and stroke induced cell death: caspases, which are the hallmark of apoptosis [7,8], and Poly(ADP-ribose) polymerases (PARP), which are nuclear proteins mainly known for their role in DNA double strand repair [9,10]. Caspases are a major player in neuronal death, but can also exacerbate inflammation and alter glial function [11]. PARP are a family of nuclear enzymes that catalyse the formation of (ADP-ribose)$_n$ chains from NAD$^+$ on acceptor proteins like histones and PARP itself, after DNA double strand breaks [12]. Among the 18 putative PARP sequences in the human genome, PARP-1 and PARP-2 are the best characterized and most abundant isoforms [13] that seem to be deeply involved in neuronal loss after ischemic damage [14]. When the damage is mild, PARP activity repairs DNA breaks and promotes cell survival, but in the presence of extensive DNA damage, over-activation of these enzymes causes massive NAD$^+$ consumption and consequent energy depletion and necrotic cell death [15]. PARP is also involved in the caspase-independent apoptosis pathway mediating Apoptosis Inducing Factor (AIF) translocation from mitochondrial matrix to nucleus, where it cleaves DNA into high molecular weight fragments [16].

However, not only neurons, but also astrocytes play a major role during HIE, being either neuroprotective or augmenting neuronal death during hypoxia, depending on the hypoxia conditions and timing [17]. The aim of the present study is to characterize an *in vitro* model widely used to test new neuroprotective molecules after hypoxia/ischemia damage, focusing on PARPs and caspases as putative molecular target. In particular (i) we first characterized the *in vitro* model of OGD (3 h OGD + 24 h re-oxygenation), in primary "pure neuronal culture" and in "mixed neurons-astrocytes culture" obtained from neonatal rats; (ii) we examined the relative contribution of glucose and oxygen deprivation, and their combination in inducing neuronal death; (iii) we utilized comparatively the most widely used biochemical viability methods (MTT and LDH) and the more recently introduced cell-based high content techniques (mitochondria function and nuclear morphology); (iv) we evaluated the effect of PARP (TIQ-A) and caspase (ZVAD-fmk) inhibitors, alone and in combination, in "pure neuronal" vs. mixed "astrocyte-neuronal" cultures subjected to OGD.

2. Materials and methods

2.1. Cell cultures

Cortical neurons from neonatal Wistar rats were prepared according to standard protocol [18,19]. Briefly, brains were removed, and cortical tissue dissected, freed from the meninges, and minced into small pieces. Cells were dispersed in Kreb's buffer (0.12 M NaCl, 4.8 mM KCl, 1.2 mM KH$_2$PO$_4$, 25.4 mM NaHCO$_3$, 14.2 mM glucose, 0.01 mg/ml phenol red, 1.5 mM MgSO$_4$) containing BSA 0.3% and 0.025% trypsin (Sigma-Aldrich) for 15 min at 37 °C, followed by mechanical trituration with a Pasteur pipette in Kreb's buffer containing 0.004% deoxyribonuclease I (DNaseI), and 0.052% soybean trypsin inhibitor (SBTI; Sigma-Aldrich). After centrifugation (500 g, 5 min), cells were resuspended in Neurobasal culture medium supplemented with 2% B27 (Gibco), 2 mM glutamine (Sigma-Aldrich), 100 U/ml penicillin, and 100 μg/ml streptomycin (Gibco) and plated onto Cultrex 2D substrate (0.25 mg/ml, Trevingen)-coated plates or coverslips. Cells were maintained in a humidified incubator at 37 °C with 5% CO$_2$. To obtain neuronal culture (99% neurons) cells were treated after 24 h with 10 μM

cytosine arabinofuranoside (Sigma-Aldrich). For mixed cultures no mitotic inhibitor was used. At 4 DIV, half of the medium was changed in both cultures.

2.2. Glutamate treatment

At 7 DIV neuronal cultures were treated with glutamate 0.5 mM. Briefly, medium was removed and cells were exposed to Krebs buffer containing or not glutamate, for 10 min. After glutamate treatment, Krebs buffer was replaced with the former conditioned medium. One group of cells were treated with MK801 10 μM from 1 h before the treatment to the end of the glutamate exposure.

2.3. OGD induction and treatments

OGD was performed using an air-tight hypoxia chamber (Billups-Rothenberg Inc., Del Mar., CA) saturated with 95% N$_2$- 5% CO$_2$ [2]. Glucose deprivation was achieved using a glucose-free Neurobasal medium, supplemented with B27, glutamine and penicillin/streptomycin, using the above-mentioned concentration. At 7 DIV cells were pre-treated for 1 h with TIQ-A 10 μM and ZVAD-fmk 30 μM (alone or in combination). MK801 10 μM was used as reference compound. Oxygen was removed by flushing the hypoxia chamber with N$_2$-CO$_2$ mixture for 6–8 min at 25 lt/min. The flushing was repeated after half the incubation time. The OGD condition was maintained for three hours, after which plates were re-oxygenated for 24 h in cell incubator in the pre-treatment culture medium.

2.4. PARP-1 activity assay

Proteins from cell lysates were quantified by Lowry assay (BioRad) following the manufacturer's instructions. The same amount of proteins were used for all the samples (400 ng). PARP enzymatic activity was measured using HT Colorimetric PARP Apoptosis Assay Kit (Trevingen), following the manufacturer's instructions in pure neuronal and mixed cultures.

2.5. MTT viability assay

Cell viability was measured by MTT colorimetric assay. Thiazolyl Blue Tetrazolium Bromide (Sigma-Aldrich) was dissolved 6.5 mg/ml in PBS and diluted 0.5 mg/ml in OptiMem (Gibco). Medium was removed and cells incubated for 3 h in incubator with the MTT solution. Formazan salts were solubilized by adding solubilisation solution (80% v/v isopropyl alcohol, 10% v/v HCl 1 N, 10% v/v Triton-X) and shaking the plates for 1 h at room temperature (RT). Absorbance was measured with a microplate reader (BioRad) at 570 nm.

2.6. LDH activity assay

LDH activity measurement was performed with PIERCE LDH Cytotoxicity Assay Kit, following the manufacturer's instructions. Both neuronal and mixed cultures were grown in a 96well plate (100,000 cells/well); after the re-oxygenation period, medium was collected and the activity of LDH enzyme in the medium was measured.

2.7. Immunocytochemistry

To evaluate neurotoxic stimulus effect on neurons and astrocytes, immunocytochemistry (ICC) was performed. Cells were seeded onto Cultrex 2D substrate (0.25 mg/ml, Trevingen)-coated coverslips and fixed after treatment with ice-cold 4% paraformaldehyde for 20 min at RT. After a fast wash in PBS, cells were incubated for 1 h with BSA 1%, 0.5% goat serum, 0.5% donkey serum in PBS- 0.3% Triton-X 100, then incubated overnight with primary antibody anti-β-III-tubulin (mouse, R&D, 1:1000), anti-GFAP (rabbit, Dako, 1:1000), anti-Iba-1 (rabbit,

Wako, 1:250), anti-active caspase 3 (rabbit, BD Pharmingen 1:200) diluted in PBS-0.3% Triton-X 100. Cells were washed with PBS and incubated with secondary antibody goat Alexa 488-conjugated anti mouse and/or goat Alexa 568-conjugated anti-rabbit (Invitrogen) for 30 min at 37 °C. After immunofluorescence staining, cells were incubated with the nuclear dye Hoechst 33258 (1 μg/ml in PBS, 0.3% Triton-X 100) for 20 min at RT. Cells were finally washed in PBS and coverslipped in glycerol and PBS (3:1, v/v) as mounting medium containing 0.1% paraphenylenediamine.

2.8. Cell-based high content screening

For HCS analysis cells were grown in 96 flat-bottom well HCS plates (NUNC; 100,000 cells/well). The mixed culture was stained following the immunocytochemistry protocol described above, using primary anti-Iba1 (rabbit, Wako, 1:250). Nuclei were stained with Hoechst 33258 as described above. Analysis of the percentage of Iba-1 positive cells was performed with Cell Insight™ CX5 High Content Screening (HCS) (ThermoFisher Scientific). Neurons and astrocytes were discriminated by nuclear size, while microglia by Iba1-immunostaining.

Mitotracker Red CMXRos (ThermoFisher Scientific) was used to stain mitochondria of living cells. After reperfusion cells were incubated with the fluorescent dye (100 nM) for 15 min at 37 °C. After a washing step using growth medium, cells were then fixed using ice-cold 4% paraformaldehyde for 20 min at RT. Cells were rinsed 2 times with PBS and stained following the immunocytochemistry protocol described above, using primary anti-GFAP (rabbit, Dako, 1:1000) and secondary anti-rabbit Alexa 488-conjugated (Invitrogen, 1:500).

Using Cell Insight™ CX5 HCS, cells were discriminated as GFAP-positive or -negative cells and fluorescence analysis of the MitoTraker fluorescence was performed on GFAP-negative cells only, identified as neurons. Cells showing a low MitoTracker fluorescence are considered with depolarized mitochondria. The software is able to detect nuclei as "object" considering each nucleus a single cell and it also detect the fluorescence in the cytoplasm belonging to the identified nucleus. This allows to clearly associate positive cells to a specific markers.

In the same cultures, the software is used to analyse the nuclear morphology based on the fluorescence intensity of the Hoechst 33258 staining and the nuclear size, using GFAP staining to differentiate neurons and astrocytes. Nuclei showing high fluorescence intensity and small size are identified as condensed/fragmented.

2.9. Fluorescence microscopy

To study the effect of the OGD on caspase-3 activation and the effect of the drugs on pure neuronal and mixed cultures we used a fluorescence microscopy approach to analyse the nuclear morphology. Immunocytochemistry was performed as described above to identify neurons and astrocytes.

Coverslips were observed using a Nikon eclipse E600 (Nikon, Italy) equipped with digital CCD camera Q imaging Retiga 20002V (Q Imaging, Surry, BC, Canada). Percentage of condensed nuclei and active caspase-3 positive cells was calculated. All images were taken at a magnification of 20× objective, 5 fields per coverslip were considered and at least 2 coverslips per condition were analysed from two independent observators. Controls using the secondary antibodies, alone, were performed and resulted negatives.

2.10. Statistical design and analysis

All data derive from at least three independent experiments. The number of technical replicates included in each experiment is indicated in the result. Prism software (GraphPad Software) was used for statistical analyses and the preparation of graphs. Data in histograms are reported as mean ± SEM. Student's t-test or one-way ANOVA and Dunnett's multiple comparison post-hoc test were used to analyse

data. Results were considered significant when the probability of their occurrence as a result of chance alone was <5% ($P < 0.05$).

3. Results

3.1. Cell system, glutamate toxicity, OGD characterization and analytical methods

We first characterized the cell populations obtained in the presence ("pure neural") and in the absence ("mixed neural-astrocyte") of Ara-C treatment. Representative micrographs of mixed (A, B) and pure (C) neuronal cultures are reported in Fig. 1, where β-III-tubulin (green) identifies neurons, GFAP (red in A and C) astrocytes and Iba1 (red in B) microglia. Quantitative results are reported in Fig. 1D. The mixed culture is composed of around 50% of GFAP-positive astrocytes, around 50% of β-III-tubulin-positive neurons and 1% Iba1-positive microglial cells (Fig. 1D). "Pure" neuronal cultures were obtained by Ara-C treatment, leading to <5% of astrocytes in the culture (Fig. 1D).

Primary cortical neurons at 7 DIVs express the active form of NMDA receptors [20], especially when isolated from new-born pups [21]. In order to confirm that our culture system is sensitive to glutamate, pure neuronal cultures were used to characterize the response of neurons at 7DIV to glutamate toxicity (Fig. 1E). Cells viability in neurons exposed to 0.5 mM of glutamate for 10 min was severely affected leading to >60% of cell death compared to control ($P < 0.0001$). Treatment with the NMDA antagonist MK801 totally rescued cell viability in the cell system.

Pure neuronal and mixed neuronal-astrocytes cells systems were then used in parallel in all the experiments. We first investigated the contribution of glucose- or oxygen-deprivation, alone or in combination, to cell viability/death. The schedule of the experiment is reported in Fig. 2. The same sets of experiments were analysed by different analytical methods exploring mitochondrial function and cell death, i.e. the mitochondria-based MTT viability assay; the LDH assay based on the release of the cytoplasmic enzyme; cell-based mitochondrial membrane potential by Mitotracker and nuclear morphology by Hoechst 33258 using cell-based high content screening. Results are reported in Fig. 3, where treatments are also indicated on the X-axis. Both MTT (Fig. 3A) and LDH assay (Fig. 3B) indicated that glucose deprivation is the major trigger of cell death in both "pure" and "mixed" cultures (MTT: mixed culture $P = 0.0017$; pure neuronal culture $P < 0.0001$; LDH mixed culture $P = 0.0138$; pure neuronal culture $P = 0.0014$), while the contribution of oxygen deprivation appears to be negligible. Since these biochemical assays do not allow any discrimination between the different cell types (neurons vs. glia) present in the culture, we also used a morphological approach based on cell-specific antigen recognition and coupled to high-throughput imaging and analysis to distinguish the OGD-affected population in mixed cultures. We first analysed the mitochondrial depolarization in neurons (recognized as GFAP-negative cells) as early event in neurodegeneration [22] occurring shortly after the OGD exposure [23], confirming that neurons are much less sensitive to OGD when cultured in the presence of astrocytes (Fig. 3C; mixed culture: $P = 0.0007$; pure neuronal culture $P < 0.0001$). Using this technique we also showed that viability of astrocytes (recognized as GFAP-positive cells) is not affected by the OGD conditions used in this study (*data not shown*).

We then investigated the effect of the OGD on nuclear morphology, as a late event in neurodegeneration (Fig. 3D). In mixed cultures showing mitochondrial depolarization, astrocytes are not affected by OGD, while neurons show vulnerability to both glucose deprivation and OGD (glucose deprivation $P = 0.03$; OGD $P = 0.0008$), but not to oxygen deprivation alone. Cell death analysed by nuclear morphology in the pure neuronal culture produces results that are in line with those obtained with the MTT assay (OGD, $P < 0.0001$). Additionally, the analysis of cell death by nuclear morphology allows the determination of the affected cell type in the mixed cultures.
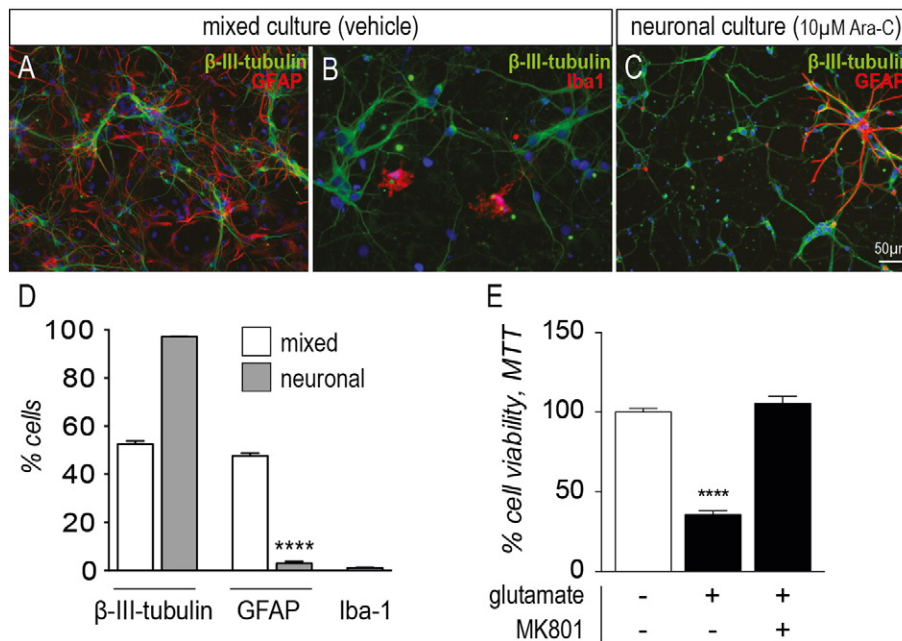
Fig. 1. Composition of the two cell systems. A–C: Representative images (fluorescence microscopy) of mixed (A and C) and neuronal (B) cultures. Neurons are labelled by anti-β-III-tubulin antibody (green); astrocytes are labelled by anti-GFAP antibody (red; A and C); microglia is labelled by anti-Iba-1 antibody (red; B). Bar = 50 μm. D: Cell composition in the two systems is quantified as a percentage of immunoreactive cells. E: Cell viability measured by MTT assay. Data were represented as percentage of cell viability, where the control group accounts for 100% of viability. Data are presented as mean ± SEM. Statistical analysis: D, Student's t-test; ****$P < 0.0001$; E, One-way ANOVA and Dunnet's multiple comparison post-test, where the control group is glutamate −/MK801 -; ****$P < 0.0001$. Abbreviations: Ara-C, cytosine arabinofuranoside; GFAP, Glial fibrillary acidic protein; Iba-1, Ionized calcium binding adaptor molecule.

3.2. Involvement of PARP and caspase-3 to OGD-induced cell death

To confirm the involvement of caspases- and PARP-pathways in the OGD model, we first measured caspase activation and PARP activity (Fig. 4B and C, respectively). Caspase activation, as visualized by caspase-3-immunoreactivity (Fig. 4A), was compared to the percentage of condensed nuclei as a marker of cell death. Caspase-3 is activated in both pure neuronal (40% of total neurons; $P < 0.0001$) and mixed cultures (20% of total neurons; $P = 0.0019$), and cell death was higher in pure neurons (80% of total neurons; $P < 0.0001$) than in mixed cultures (40% of total neurons; $P < 0.0001$) (Fig. 4B). Since caspase activation in OGD neurotoxicity is driven by glutamate [2], we utilized the NMDA receptor antagonist MK801 to counteract OGD-induced cell death. When used 1 h before OGD exposure, MK801 decreased cell death and caspase-3 activation (Fig. 4B). This analysis in the mixed cultures do not distinguished between astrocytes and neurons.

Results for the direct measure of PARP activity are shown in Fig. 4C. In mixed cultures, where cell death is lower than in pure neuronal cultures, PARP activity is not affected by OGD, while in pure neuronal cultures we observed an increase in PARP activity ($P = 0.0061$). The PARP

inhibitor TIQ-A completely abolished the increase of PAPR activity triggered by OGD. Conversely, MK801 is ineffective in counteracting PARP activation by OGD.

The effect of PARP-inhibitor (TIQ-A) and a pan-caspase inhibitor (ZVAD-fmk), alone or in combination, were tested on cell viability upon OGD (Fig. 5). Neither TIQ-A nor ZVAD-fmk affected cell viability in control cultures (concentration curve: TIQ-A and ZVAD-fmk, 0.1 nM till 10 μM, 8 points; *data not shown*). Treatments were performed 1 h before OGD exposure. When used alone, neither TIQ-A nor ZVAD-fmk counteracted OGD-induced neurotoxicity in both pure and mixed neuronal cultures. Interestingly, the co-treatment with both TIQ-A and ZVAD-fmk resulted in a partial restoration of cell viability as assessed both by biochemical (MTT, combination vs. OGD $P = 0.001$) and morphological (% condensed nuclei, combination vs. OGD, mixed cultures $P = 0.0113$; neuronal cultures $P = 0.0012$) assays.

4. Discussion

Standardization of *in vitro* models is a crucial step towards providing reliable, technically straightforward, and robust data for drug discovery and decreasing the attrition rate, as also recommended in the Good Cell Culture Practice ECVAM guidelines (European Union Reference Laboratory for alternatives to animal testing) [24]. Although used for testing neuroprotective strategies in the case of many neurological lesions and diseases, including stroke and HIE, the in vitro OGD model has not been yet fully characterized and standardized [4,25,26,27]. In this study we characterized the cytotoxic effect of OGD and its individual components, namely glucose and oxygen deprivation, in two cell systems, i.e. "pure neurons" vs. "mixed astrocyte-neuron" cultures, commonly utilized for testing of neuroprotective strategies. We concentrated on the inhibition of two main pathways involved in cell death/survival after hypoxia/ischemia damage, e.g. caspases and PARP [14,28,29,30,31]. We also compared different viability tests, based on biochemical and morphological analytical methods.

We first compared the contribution of oxygen and glucose deprivation, respectively. Very few and contradictory data consider moderate
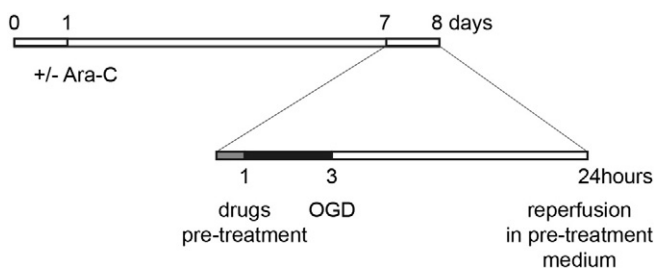

Fig. 2. Experimental design. The cell systems (+/− Ara-C) were allowed to mature for 7 days and then pre-treated with the drugs 1 h before OGD exposure. OGD lasted 3 h, and viability was then analysed after 24 h of reperfusion. Abbreviations: Ara-C, cytosine arabinofuranoside; OGD, oxygen-glucose deprivation.
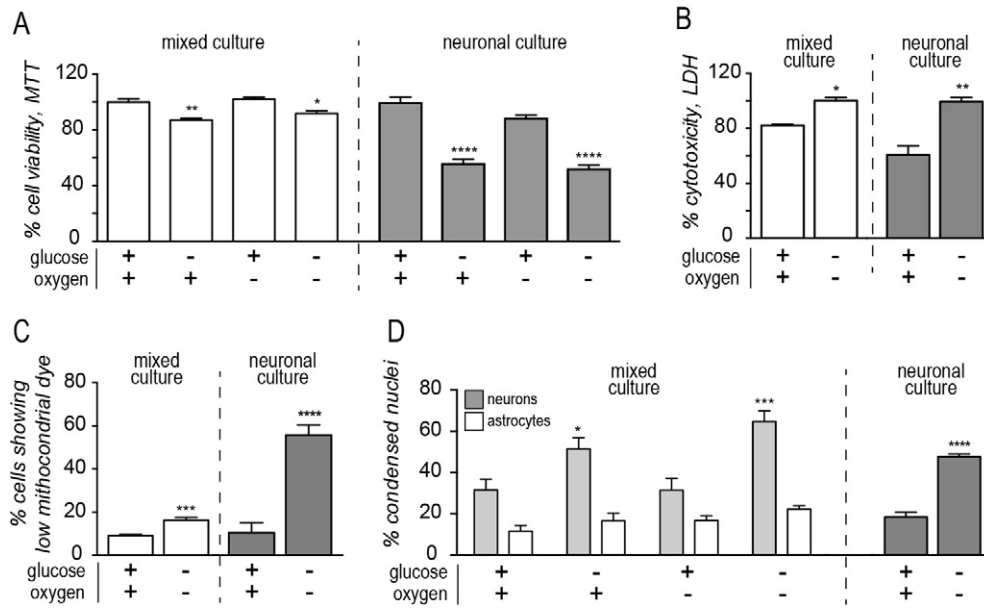
Fig. 3. Relative contribution of oxygen- and glucose-deprivation to cell death in the OGD model. A: Cell viability measured by MTT assay. Data were represented as percentage of cell viability, where the control group accounts for 100% of viability. B: Cell viability measured by LDH assay in the culture media. Data are presented as a percentage of the OGD value. C: HCS analysis of mitochondria depolarization as measured using MitoTracker, where cells showing low levels of mitochondrial dye were identified as cells with depolarized mitochondrial membranes. D: HCS analysis of nuclear morphology. Condensed and fragmented nuclei are represented as percentage of the total number in the respective cell populations (neurons and astrocytes). Data are presented as mean ± SEM. Statistical analysis: B, C and neuronal cultures in D, Student's *t*-test; *$P < 0.05$; **$P < 0.01$; ***$P < 0.001$; ****$P < 0.0001$; A and mixed cultures in D, One-way ANOVA and Dunnet's multiple comparison post-test, where the control group is glucose+/oxygen+ in the respective cell system; *$P < 0.05$; **$P < 0.01$; ****$P < 0.0001$.

(1–2% oxygen) or severe (absence) hypoxia *in vitro* as a cell death in-ducing factor [32,33,34], or as protective in association with hypoxia-in-ducible factors-1 (HIF-1) up-regulation and VEGF action [35]. We found that the absence of glucose is the major trigger of cell death in both pure and mixed neuronal cultures in the standard OGD conditions used in this study. This is in line with previously published data, indicating
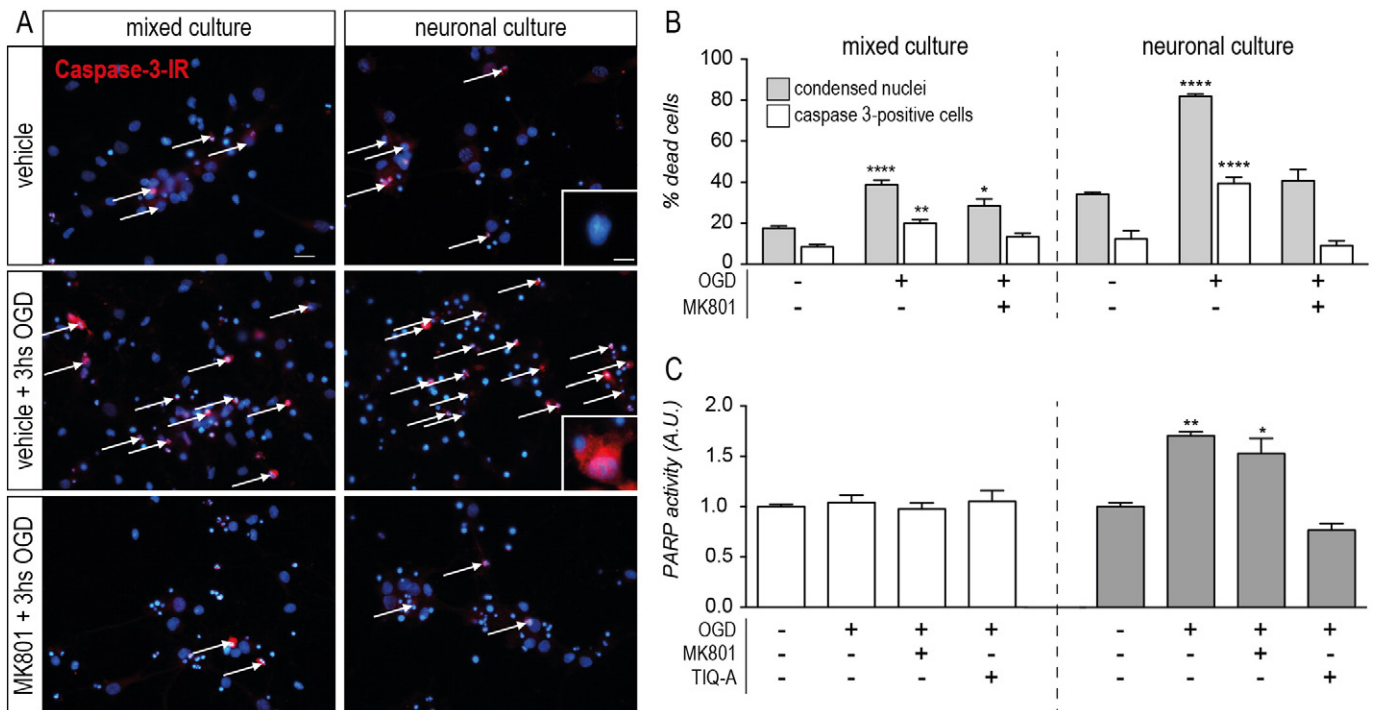
Fig. 4. Caspase-3 and PARP activation after OGD. A: Representative images of active caspase-3 (red)/Hoechst 33258 (blue) staining (fluorescence microscopy), in mixed and pure neuronal cultures, after OGD and after OGD + MK801. Bar: 20 μm. Arrows indicate example of "cleaved-caspase-3 positive cells". High magnification images of single negative- (neuronal culture, vehicle) and positive-cells (neuronal culture, vehicle +3 hs OGD) are included in the figure. Bar = 5 μm B: Quantitative analysis of condensed/fragmented nuclei and active caspase-3 positive cells in mixed and pure neuronal cultures. C: PARP activity in mixed and pure neuronal cultures after OGD, OGD + MK801 and OGD + TIQ-A. Data are presented as mean ± SEM. Statistical analysis: One-way ANOVA and Dunnet's multiple comparison post-test, where the control group is OGD−/MK801- in the respective cell system; *$P < 0.05$; **$P < 0.01$; ****$P < 0.0001$. Abbreviations: OGD, oxygen-glucose deprivation.
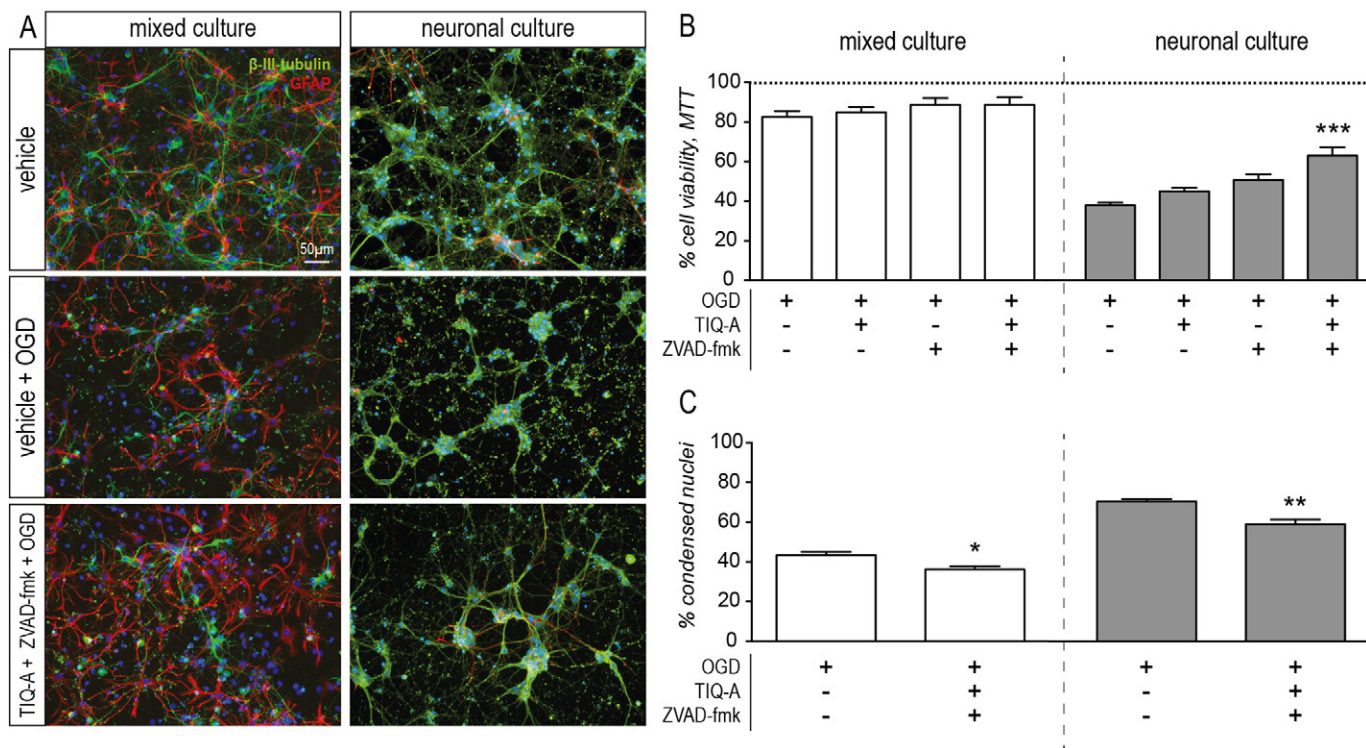
Fig. 5. Effect of Caspases and PARP inhibition in OGD treated cultures. A: Representative images of mixed and neuronal cultures (fluorescence microscopy), after OGD and OGD + TIQ-A + ZVAD-fmk. Neurons are labelled by anti-β-III-tubulin (green); astrocytes are labelled by anti-GFAP (red). Bar = 50 μm. B: Cell viability measured by MTT assay. Data were represented as percentage of cell viability, where the control group represents 100% of viability (horizontal dotted line). C: Quantitative analysis of condensed/fragmented nuclei in mixed and pure neuronal cultures. Data are presented as mean ± SEM. Statistical analysis: B, One-way ANOVA and Dunnet's multiple comparison post-test, where the control group is the OGD, ***$P < 0.001$. C, Student's t-test, *$P < 0.05$; **$P < 0.01$. Abbreviations: GFAP, Glial fibrillary acidic protein; OGD, oxygen-glucose deprivation.

glucose deprivation and glucose reperfusion as important triggers of neuronal death [36], also involving PARP-1 activation [37]. However, it should be pointed out that in standard culture conditions cells are exposed to 95% of air corresponding to 20% of oxygen, which is much higher than physiological *in vivo* condition (2.5–5.3%) [38]. Actually, a reduction of the atmospheric oxygen concentration from 21% to 3% did not modify cell death rate of neural precursors derived from different brain regions [39] and is considered a useful tool to promote neural differentiation [40].

As already indicated by a number of studies, we also confirmed that mixed culture are less sensitive to OGD, and the astrocytes are resistant to OGD in experimental conditions similar to those used in this study [2, 41]. However, the OGD experimental conditions differentially affect astrocytes. In fact, the activation of caspase-3 and -7 has been described in astrocytes after 75 min OGD [30] and astrocyte sensitivity to OGD has been described after 3 days of reoxygenation [43]. Moreover, depending on the OGD timing [30] and in combination with the mitochondrial damage [44], the caspase-9 mediated intrinsic apoptosis pathway is also involved in OGD-induced cell damage, leading to caspase-3 activation. A lactate-depending mechanism related to the glycogen storage confers astrocyte resistance to OGD [42,45]. We then evaluated if the presence of astrocytes in the culture affect neuron vulnerability to OGD. By using a morphological method in order to distinguish different cell population in the mixed culture, we found the same vulnerability of neurons compared to the pure neuronal cultures. It is well described the neuroprotective effect of astrocytes in mixed cultures against glutamate excitotoxicity [46]. However, when the injury involve a mitochondrial damage (i.e. during OGD exposure) astrocytes increased the vulnerability of neurons in the co-culture [47]. The neuroprotective effect depends on the OGD timing [45] and is not visible in biochemical assays, thus suggesting that morphological HCS methods should be preferred for

studying potential neuroprotective agents in astrocytes-neurons mixed cultures.

Moreover, we confirmed the activation of caspase-3 in both "pure" and "mixed" cultures after OGD exposure and 24 hr reperfusion, which is strongly reduced by the glutamate receptor inhibitor MK801. By using morphological viability assay, it is possible to study the OGD response of neuronal cultures from the early stages (mitochondrial damage) to the late apoptosis marker (condensed nuclei) throughout the intermediate steps of the intrinsic apoptosis pathway (caspase-3 activation), leading to more descriptive data than biochemical viability assays (MTT and LDH assays). Moreover we described the use of the cell-based High Content Screening in the study of OGD-induced cell death in pure and neuronal cultures, as already reported by our group [48], show different sensitivity compared to biochemical and conventional microscopy methods. The possibility to standardize methods in order to better dissect the mechanisms underlying cell death during hypoxia/ischemia can push forward the researches in the field.

We then investigated the effect of PARP-inhibitor TIQ-A [49] and the pan-caspase inhibitor ZVAD-fmk [50] on OGD in pure and mixed cultures, alone or in combination. We observed that the TIQ-A and ZVAD-fmk co-administration exerts a partial neuroprotective effect in pure neuronal cultures, while the effect observed in the mixed culture is very modest and can be appreciated only when using morphological methods.

A neuroprotective effect of TIQ-A in fetal mice cortical neurons treated with Ara-C but plated on a confluent astrocyte layer has been described [44,51]. However, the cell composition of the culture was not indicated in these studies. In contrast to these data, we saw no effects by TIQ-A on OGD induced cell death, using both biochemical and morphological assays, in pure neuronal and mixed cultures. Moreover, upon OGD, we found an increase in PARP enzymatic activity in the

pure but not in the mixed neuronal culture, thus suggesting that the presence of astrocytes dampens PARP activation.

Also, published data on caspase inhibition effectiveness in relation to neuroprotection after OGD are contradictory, pointing to either protection [50] or total inefficiency in blocking the death process [52] depending on the *in vitro* model utilized. In our experimental conditions, caspase inhibition, as well as PARP inhibition, do not counteract OGD-induced cell death in either pure or mixed cultures. Nevertheless, our data support a combinatorial approach to prevent neuronal death upon OGD, being the combination of z-VAD and TIQ-A neuroprotective. Our findings are in line with results reported by Yap and colleagues on the combination of PARP inhibitor 3-AB and caspase inhibitor ZVAD-fmk in the MCAO model as they observed an additive effect in the reduction of the infarcted area after the combination treatment with the two inhibitors [53]. In fact, mounting evidence indicates that a hybrid phenotype of cell death between apoptosis and necrosis, called necroptosis, can be observed in neuronal cells after ischemia induction [26,54].

In this scenario, in which multiple cellular and molecular mechanisms activated upon OGD could possibly lead to either neuron death or neuron recovery, the astrocyte/neuron interplay has a major role [55] and this should be reflected in the type of the cell system utilized for testing or developing neuroprotective strategies. The choice of a proper well-standardized *in vitro* culture system coupled with HCS can indeed improve the translational power of the OGD model.

Acknowledgements

References

[1] L. Hlatky, R.K. Sachs, E.L. Alpen, Joint oxygen-glucose deprivation as the cause of necrosis in a tumor analog, J. Cell. Physiol. 134 (1988) 167–178.

[2] M.P. Goldberg, D.W. Choi, Combined oxygen and glucose deprivation in cortical cell culture: calcium-dependent and calcium-independent mechanisms of neuronal injury, J. Neurosci. 13 (1993) 3510–3524.

[3] R. Berger, A. Jensen, W. Paschen, Metabolic disturbances in hippocampal slices of fetal Guinea pigs during and after oxygen-glucose deprivation: is nitric oxide involved? Neurosci. Lett. 245 (1998) 163–166.

[4] S. Camos, J. Mallolas, Experimental models for assaying microvascular endothelial cell pathophysiology in stroke, Molecules 15 (2010) 9104–9134.

[5] H. Cimarosti, J.M. Henley, Investigating the mechanisms underlying neuronal death in ischemia using in vitro oxygen-glucose deprivation: potential involvement of protein SUMOylation, Neuroscientist 14 (2008) 626–636.

[6] J.J. Kurinczuk, M. White-Koning, N. Badawi, Epidemiology of neonatal encephalopathy and hypoxic-ischaemic encephalopathy, Early Hum. Dev. 86 (2010) 329–338.

[7] G.M. Cohen, Caspases: the executioners of apoptosis, Biochem. J. 326 (1997) 1–16.

[8] A.G. Porter, R.U. Janicke, Emerging role of caspase-3 in apoptosis, Cell Death Differ. 6 (1999) 99–104.

[9] M.O. Hottiger, Nuclear ADP-Ribosylation and its role in chromatin plasticity, cell differentiation, and epigenetics, Annu. Rev. Biochem. 84 (2015) 227–263.

[10] J.T. Heeres, P.J. Hergenrother, Poly(ADP-ribose) makes a date with death, Curr. Opin. Chem. Biol. 11 (2007) 644–653.

[11] N. Akpan, C.M. Troy, Caspase inhibitors: prospective therapies for stroke, Neuroscientist 19 (2013) 129–136.

[12] R.P. Strosznajder, K. Czubowicz, H. Jesko, J.B. Strosznajder, Poly(ADP-ribose) metabolism in brain and its role in ischemia pathology, Mol. Neurobiol. 41 (2010) 187–196.

[13] A.W. Oliver, J.C. Amé, S.M. Roe, V. Good, G. de Murcia, L.H. Pearl, Crystal structure of the catalytic fragment of murine poly(ADP-ribose) polymerase-2, Nucleic Acids Res. 32 (2004) 456–464.

[14] F. Moroni, Poly(ADP-ribose)polymerase 1 (PARP-1) and postischemic brain damage, Curr. Opin. Pharmacol. 8 (2008) 96–103.

[15] F. Moroni, E. Meli, F. Peruginelli, A. Chiarugi, A. Cozzi, R. Picca, P. Romagnoli, R. Pellicciari, D.E. Pellegrini-Giampietro, Poly(ADP-ribose) polymerase inhibitors attenuate necrotic but not apoptotic neuronal death in experimental models of cerebral ischemia, Cell Death Differ. 8 (2001) 921–932.

[16] S.A. Susin, H.K. Lorenzo, N. Zamzami, I. Marzo, B.E. Snow, G.M. Brothers, J. Mangion, E. Jacotot, P. Costantini, M. Loeffler, N. Larochette, D.R. Goodlett, R. Aebersold, D.P. Siderovski, J.M. Penninger, G. Kroemer, Molecular characterization of mitochondrial apoptosis-inducing factor, Nature 397 (1999) 441–446.

[17] G. Vangeison, D.A. Rempe, The Janus-faced effects of hypoxia on astrocyte function, Neuroscientist 15 (2009) 579–588.

[18] M. Fernández, S. Pirondi, T. Antonelli, L. Ferraro, L. Giardino, L. Calzà, Role of c-Fos protein on glutamate toxicity in primary neural hippocampal cells, J. Neurosci. Res. 82 (2005) 115–125.

[19] G. Del Vecchio, A. Giuliani, M. Fernandez, P. Mesirca, F. Bersani, R. Pinto, L. Ardoino, G.A. Lovisolo, L. Giardino, L. Calzà, Effect of radiofrequency electromagnetic field exposure on in vitro models of neurodegenerative disease, Bioelectromagnetics 30 (2009) 564–572.

[20] V. Hausherr, C. van Thriel, A. Krug, M. Leist, N. Schobel, Impairment of glutamate signaling in mouse central nervous system neurons in vitro by tri-ortho-cresyl phosphate at noncytotoxic concentration, Toxicol. Sci. 142 (2014) 271–284.

[21] Y.C. Lin, Z.H. Huang, I.S. Jan, C.C. Yeh, H.J. Wu, Y.C. Chou, Y.C. Chang, Development of excitatory synapses in cultured neurons dissociated from the cortices of rat embryos and rat pups at birth, J. Neurosci. Res. 67 (2002) 484–493.

[22] P. Lipton, Ischemic cell death in brain neurons, Physiol. Rev. 79 (1999) 1431–1568.

[23] E.A. Wappler, A. Institoris, S. Dutta, P.V.G. Katakam, D.W. Busija, Mitochondrial dynamics associated with oxygen-glucose deprivation in rat primary neuronal cultures, PLoS One 8 (2013), e63206.

[24] S. Coecke, M. Balls, G. Bowe, J. Davis, G. Gstraunthaler, T. Hartung, R. Hay, O.W. Merten, A. Price, L. Schechtman, G. Stacey, W. Stokes, Guidance on good cell culture practice, a report of the second ECVAM task force on good laboratory practice, Altern. Lab. Anim 33 (2005) 261–287.

[25] G. Singh, M.A. Siddiqui, V.K. Khanna, M.P. Kashyap, S. Yadav, Y.K. Gupta, K.K. Pant, A.B. Pant, Oxygen glucose deprivation model of cerebral stroke in PC-12 cells: glucose as a limiting factor, Toxicol. Mech. Methods 19 (2009) 154–160.

[26] B.P. Meloni, A.J. Meade, D. Kitikomolsuk, N.W. Knuckey, Characterisation of neuronal cell death in acute and delayed in vitro ischemia (oxygen-glucose deprivation) models, J. Neurosci. Methods 195 (2011) 67–74.

[27] S. Beraki, L. Litrus, L. Soriano, M. Monbureau, L.K. To, S.P. Braithwaite, K. Nikolich, R. Urfer, D. Oksenberg, M. Shamloo, A pharmacological screening approach for discovery of neuroprotective compounds in ischemic stroke, PLoS One 8 (2013), e69233.

[28] S. Namura, J. Zhu, K. Fink, M. Endres, A. Srinivasan, K.J. Tomaselli, J. Yuan, M.A. Moskowitz, Activation and cleavage of caspase-3 in apoptosis induced by experimental cerebral ischemia, J. Neurosci. 18 (1998) 3659–3668.

[29] A. Chiarugi, M.A. Moskowitz, Poly(ADP-ribose) polymerase-1 activity promotes NF-kappaB-driven transcription and microglial activation: implication for neurodegenerative disorders, J. Neurochem. 85 (2003) 306–317.

[30] C. Malagelada, X. Xifró, A. Miñano, J. Sabriá, J. Rodríguez-Alvarez, Contribution of caspase-mediated apoptosis to the cell death caused by oxygen-glucose deprivation in cortical cell cultures, Neurobiol. Dis. 20 (2005) 27–37.

[31] N. Badiola, C. Malagelada, N. Llecha, J. Hidalgo, J.X. Comella, J. Sabriá, J. Rodríguez-Alvarez, Activation of caspase-8 by tumour necrosis factor receptor 1 is necessary for caspase-3 activation and apoptosis in oxygen-glucose deprived cultured cortical cells, Neurobiol. Dis. 35 (2009) 438–447.

[32] P. Lewczuk, M. Hasselblatt, H. Kamrowski-Kruck, A. Heyer, C. Unzicker, A.L. Sirén, H. Ehrenreich, Survival of hippocampal neurons in culture upon hypoxia: effect of erythropoietin, Neuroreport 11 (2000) 3485–3488.

[33] A. Wick, W. Wick, J. Waltenberger, M. Weller, J. Dichgans, J.B. Schulz, Neuroprotection by hypoxic preconditioning requires sequential activation of vascular endothelial growth factor receptor and Akt, J. Neurosci. 22 (2002) 6401–6407.

[34] K.J. Banasiak, O. Burenkova, G.G. Haddad, Activation of voltage-sensitive sodium channels during oxygen deprivation leads to apoptotic neuronal death, Neuroscience 126 (2004) 31–44.

[35] D. Li, J.D. Marks, P.T. Schumacker, R.M. Young, J.R. Brorson, Physiological hypoxia promotes survival of cultured cortical neurons, Eur. J. Neurosci. 22 (2005) 1319–1326.

[36] S.W. Suh, E.T. Gum, A.M. Hamby, P.H. Chan, R.A. Swanson, Hypoglycemic neuronal death is triggered by glucose reperfusion and activation of neuronal NADPH oxidase, J. Clin. Invest. 117 (2007) 910–918.

[37] S.W. Suh, K. Aoyama, Y. Chen, P. Garnier, Y. Matsumori, E. Gum, J. Liu, R.A. Swanson, Hypoglycemic neuronal death and cognitive impairment are prevented by poly(ADP-ribose) polymerase inhibitors administered after hypoglycemia, J. Neurosci. 23 (2003) 10681–10690.

[38] I. Silver, M. Erecinska, Oxygen and ion concentrations in normoxic and hypoxic brain cells, Adv. Exp. Med. Biol. 454 (1988) 7–16.

[39] J. Milosevic, S.C. Schwarz, K. Krohn, M. Poppe, A. Storch, J. Schwarz, Low atmospheric oxygen avoids maturation, senescence and cell death of murine mesencephalic neural precursors, J. Neurochem. 92 (2005) 718–729.

[40] P. Mondragon-Teran, J.Z. Baboo, M. Mason, G.J. Lye, F.S. Veraitch, The full spectrum of physiological oxygen tensions and step-changes in oxygen tension affects the neural differentiation of mouse embryonic stem cells, Biotechnol. Prog. 27 (2011) 1700–1708.

[41] S.M. Jones, A.E. Novak, J.P. Elliott, Primary culture of cellular subtypes from postnatal mouse for in vitro studies of oxygen glucose deprivation, J. Neurosci. Methods 199 (2011) 241–248.

[42] A.M. Brown, B.R. Ransom, Astrocyte glycogen as an emergency fuel under conditions of glucose deprivation or intense neural activity, Metab. Brain Dis. 30 (2015) 233–239.

[43] E. Gouix, A. Buisson, A. Nieoullon, A. Kerkerian-Le Goff, J.S. Tauskela, N. Blondeau, L. Had-Aissouni, Oxygen glucose deprivation-induced astrocyte dysfunction provokes neuronal death through oxidative stress, Pharmacol. Res. 87 (2014) 8–17.

[44] M.H. Singh, S.M. Brooke, I. Zemlyak, R.M. Sapolsky, Evidence for caspase effects on release of cytochrome c and AIF in a model of ischemia in cortical neurons, Neurosci. Lett. 469 (2010) 179–183.

[45] C. Gao, L. Zhou, W. Zhu, H. Wang, R. Wang, Y. He, Z. Li, Monocarboxylate transporter-dependent mechanism confers resistance to oxygen- and glucose-deprivation injury in astrocyte-neuron co-cultures, Neurosci. Lett. 594 (2015) 99–104.

[46] N. Amin, B. Pearce, Glutamate toxicity in neuron-enriched and neuron-astrocytes co-cultures: effect of the glutamate uptake inhibitor L-trans-pyrrolidine-2,4-dicarboxylate, Neurochem. Int. 30 (1997) 271–276.

[47] L.A. Voloboueva, S.W. Suh, R.A. Swanson, R.G. Giffard, Inhibition of mitochondrial function in astrocytes: implications for neuroprotection, J. Neurochem. 102 (2011) 1383–1394.

[48] V.A. Baldassarro, L.S. Dolci, C. Mangano, L. Giardino, M.L. Focarete, L. Calzà, In vitro testing of biomaterials for neural repair: focus on cellular systems and high-content analysis, Biores. Open Access. 5 (2016) 201–211.

[49] A. Chiarugi, E. Meli, M. Calvani, R. Picca, R. Baronti, E. Camaioni, G. Costantino, M. Marinozzi, D.E. Pellegrini-Giampietro, R. Pellicciari, F. Moroni, Novel isoquinolone-derived inhibitors of poly(ADP-ribose) polymerase-1: pharmacological characterization and neuroprotective effects in an in vitro model of cerebral ischemia, J. Pharmacol. Exp. Ther. 305 (2003) 943–949.

[50] C. Wiessner, D. Sauer, D. Alaimo, P.R. Allegrini, Protective effect of a caspase inhibitor in models for cerebral ischemia in vitro and in vivo, Cell. Mol. Biol. 46 (2000) 53–62.

[51] F. Moroni, L. Formentini, E. Gerace, E. Camaioni, D.E. Pellegrini-Giampietro, A. Chiarugi, R. Pellicciari, Selective PARP-2 inhibitors increase apoptosis in hippocampal slices but protect cortical cells in models of post-ischemic brain damage, Br. J. Pharmacol. 157 (2009) 854–862.

[52] P.A. Jones, G.R. May, J.A. McLuckie, A. Iwashita, J. Sharkey, Apoptosis is not an invariable component of in vitro models of cortical cerebral ischaemia, Cell Res. 14 (2004) 241–250.

[53] E. Yap, W.L. Tan, I. Ng, Y.K. Ng, Combinatorial-approached neuroprotection using pan-caspase inhibitor and poly (ADP-ribose) polymerase (PARP) inhibitor following experimental stroke in rats; is there additional benefit? Brain Res. 1195 (2008) 130–138.

[54] F.J. Northington, R. Chavez-Valdez, E.M. Graham, S. Razdan, E.B. Gauda, L.J. Martin, Necrostatin decreases oxidative damage, inflammation, and injury after neonatal HI, J. Cereb. Blood Flow Metab. 31 (2011) 178–189.

[55] L.B. Tovar-y-Romo, A. Penagos-Puig, J.O. Ramírez-Jarquín, Endogenous recovery after brain damage: molecular mechanisms that balance neuronal life/death fate, J. Neurochem. 136 (2016) 13–27.

4.6 Vulnerability of primary neurons derived from Tg2576 Alzheimer mice to oxygen and glucose deprivation: role of intraneuronal amyloid-β accumulation and astrocytes. (Baldassarro et al., 2018).

The Company of Biologists

RESEARCH ARTICLE

SPECIAL COLLECTION: NEURODEGENERATION

Vulnerability of primary neurons derived from Tg2576 Alzheimer mice to oxygen and glucose deprivation: role of intraneuronal amyloid-β accumulation and astrocytes

Vito Antonio Baldassarro[1,2], Alessandra Marchesini[3], Luciana Giardino[1,4,3] and Laura Calzà[1,2,3,*]

ABSTRACT

Microvascular dysfunction is considered an integral part of Alzheimer disease (AD) pathogenesis, but the possible relationship between amyloid pathology, microvascular dysfunction and cell death is still unclear. In order to investigate the influence of intraneuronal amyloid-β (Aβ) accumulation on vulnerability to hypoxia, we isolated primary cortical neurons from Tg2576 (carrying the amyloid precursor protein APPSwe mutation) and wild-type fetal mice. We first demonstrated that neurons isolated from Tg2576 newborn mice show an increase in VEGFa mRNA expression and a decrease in the expression of the two VEGF receptors, Flt1 and Kdr, compared with wild-type cells. Moreover, APPSwe primary neurons displayed higher spontaneous and glutamate-induced cell death. We then deprived the cultures of oxygen and glucose (OGD) as an *in vitro* model of hypoxia. After OGD, APPSwe neurons display higher levels of cell death in terms of percentage of pyknotic/fragmented nuclei and mitochondrial depolarization, accompanied by an increase in the intraneuronal Aβ content. To explore the influence of intraneuronal Aβ peptide accumulation, we used the γ-secretase inhibitor LY450139, which showed that the reduction of the intracellular amyloid fully protects APPSwe neurons from OGD-induced degeneration. Conditioned medium from OGD-exposed APPSwe or wild-type astrocytes protected APPswe neurons but not wild-type neurons, during OGD. In conclusion, the presence of the mutated human APP gene, leading to the intracellular accumulation of APP and Aβ fragments, worsens OGD toxicity. Protection of APPSwe neurons can be obtained either using a γ-secretase inhibitor or astrocyte conditioned medium.

KEY WORDS: Alzheimer's disease, Primary neurons, Intraneuronal amyloid, Oxygen glucose deprivation, Glutamate, Neurovascular coupling

INTRODUCTION

Brain function is strictly dependent on an appropriate blood support and tissue perfusion, to ensure nutrient and oxygen delivery and to remove metabolic waste products (Zlokovic, 2011). The fine regulation of the blood support to the neurons is performed by the cerebrovascular unit (CVU) which provides the functional coupling between energy demand and vasodilation (Nelson et al., 2016). This histological structure includes neurons, vascular cells (endothelial cells, pericytes and vascular smooth muscle cells), glial cells (astrocytes, microglia, and oligodendrocytes) and extracellular matrix protein, which plays a part in blood–brain barrier (BBB) regulation. Notably, the paracrine mechanism, including vascular endothelial growth factor (VEGF) and related receptors, participates in the cross-talk among different cell types in both normal and ischemic conditions (Redzic et al., 2015). To highlight the importance of the glial component, namely astrocytes, the CVU is also termed 'gliovascular unit'. In the CVU, astrocytes define functional domains and contact the microvessels with endfeet plastered on the vessel wall (Nedergaard et al., 2003). This physical contact is also used to guarantee the lactate/glucose dynamic in the CVU (Barros et al., 2007).

The contribution of vascular dysfunctions to Alzheimer's disease (AD) pathogenesis is now receiving increasing attention, especially in late-onset forms of the disease (Kapasi and Schneider, 2016). Recent imaging studies in preclinical and early AD have indicated that an impairment of the CVU leading to a reduction of the cerebral blood flow is an early event in AD (Garwood et al., 2016; van de Haar et al., 2016). However, the relative contribution of the different cell types and molecular mechanisms in CVU dysfunction, and its impact on neuron vulnerability is not clear. In fact, on one hand, neurons progressively accumulate amyloid peptide in the cytoplasm, leading to an increase of the intrinsic vulnerability (Baker-Nigh et al., 2015). On the other hand, astrocytes are subject to a number of cellular and molecular regulations related to the pathological microenvironment, including their activation as a consequence of AD neuroinflammation and amyloid plaques. It is not clear whether this results in neuroprotection, in further damage or in a biphasic effect, depending on the stage of the disease (Garwood et al., 2016).

In vitro models are useful to understand the relative contribution of intrinsic neuronal vulnerability due to β-amyloid (Aβ) peptide accumulation (Baldassarro et al., 2014) and astrocyte support associated with brain hypoperfusion. In particular, oxygen and glucose deprivation (OGD) is an *in vitro* model that mimics fundamental aspects of hypoperfusion (and ischemic) damage, i.e. low oxygen pressure and low nutrient levels (Goldberg and Choi, 1993). This model has been widely used to explore cellular and molecular mechanisms in experimental set-ups mimicking ischemic lesions and trauma (Cimarosti and Henley, 2008; Baldassarro et al., 2016). However, to the best of our knowledge, no studies have been published in which OGD is applied to *in vitro* cell systems appropriate for AD, i.e. which accumulate Aβ peptides (Baldassarro et al., 2014). Thus, the aim of the study was to establish a possible

[1]Interdepartmental Centre for Industrial Research in Health Science and Technologies (ICIR - HST), University of Bologna, 40064 Ozzano Emilia, Bologna, Italy. [2]Department of Pharmacy and Biotechnology (FaBit), University of Bologna, 40127 Bologna, Italy. [3]Fondazione IRET, 40064 Ozzano Emilia, Bologna, Italy. [4]Department of Medical Veterinary Sciences (DIMEVET), University of Bologna, 40064 Ozzano Emilia, Bologna, Italy.

*Author for correspondence (laura.calza@unibo.it)

V.A.B., 0000-0003-1020-4261; A.M., 0000-0002-5834-7117; L.G., 0000-0003-3107-3264

Disease Models & Mechanisms

link between intraneuronal accumulation of Aβ and the vulnerability to a mild hypoxic/ischemic injury, using an *in vitro* model. First, we established an *in vitro* system of primary neurons and astrocytes derived from transgenic Tg2576 mice and wild-type controls. Tg2576 is a mouse model carrying a single human amyloid precursor protein mutation (APPswe) (Hsiao et al., 1996), and was chosen because of its predictive validity in pharmacological and non-pharmacological research targeting AD (Bilkei-Gorzo, 2014). These cell systems were then used to explore the contribution of intraneuronal Aβ accumulation and astrocyte-conditioned culture medium to neuron viability during OGD.

RESULTS
Cell system characterization and experimental design
Primary neurons were derived from the telencephalon of single pups, immediately characterized for the genotype. In this way, in each culture well, 100% of either wild-type (Wt) or APPswe neurons was seeded. Neurons were allowed to mature *in vitro* for 8 days, then characterized for cell composition by immunocytochemistry for neural (β-III-tubulin) and astroglial (GFAP) proteins (Fig. 1A). Both Wt and APPswe pure neuronal cultures contained a very low percentage of astrocytes (Wt, 3±2%; Tg2576, 2±3%), and no differences in cell composition between the genotypes were found. APPswe neurons were also characterized for amyloid peptide intracellular deposition using the 6E10 antibody. This antibody reacts with full-length amyloid precursor protein (APP) and the soluble form (sAPPα), as well as with the processed Aβ peptides. It is reactive to human-specific amino acid residues 1-6, within the amino acids 3-8 of Aβ. All neurons derived from
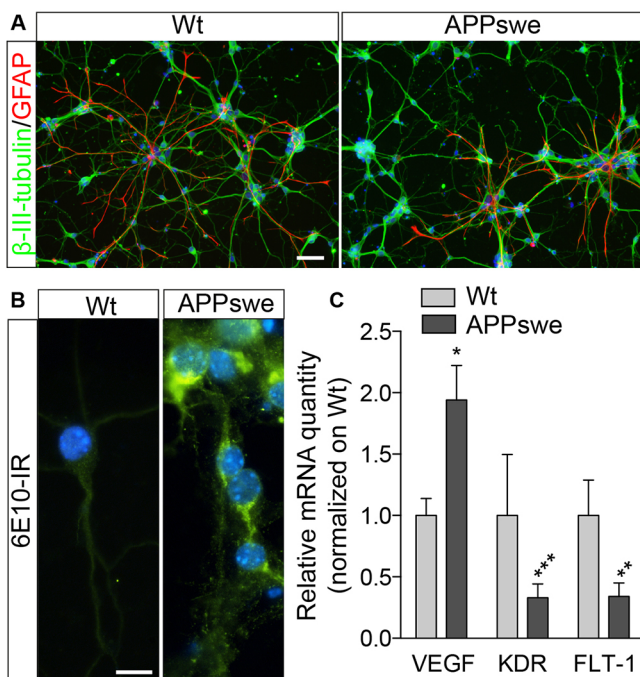
Tg2576 mice show high intensity staining, whereas Wt neurons are negative (Fig. 1B). We also investigated the expression level of VEGFa and related receptors, a regulatory factor with a key role in angiogenesis, vascular development, and neuronal survival after ischemia (Takahashi and Shibuya, 2005). Notably, *VEGFA* mRNA expression level in APPswe is twice that of Wt (P=0.0274), while type 1 (*FLT1*) and type 2 (*KDR*) VEGF receptors are strongly down-regulated (FLT-1, P=0.0092; KDR, P=0.001; Fig. 1C).

APPswe neurons are more vulnerable than Wt neurons
We then challenged Wt and APPswe neurons under conventional experimental conditions to mimic *in vitro* hypoxic/ischemic brain conditions. In particular, glutamate excitotoxicity was established by 10 min exposure to 42 μM glutamate [EC_{50} at 7 days in vitro (DIV); Ha et al., 2009] followed by 24 h withdrawal; OGD was applied for 3 h, followed by 24 h reperfusion (Goldberg and Choi, 1993; Baldassarro et al., 2016) (Fig. 2A). Cell viability was established by the contemporaneous analysis of the mitochondrial membrane potential by MitoTracker and nuclear morphology by Hoechst 33258, using cell-based high-content screening as an analytical method. MitoTracker is a mitochondrial-selective fluorescent label that allows mitochondria depolarization, an early event in neurodegeneration, to be recognized in neurons (Lipton, 1999). OGD-induced cell death is characterized by mitochondria depolarization and cells showing depolarized mitochondria can be identified as poorly MitoTracker-labelled cells (Wappler et al., 2013; Wilson et al., 2014). Vulnerability of Wt and APPswe neurons to glutamate excitotoxicity is shown in Fig. 2B. APPswe neurons showed a higher cell death compared to Wt, both in the absence and in the presence of glutamate (Fig. 2D; treatment: $F_{1,15}$, P<0.0001; genotype: $F_{1,15}$, P<0.0001). OGD resulted in cell death, as evaluated by mitochondrial function (Fig. 2C; OGD: $F_{1,33}$, P<0.0001; genotype: $F_{1,33}$, P<0.0001) and nuclear fragmentation in both Wt and APPswe neurons (Fig. 2D; OGD: $F_{1,17}$, P=0.0005; genotype: $F_{1,17}$, P<0.0001). OGD produced stronger neuron degeneration in APPswe than in Wt neurons (mitochondria, P<0.0001; nuclei, P=0.0237). Representative images of MitoTracker-positive neurons in normoxia and under OGD are presented in Fig. 2E,F,I,J. Morphological criteria for automatically distinguishing normal versus pathological nuclei (pyknotic and fragmented) and representative images of Hoechst 33258-stained nuclei after normoxia or OGD exposure are presented in Fig. 2G,H, K,L.

Intraneuronal amyloid increases neural vulnerability during OGD
In order to establish if intraneuronal accumulation of Aβ peptides contributes to the increased vulnerability of APPswe neurons compared to Wt we used the γ-secretase inhibitor LY450139. This drug reduces both soluble Aβ and amyloid plaque burden in transgenic mice, lowering $Aβ_{40}$ and $Aβ_{42}$ production and secretion by the γ-secretase enzyme complex (Abramowski et al., 2008). Neuronal cultures were treated with the γ-secretase inhibitor LY450139, starting from 48 h after seeding and for the entire duration of the experiment (Fig. 3A). LY450139 (10 μM) inhibits the generation of Aβ peptides *in vivo* and *in vitro*, as also described for primary neurons transfected with APPswe (Elvang et al., 2009; Jämsä et al., 2011). This treatment also produces a substantial decrease of cytoplasmic 6E10-immunostaining in APPswe neurons (Fig. 3B,C), which proves the effectiveness of the γ-secretase inhibition, resulting in a reduction in the intracellular levels of APP/ Aβ (Sivilia et al., 2013). Cells treated with LY450139 were then

Fig. 1. Culture characterization. (A) Representative images of double-stained cells showing β-III-tubulin-positive neurons and GFAP-positive astrocytes. Scale bar: 50 μm. (B) Representative images of 6E10-stained cells showing intracellular accumulation of the human APP protein/β-amyloid fragments. Scale bar: 10 μm. Nuclei are stained blue with Hoechst 33258. (C) mRNA expression level of VEGF and VEGF receptors FLT-1 and KDR (*VEGFA*, Wt n=15, APPswe n=11; *FLT1*, Wt n=13, APPswe n=11; *KDR*, Wt n=13, APPswe n=9). Bars represent mean+s.e.m. Statistical analysis: Student's t-test between genotypes (*P<0.05; **P<0.01; ***P<0.001).
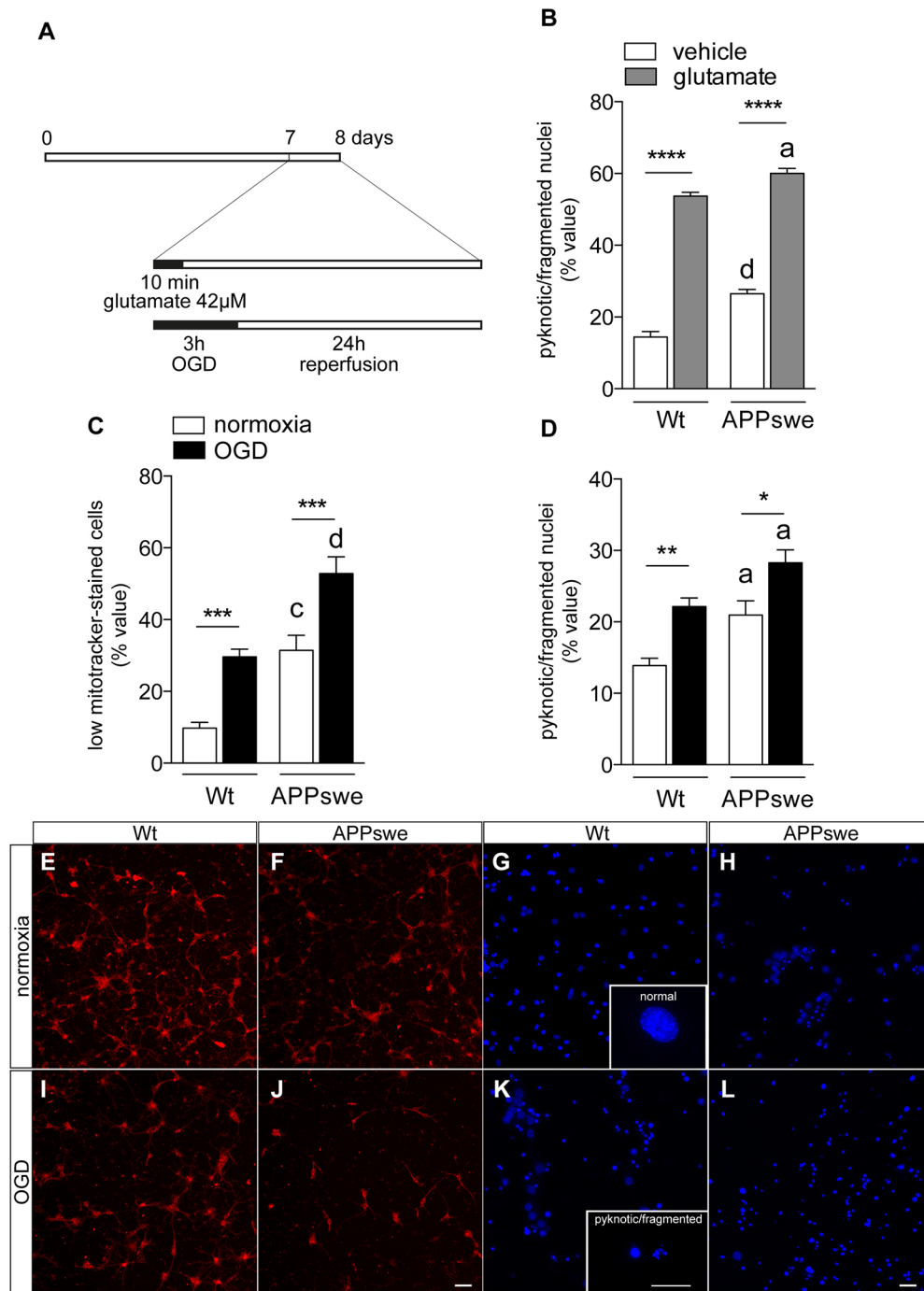
Fig. 2. Vulnerability of Wt and APPswe neurons to culture condition, glutamate excitotoxicity and OGD. (A) Experimental design. Primary neurons isolated from Wt and Tg2576 mice were exposed at 7 DIV to the challenge stimulus (42 µM glutamate or 3 h OGD). Cells were then exposed to the original culture medium for 24 h. (B) Cell viability analysis of Wt and APPswe neurons exposed to vehicle and glutamate, as established by nuclear morphology (Wt vehicle, n=4; Wt glutamate, n=5; APPswe vehicle, n=5; APPswe glutamate, n=5). (C,D) Cell viability analysis of Wt and APPswe neurons exposed to normoxia and OGD, as established by mitochondrial function (C; Wt normoxia, n=10; Wt OGD, n=10; APPswe normoxia, n=8; APPswe OGD, n=9) and nuclear morphology (D; Wt normoxia, n=6; Wt OGD, n=5; APPswe normoxia, n=5; APPswe OGD, n=5). (E-L) Representative images of MitoTracker-stained cells (E,F,I,J) and Hoechst-stained nuclei (G,H,K,L) isolated from Wt (E,I,G,K) and APPswe (F,J,H,L) mice and exposed to normoxia (E-H) or OGD (I-L). Scale bar: 50 µm (E,F,I,J) and 80 µm (G,H,K,L). G and K include high-magnification images of a normal nucleus (G) or pyknotic/ fragmented nuclei (K); scale bar: 10 µm. Bars represent mean±s.e.m. Statistical analysis: Two-way ANOVA, followed by Sidak's multiple comparison test. Asterisks represent differences between vehicle- and glutamate-treated groups (B; ****$P<0.0001$) or between normoxia- and OGD-exposed groups (C,D; *$P<0.05$; **$P<0.01$; ***$P<0.001$); letters represent differences between genotypes (a, $P<0.05$; c, $P<0.001$; d, $P<0.0001$).

exposed to OGD and analysed for mitochondrial function (Fig. 3D) and nuclear morphology (Fig. 3E). LY450139 did not modify cell viability either in Wt or APPswe neurons, but it did abolish the mitochondria dysfunction induced by OGD in APPswe neurons (Fig. 3D; normoxia versus OGD, $P=0.0028$; OGD versus OGD +LY450139, $P=0.0389$) and afford partial protection against nuclear pyknosis (Fig. 3E; normoxia versus OGD, $P=0.0268$).

Astrocyte-conditioned medium after OGD protects APPswe neurons from OGD

In order to investigate the possible contribution of the paracrine properties of Wt and APPswe astrocytes in neuronal vulnerability after OGD, we prepared conditioned medium from astrocytes

(ACM). The astrocytes were derived from Wt and APPswe mice. Cultures showing 98±2% of GFAP-positive cells and 6E10-immunoreactivity in APPswe GFAP-positive astrocytes are presented in Fig. 4B. We applied to astrocytes the same OGD protocol as used for neurons (3 h OGD and 24 h reperfusion). The culture medium was collected both after the OGD and reperfusion phases and used to treat primary neurons in the two phases of the experiment. Neuron viability after reperfusion was then established as mitochondria function (Fig. 4C) and nuclear morphology (Fig. 4D). ACM, whether from Wt or APPswe astrocytes, is not effective in protecting Wt and APPswe neurons from OGD. Conversely, ACM derived from both Wt and APPswe astrocytes fully protects APPswe neurons from OGD as measured by
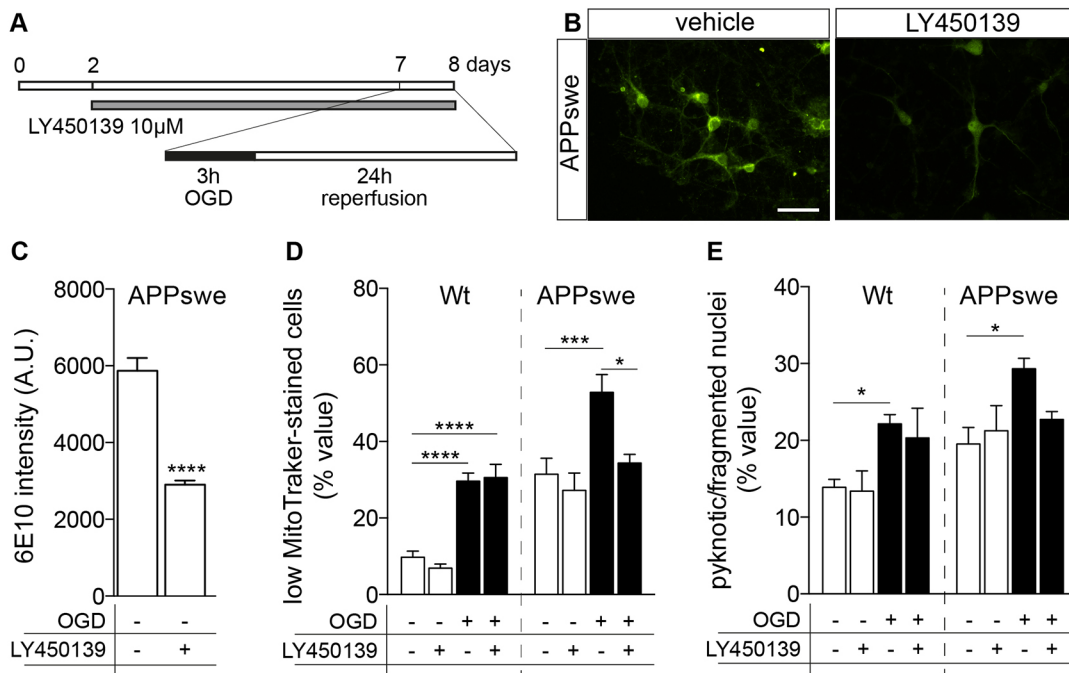
Fig. 3. Effect of γ-secretase inhibition on the vulnerability of primary neurons to OGD. (A) Experimental design. Primary neurons isolated from Wt and Tg2576 mice were treated with LY450139 from 2 DIV to the end of the experiment. At 7 DIV, cells were exposed to 3 h of OGD and 24 h of reperfusion in the previous culture medium. (B) Representative images of 6E10 immunostaining of APPswe neurons, showing the intracellular accumulation of human APP protein/Aβ fragments. Scale bar: 50 μm. (C) Quantification of 6E10 in Tg2576 cells exposed to normoxia and treated or not with LY450139 (APPswe vehicle, n=5; APPswe LY450139, n=5). (D,E) Cell viability analysis of Wt and APPswe neurons exposed to normoxia and OGD, treated or not with LY450139, as established by mitochondrial function (E; Wt normoxia, n=10; Wt normoxia, LY450139, n=6; Wt OGD, n=10; Wt OGD LY450139, n=4; APPswe normoxia, n=7; APPswe normoxia LY450139, n=6; APPswe OGD, n=8; APPswe OGD LY450139, n=4) and nuclear morphology (F; Wt normoxia, n=6; Wt normoxia LY450139, n=4; Wt OGD, n=5; Wt OGD LY450139, n=4; APPswe normoxia, n=5; APPswe normoxia LY450139, n=4; APPswe OGD, n=5; APPswe OGD LY450139, n=5). Bars represent mean±s.e.m. Statistical analysis: one-way ANOVA followed by Tukey's multiple comparisons test inside the same genotype. Asterisks represent differences between LY450139- and vehicle-treated groups (*P<0.05; ***P<0.001; ****P<0.0001).

mitochondrial function (Fig. 4D; OGD versus ACM-Wt, P=0.113; OGD versus ACM-hAPP, P<0.0001) and number of pyknotic nuclei (Fig. 4D; OGD versus ACM-Wt, P=0.0011; OGD versus ACM-hAPP, P=0.0022). No statistical differences between Wt and APPswe ACM in protecting APPswe neurons were detected (Fig. 4C; one-way ANOVA followed by Tukey's *post hoc* Wt versus APPswe ACM, P=0.1039).

DISCUSSION

Neurovascular abnormalities and aberrant glucose metabolism could be early events in the pathogenic cascade of AD and the underlying biological mechanisms are still obscure (Lourenço et al., 2015). In particular, there is a lack of studies aimed at examine the inter-related role of intracellular APP/Aβ peptide accumulation and neurovascular coupling during AD development and/or progression (Sagare et al., 2012). The aim of this study was to provide a novel *in vitro* system to dissect the relative contribution of neurons and astrocytes to cell vulnerability during hypoxic conditions in Alzheimer's disease. We thus derived primary cortical neurons and astrocytes from neonatal Tg2576 mice and Wt littermates. The experimental set-up included cells derived from single pups, which were split into different wells (technical replicates), with the single animal taken as the unit for statistical analysis (biological replicates). The experiments were analysed using a high-content approach, thus avoiding bias and providing a quite robust platform. Cell-based high-throughput technology combining cellular imaging with high-throughput data analysis (Radio and Mundy, 2008) has in fact been successfully applied to drug screening (O'Brien, 2014)

and was also used to set up standard procedures according to the European Centre for the Validation of Alternative Methods (ECVAM) Good Cellular Culture Practice guidelines (Coecke et al., 2005). We first demonstrated that primary neurons derived from mice carrying the APPswe mutation, thus accumulating APP and amyloid peptides, are more vulnerable than neurons derived from Wt mice to conventional culture conditions, glutamate and OGD. We then demonstrated that the reduction in the concentration of amyloid peptides obtained by blocking γ-secretase enzyme synthesis results in a protection of APPswe neurons from OGD-induced degeneration. Finally, we showed that conditioned medium obtained from either Wt or APPswe astrocytes exposed to OGD is neuroprotective for APPswe, but not for Wt neurons.

The intracellular concentration of Aβ42, the most toxic Aβ variant, in pyramidal (CA1) human neurons has been estimated to be much higher in sporadic AD patients than in control subjects (Umeda et al., 2011). This is due to an early dysfunction of APP processing which occurs before extracellular plaque deposition (LaFerla et al., 2007; Gouras et al., 2010). Tg2576 mice also exhibit a high level of intraneuronal Aβ peptides at the pre-plaque stage (Balducci et al., 2011; Beggiato et al., 2014) and several working hypotheses have endeavoured to clarify the possible relationship between this event and cell vulnerability and death (Bramham, 2008; Crews and Masliah, 2010; Pensalfini et al., 2014). For example, intraneuronal Aβ perturbs local protein synthesis and cytoskeleton dynamics (Bramham, 2008) and is causally related to the activation of the protein kinases responsible for intracellular tau hyperphosphorylation and caspase-3 activation (Takahashi et al., 2002; Eimer and Vassar,
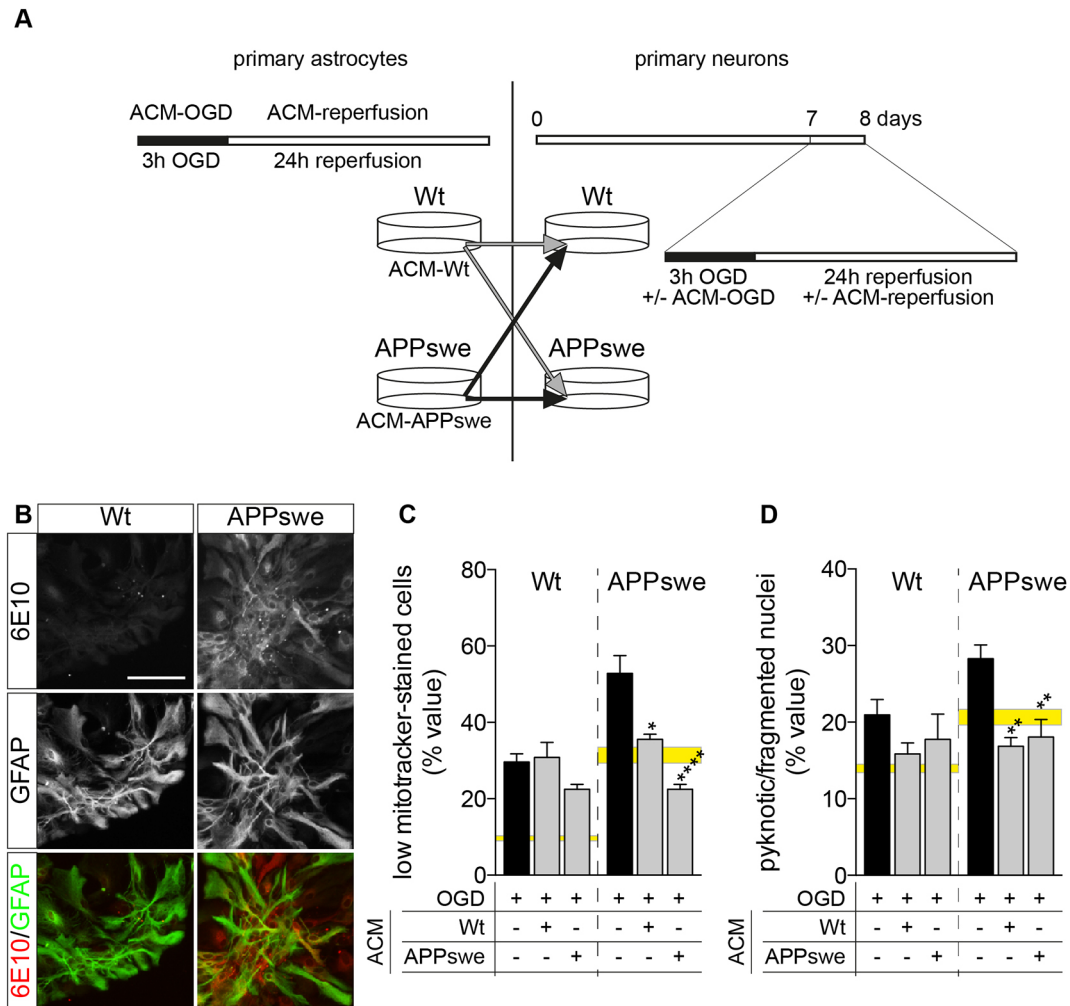
Fig. 4. Effect of astrocyte conditioned medium on the vulnerability of primary neurons to OGD. (A) Experimental design. Primary astrocytes isolated from Wt and Tg2576 mice were exposed to 3 h OGD, and conditioned medium collected. Wt and APPswe primary neurons were then exposed to Wt and APPswe ACM during normoxia or OGD and reperfusion. (B) 6E10 immunostaining of APPswe astrocytes, showing the intracellular accumulation of human APP protein/Aβ fragments in GFAP-positive cells. Scale bar: 50 µm. (C,D) Cell viability analysis of Wt and APPswe neurons exposed to normoxia and OGD, treated or not with ACM, as established by mitochondrial function (C; Wt OGD, $n=10$; Wt OGD ACM-Wt, $n=5$; Wt OGD ACM-APPswe, $n=6$; APPswe OGD, $n=9$; APPswe OGD ACM-Wt, $n=5$; APPswe OGD ACM-APPswe, $n=6$) and nuclear morphology (D; Wt OGD, $n=5$; Wt OGD ACM-Wt, $n=5$; Wt OGD ACM-APPswe, $n=4$; APPswe OGD, $n=5$; APPswe OGD ACM-Wt, $n=5$; APPswe OGD ACM-APPswe, $n=5$). The yellow horizontal bars represent normoxia values (the height of the bar represent the range of the mean value±s.e.m.). Bars represent mean+s.e.m. Statistical analysis: one-way ANOVA followed by Dunnett's multiple comparison test inside the same genotype. Asterisks represent differences between ACM-treated groups and groups exposed to OGD only (*$P<0.05$; **$P<0.01$; ****$P<0.0001$).

2013). In this study, we described how APPswe neurons are more vulnerable not only to OGD but also to glutamate excitotoxicity, that is the main driver for OGD-induced cell death (Goldberg and Choi, 1993), proving that the presence of the mutation influences the response of neurons to this stimulus. Treatment of the cultures with the γ-secretase inhibitor LY450139 results in neuroprotection, thus suggesting that intraneuronal Aβ accumulation could be responsible for the increased vulnerability to OGD observed in APPswe compared with Wt neurons. Actually, APPswe cells died in greater numbers in standard culture conditions, thus, the higher cell death under glutamate and OGD exposure could be an additive effect. However, the γ-secretase inhibition does not affect Wt viability nor the spontaneous cell death of APPswe neurons, strongly linking the inhibition of Aβ production to the protective effect.

In view of the key role of astrocytes in the CVU, we then performed experiments to dissect the possible interaction between astrocytes and neurons in our experimental systems, focusing on astrocyte-derived paracrine factors. Astrocytes are considered to be inherently neuroprotective in ischemic stroke and similar conditions (Zhao and Rempe, 2010), because of the role of astrocytes in supporting neuron energy homeostasis (Brown and Ransom, 2007). *In vitro*, co-cultures of neurons and astrocytes are more resistant to oxidative stress than pure neural cultures (Mattson and Rychlik, 1990). We have shown that conditioned medium obtained during OGD either from Wt or APPswe astrocytes is also neuroprotective in APPSwe but not in Wt neurons. After 3 h OGD and 24 h reperfusion, the percentage of low-MitoTracker-stained cells in Wt is around 30% and in APPSwe is around 53%, while the percentage of pyknotic nuclei is 22% and 35%, respectively. After 3 h OGD and 24 h reperfusion, the percentage of low-MitoTracker-stained cells in Wt is $29.61\pm2.15\%$ and in APPSwe is $54.92\pm4.76\%$, while the percentage of pyknotic nuclei is $22.16\pm1.18\%$ and $28.28\pm1.81\%$, respectively. Thus, the OGD conditions used in this study can be considered 'mild' (Yu et al., 2012; Baldassarro et al., 2016). The ACM is not effective

when used with Wt neurons, while it reduces the viability indices to Wt values when used with APPSwe neurons.

The reason for the selective effect of both ACM in APPSwe neurons only is not clear. In view of the role of astrocytes in CVU, the altered vascular endothelial growth factor (VEGFa) signalling observed in APPSwe- compared with Wt-derived cells could play a role. VEGFa and its receptors are in fact expressed in adult brain by neurons and astrocytes (Licht and Keshet, 2013; Mackenzie and Ruhrberg, 2012) and its expression is modulated by pathological conditions (Calzà et al., 2001) in humans (Boer et al., 2008) and in AD (Tarkowski et al., 2004). Here, we showed that APPSwe-derived neurons actually showed also a decreased expression of the relative receptors KDR and FLT-1. Moreover, the gene expression analysis of neurospheres derived from pre-plaque Tg2576 mice and analysed for clustering indicated that all upregulated genes in Tg2576 centred on VEGF (Baldassarro et al., 2013). It may thus be postulated that a different production of or sensitivity to paracrine factors occurs in APPSwe compared with Wt neurons. Several paracrine mechanisms between cells in the CVU playing a major role in neuron viability have been described *in vivo* and in *in vitro* systems, including growth factors (Lin et al., 2006; Li et al., 2014). Notably, VEGF seems to have a two-fold effect on neuron viability, which also depends on amyloid dosage (Sanchez et al., 2013; Dal Prà et al., 2014; Wood et al., 2015). Moreover, other potential cellular players for *in vivo* OGD neuroprotection, including endothelial cells and pericytes should be considered.

In conclusion, in this study we present an *in vitro* system aimed to dissect the contribution of the different cell types of the CVU to hypoxia and OGD. Primary neurons and astrocytes derived from transgenic animals carrying gene mutations of interest for AD are a promising tool for investigating co-morbidities and cofactors such as Aβ deposition and vascular dysfunction leading to hypoxia. Finally, the use of cell-based high-content analysis is recommended in order to improve *in vitro* data robustness.

MATERIALS AND METHODS
Primary neuronal cultures
All animal protocols described herein were carried out according to the European Community Council Directives (86/609/EEC), and comply with the guidelines published in the NIH Guide for the Care and Use of Laboratory Animals. Cortical neurons from single neonatal (within 24 h from birth) Wt or Tg2576 (Taconic, Hudson, NY, USA) mice were prepared according to standard protocols (Fernández et al., 2005; Del Vecchio et al., 2009). Briefly, brains were removed and cortical tissue dissected, freed from the meninges, and minced into small pieces. Cells were dispersed in Kreb's buffer (0.12 M NaCl, 4.8 mM KCl, 1.2 mM KH_2PO_3, 25.4 mM $NaHCO_3$, 14.2 mM glucose, 0.01 mg/ml Phenol Red, 1.5 mM $MgSO_4$) containing BSA 0.3% and 0.025% trypsin (Sigma-Aldrich) for 15 min at 37°C, followed by mechanical trituration with a Pasteur pipette in Kreb's buffer containing 0.004% deoxyribonuclease I (DNaseI, Sigma-Aldrich), and 0.052% soybean trypsin inhibitor (SBTI; Sigma-Aldrich). After centrifugation (500 g, 5 min), cells were resuspended in Neurobasal culture medium supplemented with 2% B27 (Invitrogen), 2 mM glutamine (Sigma-Aldrich), 100 U/ml penicillin, and 100 µg/ml streptomycin (pen/strep; Invitrogen) and plated onto Cultrex 2D substrate (0.25 mg/ml; Trevingen, Gaithersburg, MD, USA) coated plates or coverslips. Cells were maintained in a humidified incubator at 37°C with 5% CO2. To obtain neuronal culture (99% neurons) cells were treated after 24 h with 10 µM cytosine arabinofuranoside (Sigma-Aldrich) and at 4 DIV, half of the medium was changed. Neurons isolated from Tg2576 mice are denoted as APPSwe primary neurons.

Primary astrocyte cultures
Primary astrocytes were isolated from single 7-day-old Wt or Tg2576 mice using the same protocol as the primary neuronal cultures (Jones et al., 2011),

except that cells were plated and maintained in DMEM with 15% fetal bovine serum (FBS), non-essential amino acid mixture (Sigma-Aldrich), pen/strep (Invitrogen) and 2 mM Glutamine (Invitrogen). Cultures were seeded in culture-treated flasks at a density of 125,000 cells/cm^2 and maintained at 37°C 5% CO_2. Cells were detached with trypsin (10 min, 37°C) and replated twice before use. For the OGD exposure, astrocytes were seeded in flat-bottom 96-well plates and exposed to OGD 2 weeks after plating. Astrocytes isolated from Tg2576 mice are denoted as APPswe primary astrocytes.

Genotyping
Mouse tails were used for genotyping analysis. The mouse genomic DNA was extracted using the GenElute Mammalian Genomic DNA MiniPrep Kit (Sigma-Aldrich) according to the manufacturer's instructions and eluted in 100 µl of elution solution. DNA concentration was determined using a spectrophotometer and Tg2576 mice were identified by the presence of the mutated human APP gene (FW: 5′-GATGAGGATGGTGATGAGGTA-3′ REV: 5′-ACTGGCTGCTGTTGTAGG-3′) using the Real Time PCR technique and the SYBR Green qPCR master mix (Bio-Rad) and 0.4 µM forward and reverse primers. The amount of DNA used for each sample was 10 ng and PCR amplification conditions were: 60°C for 30 s.

Glutamate excitotoxicity
At 7 DIV, Wt and APPswe primary neurons were treated with 42 µM glutamate. Briefly, medium was removed and cells were exposed to Krebs buffer, with or without glutamate, for 10 min. After glutamate treatment, Krebs buffer was replaced with medium (Fernandez et al., 2005).

Oxygen and glucose deprivation and treatment
OGD was performed on primary cortical neurons and primary astrocytes cultures using an air-tight hypoxia chamber (Billups-Rothenberg, Del Mar, CA, USA) saturated with 95% N_2, 5% CO_2 (Goldberg and Choi, 1993). Glucose deprivation was achieved using a glucose-free Neurobasal medium, supplemented with B27, glutamine and penicillin/streptomycin as above. Oxygen was removed by flushing the hypoxia chamber with N_2-CO_2 mixture for 6-8 min at 25 l/min. The flushing was repeated after half the incubation time. The OGD condition was maintained for 3 h, after which plates were re-oxygenated for 24 h in the old medium in a cell incubator.

Wt and APPswe astrocyte media, both from the OGD and after reperfusion phases were collected, and used as astrocyte-conditioned medium (ACM) on neurons. In one set of experiments, Wt and APPswe primary cortical neurons were exposed to Wt and APPswe ACM both in the OGD and the reperfusion phases. In another set of experiments, primary cortical neurons were treated from 2 DIV to the end of the experiment (8 DIV) with 10 µM LY450139.

MitoTracker staining
Cells were stained with MitoTracker Orange (Thermo Scientific, Waltham, MA, USA) following the manufacturer's instructions. Briefly, cells were treated for 30 min at 37°C with 150 nM MitoTracker. After two washes with PBS, cells were fixed and used in the immunocytochemistry procedure.

Immunocytochemistry
At 8 DIV, cells were washed with ice-cold PBS and fixed in a solution of 4% paraformaldehyde for 20 min at room temperature (RT) and washed twice with PBS. Cells were then treated with 0.1 M PBS, 0.3% Triton X-100 containing 1% BSA and 1% normal blocking serum prepared from the species in which the secondary antibody was raised for 1 h at RT.

The following primary anti-sera were used: anti-6E10 (mouse; Covance, SIG-39320, batch no. D11AF00145; 1:1000), anti-β-III-tubulin (mouse; R&D Systems, MAB-1195, batch. no. HGQ0113121; 1:1000), anti-GFAP (rabbit; Dako, Z0334, batch no. 20005461; 1:1000) overnight at 4°C. Cells were washed with PBS and incubated with goat Alexa 488-conjugated anti-mouse, goat Alexa 568-conjugated anti-rabbit, goat Alexa 658-conjugated anti-mouse (Invitrogen) secondary antibodies for 30 min at 37°C. Cells were washed twice in PBS and incubated with the nuclear dye Hoechst

33258 (1 µg/ml) for 20 min at RT, washed with PBS and mounted with 0.1% para-phenylendiamine solution.

Cell-based high-content screening

For HCS analysis cells were grown in 96 flat-bottom well HCS plates (Nunc, Roskilde, Denmark). Analysis of condensed nuclei, cell number and lineage/differentiation markers were performed with Cell Insight CX5 High Content Screening (HCS; Thermo Scientific), using the Compartmental Analysis BioApplication. Based on nuclear staining, the software is able to recognise nuclei and calculate the percentage of high intensity/small sized condensed nuclei. Moreover, based on nuclei identification, the software is able to detect the presence of the marker-specific stain in the cell body, calculating the percentage of immunoreactive cells and fluorescence intensity. For the MitoTracker analysis, the software is able to recognize every single cell by its nuclear staining and quantifies the fluorescence intensity inside the cell body. The operator can select a fluorescence threshold that allows the software to discriminate between 'high-intensity staining' and 'low-intensity staining'. Using the same parameters and the same threshold it is possible to perform an automatic, statistically robust and objective analysis. This technique avoids also the bias of the analysis of randomly chosen fields, because the analysis is performed in all cells. From 60,000 to 80,000 cells/well were analysed.

RNA isolation and reverse transcription

Total RNA isolation was performed with the RNeasy Micro kit (Qiagen) following the manufacturer's instructions. Total RNA was eluted in RNase-free water and concentration estimated through absorbance values at 260, 280 and 320 (Nanodrop 2000 spectrophotometer, Thermo Scientific). First-strand cDNAs were obtained using the iScript cDNA Synthesis Kit (Bio-Rad), incubating at 42°C for 30 min. An RNA sample with no reverse transcriptase enzyme in the reaction mix was processed as a no-reverse transcription control sample.

Semi-quantitative real-time PCR

Semi-quantitative real-time PCR was performed using the CFX96 real-time PCR system (Bio-Rad). The reactions were performed in a final volume of 20 µl consisting of 1× SYBR Green qPCR master mix (Bio-Rad) and 0.4 µM forward and reverse primers. In order to avoid possible contamination of genomic DNA in isolated RNA, the sample with no reverse transcriptase enzyme was processed in parallel with the others and tested by real-time PCR for every pair of primers used. All primers used were designed using Primer Blast software (NCBI) and synthesized by IDT (Coralville). The following primer sequences were used: *VEGFA* (FW: 5′-AAGAGAAGGAAGAGGAGAG-3′; REV: 5′-ACCCAAGAG-AGCAGAAAG-3′); *FLT1* (FW: 5′-CGTGCAAGGAACCTCAGACA-3′; 5′-ATCATAGGGCAGCCGTTCAC-3′); *KDR* (FW: 5′-ATGTCCTTGGC-TGTGCAAGA-3′; REV: 3′-CCTTCATTGGCCCGCTTAAC); *GAPDH* (FW: 5′-GGCAAGTTCAATGGCACAGTCAAG-3′; REV: 5′-ACATAC-TCAGCACCAGCATCACC-3′) was used as a housekeeping gene to normalize the amount of reverse-transcribed RNA used for PCR. Thermal profile of PCR reactions consisted first of a denaturation step (95°C, 2 min) and 40 cycles of amplification (95°C for 15 s and 60°C for 60 s). At the end of the amplification cycles, the melting curve of amplified products was performed according to the following temperature/time scheme: heating from 55°C to 95°C with a temperature increase of 0.5°C/s.

Primer efficiency values for all primers were 95-102%. The $2^{(-\Delta\Delta CT)}$ method was used for the calculation of gene expression.

Statistical analysis

The number of wells per animal varied according to the cell isolation yield. For mRNA analysis, each value derived from a single animal. For HCS analysis, individual data were obtained from the mean value of the wells obtained from a single animal culture. Exclusion criteria in data analysis were pre-established for each assay as follows. mRNA analysis: samples in which curves not fitting the melting temperature or in which a double peak was observed were excluded from the analysis; HCS analysis: wells in which the software was unable to automatically identify the nuclei were excluded from the analysis. The final number of data per group is reported in the figure legends.

Data are reported as mean±s.e.m. Prism software (GraphPad) was used for statistical analyses and graph generation. Student's *t*-test, two-way ANOVA and Sidak's multiple comparison or one-way ANOVA and Dunnett's or Tukey's multiple comparison *post hoc* were used to analyse data, as specified in the figure legends. Results were considered significant when the probability of their occurrence as a result of chance alone was less than 5% ($P<0.05$).

Competing interests
The authors declare no competing or financial interests.

Author contributions
V.A.B.: experimental activities and manuscript preparation. A.M.: experimental activities and manuscript preparation. L.G.: study design and manuscript preparation. L.C.: study design, data analysis, manuscript preparation.

References

Abramowski, D., Wiederhold, K.-H., Furrer, U., Jaton, A.-L., Neuenschwander, A., Runser, M.-J., Danner, S., Reichwald, J., Ammaturo, D., Staab, D. et al. (2008). Dynamics of Abeta turnover and deposition in different beta-amyloid precursor protein transgenic mouse models following gamma-secretase inhibition. *J. Pharmacol. Exp. Ther.* **327**, 411-424.

Baker-Nigh, A., Vahedi, S., Davis, E. G., Weintraub, S., Bigio, E. H., Klein, W. L. and Geula, C. (2015). Neuronal amyloid-β accumulation within cholinergic basal forebrain in ageing and Alzheimer's disease. *Brain* **138**, 1722-1737.

Baldassarro, V. A., Lizzo, G., Paradisi, M., Fernández, M., Giardino, L. and Calzà, L. (2013). Neural stem cells isolated from amyloid precursor protein-mutated mice for drug discovery. *World J. Stem Cells* **5**, 229-237.

Baldassarro, V. A., Calzà, L., Fernandez, M., Giardino, L., Gliuliani, A., Lorenzini, L., Mangano, C., Sivilia, S. (2014). Alzheimer's disease: discussing the bench-to-bed" and the "Bed-to-Bench" pathway linking preclinical and clinical research. In *Lost in Translation* (ed. R. Srivastava, W. Maksymowicz and W. Lopaczynski), pp. 409-442. World Scientific.

Baldassarro, V. A., Marchesini, A., Facchinetti, F., Villetti, G., Calzà, L., Giardino, L. (2016). Cell death in pure-neuronal and neuron-astrocyte mixed primary culture subjected to oxygen-glucose deprivation: the contribution of poly (ADP-ribose) polymerases and caspases. *Microchem. J.* doi:10.1016/j.microc.2016.11.008.

Balducci, C., Mehdawy, B., Mare, L., Giuliani, A., Lorenzini, L., Sivilia, S., Giardino, L., Calzà, L., Lanzillotta, A., Sarnico, I. et al. (2011). The γ-secretase modulator CHF5074 restores memory and hippocampal synaptic plasticity in plaque-free Th2576 mice. *J. Alzheimers Dis.* **24**, 799-816.

Barros, L. F., Bittner, C. X., Loaiza, A. and Porras, O. H. (2007). A quantitative overview of glucose dynamics in the gliovascular unit. *Glia* **55**, 1222-1237.

Beggiato, S., Giuliani, A., Sivilia, S., Lorenzini, L., Antonelli, T., Imbimbo, B. P., Giardino, L., Calzà, L. and Ferraro, L. (2014). CHF5074 and LY450139 sub-acute treatments differently affect cortical extracellular glutamate levels in pre-plaque Tg2576 mice. *Neuroscience* **266**, 13-22.

Bilkei-Gorzo, A. (2014). Genetic mouse models of brain ageing and Alzheimer's disease. *Pharmacol. Ther.* **142**, 244-257.

Boer, K., Troost, D., Spilet, W. G. M., van Rijen, P. C., Gorter, J. A. and Aronica, E. (2008). Cellular distribution of vascular endothelial growth factor A (VEGFA) and B (VEGFB) and VEGF receptors 1 and 2 in focal cortical dysplasia type IIB. *Acta Neuropathol.* **115**, 683-696.

Bramham, C. R. (2008). Local protein synthesis, actin dynamics, and LTP consolidation. *Curr. Opinion Neurobiol.* **18**, 524-531.

Brown, A. M. and Ransom, B. R. (2007). Astrocyte glycogen and brain energy metabolism. *Glia* **55**, 1263-1271.

Calzà, L., Giardino, L., Giuliani, A., Aloe, L. and Levi-Montalcini, R. (2001). Nerve growth factor control of neuronal expression of angiogenetic and vasoactive factors. *Proc. Natl. Acad. Sci. USA* **98**, 4160-4165.

Cimarosti, H. and Henley, J. M. (2008). Investigating the mechanisms underlying neuronal death in ischemia using in vitro oxygen-glucose deprivation: potential involvement of protein SUMOylation. *Neuroscientist* **14**, 626-636.

Coecke, S., Balls, M., Bowe, G., Davis, J., Gstraunthaler, G., Hartung, T., Hay, R., Merten, O.-W., Price, A., Schechtman, L. et al. (2005). Guidance on good

cell culture practice. A report of the second ECVAM task force on good laboratory practice. *Altern. Lab. Anim.* **33**, 261-287.

Crews, L. and Masliah, E. (2010). Molecular mechanisms of neurodegeneration in Alzheimer's disease. *Hum. Mol. Genet.* **19**, R12-R20.

Dal Prà, I., Armato, U., Chioffi, F., Pacchiana, R., Whitfield, J. F., Chakravarthy, B., Gui, L. and Chiarini, A. (2014). The Aβ peptides-activated calcium-sensing receptor stimulates the production and secretion of vascular endothelial growth factor-A by normoxic adult human cortical astrocytes. *Neuromolecular Med.* **16**, 645-657.

Del Vecchio, G., Giuliani, A., Fernandez, M., Mesirca, P., Bersani, F., Pinto, R., Ardoino, L., Lovisolo, G. A., Giardino, L. and Calzá, L. (2009). Effect of radiofrequency electromagnetic field exposure on in vitro models of neurodegenerative disease. *Bioelectromagnetics* **30**, 564-572.

Eimer, W. A. and Vassar, R. (2013). Neuron loss in the 5XFAD mouse model of Alzheimer's disease correlates with intraneuronal Aβ42 accumulation and Caspase-3 activation. *Mol. Neurodegener.* **8**, 2.

Elvang, A. B., Volbracht, C., Pedersen, L. Ø., Jensen, K. G., Karlsson, J.-J., Larsen, S. A., Mørk, A., Stensbøl, T. B. and Bastlund, J. F. (2009). Differential effects of γ-secretase and BACE1 inhibition on brain Aβ levels in vitro and in vivo. *J. Neurochem.* **110**, 1377-1387.

Fernández, M., Pirondi, S., Antonelli, T., Ferraro, L., Giardino, L. and Calzà, L. (2005). Role of c-Fos protein on glutamate toxicity in primary neural hippocampal cells. *J. Neurosci. Res.* **82**, 115-125.

Garwood, C. J., Ratcliffe, L. E., Simpson, J. E., Heath, P. R., Ince, P. G. and Wharton, S. B. (2016). Review: Astrocytes in Alzheimer's disease and other age-associated dementias; a supporting player with a central role. *Neuropathol. Appl. Neurobiol.* doi: 10.1111/nan.12338.

Goldberg, M. P. and Choi, D. W. (1993). Combined oxygen and glucose deprivation in cortical cell culture: calcium-dependent and calcium-independent mechanisms of neuronal injury. *J. Neurosci.* **13**, 3510-3524.

Gouras, G. K., Tampellini, D., Takahashi, R. H. and Capetillo-Zarate, E. (2010). Intraneuronal β-amyloid accumulation and synapse pathology in Alxheimer's disease. *Acta Neuropathol.* **119**, 523-541.

Ha, J. S., Lee, C.-S., Maeng, J.-S., Kwon, K.-S. and Park, S. S. (2009). Chronic glutamate toxicity in mouse cortical neuron culture. *Brain Res.* **1273**, 138-143.

Hsiao, K., Chapman, P., Nilsen, S., Eckman, C., Harigaya, Y., Younkin, S., Yang, F. and Cole, G. (1996). Correlative memory deficits, Abeta elevation, and amyloid plaques in transgenic mice. *Science* **274**, 99-102.

Jämsä, A., Belda, O., Edlund, M. and Lindström, E. (2011). BACE-1 inhibition prevents the γ-secretase inhibitor evoked Aβ rise in human neuroblastoma SH-SY5Y cells. *J. Biomed. Sci.* **18**, 76.

Jones, S. M., Novak, A. E. and Elliot, J. P. (2011). Primary culture of cellular subtypes from postnatal mouse for in vitro studies of oxygen glucose deprivation. *J. Neurosci. Methods* **199**, 241-248.

Kapasi, A. and Schneider, J. A. (2016). Vascular contributions to cognitive impairment, clinical Alzheimer's disease, and dementia in older persons. *Biochim. Biophys. Acta* **1862**, 878-886.

LaFerla, F. M., Green, K. N. and Oddo, S. (2007). Intracellular amyloid-beta in Alzheimer's disease. *Nat. Rev. Neurosci.* **8**, 499-509.

Li, Y.-N., Pan, R., Qin, X.-J., Yang, W.-L., Qi, Z., Liu, W. and Liu, K. J. (2014). Ischemic neurons activate astrocytes to disrupt endothelial barrier via increasing VEGF expression. *J. Neurochem.* **129**, 120-129.

Licht, T. and Keshet, E. (2013). Delineating multiple functions of VEGF-A in the adult brain. *Cell. Mol. Life Sci.* **70**, 1727-1737.

Lin, C.-H., Cheng, F.-C., Lu, Y.-Z., Chu, L.-F., Wang, C.-H. and Hsueh, C.-M. (2006). Protection of ischemic brain cells is dependent on astrocyte-derived growth factors and their receptors. *Exp. Neurol.* **201**, 225-2233.

Lipton, P. (1999). Ischemic cell death in brain neurons. *Physiol. Rev.* **79**, 1431-1568.

Lourenço, C. F., Ledo, A., Dias, C., Barbosa, R. M. and Laranjinha, J. (2015). Neurovascular and neurometabolic derailment in aging and Alzheimer's disease. *Front. Aging Neurosci.* **7**, 103.

Mackenzie, F. and Ruhrberg, C. (2012). Diverse roles for VEGF-A in the nervous system. *Development* **139**, 1371-1380.

Mattson, M. P. and Rychlik, B. (1990). Glia protect hippocampal neurons against excitatory amino acid-induced degeneration: involvement of fibroblast growth factor. *Int. J. Dev. Neurosci.* **8**, 399-415.

Nedergaard, M., Ransom, B. and Goldman, S. A. (2003). New roles for astrocytes: redefining the functional architecture of the brain. *Trends Neurosci.* **26**, 523-530.

Nelson, A. R., Sweeney, M. D., Sagare, A. P. and Zlokovic, B. V. (2016). Neurovascular dysfunction and neurodegeneration in dementia and Alzheimer's disease. *Biochim. Biophys. Acta* **1862**, 887-900.

O'Brien, P. J. (2014). High-content analysis in toxicology: screening substances for human toxicity potential, elucidating subcellular mechanisms and in vivo use as translational safety biomarkers. *Basic Clin. Pharmacol. Toxicol.* **115**, 4-17.

Pensalfini, A., Albay, R., III, Rasool, S., Wu, J. W., Hatami, A., Arai, H., Margol, L., Milton, S., Poon, W. W., Corrada, M. M. et al. (2014). Intracellular amyloid and the neuronal origin of Alzheimer neuritic plaques. *Neurobiol. Dis.* **71**, 53-61.

Radio, N. M. and Mundy, W. R. (2008). Developmental neurotoxicity testing in vitro: models for assessing chemical effects on neurite outgrowth. *Neurotoxicol* **29**, 361-376.

Redzic, Z. B., Rabie, T., Sutherland, B. A. and Buchan, A. M. (2015). Differential effects of paracrine factors on the survival of cells of the neurovascular unit during oxygen glucose deprivation. *Int. J. Stroke* **10**, 407-414.

Sagare, A. P., Bell, R. D. and Zlokovic, B. V. (2012). Neurovascular dysfunction and faulty amyloid β-peptide clearance in Alzheimer disease. *Cold Spring Harb. Perspect Med.* **2**, a011452.

Sanchez, A., Tripathy, D., Luo, J., Yin, X., Martinez, J. and Grammas, P. (2013). Neurovascular unit and the effects of dosage in VEGF toxicity: role for oxidative stress and thrombin. *J. Alzheimers Dis.* **34**, 281-291.

Sivilia, S., Lorenzini, L., Giuliani, A., Gusciglio, M., Fernandez, M., Baldassarro, V. A., Mangano, C., Ferraro, L., Pietrini, V., Baroc, M. F. et al. (2013). Multi-target action of the novel anti-Alzheimer compound CHF5074: in vivo study of long term treatment in Tg2576 mice. *BMC Neurosci.* **14**, 44.

Takahashi, H. and Shibuya, M. (2005). The vascular endothelial growth factor (VEGF)/VEGF receptor system and its role under physiological and pathological conditions. *Clin. Sci.* **109**, 227-241.

Takahashi, R. H., Milner, T. A., Li, F., Nam, E. E., Edgar, M. A., Yamaguchi, H., Beal, M. F., Xu, H., Greengard, P. and Gouras, G. K. (2002). Intraneuronal Alzheimer abeta42 accumulates in multivesicular bodies and is associated with synaptic pathology. *Am. J. Pathol.* **161**, 1869-1879.

Tarkowski, E., Issa, R., Sjögren, M., Wallin, A., Tarkowski, A. and Kumar, P. (2004). Increased intrathecal levels of the angiogenic factors VEGF and TGF-beta in Alzheimer's disease and vascular dementia. *Neurobiol. Aging* **23**, 237-243.

Umeda, T., Tomiyama, T., Sakama, N., Tanaka, S., Lambert, M. P., Klein, W. L. and Mori, H. (2011). Intraneuronal amyloid β oligomers cause cell death via endoplasmic reticulum stress, endosomal/lysosomal leakage, and mitochondrial dysfunction in vivo. *J. Neurosci. Res.* **89**, 1031-1042.

van de Haar, H. J., Jansen, J. F. A., van Osch, M. J. P., van Buchem, M. A., Muller, M., Wong, S. M., Hofman, P. A. M., Burgmans, S., Verhey, F. R. J. and Backes, W. H. (2016). Neurovascular unit impairment in early Alzheimer's disease measured with magnetic resonance imaging. *Neurobiol. Aging* **45**, 190-196.

Wappler, E. A., Institoris, A., Dutta, S., Katakam, P. V. G. and Busija, D. W. (2013). Mitochondrial dynamics associated with oxygen- glucose deprivation in rat primary neuronal cultures. *PLoS ONE* **8**, e63206.

Wilson, M. S., Graham, J. R. and Ball, A. J. (2014). Multiparametric High Content Analysis for assessment of neurotoxicity in differentiated neuronal cell lines and human embryonic stem cell-derived neurons. *Neurotoxicology* **42**, 33-48.

Wood, L. B., Winslow, A. R., Proctor, E. A., McGuone, D., Mordes, D. A., Frosch, M. P., Hyman, B. T., Lauffenburger, D. A. and Haigis, K. M. (2015). Identification of neurotoxic cytokines by profiling Alzheimer's disease tissues and neuron culture viability screening. *Sci. Rep.* **5**, 16622.

Yu, Z., Xu, J., Liu, N., Wang, Y., Li, X., Pallast, S., van Leyen, K. and Wang, X. (2012). Mitochondrial distribution of neuroglobin and its response to oxygen-glucose deprivation in primary-cultured mouse cortical neurons. *Neuroscience* **218**, 235-242.

Zhao, Y. and Rempe, D. A. (2010). Targeting astrocytes for stroke therapy. *Neurotherapeutics* **7**, 439-451.

Zlokovic, B. V. (2011). Neurovascular pathways to neurodegeneration in Alzheimer's disease and other disorders. *Nat. Rev. Neurosci.* **12**, 723-738.

Disease Models & Mechanisms

4.7 Foetal and adult oligodendrocyte precursor cells are differentially vulnerable to inflammation and oxygen-glucose deprivation (Baldassarro et al., unpublished – B).

Foetal and adult oligodendrocyte precursor cells are differentially vulnerable to inflammation and oxygen-glucose deprivation.

Vito A. Baldassarro[1,2], Alessandra Marchesini[3], Luciana Giardino[1,3,4], Laura Calzà[1,2,3]

[1]Health Science and Technologies Interdepartmental Center for Industrial Research (HST-ICIR), University of Bologna, Italy; [2]Department of Pharmacy and Biotechnology, University of Bologna, Italy; [3]IRET Foundation, Ozzano Emilia, Italy; [4]Department of Veterinary Medical Sciences, University of Bologna, Italy.

Correspondence:

Laura Calzà

CIRI-SDV, University of Bologna

Via Tolara di Sopra 41/E

40064 Ozzano Emilia (Bologna)

ITALY

laura.calza@unibo.it

Abstract

Acute traumatic or vascular lesions of the central nervous system are characterized by an extensive myelin loss, when occurring in the adult life, or impaired myelination, when occurring during early postnatal stage. Hypoxia and inflammation characterize both conditions, severely affecting the myelin repair or myelin development, respectively. Both processes are dependent on oligodendrocyte precursor cells (OPCs) and its capability to differentiate into mature, myelinating oligodendrocyte (OL).

In this study we investigated the response of OPC derived from neural stem cells (NSCs) isolated from foetal and adult brains to in inflammatory and hypoxic insults, focusing on OPC survival and differentiation. OPCs were exposed to a cytokine cocktail, to mimic inflammation, or to oxygen-glucose deprivation (OGD), to mimic hypoxic condition. After exposure to inflammatory cytokines, the differentiation of both foetal and adult OPCs is completely abolished. On the contrary, when exposed to OGD, only foetal- and not adult-brain derived OPC degenerate. Moreover, foetal OGD-induced cell death is characterized by a delayed onset.

These results indicate than the biological response of OPC to inflammation and demyelination are different in foetal and adult cells. The understanding of the underlying molecular mechanism will strongly contribute to differentiate myelination enhancing and neuroprotective therapies for neonatal and adult CNS lesions.

Keywords

1. *Introduction*

The myelin loss is a major pathological event in traumatic and vascular lesions of the central nervous system (CNS), and it is also considered a major cause of neurodegeneration and chronic disabilities (Verden and Macklin, 2016). The underlying pathogenic mechanisms include the myelin breakdown by oxidative stress products and oligodendrocyte (OL) cell death. Moreover, also oligodendrocyte precursor cells (OPC), the cell responsible for myelin development during early postnatal age and of myelin repair during the adult life, undergoes to extensive degeneration (Alizadeh et al., 2015) and impaired differentiation into mature OL (van Tilborg et al., 2017).

During the adult life, myelin damages can be efficiently and correctly repaired and functions restored (Crawford et al., 2013) thanks to OPCs, which proliferate, migrate to the unmyelinated axons and differentiate in mature oligodendrocytes (OLs) after lesion (Trotter et al., 2010). Since OPCs are the cells responsible for both developmental myelination and myelin repair during the adult life, it has been suggested that remyelination in adulthood is resembling the developmental myelination mechanism (Franklin & Hinks 1999). However, morphological differences between the two processes lead to the view that these two mechanisms are differentially regulated (Miron, 2011) Moreover, we also demonstrated that PARP expression and activity, such as the effect to PARP inhibition exposure is substantially different in OPC derived from foetal or adult brain, impacting on cell survival and differentiation (Baldassarro et al., 2017).

Two main pathological mechanisms are involved in myelin injury and demyelination, both in foetal (e.g. neonatal hypoxia/ischemia) and adult lesions (e.g. multiple sclerosis, MS; spinal cord and brain trauma, stroke), i.e. inflammation and hypoxia/ischemia (HI; Calzà et al., 2017).

Inflammation has a dual role on myelin and OPC pathobiology, being a promoter of myelin repair in some conditions, and a severe inhibitor in other conditions (Tognatta and Miller, 2016). In fact, depending on the severity of the inflammation, an overproduction of cytokines/chemokines may lead to excessive inflammation and OL cell death (Patel and Klein, 2011). This has been considered for many years the cause of remyelination failure in several conditions, usually characterized by the establishment of severe (and chronic) inflammatory microenvironment. More recently, the role of OPC differentiation block has been indicated as preeminent event to explay remyelination failure in multiple sclerosis (Irvine and Blakemore, 2008) and spinal cord injury (Mekhail et al., 2012), and stroke both in experimental animals and humans. In particular, in lesion models of inflammatory/demyelinating diseases local OPCs in the white matter proliferate and part of them differentiates into astrocytes, while the remaining cells are mainly blocked in a progenitor phenotype (Sozmen et al., 2016).

HI also occurs in acute injuries, like trauma and stroke. In these conditions, most of the white matter infarcts are believed to be secondary to vascular occlusion and endothelial cell dysfunction (El Waly et al., 2014). Three hours after HI, OLs show swelling and vacuolization, followed by retraction and cell death in 24 hours (Pantoni et al., 2006; McIver et al., 2010). Oxygen deprivation is the major cause of neonatal encephalopathy, a common cause of neonatal brain injury that affects 1 to 3 per 1000 live births in developed countries and up to 26 per 1000 live births in the developing world. The pattern of injury depends on the brain developmental time, and on the severity of the insult (Rocha-Ferreira and Hristoya, 2016). In particular, since myelination occurs from late embryonic gestation throughout post-natal life and continues until adult life (Fancy et al., 2011), a myelination impairment is a typical event when HI occurs at neonatal stages (Rocha-Ferreira and Hristoya, 2016). At this age, late OPC are highly susceptible to HI, and the activation of the Cdk2 pathway induces OPCs proliferation, delayed/impaired maturation of OLs and apoptosis (Back et al., 2002;

Jablonska et al., 2012). HI also induces an inflammatory response that has the positive role to remove damaged cells, debris and lipids, followed by a switch from pro- to anti-inflammatory profile that stimulates repair processes (Rocha-Ferreira et al., 2016). Several cell types are involved in this complex event, which is quite different in neonatal and adult life. After HI in adult CNS, leukocytes are activated within hours and migrate into the brain/spinal cord injured site, where cytokines are produced in large amounts. On the contrary, HI in new-borns induces an immediate (minutes) innate immune response. Age differences in HI-response mechanisms also include the cross-talk between excitotoxic, oxidative and inflammatory injury, determining the so-called "windows of susceptibility" during late foetal and early postnatal brain (Liu et al., 2013).

Thus, on spite of the fact that OPCs are the cells responsible for both myelin formation during development and myelin repair during the adulthood, and in spite of the fact that most OPCs that populate adult CNS are generated during prenatal stages (REF), the response of this cells to lesion including their capability to evolve into myelinating OL is quite different (Calzà et al., 2017).

In the present study we then analysed *in vitro* response of foetal and adult OPCs to stimuli responsible for myelin loss *in vivo*. In order to follow all developmental stages of OPC, we derived these cells from neural stem cells (NSCs) obtained from foetal forebrain and adult subventricular zone. We then exposed these cell systems to experimental conditions mimicking *in vitro* inflammation (cytokine cocktail composed by TGF-b1, TNF-a, IL-1b, IL-6, IL-17 and IFN-c) and HI model (oxygen-glucose deprivation, OGD), to investigate survival and differentiation. Results from this study could have important implication in the development of myelin enhancing therapies and neuroprotection strategies.

2. *Materials and methods*

2.1 *Cell preparation and cultures*

All animal protocols described herein were carried out according to the European Community Council Directives (86/609/EEC), and comply with the guidelines published in the *NIH Guide for the Care and Use of Laboratory Animals*.

Foetal and adult NSCs were isolated from E.13-14 foetal forebrain or 2.5 month old adult sub-ventricular zone (SVZ), following the Ahlenius and Kokaia protocol (Ahlenius and Kokaia, 2010). Oligodendrocyte differentiation was performed following the Chen protocol (Chen et al., 2007) with some modifications. Tissues were enzymatically dissociated using trypsin (SIGMA), hyaluronidase (SIGMA) and DNase (SIGMA), than mechanically dissociated by piepetting. The solution was filtered, centrifuged and the resulting pellet was washed twice in HBSS. After 7 minutes centrifugation at $400 \times g$, the cellular pellet was resuspended in serum-free medium (DMEM/F12 GlutaMAX 1 x; 8 mmol/L HEPES; 100 U/100 µg Penicillin/Streptomycin; 0.1 x B27; 1 x N-2; 20 ng/mL bFGF; 20 ng/mL EGF) and, after cell count, cells were plated in suspension at a density of 10 cells/µl in a final volume of 3 mL in low-attachment 6-well plates (NUNC). Half medium was changed every three days, centrifuging the cell suspension at $300 \times g$ for 5 minutes and gently resuspending the cellular pellet in fresh medium. Neurospheres were allowed to proliferate until they attained a diameter of about 100µm.

To obtain oligospheres, primary neurospheres were centrifuged at 300 x g for 5 minutes. The pellet was mechanically dissociated by pipetting and cells were counted and plated again at a density of 10 cells/µl in a final volume of 3 mL of OPCs medium (DMEM/F12 GlutaMAX 1 x; 8 mmol/L HEPES; 100 U/100 µg Penicillin/Streptomycin; $0.1 \times B27$; $1 \times N-2$; 20 ng/mL bFGF; 20 ng/mL PDGF) in low-attachment 6-well plates (NUNC). Oligospheres were centrifuged and the pellet was mechanically dissociated to obtain a single cell suspension.

After cell count, cells were plated at a density of 3000 cells/cm^2 on poly-D,L-ornithine (50μg/ml)/laminin (5μg/ml) coating, in OPC medium.

In order to induce oligodendrocyte differentiation and maturation, after 3 DIVs OPC medium was replaced with the oligodendrocyte differentiation medium (DMEM/F12 GlutaMAX 1 x; 8 mmol/L HEPES; 100 U/100 μg Penicillin/Streptomycin; 0.1 x B27; 1 x N-2; 50 nM T3; 10 ng/ml CNTF; 1x *N*-acetyl-L-cysteine -NAC-).

2.2 *Cytokines exposure*

After the primary neurospheres splitting, foetal and adult cultures were divided in two groups: one treated with a mix of six different cytokines (TGF-b1, TNF-a, IL-1b, IL-6, IL-17 and IFN-c; 20 ng/mL each) and the other treated with vehicle (0.04% of the cytokines solvent: 10% glycerol/100 nM glycine/25 nM Tris, pH 7.3). After oligospheres expansion, medium was changed with the standard one, without cytokines, in both groups.

2.3 *Oxygen-glucose deprivation*

OGD was performed using an air-tight hypoxia chamber (Billups-Rothenberg Inc., Del Mar., CA) saturated with 95% N2- 5% CO2 (Goldberg and Choi, 1993). Glucose deprivation was achieved using a glucose-free complete medium. Oxygen was removed by flushing the hypoxia chamber with N2-CO2 mixture for 6-8 min at 25 l/min. The flushing was repeated after half the incubation time. The OGD condition was maintained for 3 h, after which plates were re-oxygenated for 24 h in the old medium in a cell incubator.

2.4 *Immunocytochemistry*

Indirect immunofluorescence was used to identify OPCs (NG2-positive cells), mature (CNPase-positive cells) and myelinating (MBP-positive cells) oligodendrocytes, neurons (β-III-tubulin-positive cells), astrocytes (GFAP-positive cells) and deyodinases 3 expressing

cells (D3). The following primary antisera were used: mouse anti-β-III-tubulin (R&D system, Trento, Italy) 1:3000; rabbit anti-GFAP (Glial Fibrillary Acidic Protein, Dako) 1:1000; rabbit anti-NG2 (chondroitin sulphate proteoglycan, neural/glial antigen 2, Millipore, Merck S.p.a., Milan, Italy) 1:350; mouse anti-CNPase (2', 3'-cyclic nucleotide 3'-phosphodiesterase, Millipore) 1:500; rabbit anti-MBP (Myelin Basic Protein, Dako) 1:500; goat anti-D3 (deyodinase type 3, Santa Cruz Biotechnology) 1:100. Donkey Alexa 488-conjugated anti mouse IgG. donkey Alexa 568-conjugated anti-rabbit IgG, 1:500 (Invitrogen) and DyLight488-conjugated affinity-pure donkey anti-Goat IgG (Jackson Immunoresearch) 1:100 were used as secondary antisera. After immunofluorescence staining, cells were incubated with the nuclear dye Hoechst 33258 (1 μg/mL in PBS, 0.3% Triton-X 100) for 20 min at RT. Cells were finally washed in PBS and mounted in glycerol and PBS (3:1, v/v) containing 0.1% paraphenylendiamine.

2.5 *Fluorescence microscopy*

Fluorescence microscopy was used to quantify the percentage od D3-expressing cells in foetal cultures 24 hours after OGD exposure.

Images were captured using a Nikon Eclipse E600 microscope equipped with digital CCD camera Q Imaging Retiga-2000RV (Q Imaging, Surrey, BC, Canada). Measurements were performed using Nis-Elements AR 3.2 software.

Five random filed per glass (duplicate for group) were analysed. D3-positive cell percentage was calculated on the total number of cells per field, identified by the nuclear saining.

2.6 *High Content Screening*

For HCS analysis cells were grown in 96 flat-bottom well HCS plates (NUNC). Analysis of condensed nuclei, cell number and lineage/differentiation markers were performed with Cell

Insight™ CX5 High Content Screening (HCS; Thermo Scientific), using the *Compartmental analysis* BioApplication. Based on nuclear staining, the software is able to recognise nuclei and calculate the percentage of high intensity/small sized condensed nuclei. Moreover, based on the nuclei identification, the software is able to detect the presence of the marker-specific stain in the cell body, calculating the percentage of the immunoreactive cells. Lineage/differentiation markers analysis was performed only on cells showing intact nuclei, excluding condensed nuclei from the percentage calculation.

2.7 *Statistical Analysis*

Experiments were performed in triplicate for cell number and viability and in duplicate for cell markers analysis. Data are reported as mean ± SEM. Prism software (GraphPad) was used for statistical analyses and graph generation. Student's t test or two-way ANOVA (for the time course of OGD vulnerability of foetal OPCs) were used to analyse data. Results were considered significant when the probability of their occurrence as a result of chance alone was less than 5% ($P < 0.05$).

3. *Results*

3.1 *The cells systems.*

OPCs were obtained driving NSCs differentiation by specific factors. After neurospheres splitting, PDGF was substituted to EGF in the culture medium, starting the OPCs differentiation, obtaining oligospheres in suspensions. In order to obtain OPCs cultures, oligospheres were sedded as single cell suspension and, after 3 days, bFGF/PDGF medium was substituted by T3 containing medium, allowing the OLs maturation for 12 DIVs (Figure 1A).

NSCs-derived cultures are mixed cultures composed by OPCs, OLs and astrocytes, with a small percentage of neurons (Baldassarro et al., 2017). Lineage progression from NG2-positive OPC (DIV0) through CNPase- mature OL as far as myelinating CNPase/MBP-positive OL is illustrated in Fig. 1B-D (representative images). The culture composition changes during the 12 DIV differentiation period, starting from DIV0, where the majority of cells are NG2 positive (NG2-positive cells 80%; CNPase-positive cells 5%), passing thorough DIV 6, where CNPase cells are growing in number (NG2-positive cells 60%; CNPase-positive cells 30%), reaching the end of the differentiation with CNPase/MBP positive cells representing the majority of cells (CNPase-positive cells; 70% in foetal and 45% in adult cultures; MBP-positive cells, 40% in foetal and 30% in adult cultures). Both cultures show around 40% of GFAP-positive cells at 12 DIVs, and a small percentage (6-8%) of beta-III-tubulin positive cells (neurons).

3.2 Inflammatory cytokines block foetal and adult OPCs differentiation.

In this experiment, NSCs-derived OPCs were exposed at the inflammatory cytokines mix during the oligospheres phase, during replication and in absence of differentiating stimuli. The cytokine mix was composed by TGF-b1, TNF-a, IL-1b, IL-6, IL-17 and IFN-c. This cocktail was choose from in vivo experiments, detected in EAE model, the animal model of MS, and we already demonstrated that, when used in these experimental conditions, block adult OPCs differentiation (Fernandez et al., 2016). Three days after the OPCs cell seeding, cells were triggered to differentiation into OPCs by T3 (Fig 2A). Cells were analysed at the end of the differentiation phase for cell number, cell death and positivity for markers expressed at different maturation stages (12 DIV, black arrow in Fig 2A) by HCS technology. Both foetal and adult OPCs cultures treated with the cytokine mix show an increase in the total cell number at the end of the differentiation phase compared to the vehicle-treated cells (Student's t test: foetal, $p < 0.0001$; adult, $p = 0.0009$; Fig 2B). Cytokines treatment during the

proliferation phase do not induce cell death in both foetal and adult cultures. However, in the opptiste way, cytokines-treated foetal cells show a lower percentage of dead cells compared to vehicle-treated cells (p = 0.0007; Fig 2C).

At the end of the differentiation period, cytokines-treated cells show a different cell composition compared to vehicle-treated cells. As already described (Fernandez et al., 2016), in adult cultures, cytokine treatment of OPCs determines an increase in the percentage of NG2-positive cells (Student's t test, p = 0.0025), which is not observed in the foetal cultures (Student's t test, p = 0.5076). However, in both foetal and adult cultures, OPCs differentiation is drastically reduced in the cytokines- compared to the vehicle-treated, as indicated by the percentage of mature (CNPase-positive cells) and myelinating (MBP-positive cells) OLs (Student's t test: CNPase, foetal, p < 0.0001, adult, p = 0.0273; MBP, foetal p < 0.0001, adult, p = 0.0036). Moreover, also differentiation into astrocyte is decreased by cytokines exposure in both foetal and adult cultures, compared to vehicle-treated cells (Student's t test: foetal, p = 0.0030; adult p = 0.0001; Fig 2 D-L).

3.3. *Foetal but not adult OPCs are vulnerable to OGD-induced cell death*

We then tested foetal and adult OCDs vulnerability to OGD, the most widely used *in vitro* model for HI. The OGD model was previously set up and characterized in primary pure neuronal and mixed neurons/astrocytes cultures (Baldassarro et al., 2018), demonstrating that 3 hours of OGD followed by 24 hours of reoxygenation/reperfusion is able to induce neuronal cell death.

OGD was thus tested in the NSCs-derived OPCs, during the proliferation of seeded OPCs, 24 hours before the T3-mediated differentiation induction (Figure 3 A). OGD induces a reduction in cell number after the differentiation phase in foetal (p < 0.0001), and an increase in adult cultures (p < 0.0001; Fig 3 B). The cell number reduction in foetal cultures is associated to a

drastic increase of cell death (p < 0.0001), effect not observed in adult cultures (p = 0.1247; Fig 3 C).

In order to investigate the foetal OPC vulnerability according to the phases of the H/I pathogenic mechanism, we exposed foetal OPCs to OGD as previously described and we analysed the cell number and cell viability, by HCS technology, at three different time points: after reoxygenation phase (before adding the T3-induced differentiation stimulus to the culture; 0 DIV), and at 6 and 12 DIVs after T3 exposure. Results were analysed by two-ways ANOVA, considering the culture time (0, 6 and 12 DIVs) and condition (OGD and normoxia). As showed in the previous experiments, both cell number and cell death are affected by OGD (two-ways ANOVA for cell number; culture condition, p < 0.0001, $F_{(2,60)}$ = 33.48; time, p < 0.0001, $F_{(1,30)}$ = 57.35; interaction, p < 0.0001, $F_{(2, 60)}$ = 106.4; two-ways ANOVA for cell death, culture condition, p < 0.0001, $F_{(1,30)}$ = 118.4; time, p < 0.0001, $F_{(2,60)}$ = 114.6; interaction, p < 0.0001, $F_{(2, 60)}$ = 110.2). However, cell death is a late responce, with an effect observed only at 12 DIVs (Sydak post-hoc: normoxia vs. OGD; cell number, p < 0.0001; cell death, p < 0.0001; Fig 3 D-E).

As already indicated, the OPC preparation derived from NSC also contains astrocytes, and few neurons. In order to establish the cell population affected by OGD, we used Cell Insight™ CX5 HCS. The software identify nuclear size and morphology (normal nucleus for living cells; condensed nuclei for dead cells), and the associated cytoplasm immunostaining for astrocytes (GFAP), neurons (b-III-tubulin), OPC (NG2), mature OL (CNPase) and myelinating OL (MBP), thus allowing the identification of degenerating cell type. The final percentage of astrocyte and neurons in the differentiated cultures are not affected by OGD (Student's t test: foetal, GFAP, p = 0.3137, foetal beta-III-tubulin, p = 0.2998; adult, GFAP, p = 0.1530, beta-III-tubulin, p = 0.9914). On the contrary, OGD exposure causes a decrease in the number of NG2-, CNPase- and MBP-positive cells in foetal- (Student's t test: NG2, p = 0.0158; CNPase, p < 0.0001; MBP, p = 0.0002) cultures while adult-derived cultures

163

(Student's t test: CNPase, p = 0.6283; MBP, p =0.3606) do not show differences in the mature and myelinating OLs. However, adult cultures exposed to OGD show an increase in the number of NG2-positive cells, compared to normoxia-exposed cultures (p = 0.0025; Figure 4 A).

With regard to the lineage composition of dead cells, foetal-derived cultures show an increase in cell death in NG2, CNPase and MBP-positive cells (NG2, p = 0.0002; CNPase, p = 0.0028; MBP, p = 0.0095), without affecting astrocytes and the small percentage of neurons (Student's t test: GFAP, p = 0.0880; beta-III-tubulin, p = 0.1272). Adult-derived cultures, as expected by the analysis of the whole culture, do not show cell death in any population (Student's t test: NG2, p = 0.4690; CNPase, p = 0.2321; MBP, p = 0.3568; GFAP, p = 0.8302; beta-III-tubulin, p = 0.4015; Figure 4 B-J).

Moreover, after the reoxygenation phase (0 DIV, Figure 5 A), foetal-derived cultures show an increase in D3-positive cells (p = 0.0009; Fig 5 B-D).

4. *Discussion*

The most investigated example of the role of inflammation in remyelination failure is multiple sclerosis (MS), the most diffuse inflammatory/demyelinating disease in humans (Goodin, 2014). In the acute focal phase of the disease, remyelination is efficient (Rodgers et al., 2013), however this process progressively fails (Boyd et al., 2013; Lassmann et al., 2012), and the most accredited hypothesis for remyelination failure is the block of OPCs differentiation and maturation into myelinating OL (Kuhlmann et al., 2008; Miller and Mi, 2007). The block of this process leads to an inefficient myelin repair (Zhang et al., 2015).

Numerous *in vitro* and *in vivo* studies have indicated that inflammatory cytokines are involved in OPCs differentiation block, affecting cell cycle exit and the expression of genes encoding

for proteins regulating and determining remyelination (Chew et al., 2005; Falahati et al., 2013; Kang et al., 2013; Su et al., 2011; Tanner et al., 2011; Fernandez et al., 2016).

Less data are instead available on the mechanism of OPC differentiation block in neonatal age. Here we showed that both foetal and adult NSCs-derived OPCs are vulnerable to cytokines exposure, that leads to a differentiation block, thus confirming the differentiation block observed in adult NSCs-derived OPCs alredy described (Fernandez et al., 2016).

A different vulnerability to OGD is instead observed in foetal and adult OPCs. Adult OPCs are not vulnerable to 3 hours of OGD followed by 24 hours of reoxygenation/reperfusion, before the T3-mediated differentiation induction, in terms of cell viability and differentiation process, while foetal cultures are highly susceptible, leading to an increase in cell death and a reduction in cell number. Moreover, we showed that the OGD-cell death induction, is a slow process and selective for OPCs/OLs.

The impaired OLs maturation in OGD seems to be maturation stage-dependent, where PreOLs (late OPCs) are the most susceptible cells, followed by early OPCs and mature OLs, which implies that death of PreOLs causes subsequent failure of myelination (Back et al., 2002). *In vitro* experiments demonstrated that oxygen-glucose deprivation (OGD) in primary OPCs, induces intracellular Ca^{2+} overload, mitochondrial damage and ROS generation (via ERK1/2 pathway), resulting in PreOLs death (Cai et al., 2016). Calcium overload leads also to lipases, endonucleases and proteases activation, leading to the cytoskeleton disaggregation (Rocha-Ferreira et al., 2016).

A complex dysregulation of the TH tissue signalling is present in acute phase of EAE (experimental allergic encephalomyelitis), the rodents and primate animal model of MS

(Dell'Acqua et al., 2012; D'Intino et al., 2011; Fernandez et al., 2016), which correlates with the rise of inflammatory cytokines released by peripheral cells and resident microglia (Borjini et al., 2016).

This pathological characteristic of severe demyelinating disease, was causally linked to an increase in D3-positive cells and D3 expression both *in vivo* and *in vitro*, causing the inactivation of T3 and subsequent differentiation block. The hypothesis has been confirmed by *in vitro* studies in our lab, where we demonstrated that the inhibition of D3 restores the OPC differentiation during exposure to the inflammatory cytokine cocktail (Fernandez et al., 2016).

An increase in D3 activity and mRNA expression level has been described in other neurological conditions characterized by inflammation and demyelination, e.g., ischemia-induced hypoxic brain damage (Jo et al., 2012) and nerve lesion (Li et al., 2001).

In the present study we demonstrated that foetal cells show an up-regulation of D3 enzyme 24 hours after the OGD-exposure, pointing the focus of the future studies on the implication of THs metabolism dysregulation OGD-mediated.

Another possible mechanism refers to glutamate excitotoxicity. It is well described that HI-induced cell death is linked to glutamate receptors overactivation and consequent excitotoxicity. Glutamate receptors expression and functions are also dynamics throughout the OPCs differentiation process, while little is known about differences in their expression and function between foetal and adult primary or NSCs-derived OPCs.

In particular, for many years, AMPA/kainite, but not NMDA receptors, have been considered the mediator of glutamate excitotoxicity in glial cells (Tekkök and Goldberg, 2001) and, in particular, the HI-induced cell death glutamate-mediated in pre OLs (Deng et al., 2003). However, more recently it has been demonstrated that NMDA receptors play a role during development myelination (Káradóttir et al., 2007) and are partners in the OL myelinating

processes. A different expression of these receptors during the differentiation process, could also explain the different sensitivity to glutamate in different stages. In particular OPCs show higher expression of AMPA/kainite receptor, mGluR while, postmitotic OLs have higher NMDA receptor expression (Butts et al., 2008).

We previously demonstrated that adult OPCs show a more mature phenotype in early stages of differentiation, while achieving a less yield of maturation compared to foetal (Baldassarro et al., unpublished). Future studies will clarify the role of glutamate exitotoxicity in OGD-induced cell death in foetal OPCs, and consequent different role of glutamate receptors in adult-derived cells.

The understanding of differences in response of foetal and adult OPCs to demyelination stimuli, and their origin, will contribute to the development of myelination promoting therapies in foetal/neonatal and adult pathologies.

Acknowledgements

References

Alhenius H and Kokaia Z. Isolation and generation of neurosphere cultures from embryonic and adult mouse brain. Methods Mol Biol, 2010; 633: 241-252.

Alizadeh A, Dyck SM and Karimi-Abdolrezaee S. Myelin damage and repair in pathologic CNS: challenges and prospects. Front Mol Neurosci, 2015. 8: 35.

Baldassarro VA, Marchesini A, Giardino L and Calzà L. PARP activity and inhibition in fetal and adult oligodendrocyte prectursor cells: Effect on cell survival and differentiation. Stem Cell Res, 2017. 22: 54-60.

Baldassarro VA, Marchesini A, Facchinetti F, Villetti G, Calzà L and Giardino L. Cell death in pure-neuronal and neuron-astrocyte mixed primary culture subjected to oxygen-glucose deprivation: The contribution of poly(ADP-ribose) polymerases and caspases. Microchem J, 2018. 136: 215-222.

Baldassarro VA, Krezel W, Giardino L and Calzà L. Nuclear receptors and foetal vs. adult oligodendrocyte precursor cells differentiation. unpublished

Back SA, Han BH, Luo NL, Chricton CA, Xanthoudakis S, Tam J, Arvin KL and Holtzman DM. Selective vulnerability of late oligodendrocyte progenitors to hypoxia-ischemia. J Neurosci, 2002. 22: 455-463.

Borjini N, Fernández M, Giardino L and Calzà L. Cytokine and chemokine alterations in tissue, CSF, and plasma in early presymptomatic phase of experimental allergic encephalomyelitis (EAE), in a rat model of multiple sclerosis. J Neuroinflammation, 2016. 13: 291.

Boyd A, Zhang H and Williams A. Insufficient OPC migration into demyeli- nated lesions is a cause of poor remyelination in MS and mouse models. Acta Neuropathol, 2013. 125: 841–859.

Butts BD, Houde C and Mehmet H. Maturation-dependent sensitivity of oligodendrocyte lineage cells to apoptosis: implications for normal development and disease. Cell Death Diff, 2008. 15: 1178-1186

Cai Q, Ma T, Li C, Tian Y and Li H. Catalpol Protects Pre-Myelinating Oligodendrocytes against Ischemia-induced Oxidative Injury through ERK1/2 Signaling Pathway. Int J Biol Sci, 2016. 12: 1415-1426.

Calzà L, Baldassarro VA, Fernandez M, Giuliani A, Lorenzini L and Giardino L. Thyroid hormone and the white matter of the central nervous system: from development to repair. Vit and Horm, 2017. In press.

Chen Y, Balasubramaniyan V, Peng J, Hurlock EC, Tallquist M, Li J and Lu QR. Isolation and culture of rat and mouse oligodendrocyte precursor cells. Nat Proc, 2007; 2: 1044-1051.

Chew LJ, King WC, Kennedy A andGallo V. Interferon-gamma inhibits cell cycle exit in differentiating oligodendrocyte progenitor cells. Glia, 2005. 52: 127–143.

Crawford AH, Chambers C and Franklin RJ. Remyelination: The true regeneration of the central nervous system. Journal of Comparative Pathology, 2013. 149: 242–254.

Dell'Acqua ML, Lorenzini L, D'Intino G, Sivilia S, Pasqualetti P, Panetta V, Paradisi M, Filippi MM, Baiguera C, Pizzi M, Giardino L, Rossini PM and Calzà L. Functional and molecular evidence of myelin- and neuroprotection by thyroid hormone administration in experimental allergic encephalomyelitis. Neuropathology and Applied Neurobiology, 2012; 38: 454–470.

Deng W, Yue Q, Rosenberg PA, Volpe JJ and Jensen FE. Oligodendrocyte excitotoxicity determined by local glutamate accumulation and mitochondrial function. J Neurochem, 2006. 98: 213-222.

D'Intino G, Lorenzini L, Fernandez M, Taglioni A, Perretta G, Del Vecchio G, Villoslada P, Giardino L and Calzà L. T3 administration ameliorates the demyelination/remyelination ratio in a non-human primate model of multiple sclerosis by correcting tissue hypothyroidism. Journal of Neuroendocrinology, 2011; 23: 778–790.

El Waly B, Macchi M, Cayre M and Durbec P. Oligodendrogenesis in the normal and pathological central nervous system. Front. Neurosci, 2014. 8: 145

Falahati S, Breu M, Waickman AT, Phillips AW, Arauz EJ, Snyder S, Porambo M, Goeral K, Comi AM, Wilson MA, Johnston MV and Fatemi A. Ischemia- induced neuroinflammation is associated with disrupted development of oli- godendrocyte progenitors in a model of periventricular leukomalacia. Dev Neurosci, 2013. 35: 182–196.

Fernández M, Baldassarro VA, Sivilia S, Giardino L and Calzà L. Inflammation severely alters thyroid hormone signaling in the central nervous system during experimental allergic encephalomyelitis in rat: Direct impact on OPCs differentiation failure. Glia, 2016. 64: 1573-1589.

Franklin RJM and Hinks GL. 1999. Understanding CNS remyelination: Clues from developmental and regeneration biology. J Neurosci Res 58:207–213.

Goldberg MP and Choi DW. Combined oxygen and glucose deprivation in cortical cell culture: calcium-dependent and calcium-independent mechanisms of neuronal injury. J Neurosci, 1993; 13: 3510-3524.

Goodin DS. The epidemiology of multiple sclerosis: Insights to disease pathogenesis. Handb Clin Neurol, 2014. 122: 231–266.

Irvine KA and Blackmore WF. Remyelination protects axons from demyelination-associated axon degeneration. Brain, 2008. 131: 1464-1477.

Jablonska B, Scafidi J, Aguirre A, Vaccarino F, Nguyen V, Borok E, Horvath TL, Rowitch DH and Gallo V. Oligodendrocyte regulation after Neuonatal Hypoxia requires FoxO1-mediated p27kip1 expression. J Neurosci, 2013. 32: 14775-14793.

Jo S, Kalloò I, Bardóczi Z, Arrojo e Drigo R, Zeo˙ld A, Liposits Z, Oliva A, Lemmon VP, Bixby JL, Gereben B and Bianco AC. Neuronal hypoxia induces Hsp40-mediated nuclear import of type 3 deiodinase as an adaptive mechanism to reduce cellular metabolism. J Neurosci, 2012. 32: 8491-8500.

Kang Z, Wang C, Zepp J, Wu L, Sun K, Zhao J, Chandrasekharan U, DiCorleto PE, Trapp BD, Ransohoff RM and Li X. Act1 mediates IL-17-induced EAE pathogenesis selectively in NG21 glial cells. Nat Neurosci, 2013; 16: 1401–1408.

Káradóttir R and Attwell D. Neurotransmitter receptors in the life and death of oligodendrocytes. Neuroscience, 2007. 145: 1426-1438.

Kuhlmann T, Miron V, Cui Q, Wegner C, Antel J and Bruck W. Differentiation block of oligodendroglial progenitor cells as a cause for remyelination failure in chronic multiple sclerosis, Brain, 2008. 131: 1749–1758.

Lassmann H, van Horssen J and Mahad D. Progressive multiple sclerosis: Pathology and pathogenesis. Nat Rev Neurol, 2012. 8: 647–656.

Li WW, Le Goascogne C, Ramaugé M, Schumacher M, Pierre M and Courtin F. Induction of type 3 iodothyronine deiodinase by nerve injury in the rat peripheral nervous system. Endocrinol, 2001. 142: 5190–5197.

Liu C, Li Y, Yu J, Feng L, Hou S, Liu Y, Guo M, Xie Y, Meng J, Zhang H, Xiao B, Ma C. Targeting the shift from M1 to M2 macrophages in experi- mental autoimmune encephalomyelitis mice treated with fasudil. PLoS One, 2013. 8: e54841–54854.

McIver SR, Muccigrosso M, Gonzales ER, Lee JM, Roberts MS, Sands MS and Goldberg MP. Oligodendrocyte degeneration and recovery after focal cere- bral ischemia. Neuroscience, 2010. 169: 1364–1375.

Mekhail M, Almazan G and Tabrizian M. Oligodendrocyte-protection and remyelination post-spinal cord injuries: A review. Progress in Neurobiology, 2012. 96, 322–339.

Miller RH and Mi S. Dissecting demyelination. Nat Neursci, 2007. 10: 1351-1354.

Miron VE, Kuhlmann T and Antel JP. CElls of the oligodendrocglial lineage, myelination, and remyelination. Biochimica et Biophysica Acta, 2011. 1812: 184-193.

Pantoni L, Sarti C, Alafuzoff I, Jellinger K, Munoz DG, Ogata J and Palumbo V. Postmortem examination of vascular lesions in cognitive impair- ment: a survey among neuropathological services. Stroke, 2006. 37: 1005–1009.

Patel JR and Klein RS. Mediators of oligodendrocyte differentiation during remyelination. FEBS Lett, 2011; 585: 3730-3737.

Rocha-Ferreira E and Hristova M. Plasticity in the neonatal brain following hypoxic-ischemic injury. Neural Plast, 2016. 2016: 4901014.

Rodgers JM, Robinson AP and Miller SD. Strategies for protecting oligo- dendrocytes and enhancing remyelination in multiple sclerosis. Discov Med, 2013. 16: 55-63.

Sozmen EG, Rosenzweig S, Llorente IL, DiTullio DJ, Machnicki M, Vinters HV, Havton LA, Giger Rj, Hinman JD and Carmichael ST. Nogo receptor blockade overcomes remyelination failure after white matter stroke and stimulates functional recovery in aged mice. Proceedings of the National Academy of Sciences of the United States of America, 2016. 113: E8453–E8462.

Su Z, Yuan Y, Chen J, Zhu Y, Qiu Y, Zhu F, Huang A and He C. Reactive astrocytes inhibit the survival and differentiation of oligodendrocyte precursor cells by secreted TNF-a. J Neurotrauma, 2011. 28: 1089–1100.

Tanner DC, Cherry JD and Mayer-Pro€schel M. Oligodendrocyte progenitors reversibly exit the cell cycle and give rise to astrocytes in response to interferon-c. J Neurosci, 2011. 31: 6235–6246.

Tekkök SB and Goldberg MP. AMPA/Kainate Receptor Activation Mediates Hypoxic Oligodendrocyte Death and Axonal Injury in Cerebral White Matter. J Neurosci, 2001. 21: 4237-4248.

Tognatta R and Miller RH. Contribution of the oligodendrocyte lineage to CNS repair and neurodegenerative pathologies. Neuropharmacology, 2016; 110: 539-547.

Trotter J, Karram K and Nishiyama A. NG2 cells: Properties, progeny and origin. Brain Res Rev, 2010. 63: 72–82.

van Tilborg E, de Theije CGM, van Hal M, Wagenaar N, de Vries LS, Benders MJ, Rowitc DH and Nijboer CH. Originand dynamics of oligodendrocytes in the developing brain: Implications for perinatal white matter injury. Glia, 2018. 66: 221-238.

Verden D and Macklin WB. Neuroprotection by central nervous system remyelination: Molecular, cellular, and functional considerations. J Neurosci Res, 2016. 94: 1411-1420.

Zhang Y, Luo X, Wu D and Xu Y. ROR nuclear receptors: structures, related diseases and drug discovery. Acta Pharmacologica Sinica, 2015. 36: 71-87.

Legend to the figures.

Figure 1. Experimental design

(A) After NSCs isolation and neurospheres expansion, in presence of bFGF and EGF, oligospheres were generated by spheroids disgregation and bFGF/PDGF exposure. Oligospherese were than dissociated and single cell cultures were seeded in the same medium. After 3 DIVs, medium was changed and cells were exposed to T3, in order to differentiate, for 12 DIVs.

(B-D) Representative images of culture progress from OPCs (NG2-positive cells, 0 DIV, B), through mature OLs (CNPase-positive cells, 6 DIV, C) to mature/myelinating OLs (CNPase/MBP-positive cells, 12 DIV, D).

Abbreviations: CNPase, 2',3'-cyclic nucleotide 3'-phosphodiesterase; MBP, myelin basic protein; NG2, chondroitin sulphate proteoglycan, neural/glial antigen 2.

Figure 2. Cytokines exposure effect on viability and differentiation in foetal and adul NSCs-derived OPCs.

(A) Experimental design. Cells were exposed to cytokine mix during the oligospheres proliferation phase. Three days after cell seeding, differentiation was induced by T3 exposure. Cells were analysed at the end of the differentiation phase (black arrow, 12 DIV).

(B) Graph shows the cell number at the end of the differentiation phase (12 DIV), in foetal and adult cultures, exposed to vehicle or cytokine mix. Bars represent the total cell number per well.

(C) Graph shows the cell death at the end of the differentiation phase (12 DIV), in foetal and adult cultures, exposed to vehicle or cytokine mix. Bars represent the percentage of cells showing condensed nuclei, on the total number of cells per well.

(D) Graph shows the percentage of lineage specific positive cells at the end of the differentiation phase (12 DIV) in foetal and adult cultures, exposed to vehicle or cytokines mix. The percentage of OPCs (NG2-positive cells), mature OLs (CNPase-positive cells), myelinating OLs (MBP-positive cells) and astrocytes (GFAP-positive cells), was calculated on the total cell number, showing a normal nuclear morphology, per well.

(E-L) Images show CNPase-positive (E, F, I, J) and MBP-positive (G, H, K, L) detected in foetal (E, I, G, K) and adult (F, J, H, L) cultures exposed to vehicle (E-H) or cytokines mix (I-L). White bar in image L: 50 μm.

Bars represent mean value + SEM. Statistical analysis: Student's t test; * $p < 0.05$, ** $p < 0.01$, *** $p < 0.001$, **** $p < 0.0001$.

Abbreviations: CNPase, 2',3'-cyclic nucleotide 3'-phosphodiesterase; GFAP, Glial fibrillary acidic protein; MBP, myelin basic protein; NG2, chondroitin sulphate proteoglycan, neural/glial antigen 2.

Figure 3. OGD effect on viability of foetal and adul NSCs-derived OPCs and effect on D3 expression.

(A) Experimental design. Cells were exposed to 3 hours OGD, followed by 24 hours of reoxygeneation, one day before the T3-mediated differentiation induction.

(B) Graph shows the cell number at the end of the differentiation phase (12 DIV), in foetal and adult cultures, exposed to normoxia or OGD. Bars represent the total cell number per well.

(C) Graph shows the cell death measured at the end of the differentiation phase (12 DIV), in foetal and adult cultures, exposed to normoxia or OGD. Bars represent the percentage of cells showing condensed nuclei, on the total number of cells per well.

(D) Graph shows the cell number at 0, 6 and 12 DIV in foetal cultures, exposed to normoxia or OGD. Bars represent the total cell number per well.

(E) Graph shows the cell death measured at 0, 6 and 12 DIV in foetal cultures, exposed to normoxia or OGD. Bars represent the percentage of cells showing condensed nuclei, on the total number of cells per well.

Bars represent mean value + SEM. Statistical analysis: Student's t test (B, C, F) and two-way ANOVA, followed by Tukey's post-hoc (D, E); *** $p < 0.001$, **** $p < 0.0001$.

Abbreviations: OGD, oxygen-glucose deprivation.

Figure 4. OGD effect on differentiation and lineage-specific cell death induction in foetal and adult NSCs-derived OPCs.

(A) Graph shows the percentage of lineage specific positive cells at the end of the differentiation phase (12 DIV) in foetal and adult cultures, exposed to normoxia or OGD. The percentage of OPCs (NG2-positive cells), mature OLs (CNPase-positive cells), myelinating OLs (MBP-positive cells), astrocytes (GFAP-positive cells) and neurons (beta-III-tubulin), was calculated on the total cell, showing a normal nuclear morphology, number per well.

(B) Graph show the percentage of lineage specific positive cells showing also a condensed nuclei, at the end of the differentiation phase (12 DIV) in foetal and adult cultures, exposed to normoxia or OGD. The percentage of OPCs (NG2-positive cells), mature OLs (CNPase-positive cells), myelinating OLs (MBP-positive cells), astrocytes (GFAP-positive cells) and neurons (beta-III-tubulin), was calculated on the total cell, showing a normal nuclear morphology, number per well.

(C-J) Images show NG2-positive (C, D, G, H) and CNPase/MBP-positive (E, F, I, J) detected in foetal (C, G, E, I) and adult (D, H, F, J) cultures exposed to normoxia (C-F) or OGD (G-J). White bar in image J: 50 μm.

Bars represent mean value + SEM. Statistical analysis: Student's t test; ** p < 0.01, *** p < 0.001, **** p < 0.0001.

Abbreviations: CNPase, 2',3'-cyclic nucleotide 3'-phosphodiesterase; GFAP, Glial fibrillary acidic protein; MBP, myelin basic protein; NG2, chondroitin sulphate proteoglycan, neural/glial antigen 2.

Figure 5. OGD effect on D3 expression.

(A) Experimental design. Cells were exposed to 3 hours OGD, followed by 24 hours of reoxygeneation, one day before the T3-mediated differentiation induction. D3 gene expression was analysed in both normoxia and OGD exposed foetal cultures at 0 DIV, after the reoxygenation phase.

(B-D) Graph shows the percentage of D3-positive cells before the T3-mediated differentiation induction (0 DIV) in foetal cultures, exposed to normoxia or OGD (B). Images show D3-

positive cells detected in foetal cultures exposed to normoxia (C) or OGD (D). White bar in image H: 50μm.

Bars represent mean value + SEM. Statistical analysis: Student's t test *** p < 0.001.

Abbreviations: D3, deyodinases 3; OGD, oxygen-glucose deprivation.

A

NSCs isolation · neurospheres proliferation · neurospheres splitting · oligospheres proliferation · OPCs seeding · differentiation induction · OPCs differentiation

bFGF, EGF · bFGF, PDGF · bFGF, PDGF · **T3**, CNTF, NAC

PROLIFERATION · DIFFERENTIATION

B NG2 · DIV 0

C CNPase/MBP · DIV 6

D CNPase/MBP · DIV 12

Figure 1

Figure 2

A

NSCs isolation | neurospheres proliferation | splitting | oligospheres proliferation | OPCs seeding | differentiation induction | OPCs differentiation

bFGF, EGF | bFGF, PDGF | bFGF, PDGF | **T3**, CNTF, NAC

PROLIFERATION | DIFFERENTIATION

3 hs OGD | 24 hs reoxygenation

DIV 0 | 6 | 12

B Cell number (12 DIV)

Fetal | Adult

n cells / well

OGD − + − +

C Cell death (12 DIV)

Fetal | Adult

% condensed nuclei

OGD

D Cell number

n cells / well

- ■ - Fetal Normoxia
- ▲ Fetal OGD

0 6 12
DIV

E Cell death

% condensed nuclei

0 6 12
DIV

Figure 3

Figure 4

A

NSCs isolation | neurospheres proliferation | splitting | oligospheres proliferation | OPCs seeding | differentiation induction | OPCs differentiation

bFGF, EGF   bFGF, PDGF   bFGF, PDGF   **T3**, CNTF, NAC

PROLIFERATION   DIFFERENTIATION

3 hs OGD   24 hs reoxygenation

DIV 0   6   12

B

D3 in fetal OPCs (0 DIV)

% D3 - positive cells

80
60
40
20
0

Normoxia   OGD

***

C Normoxia   **D** OGD
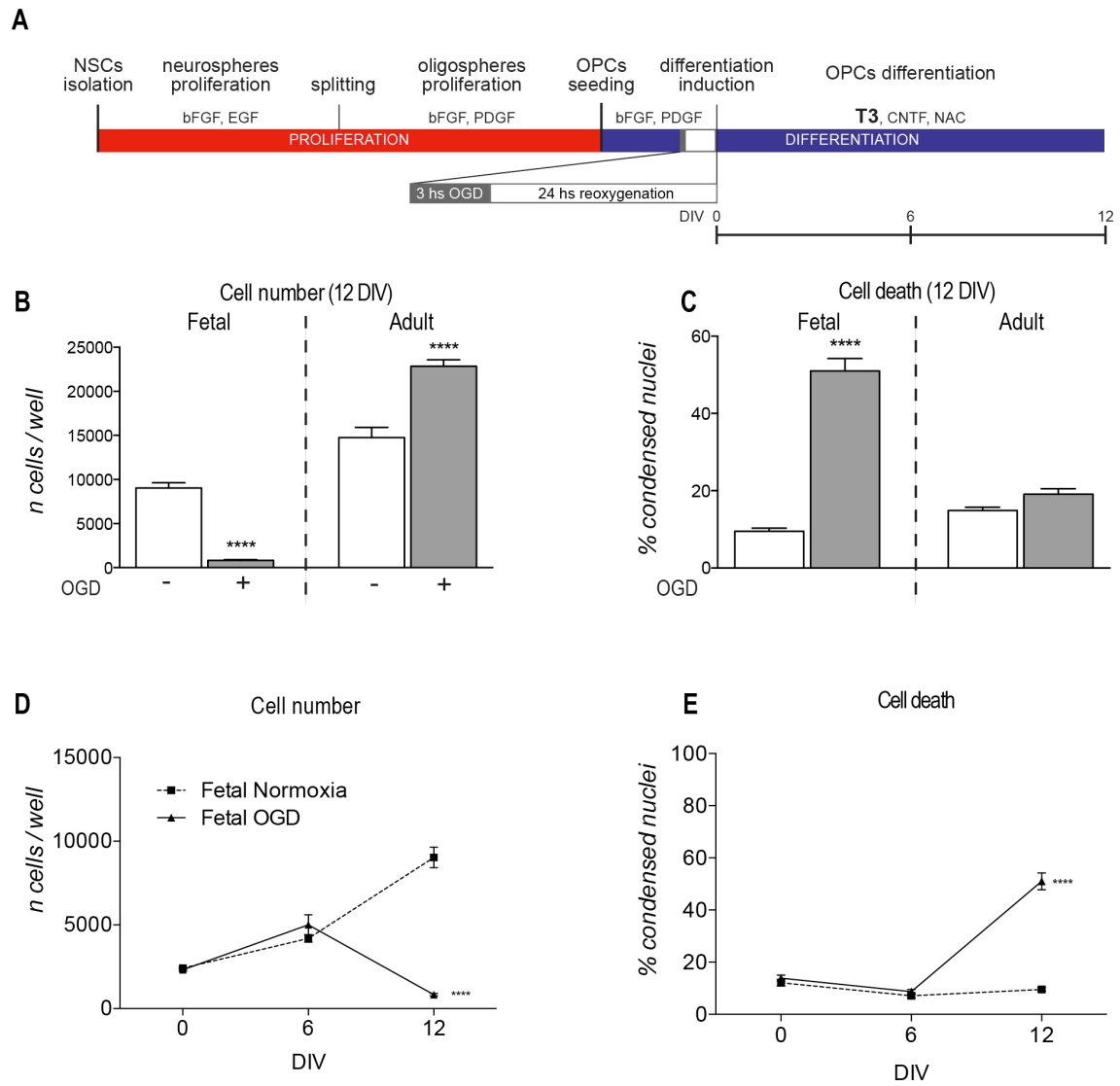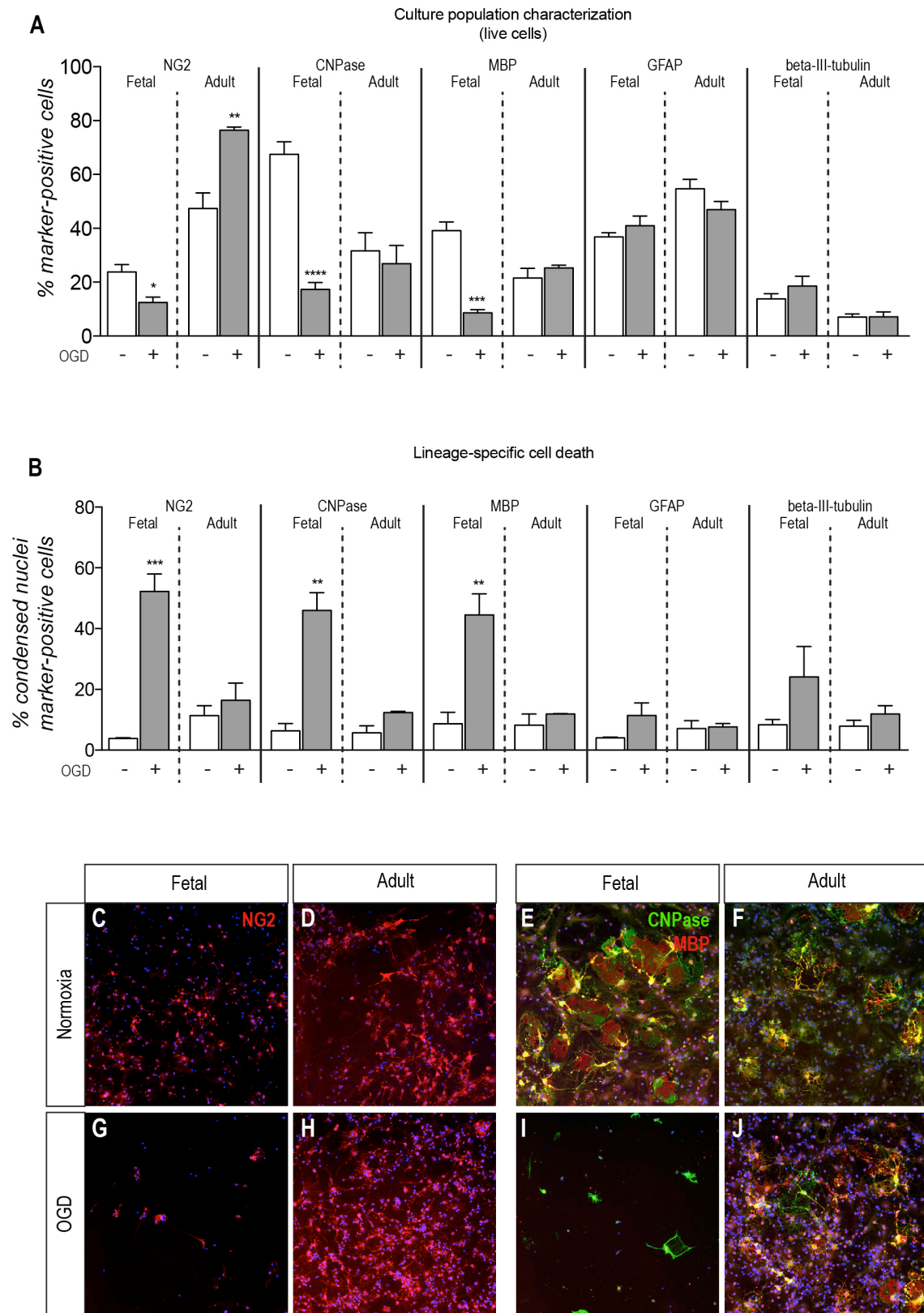
Figure 5

4.8 Inflammation severely alters thyroid hormone signaling in the central nervous system during experimental allergic encephalomyelitis in rat: Direct impact on OPCs differentiation failure (Fernandez et al., 2016).
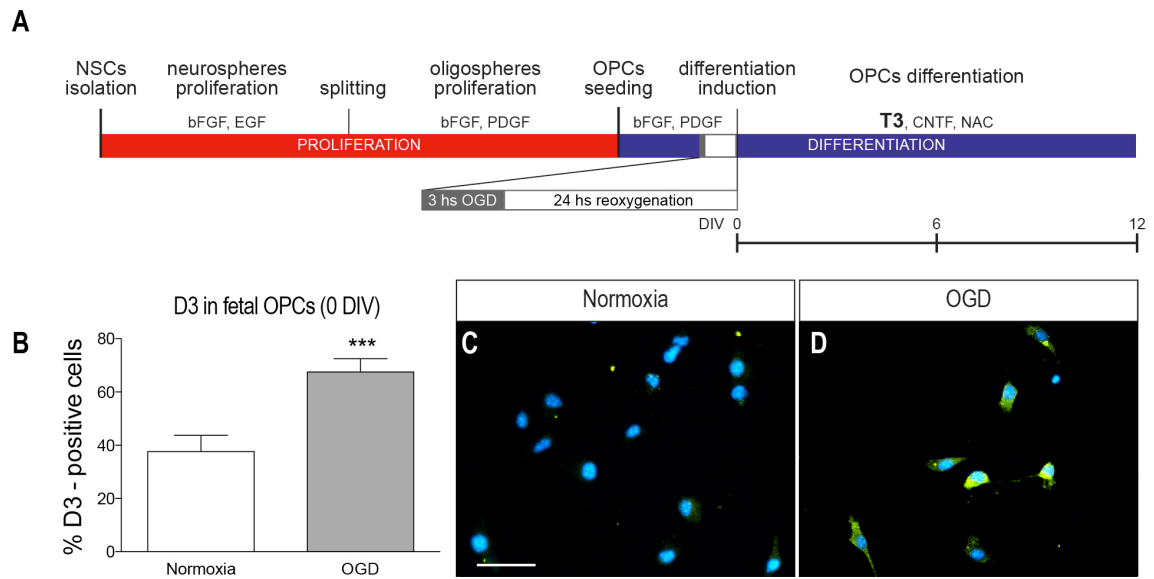
Inflammation Severely Alters Thyroid Hormone Signaling in the Central Nervous System During Experimental Allergic Encephalomyelitis in Rat: Direct Impact on OPCs Differentiation Failure

Mercedes Fernández,[1] Vito A. Baldassarro,[1,2] Sandra Sivilia,[3] Luciana Giardino,[3,4] and Laura Calzà[1,2,4]

Differentiation of oligodendrocyte precursor cells (OPCs) into myelinating oligodendrocytes is severely impaired by inflammatory cytokines and this could lead to remyelination failure in inflammatory/demyelinating diseases. Due to the role of thyroid hormone in the maturation of OPCs and developmental myelination, in this study we investigated (i) the possible occurrence of dysregulation of thyroid hormone signaling in the CNS tissue during experimental neuroinflammation; (ii) the possible impact of inflammatory cytokines on thyroid hormone signaling and OPCs differentiation *in vitro*. The disease model is the experimental allergic encephalomyelitis in female Dark-Agouti rats, whereas *in vitro* experiments were carried out in OPCs derived from neural stem cells. The main results are the following: (i) a strong upregulation of cytokine mRNA expression level was found in the spinal cord during experimental allergic encephalomyelitis; (ii) thyroid hormone signaling in the spinal cord (thyroid hormone receptors; deiodinase; thyroid hormone membrane transporter) is substantially downregulated, due to the upregulation of the thyroid hormone inactivating enzyme deiodinase 3 and the downregulation of thyroid hormone receptors, as investigated at mRNA expression level; (iii) when exposed to inflammatory cytokines, deiodinase 3 is upregulated in OPCs as well, and OPCs differentiation is blocked; (iv) deiodinase 3 inhibition by iopanoic acid recovers OPCs differentiation in the presence on inflammatory cytokines. These data suggest that cellular hypothyroidism occurs during experimental allergic encephalomyelitis, possibly impacting on thyroid hormone-dependent cellular processes, including maturation of OPCs into myelinating oligodendrocytes.

Introduction

Multiple sclerosis (MS) is the most diffuse inflammatory/demyelinating disease in humans (Goodin, 2014). The focal phase of MS is characterized by inflammation and acute damage of the myelin sheath and axons. At this stage, myelin repair may be robust and efficient, early lesions correctly repaired and function restored (Rodgers et al., 2013). This process is ensured by the presence of oligodendrocyte precursor cells (OPCs) (Trotter et al., 2010) that proliferate and differentiate into mature, myelinating oligodendrocytes (OL) (Boulanger and Messier, 2014). However, for unknown reasons this process progressively fails in MS (Boyd et al., 2013; Lassmann et al., 2012). Currently, a blockade of OPCs maturation is regarded as a pre-eminent cause of remyelination

failure in MS (Kuhlmann et al., 2008; Miller and Mi, 2007), suggesting the hypothesis that remyelination depends on successful OPCs differentiation (Zhang et al., 2015a).

The reasons for OPCs differentiation block in MS are unknown. *In vitro* and *in vivo* studies have indicated that inflammatory cytokines impair OPCs differentiation, inhibiting cell cycle exit and the expression of myelin-related genes (Chew et al., 2005; Falahati et al., 2013; Kang et al., 2013; Su et al., 2011; Tanner et al., 2011). However, the intracellular machinery supporting the cytokine-induced OPCs differentiation block has been not identified.

Thyroid hormone (TH) is one of the best characterized differentiating agents of OPCs, inducing cell-cycle arrest and transcription of premyelinating genes (Billon et al., 2002; Casaccia-Bonnefil and Liu, 2003; Dugas et al., 2012). The circulating prohormone thyroxine (T4) secreted by the thyroid gland is converted into the active form (triiodothyronine, T3) by astrocytes in the CNS through the enzyme deiodinase 2 (D2) (Bianco et al., 2002; Calzà et al., 2015; Morte and Bernal, 2014). TH tissue homeostasis is then guaranteed by deiodinase 3 (D3), which inactivates T4 to reverse-T3 (rT3) and T3 to 3,5-diiodo-l-thyronine (T2). Therefore, a local TH metabolism also supported by TH membrane transporters (Bernal et al., 2015; Lee et al., 2015) guarantees the appropriate intracellular content of TH in the CNS and the TH-dependent genomic (via nuclear receptor, TRs) and nongenomic effects (Dentice et al., 2013). Direct action of T3 has been found in purified OPCs, where T3 induces cell cycle exit and terminal differentiation into myelinating oligodendrocytes (Raff, 2006), also regulating the expression of myelin protein-encoding genes (Strait et al., 1997).

Inflammatory cytokines impair OPCs differentiation (Kuhlmann et al., 2008), alter TH tissue metabolism and intracellular T3 availability (de Vries et al., 2015). These data supported the attempt to use TH to overcome OPCs differentiation block during experimental inflammatory-demyelinating diseases. Our previous work showed that a short *in vivo* TH administration during experimental allergic encephalomyelitis (EAE) promotes OPCs maturation, protects myelin sheaths and axons, and ultimately improves functional and clinical outcome in rat and non-human primates Callithrix Jacchus (Calzà et al., 2002, 2015; Dell'Acqua et al., 2012; D'Intino et al., 2011; Fernández et al., 2004a,b). TH supplementation also restores oligodendroglial lineage and OL maturation from neural stem/progenitor cells (NSCs) derived from inflamed animal brains (Fernández et al., 2009). These results have been confirmed by other labs in the cuprizone demyelination model in mouse (Harsan et al., 2008) and rat (Castelo-Branco et al., 2014; Franco et al., 2008; Silvestroff et al., 2012). Contrasting results have been obtained by TH treatment in perinatal inflammation-induced white

matter injury, either positive (perinatal hypoxa-ischemia, Hung et al., 2013; intraventricular hemorrhage, Vose et al., 2013), or no effects (white matter injury induced by interleukin-1β, Schang et al., 2014). The substantial differences in adult vs. neonatal models, make quite difficult to compare these data sets, also considering the delicate balance between maternal-derived TH and the perinatal development of fetal thyroid function (Moog et al., 2015).

To establish whether a dysregulation of TH cellular signaling induced by inflammation is causally linked to differentiation failure of OPCs, two sets of experiments were performed. It was first investigated whether the increase in inflammatory cytokines that occurs in the CNS of the animal model of MS is linked to a dysregulation of the molecular mediators of TH action. Then, the hypothesis that intracellular hypothyroidism induced by inflammatory cytokines is responsible for OPCs differentiation failure was tested *in vitro* in OPCs derived from adult NSCs, by using the deiodinase inhibitor iopanoic acid (IOP) as pharmacological tool.

Materials and Methods
Animals, EAE Induction, and Disease follow-up
Dark-Agouti (DA, Harlan, Italy) female rats, 150–175 g body weight, were used. For EAE induction rats were immunized using 0.15 g/mL guinea pig spinal cord in complete Freund's adjuvant (CFA, Sigma, St. Louis, MO), 50% v/v, to which 5 mg/mL of heat-inactivated Mycobacterium (Difco H37Ra) was added. Two control groups were included: intact, un-injected animals, and adjuvant-injected animals (complete Freund's adjuvant + heat-inactivated Mycobacterium). Rats were regularly weighed and examined for clinical signs of EAE by two independent observers and scored as follows: 1 = loss of tail tone, 2 = mono or bilateral weakness of hind legs or middle ataxia, 3 = ataxia or paralysis, 4 = severe hind leg paralysis, 5 = severe hind leg paralysis and urinary incontinence. During the acute phase, animals were fed with humid pellets on the cage floor. Experimental groups intended for molecular biology and proteomic studies were the followings: control $n = 10$; EAE-acute [11 days post immunization (DPI)] $n = 9$; Adjuvant-acute (11 DPI) $n = 8$; EAE-relapsing-remitting (RR, 18 DPI) $n = 7$; Adjuvant-RR (18 DPI) $n = 8$. Additional control ($n = 5$) and EAE-acute animals ($n = 5$) were used for immunohistochemistry (IHC) experiments.

At the time of sacrifice, CSF and blood were collected. Then thoracic and lumbar tracts of the spinal cord (TSC, LSC) were dissected, immediately snap frozen and stored at −80°C till used. TSC was used for microdissection, LSC was used for molecular biology studies. Plasma samples and CSF were stored at −80°C till used.

All animal protocols described herein were carried out according to the European Community Council Directives (86/609/EEC), approved by the intramural ethical committee for animal experimentation of Bologna University and Ministry of Health (no. 158/2013-B), and comply with the guidelines published in the NIH Guide for the Care and Use of Laboratory Animals.

Inmunohistochemistry

Lumbar spinal cord tissues were frozen after fixation in 4% paraformaldehyde and picric acid saturated aqueous solution in 0.1 M Sörensen buffer pH 7, and 14 μm thick coronal sections (Microm HN550, Bio-Optica, Milan, Italy) were processed for inmunohistochemistry and myelin staining. Sections were incubated with the primary antibodies diluted in PBS-0.3% Triton X-100 overnight at 4°C. Primary antibodies and dilutions used were: mouse anti OX42 (AbD Serotec, Raleigh, NC), 1:250; mouse anti NG2 (membrane-spanning chondroitin sulphate proteoglycan, Millipore, Merck S.p.a., Milan, Italy), 1:100; mouse anti CNPase (2′,3′-cyclic nucleotide 3′-phosphodiesterase, Millipore) 1:250; rabbit anti MBP (Myelin Basic Protein, Dako) 1:100; rabbit anti GFAP (Glial Fibrillary Acidic Protein, Dako) 1:500; mouse anti NeuN (Neuron-Specific Nuclear Protein, Millipore) 1:250; goat anti D3 (Deiodinase type 3, Santa Cruz Biotechnology), 1:50. After rinsing in PBS, the sections were incubated at 37°C for 30 min with the secondary antisera: DyLight488-conjugated affinity-pure goat anti-mouse IgG (ThermoScientific), DyLight488-conjugated affinity-pure donkey anti-goat IgG (Jackson Immunoresearch), Rhodamine Red^{TM}-X-conjugated affinity-pure donkey anti-mouse IgG (Jackson Immunoresearch) and Rhodamine Red^{TM}-X-conjugated affinity-pure donkey anti-rabbit IgG (Jackson Immunoresearch) diluted in PBS-0.3% Triton X-100. For nuclear staining, sections were incubated for 20 min in PBS-0.2% Triton X-100 containing 1 μg/mL Hoechst 33258 (Invitrogen^{TM}). Sections were then rinsed in PBS and mounted in phenylenediamine solution (0.1% 1,4-phenylenediamine, 50% glycerine, carbonate/bicarbonate buffer pH 8.6, Sigma). Control slices incubated with only secondary antibodies were processed in parallel. FluoroMyelin^{TM} Fluorescence Myelin staining (Molecular Probes, Eugene, OR) was also performed, following manufacturer's specifications. Images were captured using a Nikon Eclipse E600 microscope equipped with digital CCD camera Q Imaging Retiga-2000RV (Q Imaging, Surrey, BC, Canada). Measurements were performed using Nis-Elements AR 3.2 software. The NG2 immunoreactive area was calculated as area fraction (percentage of NG2 immunoreactive area). The mean intensity of D3 in NeuN positive neurons was calculated in a region of interest (ROI). Confocal microscopy was used to study the co-presence of neuronal marker (NeuN), astrocytic marker (GFAP) microglial marker (OX42) and oligodendrocytic markers (NG2 and CNPase) with D3. Sections were scanned with a Nikon Ti-E fluorescence microscope coupled to an A1R confocal system (Nikon). A diode laser system with 405 wavelength output, air-cooled Argon-Ion laser system with 488 wavelength output and Yellow diode-pumped solid state laser system with 561 wavelength output were used. Images were acquired with 20× and oil immersion 60× with an optical resolution of 0.18 micron, using Nis-Elements AR 3.2 software. All the z-stacks were collected in compliance with optical section separation (z-interval) values suggested by Nis-Elements AR 3.2 software. Then, the 60× z-stacks were elaborated by using IMARIS software 8.0.1 (Bitplane, Zurich, Switzerland) (Fig. 6E). An isosurface of the cell body of a single cell was created using the cell marker fluorescence channel (NG2, CNPase or GFAP) of the raw image (cell identification and surface extraction, Fig. 6). The voxels corresponding to the D3- (red) and cell markers (green) immunostaining inside the object delimitated by the surface was then isolated (masked channels), and the voxels in both green and red channels were visualized in 3D projection.

RNA Isolation and Retrotranscription

Half of the lumbar spinal cord was used for the isolation of RNA by RNeasy Mini kit (Qiagen, Milan, Italy). Total RNA was eluted in RNase free water. The RNA obtained was subjected to DNase treatment (1 U/μL) in 1× DNase buffer in the presence of RNase (4 U/μL, Fermentas, Life Sciences, Italy), incubating at 37°C for 30 min. First strand cDNAs were obtained using the enzyme M-Moloney murine leukemia virus (M-MuLV) reverse transcriptase (20 U/μL) (Fermentas) in the presence of 1× first strand buffer, 2 mM of each d(NTP) (Fermentas), 5 μM p(dN)6 random primers (Roche, Molecular Biochemicals) and 25 ng/μL oligo(dT)18 (Fermentas), incubating at 42°C for 60 min. An RNA sample with no reverse transcriptase enzyme in the RT reaction mix was processed as a no RT control sample. The cDNA obtained was stored at −20°C till used for PCR.

Semiquantitative Real-Time PCR

Semiquantitative real-time PCR was performed using the Mx3005PTM real-time PCR system (Stratagene, CA). The reactions were performed in a final volume of 25 μL consisting of 1× SYBR Green qPCR master mix (Fermentas) and 0.4 μM forward and reverse primers. In order to avoid possible contamination of genomic DNA in isolated RNA, the sample with no reverse transcriptase enzyme (no RT sample) was processed in parallel with the others and tested by real-time PCR for every pair of primers used. All primers used were designed using Beacon Designer software (BD 5.1, Premier Biosoft International, Palo Alto, CA) or Primer BLAST and synthesized by IDT (Coralville, IA). The primer sequences, National Center for Biotechnology Information (NCBI) genbank reference sequence accession number and size of amplified products are set out included in Table 1. GAPDH was used as housekeeping gene to normalize the amount of retrotranscribed RNA used for PCR. Thermal profile of PCR reactions consisted first of an activation step of master mix Taq polymerase (95°C, 10 min), then two steps of: (1) denaturation (95°C, 10 min); (2) annealing/extension (40 cycles of: 95°C for 15 s, 60°C for 30–60 s); at the end of amplification cycles the melting curve of amplified products was performed according to the following temperature/time scheme: heating from 55°C to 95°C with a temperature increase of 0.5°C/s.

The efficiency of the primers used for real-time PCR reactions was calculated by amplifying control cDNA serial dilution in the presence of each pair of primers, under the conditions described above. Standard curve slope and primer efficiency were calculated with the MxPro QPCR software 3.1 (Stratagene, CA), obtaining efficiency values for all primers used in the range of 95–102%; the $2^{(-\Delta\Delta CT)}$ method for the calculation of gene expression relative to a given group was taken as "reference" having a value of 1 (User Bulletin #5, Guide to Performing Relative Quantitation of Gene Expression Using Real-Time Quantitative PCR Applied Biosystems).

The specificity of real-time PCR reactions was evidenced by both melting curves which yielded a single peak at the corresponding

TABLE 1: Primer Sequences Description

Gene	NCBI ACC. N.	Primer sequences	Size (bp)
TRα1	NM_001017960	F: 5′-gcaaacacaacattccgc-3′ R: 5′-tcctgatcctcaaagacctc-3′	108
TRα2	NM_031134	F: 5′-gcaaacacaacattccgc-3′ R: 5′-caccaaactgctgctcaa-3′	160
TRβ	NM_012672	F: 5′-gcaaacacaacattccgc-3′ R: 5′-caccaaactgctgctcaa-3′	198
MTC8	NM_147216	F: 5′-caatggtgtggtgtctgc-3′ R: 5′-cggtaggtgagtgagagc-3	150
D-2	U53505	F: 5′-ctcctcacggtagacttg-3′ R: 5′-gttccagacacagcgtag-3′	189
D-3	NM_017210	F: 5′-gcatccgcaagcatttcc-3′ R: 5′-ggcatctcctccaccttcac-3′	85
GAPDH	NM_17701	F: 5′-ggcaagttcaatggcacagtcaag-3′ R: 5′-acatactcagcaccagcatcacc-3′	125
Klf9	NM_057211.1	F: 5′-agtggcttcgaaggggaaac-3′ R: 5′-tccgagcgcgagaacttttt-3′	174
INF-γ	NM_138880.02	F: 5′-agcatcgccaagttcgaggtga-3′ R: 3′-agcaccgactcctttttccgct-5′	124
IL-1β	NM_031512	F: 5′-tcgttgcttgtctctccttg-3′ R: 3′-tcgttgcttgtctctccttg-5′	118
TNF-α	NM_012675.3	F: 5′-tcgtgcctcagcctcttctcatt-3′ R: 3′-ggctacgggcttgtcactc-5′	186
TGF-β	NM_021578	F: 5′-caattcctggcgttaccttg-3′ R: 3′-agccctgtattccgtctcct-5′	122
TREM-2	NM_001106884	F: 5′-acacccttgctggaactgtc-3′ R: 3′-gaaacctgactggaggtgct-5′	233
CD40	NM_134360	F: 5′-atgccaaccgtgcgactc-3′ R: 3′-taacctgaagcccttgattgag-5′	101

Detailed information about gene, NCBI (National Center for Biotechnology Information) genbank accession number, forward (F) and reverse (R) sequences and size of PCR product (base pair, bp) has been included.
Abbreviations: TR, thyroid receptor; MCT8, monocarboxylate transporter 8; D2, deiodinase type 2; D3, deiodinase type 3; GAPDH, glyceraldehyde-3-phosphate dehydrogenase, KLF9, kruppel-like factor 9; IL-1β, interleikin 1 beta; TNF-α, tumor necrosis factor alpha; TGF-β, trasforming growth factor beta; TREM2, triggering receptor expressed on myeloid cells 2; CD40, TNF receptor superfamily member 5.

melting temperature (Tm) and electrophoresis in agarose gel (2,5%) of random amplified products which showed a single band of the expected size for each pair of primers used (results not shown).

Cytokines and TH Assay in CSF and Plasma

xMAP technology and Luminex platform (Luminex 200™ Luminex Corporation, Austin, TX) provided with Luminex xPONENT 3.1 (Luminex) and Milliplex Analyst 3.5.5 softwares (Millipore Corporation, Billerica, MA) were used to quantify cytokines/chemokines (TGFβ1, IL-1β, MCP-1, TNF-α and RANTES) in the CSF and T3, T4, and TSH in plasma. The Milliplex MAP kit (Millipore) for TGFβ1; the rat cytokine/chemokine magnetic bead panel kit

(RECYTMAG-65K, Millipore) for IL-1β, MCP-1, TNF-α, and RANTES; the Milliplex MAP kit Rat-THY-30K (Millipore Corporation) were used.

CSF samples were centrifuged at 4,000g for 10 min at 4°C before being processed. In brief, 25 μL CSF samples were incubated with specific monoclonal antibodies-conjugated bead population overnight at 4°C. Washed beads were then incubated with the detection antibody solution at RT for 30 min, then with the streptavidin–phycoerythrin conjugated solution. After washing, beads were resuspended in the sheath fluid, shacked for 10 min and then read.

For TH assays, plasma samples were centrifuged at 4,000g for 10 min at 4°C. In brief, plasma samples were incubated with specific

monoclonal antibodies-conjugated beads (anti-T3/anti-T4/anti-TSH) and HRP-conjugated solution overnight at 4°C. Washed beads were incubated with the detection antibody solution (20–25°C, 30 min) and then with the streptavidin–phycoerythrin conjugated solution (20–25°C, 30 min). The samples MFI (mean fluorescence intensity) for each analyte was interpolated in the corresponding standard curve to obtain the pg/mL values (Milliplex Analyst 3.5.5 software). Reverse T3 ELISA kit was used for quantification of plasma levels of rT3 (Uscn, Life Science), following the manufacturer's instructions.

Laser Capture Microdissection and Gene Expression Analysis

Laser capture microdissection (LCM) was performed in TSC using a NIKON Eclipse TE 2000-S and SLμCUT laser microdissection system (MMI Molecular Machines & Industries AG, Glattbrugg, Switzerland). The whole procedure was carried out in an RNase-free environment. Solutions were prepared in diethyl pyrocarbonate (DEPC, Sigma)-treated water and working surfaces were decontaminated with RNase decontamination solution (RNaseZap, Sigma). The laser microdissection-isolation caps and membrane slides (metal frame coated with 1.5 μm thick PEN membrane) used were nuclease and nucleic acid free (MMI). Stored tissue at −80°C was equilibrated to −20°C for at least 5 h, then embedded in optimum cutting temperature (OCT) compound and sectioned (20 μm thickness) on a cryostat (Microm). Sections were fixed in EtOH decreasing concentration scale, then stained in toluidine RNase-treated, dehydrated in EtOH increasing concentration scale, air-dried and immediately processed for LCM. Inflammatory infiltrates from each EAE-RR animal, corresponding to a total area of 2×10^6 μm^2, were cut and captured in a separate cap. In the case of control animals, a similar area was captured.

RNA isolation was performed with the RNeasy Micro kit (Qiagen), following the manufacturer's instructions. The RNA obtained, quantified with the Nanodrop 2000 spectrophotometer, was around 800 ng from each captured animal area. Retrotranscription was performed with the Maxima Reverse Transcriptase enzyme (Thermo Scientific) following the manufacturer's instructions. Semiquantitative real-time PCR of cDNA obtained from laser capture microdissected RNA was performed as described above. D3 gene expression was studied; GAPDH was used as housekeeping gene. Thermal profile of PCR reactions consisted of two first steps of: (1) denaturation (95°C, 10 min); (2) annealing/extension, 40 cycles of: 95°C for 15 s, 57°C for 30 s. The amount of cDNA used for D3 and GAPDH PCR reactions was 10 ng.

Cell Culture and Treatment

Adult NSCs were isolated following the Ahlenius and Kokaia protocol (Ahlenius and Kokaia, 2010) and oligodendrocyte differentiation was performed following the Chen protocol (Chen et al., 2007) with some modifications, as described in Fig. 3A. Brains from five month old rats were collected in a 50 mL tube containing ice-cold HBSS (Life Technologies, Milan, Italy).

The subventricular zone (SVZ) was isolated from 1 mm thick coronal slices and triturated in cold HBSS. The HBSS was then removed and the tissues enzymatically dissociated (1× HBSS; 5.4 mg/mL D-glucose (Sigma); 15 mmol/L HEPES (Life Technologies); 1.33 mg/mL Trypsin (Sigma); 0.7 mg/mL hyaluronidase (Sigma); 80 U/mL DNase (Sigma). After 15 min incubation at 37°C tissues were pipetted several times to favor dissociation and incubated again at 37°C for 10 min. The solution was filtered through a 70 μm filter and then centrifuged at 400g for 5 min. The resulting pellet was washed twice, first with a sucrose-HBSS solution (0.3 g/mL sucrose in 0.5× HBSS), 500 × g 10 min), then with a solution consisting of BSA (40 mg/mL) and HEPES (0.02 mol/L) in EBSS. After 7 min centrifugation at 400g, the cellular pellet was resuspended in serum-free medium (DMEM/F12 GlutaMAX 1×; 8 mmol/L HEPES; 100 U/100 μg penicillin/streptomycin; 0.1× B27; 1× N-2; 20 ng/mL bFGF; 20 ng/mL EGF) and, after cell count, cells were plated at a density of 10 cells/μL in a final volume of 3 mL in low-attachment 6-well plates (NUNC). Medium was changed every three days, centrifuging the cell suspension at 300g for 5 min and gently resuspending the cellular pellet in fresh medium. Neurospheres were allowed to proliferate until they attained a diameter of about 100 μm.

To obtain oligospheres, primary neurospheres were centrifuged at 300g for 5 min. The pellet was mechanically dissociated by pipetting and cells were counted and plated again at a density of 10 cells/μL in a final volume of 3 mL of OPCs medium (DMEM/F12 GlutaMAX 1×; 8 mmol/L HEPES; 100 U/100 μg Penicillin/Streptomycin; 0.1× B27; 1× N-2; 20 ng/mL bFGF; 20 ng/mL PDGF) in low-attachment 6-well plates (NUNC).

At this step, cells were divided into two groups: one treated with a mix of six different cytokines (TGF-β1, TNF-α, IL-1β, IL-6, IL-17 and IFN-γ; 20 ng/mL each) and the other treated with vehicle (0.04% of the cytokines solvent: 10% glycerol/100 nM glycine/25 nM Tris, pH 7.3). Images of oligospheres were taken at 3, 5 and 7 DIV.

Oligospheres were centrifuged at 300g for 5 min and the pellet was mechanically dissociated to obtain a single cell suspension. After cell count, cells were plated at a density of 3,000 cells/cm^2 on poly-D,L-ornithine (50 μg/mL)/laminin (5 μg/mL) coating, in OPCs medium, containing 20 ng/mL bFGF and 20 ng/mL PDGF.

After 3 DIV, OPCs medium was replaced with the oligodendrocyte differentiation medium [DMEM/F12 GlutaMAX 1×; 8 mmol/L HEPES; 100 U/100 μg penicillin/streptomycin; 0.1× B27; 1× N-2; 50 nM T3; 10 ng/mL CNTF; 1× N-acetyl-L-cysteine (NAC)].

The cytokine treated group was then divided into two subgroups: one treated with vehicle and the other treated with IOP (10 μM). Another vehicle-exposed experimental group was treated with the cytokine mix during the differentiation phase, while the control group was treated with vehicle. Oligodendrocyte differentiating factors (T3, CNTF and NAC) were refreshed every two days.

Population Doubling

Oligosphere images were analyzed using Image Proplus software (Media Cybernetics, Bethesda, MD). Counting procedure was performed as already described (Baldassarro et al., 2013) calculating the cell number based on spheres and single cell area. Population doubling was calculated using the following formula: PD = log10(N/N0) × 3.33, where PD is the Population Doubling, N and N0 are the final and initial number of cells, respectively.

Immunocytochemistry

At 12 DIV after the differentiation induction, cells were fixed (cold 4% paraformaldehyde, 20 min), washed (two PBS washes, 10 min each) and incubated overnight at 4°C with primary antibodies diluted in PBS/0,3% Triton X-100. Primary antibodies and dilutions used were: mouse anti beta-III-tubulin (R&D system, Trento, Italy) 1:3000; rabbit anti PDGFαR (platelet derived growth factor alpha receptor, Santa Cruz Biotechnology) 1:300; mouse anti NG2 (membrane-spanning chondroitin sulphate proteoglycan, Millipore), 1:300; mouse anti CNPase (2′,3′-cyclic nucleotide 3′-phosphodiesterase, Millipore) 1:500; rabbit anti MBP (Myelin Basic Protein, Dako) 1:500; rabbit anti GFAP (Glial Fibrillary Acidic Protein, Dako) 1:1,000; goat anti D3 (Deiodinase type 3, Santa Cruz Biotechnology), 1:100.

Cells were washed twice using PBS and incubation of secondary antibodies was performed at 37°C for 30 minutes. Secondary antisera and dilutions used were: Alexa488-coniugated affinity-pure Donkey anti-Mouse IgG (Life Technologies, Eugene, OR) 1:500, Alexa568-conjugated affinity-pure Donkey anti-Mouse IgG (Molecular Probe, Eugene, OR) 1:500, DyLight488-conjugated affinity-pure Donkey anti-Goat IgG (Jackson Immunoresearch) 1:100, Alexa568-conjugated affinity-pure Donkey anti-Rabbit IgG (Life Technologies) 1: 500, and RRX-conjugated Donkey anti-rabbit IgG (Jackson Immunoresearch) 1:500, all diluted in PBS/0.3% Triton X-100. After two washes with PBS, cells were incubated with Hoechst 33258 (1 μg/mL in PBS/0.2% Triton X-100) for 30 min at RT. After the last two washes in PBS, cells were mounted with phenylenediamine solution (0.1% 1,4-phenylenediamine; Sigma, 50% glycerine; Sigma, carbonate/bicarbonate buffer pH 8.6). Controls were always performed on secondary antibodies.

Each antibody staining was performed in duplicate and at least five random fields per glass were analyzed using NIS-Elements Microscope Imaging Software (Nikon, Shinjuku, Tokyo, Japan).

Hoechst staining was used to identify the total cell number and condensed nuclei, while the different markers were used to identify specific lineage (beta-III-tubulin for neurons, GFAP for astrocytes, NG2 for OPCs, CNPase for mature oligodendrocytes and MBP for myelinating oligodendrocytes). The lineage analysis was performed on cells presenting intact, non-condensed nucleus.

Statistical Analysis

GraphPad Software (San Diego, CA) was used for statistics and graph preparation. Data are expressed as mean + SEM. Student's t test and one-way analysis of variance (ANOVA) followed by *post hoc* tests were used for statistical analyses. Results were considered significant when the probability of their occurrence by chance alone was less than 5%. Details on the tests are reported in results and figure captions.

Results

Inflammatory Cytokines Expression Level During EAE

In the first set of experiments, the expression profile and content of inflammatory cytokines and tissue expression of TH molecular mediators in the acute and RR phase of EAE were investigated. EAE clinical progression was monitored by the neurological disability score and body weight (Fig. 1A,B). Neurological deficit appeared on 9–10 DPI, with a rapid increase in disability which in most rats reached the highest clinical score on 11–13 DPI (acute phase), followed by a short remission and a second relapse phase (RR) with a similar disability score observed in the acute phase. Body weight dropped drastically in the acute phase without recovery during RR (Fig. 1B, group effect $P < 0.0001$). Adjuvant injected animals, developed arthritis and also ceased body weight increase (group effect $P < 0.0001$).

Histopathology (inflammation and demyelination) was evaluated at the two investigated times (acute: 11DPI; RR: 18DPI) in the fasciculus gracilis, in the dorsal horn of the spinal cord (Fig. 1C), as this is the most affected CNS structure in rodent models of EAE (Robinson et al., 2014). As expected, microglial reaction starts in the acute phase, when OX42-IR cells retract elongation, taking on a rounder morphology (see Fig. 1C, control compared with EAE 11DPI) and converge around blood vessels (see arrows around the sulcal branches of the posterior spinal artery). Demyelination signs appear in the acute phase, as revealed by the slight decrease in fluoromyelin staining intensity in the peripheral, submeningeal part of the dorsal funiculus (Fig. 1C, EAE11DPI, see stars), appearing very extensive at 18DPI, in the areas characterized by microglia concentration (asterisks).

The expression of genes that encode for cytokines/chemokines involved in neuroinflammation processes was studied in the LSC by real-time PCR (Fig. 1D). The pattern of mRNA expression was similar for all investigated genes. The cytokine IL-1β mRNA was strongly upregulated in EAE-acute animals (around 150-fold vs the control group) and in EAE-RR animals (around 30-fold vs the control group; CNT vs EAE-acute, $P < 0.0001$; CNT vs EAE-RR, $P < 0.0001$). The expression of TNF-α mRNA increased significantly in the EAE group of animals in the two investigated phases of the disease, around eightfold versus the control group (CNT vs EAE-acute, $P < 0.0001$; CNT vs EAE-RR, $P < 0.0001$). The INF-γ mRNA was also strongly upregulated in EAE-acute (around 500-fold vs control), and in EAE-RR animals (around 200-fold vs control; CNT vs EAE-acute, $P = 0.0001$; CNT vs EAE-RR, $P = 0.0006$). CD40 mRNA increased around 20-fold versus the control group in EAE acute and RR (CNT vs EAE-acute, $P < 0.0001$; CNT vs EAE-RR, $P < 0.0001$). TGF-β mRNA expression was upregulated in EAE-acute and EAE-RR (around eightfold vs the control group; CNT vs EAE-acute, $P < 0.0001$; CNT vs EAE-RR, $P < 0.0001$). Finally, TREM2 mRNA was significantly increased in EAE-RR group of animals, (around 4.5-fold vs controls; CNT vs EAE-RR, $P = 0.0025$). It should be noted that the overexpression of INF-γ mRNA in EAE-acute
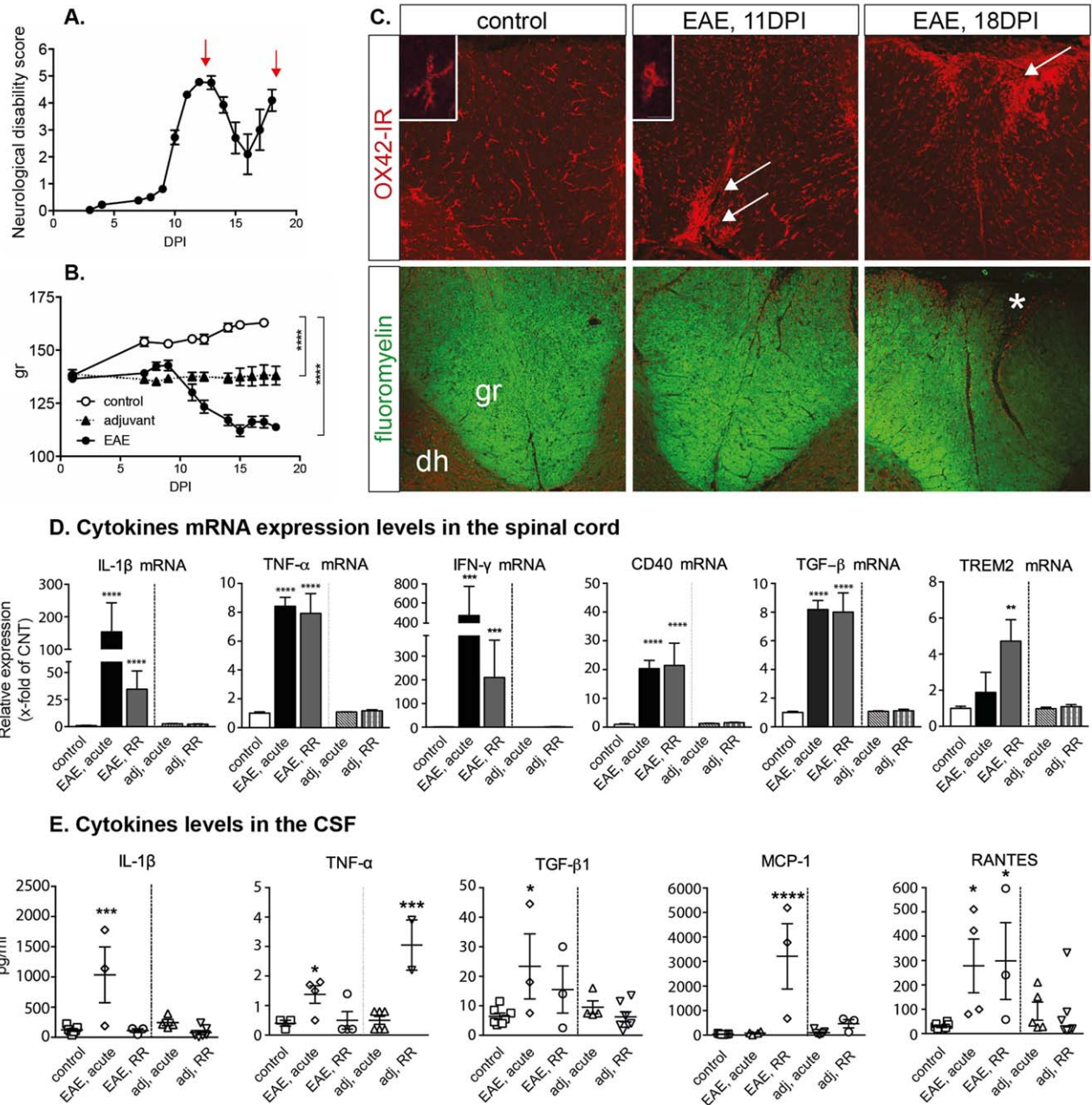
Clinical course and spinal cord pathology

FIGURE 1: EAE clinical course, histopathology and cytokine expression. Neurological disability score (**A**) and animals' body weight (**B**). The red arrows indicate the days of sacrifice at 11 and 18 DPI. Statistical analysis: two-way ANOVA, ****$P < 0.0001$. (**C**) Spinal cord histopathology. Micrographs illustrate OX42-IR microglia and fluoromyelin staining in control, EAE acute phase (11DPI) and remission-relapsing phase (18 DPI). Arrows indicate microglia accumulation around vessels; asterisks indicate microglial reaction and associated demyelination. Scale bar 50 μm. (**D**) Cytokine mRNA expression level in the LSC (control: $N = 10$; EAE-acute: $n = 9$; Adjuvant-acute: $n = 8$; EAE-relapsing-remitting: $n = 7$; adjuvant-RR: $n = 8$). Results obtained after analysis through the $2^{(-\Delta\Delta CT)}$ method. Statistical analysis: one-way ANOVA and Dunnett's *post hoc* test, **$P < 0.01$; ***$P < 0.001$. E: Cytokine/Chemokine levels in the CSF. Results are presented as individual values (pg/mL) and the mean $\pm$ SEM is also shown. Statistical analysis: one-way ANOVA and Dunnett's *post hoc* test, *$P < 0.05$; **$P < 0.01$; ***$P < 0.001$; ****$P < 0.0001$. Abbreviations: ADJ, adjuvant; DPI, days post immunization; dh, dorsal horn; EAE, experimental allergic encephalomyelitis; CD40, cluster of differentiation 40; gr, fasciculus gracilis; INF-γ, interferon γ; IL-1β, interleukin 1β; MCP-1, monocyte chemotactic protein-1; TGF-β, transforming growth factor β; TNF-α, tumor necrosis factor-α; TREM2, triggering receptor expressed on myeloid cells 2; RANTES, regulated on activation, normal T cell expressed and secreted; RR, relapsing-remitting.

animals is the highest EAE-induced upregulation observed compared with the other cytokines/chemokines investigated.

IL-1β, TNF-α, TGF-β, MCP-1, and RANTES in CSF samples (Fig. 1E) was then simultaneously quantified. IL-1β protein was significantly increased in EAE-acute group compared with control animals ($P = 0.0004$). This increase was not observed in the EAE-RR experimental group. TNF-α was also increased in EAE-acute animals compared with controls ($P = 0.0256$). Moreover, the level of this cytokine was significantly higher in ADJ-RR compared with the control group of animals ($P = 0.0002$). MCP-1 chemokine also increased in EAE animals and this difference was significant in the group of EAE-acute animals (CNT vs EAE-acute, $P < 0.0001$), whereas RANTES chemokine was increased in the EAE-RR group of animals (CNT vs EAE-acute, $P = 0.0265$ CNT vs EAE-RR, $P = 0.0310$). The level of TGF-β was increased in EAE animals, as it was significantly higher in the acute phase of the disease (CNT vs EAE-acute, $P = 0.0294$).

The Expression of TH-Signaling Genes Is Altered in the Nervous Tissue During EAE

We first investigated the impact of the extensive inflammation described above on the expression of genes encoding for the TH transporter MCT8, the different genes encoding for the nuclear receptors (TRα1, TRα2, TRβ) and the activating (D2) and inactivating (D3) enzymes by real-time PCR (Fig. 2A). There is a significant decrease in the expression of MTC8 in the EAE-RR group (CNT vs EAE-RR, one-way ANOVA $P = 0.0265$). The MTC8 mRNA level is also lower in adjuvant-RR animals ($P < 0.0001$). The expression level of mRNA encoding for TR subtypes α1, α2 and β is decreased in EAE animals compared with the control group in both investigated phases of the disease. Statistical analysis performed through one-way ANOVA and Dunnett's multiple comparisons test gave the following P values: TRα1, CNT vs EAE-acute, $P = 0.0022$; CNT vs EAE-RR, $P = 0.0067$; TRα2, CNT vs EAE-acute, $P = 0.0253$; CNT vs EAE-RR, $P = 0.0161$; TRβ, CNT vs EAE-acute, $P = 0.0164$; CNT vs EAE-RR, $P = 0.0008$. The mRNA of TRβ was also downregulated in the adjuvant-RR group ($P = 0.0207$). D2 mRNA did not show any significant difference in EAE animals compared with controls. In contrast, D2 mRNA level in adjuvant-RR group was lower than in control animals ($P = 0.0037$). The expression of D3 was instead subjected to a strong upregulation in EAE animals in the acute phase (around 30 times) and to a more moderate upregulation in the EAE-RR group (around 10 times) compared with controls ($P < 0.0001$).

In an attempt to correlate the observed changes in TH signaling with EAE histopathology (inflammation and demyelination), the mRNA expression in microdissected samples of the spinal cord was analyzed. The focus was laid on the gene and the time showing the most extensive regulation, i.e., D3 in the acute phase, and an SC area with extensive inflammation and cellular infiltrates. Micrographs in Fig. 2B show representative images of toluidine stained sections of the spinal cord in control and acute-EAE animals. Extensive cellular infiltrates enriched by peripheral cells were observed in the white matter and around vessels penetrating the grey matter (arrows). As in the whole LSC tissue, an upregulation of D3 mRNA (Student's t test, $P = 0.0003$) was found in TSC microdissected areas of acute-EAE compared with control animals.

Finally, TH levels were quantified in plasma (Fig. 2C). The working dynamic ranges of the standard curves were: 10,000–13.77 pg/mL for T3 and TSH; 200,000–274.33 pg/mL for T4. T3 plasmatic levels do not differ significantly across the experimental groups studied. T4 and TSH are significantly decreased in acute-EAE compared with control animals (Student's t test, $P = 0.0332$ and $P = 0.0004$, respectively). No changes in rT3 plasma levels were observed (results not shown).

In Vitro *Exposure to Inflammatory Cytokines Impairs OPCs Differentiation*

In order to answer the question of whether the inflammatory cytokines upregulated during EAE impair OPCs differentiation, *in vitro* studies deriving OPCs from oligospheres under T3 exposure were performed (Chen et al., 2007). This cell system (OPCs-enriched) was preferred to primary OPCs isolation, because T3 stimulation is necessary for NSC specification in the oligodendrocyte lineage and for OL differentiation and maturation (Castelo-Branco et al., 2014). The schedule of the experiment is presented in Fig. 3A. After 12 days differentiation, $17.2 \pm 2.2\%$ OPCs (NG2-positive cells) were obtained, while mature OL ranged from $40.0 \pm 3.8\%$ (CNPase) to $22.3 \pm 1.9\%$ (MBP). The morphology of the cells was consistent with the respective differentiation phase (Fig. 3E,F, vehicle). In all groups, GFAP-positive astrocytes account for $29.9 \pm 3.7\%$ of the cell population, while $6.2 \pm 4.1\%$ of the cells are beta-III-tubulin positive (data not shown, average values $\pm$ standard deviation from three independent experiments).

Inflammatory cytokines have different roles on OPCs biology, on the proliferation and differentiation phases, respectively. We then used two exposure schemes to investigate the effect of cytokines on OPCs, i.e. (i) exposure during the proliferation phase of OPCs *in vitro* generation and (ii) exposure during OL *in vitro* differentiation (see Fig. 3A). The cytokines mix was composed of TGF-β1, TNF-α, IL1-β, IL-6, IL-17, and IFN-γ, as derived in Results section (Fig. 1D,E). The exposure to the cytokines mix during oligosphere
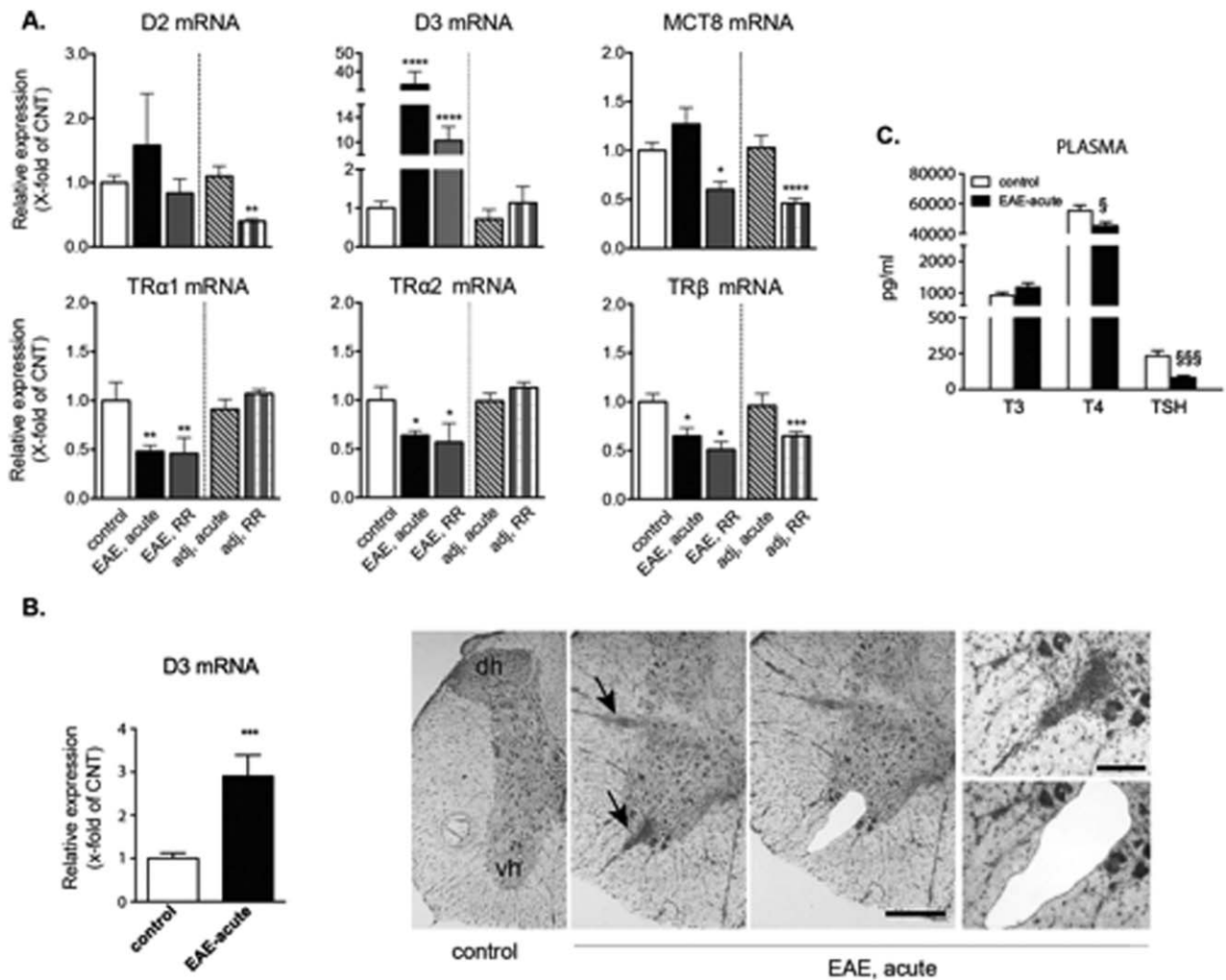
FIGURE 2: Thyroid hormone signaling related genes and proteins in EAE. (A) Thyroid hormone system molecules mRNA expression level in the LSC (control: $N = 10$; EAE-acute: $n = 9$; adjuvant-acute: $n = 8$; EAE-relapsing-remitting: $n = 7$; adjuvant-RR: $n = 8$). Results are obtained after analysis by the $2^{(-\Delta\Delta CT)}$ method. Statistical analysis: one-way ANOVA and Dunnett's *post hoc* test, *$P < 0.05$; ***$P < 0.01$; ***$P < 0.001$; ****$P < 0.0001$. B: Expression analysis of D3 mRNA in microdissected areas of the spinal cord in EAE vs control animals. Micrographs show the toluidine blue staining of a coronal section of thoracic spinal cord in control and EAE rats, where cellular infiltrates included in the microdissected areas are illustrated (arrows). Results are obtained after analysis by the $2^{(-\Delta\Delta CT)}$ method. Statistical analysis: Student's *t* test, ***$P < 0.001$. Bars: 250 μm; 100 μm. C: T3, T4 and TSH levels in plasma in control and acute EAE. Statistical analysis: Student's *t* test, §$P < 0.05$ and §§§$P < 0.001$. Abbreviations: D2, D3, deiodinase enzyme type 2, and 3; dh, dorsal horn; EAE, experimental allergic encephalomyelitis; MCT8, monocarboxylate transporter 8; TH, thyroid hormone; TR, thyroid hormone receptor; TSH, thyroid stimulating hormone; vh, ventral horn.

generation increased the proliferation index (Fig. 3B) after 5 ($P = 0.0176$) and 7 ($P = 0.0062$) DIVs compared with the vehicle group, resulting in a higher number of cells at 12 DIV after seeding (Fig. 3C, $P < 0.0001$). The percentage of condensed nuclei was not different in cytokines- and vehicle-exposed cells. Conversely, the exposure to cytokines during the differentiation phase provoked a decrease in the number of cells at 12DIV compared with vehicle cells ($P = 0.0111$; Fig. 3C), and an increase in the percentage of condensed nuclei ($P = 0.0002$) (Fig. 3D), thus indicating a toxic effect of cytokines in differentiating OPCs.

Next, the effect of cytokine exposure on OPCs differentiation and OL maturation was analyzed, labeling antigens expressed at different stages of OL maturation. Representative micrographs at 12DIV are shown in Fig. 3E and the quantification results in Fig. 3F. Cytokine exposure during proliferation or differentiation results in an increase of NG2-IR cells ($P = 0.0015$ and $P = 0.0022$, respectively). The percentage of mature, myelinating OL, as normalized according to the cell survival in the different conditions dramatically decreases when cytokines are present in the culture medium during proliferation (CNPase, $P = 0.0002$; MBP, $P = 0.0030$), while
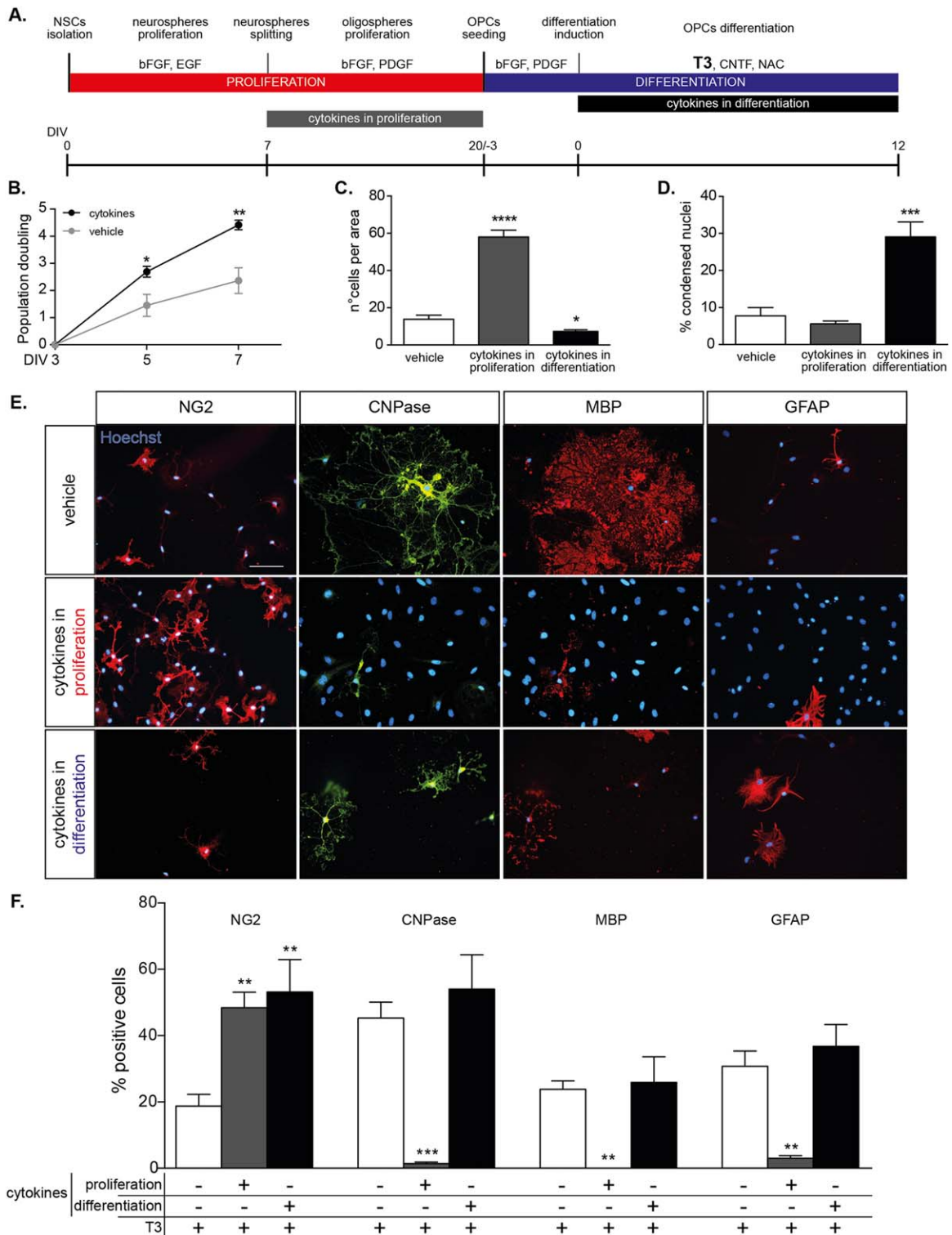
FIGURE 3: Effect of OPC-enriched cultures cytokine exposure on OPCs proliferation and differentiation. (**A**) Design of the *in vitro* experiments. (**B**) Proliferation index during oligosphere proliferation. Total number of cells (**C**) and percentage of condensed nuclei (**D**) after cell seeding at 12 DIVs of differentiation. (**E**) Representative images of NG2-, CNPase-, MBP- and GFAP-IR cells from the three experimental groups at 12 DIV. (**F**) lineage marker analysis of the different groups. Two biological replicates and at least 10 fields per group were analyzed. Statistical analysis: one-way ANOVA followed by Tukey posttest, *$P<0.05$; **$P<0.01$; ***$P<0.001$; ****$P<0.0001$. Abbreviations: bFGF, basic fibroblast growth factor; CNTF, ciliary neurotrophic factor; CNPase, 2′,3′-cyclic nucleotide 3′-phosphodiesterase.; EGF, epidermal growth factor; GFAP, glial fibrillary acid protein; NAC, *N*-acetyl-L-cysteine; NG2 chondroitin sulphate proteoglycan, neural/glial antigen 2; NSC, neural stem cells; MBP, myelin basic protein; OPCs, oligodendrocyte precursor cells; PDGF, platelet derived growth factor.
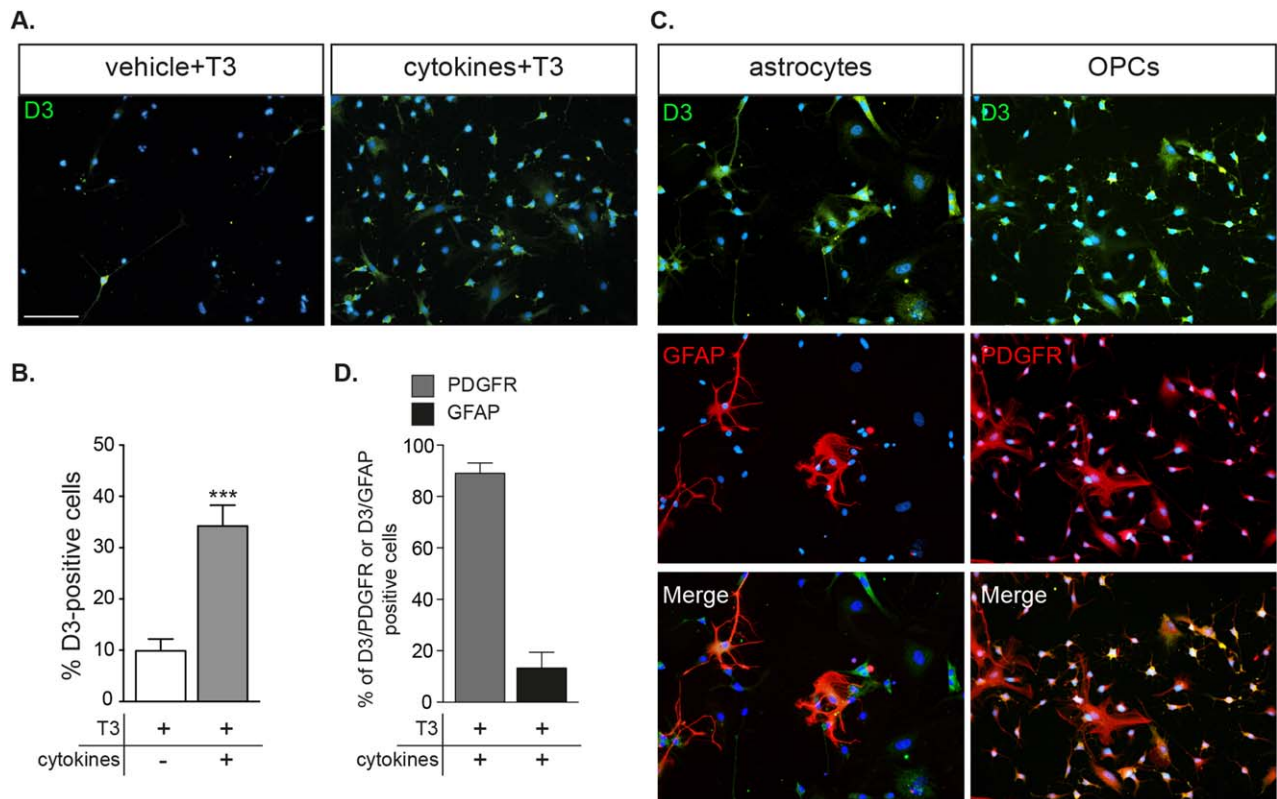
FIGURE 4: Effect of OPC-enriched cultures cytokine exposure on D3 expression and effect of deiodinase inhibition on OL differentiation. (A) Representative images of D3-positive cells in the vehicle- and cytokine-exposed groups. (B) Percentage of D3-positive cells in the vehicle- and cytokine-exposed groups. (C) Representative images of double staining GFAP/D3 and PDGFαR/D3. (D) Percentage of D3 positive cells that are also positive for PDGFαR or GFAP. Grey bar: PDGFαR/D3; black bar: NG2/D3. Statistical analysis: Student's t test, ***$P < 0.001$. Bar: 50 μm. Abbreviations: D3, deiodinase-3; GFAP, glial fibrillary acidic protein; NG2 chondroitin sulphate proteoglycan, neural/glial antigen 2; OPCs, oligodendrocyte precursor cells; PDGFαR, platelet derived growth factor α receptor; T3 thriiodothironin.

no changes are observed when cytokines are present in the differentiation phase only. Notably, GFAP-positive cells follow the same profile as mature OL, and are drastically decreased after cytokine exposure during proliferation ($P = 0.0013$).

An Appropriate Intracellular Content of TH Is Required to Overcome the Block of OPCs Differentiation Induced by Inflammation

In view of the results from *in vivo* experiments, which indicated that the T3 inactivating enzyme D3 is strongly upregulated in acute EAE, and in order to determinate whether cellular hypothyroidism due to inflammatory cytokines causes the OPCs differentiation block, we first focused in the study of D3 in the cell system exposed to the cytokines mix. After 12 DIVs of differentiation, less than 10% of cells express a detectable level of D3 in the control OPCs-enriched culture. The exposure to cytokines during the proliferation phase leads to an increase of over 35% in D3-IR cells ($P = 0.0001$) (Fig. 4A,B). Moreover, in order to identify the cell type expressing D3, cultures were double stained for D3 and cell markers for astrocytes (GFAP) or early OPCs (PDGFαR). As showed in

Fig. 4C,D, the majority of cells expressing D3 are PDGFαR-positive ($89.0 \pm 4.0\%$), while the remaining cells are astrocytes. Thus, it could be hypothesized that the increase in D3 protein in the cell system may lower T3 availability, leading to a cellular hypothyroidism in OPCs. This could determine the impairment of OPCs cell cycle exit, as is suggested by the high number of NG2-positive cells corresponding to proliferating OPCs, and the low number of CNPase- and MBP-positive cells corresponding to mature OL.

To test this hypothesis, the nonspecific deiodinase enzyme inhibitor IOP was introduced into the cell system. IOP has been used to study rodent and human deiodinase biochemical properties (St Germain et al., 2009). IOP was used with the intent to inhibit D3 and restore T3 intracellular content in an environment characterized by the presence of T3, inflammatory cytokines, OPCs and astrocytes (Fig. 5A). IOP was added to the culture in the differentiation phase, 24 h before adding T3 (Fig. 5B). IOP exposure partially restored the maturation of OL from OPCs (Fig. 5C). More specifically, the following percentages of cells along the maturation lineage of OPCs were obtained (Fig. 5D): (i) in the presence of T3, alone: NG2 17.1%, CNPase 40%, MBP 22.3%; (ii) in the presence of
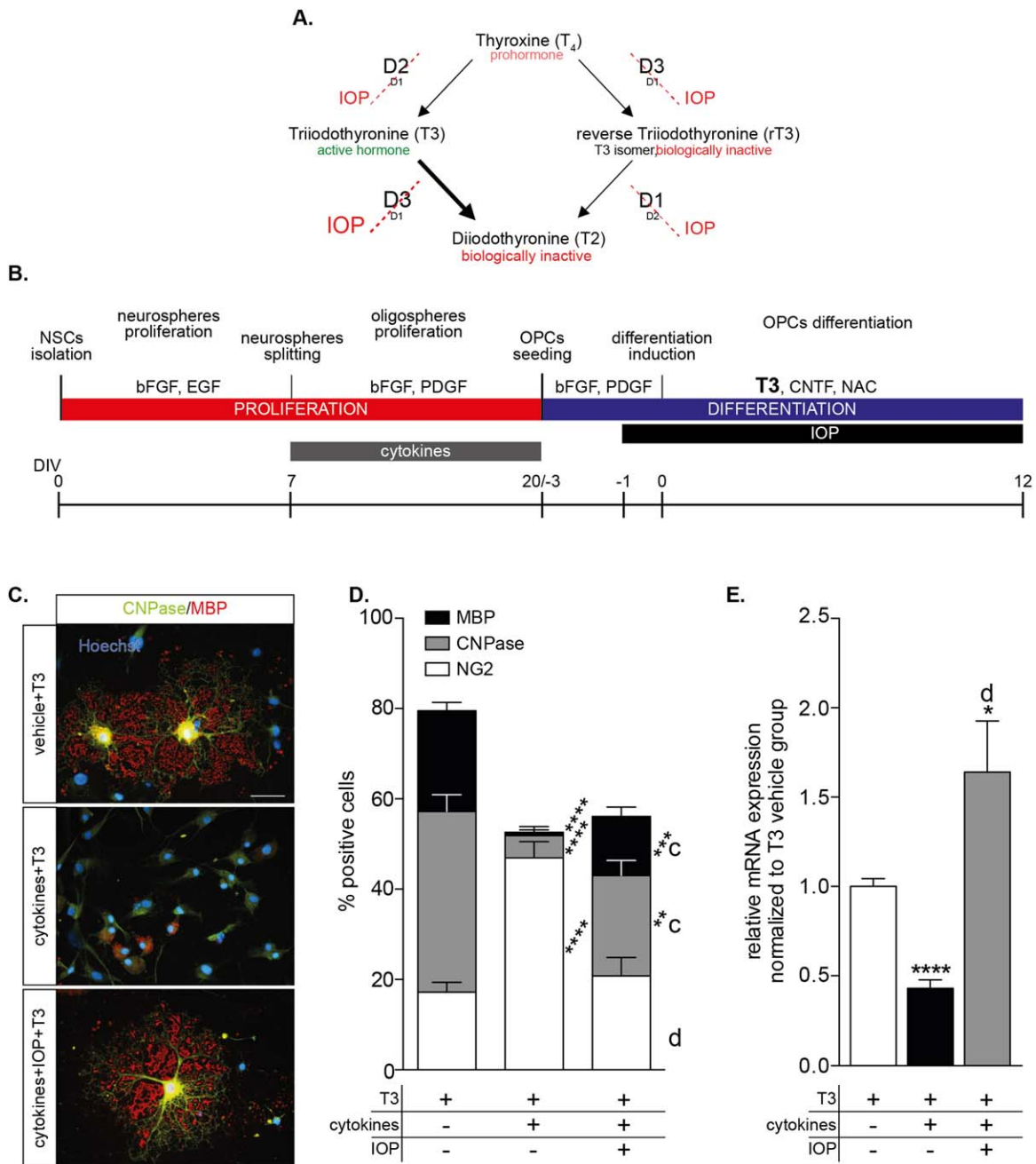
FIGURE 5: Effect of deiodinase inhibition on OL differentiation in cytokines exposed OPC-enriched cultures. **(A)** Pathway of TH tissue metabolism, and effect of IOP. **(B)** Protocol of OPCs proliferation and differentiation, cytokine exposure and IOP treatments. **(C)** Cell morphology and lineage analysis after D3 inhibition induced by IOP treatment. **(D)** Graph shows the cell lineage analysis. **(E)** mRNA expression relative quantification of the Klf9 gene, normalized to the T3-vehicle group. Two biological replicates and at least 10 fields per group were analyzed. Statistical analysis: A: Student's t test, ***$P < 0.001$. (D and E) One-way ANOVA and by Tukey's *post hoc* test. Asterisks represent differences between treated groups and T3-only exposed group (**$P < 0.01$; ***$P < 0.001$; ****$P < 0.0001$), while letters represent differences between cytokine-only exposed group and cytokines + IOP treated group (c = $P < 0.001$; d = $P < 0.0001$). Bar: 20 μm. Abbreviations: bFGF, basic fibroblast growth factor; CNTF, ciliary neurotrophic factor; CNPase, 2′,3′-cyclic nucleotide 3′-phosphodiesterase; D3, deiodinase-3; EGF, epidermal growth factor; IOP, iopanoic acid; NAC, N-acetyl-L-cysteine; NG2 chondroitin sulphate proteoglycan, neural/glial antigen 2; NSC, neural stem cells; MBP, myelin basic protein; OPC, oligodendrocyte precursor cells; PDGF, platelet derived growth factor.

T3 + cytokines (vs T3 alone): NG2 46.9% ($P < 0.0001$); CNPase 4.9% ($P < 0.0001$); MBP 0.7% ($P < 0.0001$); (iii) in the presence of T3 + cytokines + IOP (vs T3 + cytokines):

NG2 20.7% ($P < 0.0001$), CNPase 22.3% ($P = 0.0008$), MBP 13.1% ($P < 0.0001$). The morphology of the cells is consistent with lineage progression.
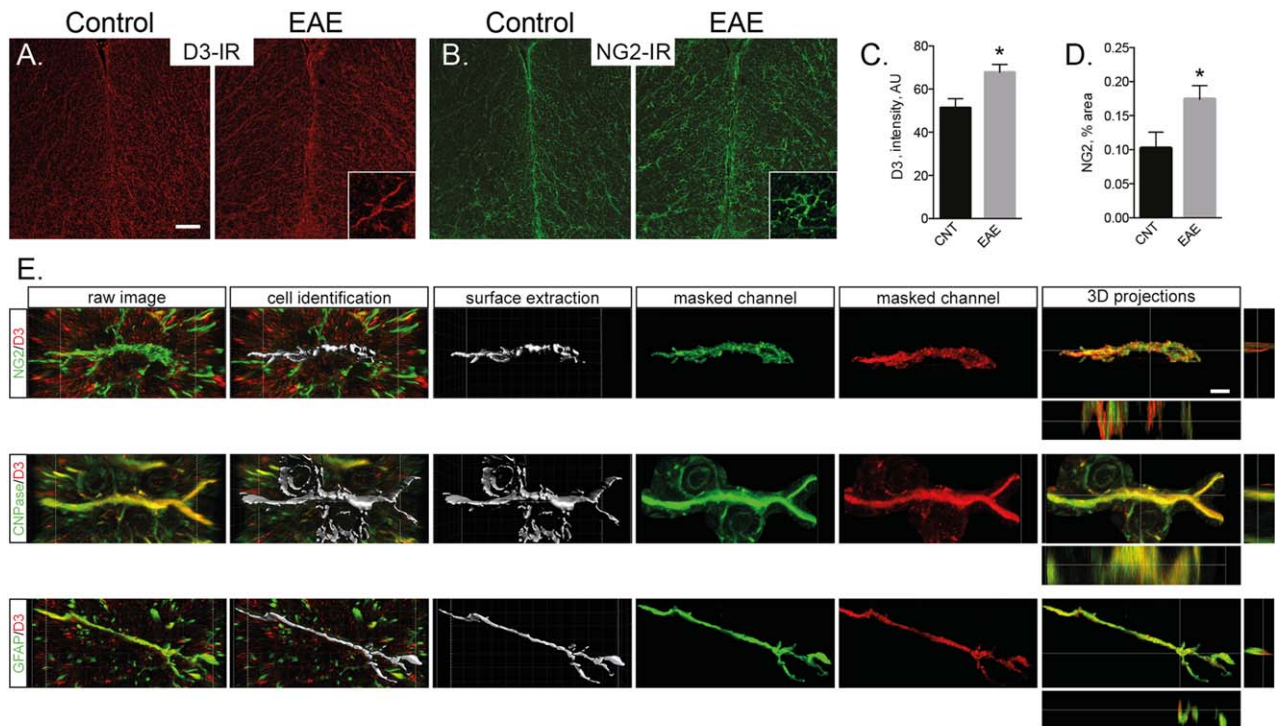
FIGURE 6: D3 immunostaining in different cell types in the lumbar spinal cord. Representative images of D3 (**A**) and NG2 (**B**) staining in the ventral spinal cord in control and EAE-acute animals. High magnification of stained cells are included in the EAE images. (**C**) D3 staining intensity in control and EAE spinal cord. (**D**) NG2-IR percentage area in control and EAE spinal cord. (**E**) 3D visualization and images elaboration of NG2, CNPase and GFAP-positive cells double stained for D3. Images were elaborated by using IMARIS software, extracting the single cell volume (grey surface) from the whole image. Co-distribution of D3 was visualized in 3D elaborated images (see text for image analysis procedure). Bars: A–B, 50 μm; E, 5 μm. Abbreviations: A.U. arbitrary units; D3, deiodinase-3; GFAP, glial fibrillary acid protein; NG2 chondroitin sulphate proteoglycan, neural/glial antigen 2; CNPase, 2′,3′-cyclic nucleotide 3′-phosphodiesterase.

Since both astrocytes and OPCs are present in the cell system, and the correction of cellular hypothyroidism operated by IOP could thus be either direct in OPCs, or indirect through astrocytes, the expression level of the transcription factor, Kruppel-like factor 9 (Klf9), was ultimately studied; this is a key gene in driving OPCs differentiation *in vitro* (Dugas et al., 2012), which is strongly induced by T3. Since cytokine exposure induces a huge decrease in Klf9 mRNA ($P < 0.0001$), the treatment with IOP successively re-established the expression of this transcription factor ($P < 0.012$) (Fig. 5E).

D3 Is Expressed in CNS Cells During EAE

In order to determine whether the *in vitro* data could somehow mimic the *in vivo* condition, double labeling experiments were performed in fixed LSC tissue from control- and acute EAE-animals (Figs. 1 and 6, supporting results). As expected, the TH-inactivating enzyme D3 in control animals is expressed in neurons (see Fig. 1F, supporting results), while it is not observed in astrocytes, microglial cells, OPCs or OL. While no changes were observed in D3 staining intensity in neurons (Fig. 1H, supporting results, motoneurons in the ventral horn of the LSC), an upregulation was observed in the white matter in acute EAE (Fig. 6A,C, sampled in the dorsal funiculus of the LSC), where also an upregulation of the NG2 immunoreactive area was observed (Fig. 6B,D). In particular, D3 appears in OPCs, OL and astrocytes. High-power confocal analysis exploring the co-localization of D3 with cell markers is reported in Fig. 6E, along with the step-by-step image analysis procedure used to examine the multiple z-plane scanning and its lateral projections. The co-distribution of red and green channels, corresponding to the D3-IR in NG2-, CNPase- and GFAP-IR cells, is quite evident, whereas it is not observed in OX42-IR cells (Fig. 1G, supporting results). At this time, and according to well established results, an activation of microglia (OX42-IR cells, Fig. 1C, supporting results) and a downregulation of MBP-IR (Fig. 1E, supporting results) is observed in the dorsal horn of the spinal cord, along with an initial astrogliosis (Fig. 1D, supporting results).

Discussion

The role of T3 in oligodendrogenesis and developmental myelination has been known for more than twenty years in rodents and humans (Bernal, 2005). T3 induces more OLs to be generated from stem and neural stem cells (Fernández

et al., 2004a; Kang et al., 2007; Whittemore et al., 1999) driving cell cycle exit and terminal differentiation into myelinating OL (Casaccia-Bonnefil and Liu, 2003; Raff, 2006) and regulates the expression of genes encoding for myelin proteins (Baxi et al., 2014; Strait et al., 1997). The critical role of intracellular T3 in appropriate myelination was further confirmed by the discovery of the mutation of MCT8 in the Allan-Herndon-Dudley syndrome (Schwartz et al., 2005), leading to severe hypomyelination and TH metabolism impairment in the brain (López-Espíndola et al., 2014). Lastly, TH is recommended in OPCs differentiation protocols (Chen et al., 2007).

According to the so-called "recapitulation hypothesis", remyelination after myelin damage follows some myelination steps and mechanisms occurring during development (Franklin and Hinks, 1999). However, a number of myelination inhibitory factors are present in the adult diseased microenvironment (Fancy et al., 2011). Herein it is suggested that altered TH tissue metabolism induced by inflammatory cytokines could be one of these factors, thus extending to the CNS the evidence described in peripheral tissues, and indicating that cytokines affect a variety of genes involved in TH metabolism, including D2 and D3 (Boelen et al., 2011; de Vries et al., 2015).

By means of *in vivo* experiments, it was first demonstrated that a complex dysregulation of the TH tissue signaling is present in acute EAE, which correlates with the rise of inflammatory cytokines released by peripheral cells and resident microglia (Rodgers and Miller, 2012). The present study confirms the dramatic rise in mRNA tissue expression level for several cytokines, some of which (IL-1β, TNF-α, and TGF-β) also increased in the CSF. Also confirmed was the upregulation of TREM2, a membrane receptor expressed on microglial cells during EAE (Piccio et al., 2007), and CD40, associated with anti-inflammatory M2 microglia (Liu et al., 2013).

In parallel, a 30-fold upregulation was found in the T3 inactivating enzyme D3 mRNA, while no significant changes were found in the D2 gene expression. Notably, in microdissected inflammatory infiltrates a modest (threefold) upregulation of D3 mRNA was observed. The expression level of all TRs isoforms was decreased. In brain tissue, D2 is mainly localized in astrocytes and D3 in neurons (Courtin et al., 2005). In EAE, D3 protein is detectable also in astrocytes, NG2-IR OPCs and CNPase-IR OL. Thus, not only peripheral cells infiltrating the spinal cord parenchyma during EAE (Boelen et al., 2009) but also resident cells express high levels of the T3-inactivating enzyme. Although the different preparation of whole and microdissected tissue for mRNA expression analysis makes hard a direct comparison between these results, we can argue that D3 regulation in astrocytes, OPCs

and OL is even higher that in peripheral cells infiltrating spinal cord parenchyma.

Notably, an increase in D3 activity and mRNA expression level has been described in other neurological conditions characterized by inflammation and demyelination, e.g., ischemia-induced hypoxic brain damage (Jo et al., 2012) and nerve lesion (Li et al., 2001). Finally, a downregulation of all TRs was also found, including TRα, responsible for oligodendroglial lineage induction from NSC (Marziali et al., 2015), as well as TRβ, responsible for OPCs maturation into oligodendrocytes (Baxi et al., 2014).

A decrease was observed in T4 and TSH plasma levels, possibly indicating that the TH negative feedback in the pituitary and hypothalamus is altered, as already described in severe systemic inflammation (Docter et al., 1993; de Vries et al., 2015), and in the non-human primate model of MS (D'Intino et al., 2011).

The overall scenario emerging from our *in vivo* data, namely D3 overexpression and TR downregulation, supports the hypothesis that inflammation leads to a substantial tissue hypothyroidism during EAE, and this could impact on cellular processes requiring an appropriate TH drive, including OPCs differentiation into myelinating OL. Indeed, extensive *in vitro* and *in vivo* evidence indicates that OPCs maturation into myelinating oligodendrocytes is a T3-dependent process. *In vitro* studies have quite elegantly described the role of T3 and TRs as key components of the molecular machinery triggering OPCs out of the cell cycle toward mature OL (Durand and Raff, 2000). The absence of all TRs results in the persistence of OPCs proliferation and the absence of differentiation in adult optic nerves, leading to a default in myelination (Baas et al., 2002). T3 is also necessary in the signaling cascade that promotes myelin repair, possibly involving the transcription factor Kruppel-like factor 9 (Klf9) (Dugas et al., 2012).

To directly test if cytokine-induced alteration of intracellular T3 availability is involved in OPCs differentiation failure during inflammation, *in vitro* studies were performed using OPCs derived from NSCs obtained from the SVZ of adult rats. In this cell system, OPCs, mature OLs and astrocytes are present. We described that OPC maturation was impaired after cytokines exposure during proliferation. Notably, these effects are maintained also when cytokines are withdrawn from the medium, suggesting that cells maintain the "inflammatory priming" initiated by cytokine exposure, as already suggested in ischemia (Falahati et al., 2013). On the contrary, cytokines exposure during differentiation is cytotoxic, but does not abolish OL maturation of the surviving cells.

This dual effect according to the culture phase could at least partially explain the contrasting data on the effect of

inflammatory cytokines on proliferation and differentiation of NSCs described so far in EAE models. In fact, while several papers agree on the increased proliferation of NSCs in the SVZ during acute EAE (Calzà et al., 1998, 2002; Picard-Riera et al., 2002; Pluchino et al., 2008; Tepavcevic et al., 2011) and MS (Nait-Oumesmar et al., 2007), contrasting results are reported using different OPC *in vitro* systems. IFN-γ either inhibits (1-day postnatal rat purified OPCs primary cultures and adult mice SVZ derived OPCs, Chew et al., 2005; Pluchino et al., 2008, respectively) or induces (7-days postnatal O/2A OPC primary cultures from the corpus callosum, Tanner et al., 2011) cell cycle exit in OPCs, also abrogating differentiation into OL induced by T3 (Tanner et al., 2011). TNF-α is cytotoxic and inhibits OPCs differentiation (primary OPCs, Su et al., 2011). IL-17 prevents OPCs maturation (OPCs-enriched primary culture from foetal mice NPCs, Kang et al., 2013). IL-1β, IL-6, TGF-β1, and TNF-α produced as a result of ischemia shifted OPCs toward the more immature form (1-day postnatal rat ischemia, Falahati et al., 2013).

Under cytokine exposure, a dramatic rise in the number of D3-positive cells was observed. Notably, over 80% of PDGFαR-IR OPCs and less than 20% of GFAP-IR astrocyte express D3 under cytokine exposure, thus corroborating what happens *in vivo* during EAE. In order to contrast the possible T3 degradation induced by D3, and to maintain an appropriate T3 concentration in the culture medium for OPCs differentiation, the deiodinase inhibitor IOP was introduced into the cell system. IOP is used as radiocontrast medium and in the treatment of drug-resistant hyperthyroidism (Allahabadia et al., 2000). IOP blocks conversion of T4 to T3 by competitively inhibiting D1 and D2, and blocks T3 inactivation by inhibiting D3 (Huang et al., 2011), thus increasing T3 availability. In our system, when used in the presence of T3 and cytokines, it restores the capability to express differentiation markers (CNPase and MBP), also restoring OL mature morphology. It may thus be concluded that IOP inhibits D3, thereby restoring an appropriate T3 content in OPCs that overcome the cytokine-induced OPCs differentiation block.

This mechanism could explain the positive results observed in *in vivo* TH supplementation in different demyelination models, and also suggests downstream mechanisms. TH supplementation, possibly by binding TR and TREs, actually restores the expression on a number of key genes for OPCs differentiation (Zhang et al., 2015b). Among others: Olig1/2 (D'Intino et al., 2011; Harsan et al., 2008), which are key determinants for OPCs maturation (Meijer et al., 2012; Zhu et al., 2012); sonic hedgehog, the activation of which is necessary to promote remyelination by fingolimod in EAE (Zhang et al., 2015a); Klf9, the activation of which is necessary and sufficient to promote OL differentiation *in vitro* (Denver and Williamson, 2009), and remyelination *in*

vivo (Dugas et al., 2012). Once again, IOP was able to extensively re-establish Klf9 mRNA expression level, which was almost suppressed by cytokine exposure. Therefore, as the appropriate balance between intracellular production and degradation of TH is necessary during cellular differentiation (Dentice et al., 2013), it follows that a hormone replacement therapy should be considered as supporting therapy to overcome OPCs differentiation inhibition observed in inflammatory demyelinating diseases (Kremer et al., 2011; Watzlawik et al., 2010). This conclusion could be also extended to the cerebral white matter injury in the premature infant, where a transient hypothyroxinemia is described (Elitt and Rosenberg, 2014; van Tilborg et al., 2015). However, to pursue this aim, many other aspects need to be thoroughly investigated from both a neurobiological and a clinical point of view, starting from the need to avoid potential hyperthyroidism side effects, and considering the substantially different profile of thyroid function and tissue signaling in perinatal period and adult life (Calzà et al., 2015; Moog et al., 2015).

References

Ahlenius H, Kokaia Z. 2010. Isolation and generation of neurosphere cultures from embryonic and adult mouse brain. Methods Mol Biol 633:241–252.

Allahabadia A, Daykin J, Holder RL, Sheppard MC, Gough SCL, Franklyn JA. 2000. Age and gender predict the outcome of treatment for Graves' hyperthyroidism. J Clin Endocrinol Metab 85:1038–1042.

Baas D, Legrand C, Samarut J, Flamant F. 2002. Persistence of oligodendrocyte precursor cells and altered myelination in optic nerve associated to retina degeneration in mice devoid of all thyroid hormone receptors. Proc Natl Acad Sci USA 99:2907–2911.

Baldassarro VA, Lizzo G, Paradisi M, Fernández M, Giardino L, Calzà L. 2013. Neural stem cells isolated from amyloid precursor protein-mutated mice for drug discovery. World J Stem Cells 5:229–237.

Baxi EG, Schott JT, Fairchild AN, Kirby LA, Karani R, Uapinyoying P, Pardo-Villamizar C, Rothstein JR, Bergles DE, Calabresi PA. 2014. A selective thyroid hormone β receptor agonist enhances human and rodent oligodendrocyte differentiation. Glia 62:1513–1529.

Bernal J. 2005. Thyroid hormones and brain development. Vitam Horm 71:95–122.

Bernal J, Guadaño-Ferraz A, Morte B. 2015. Thyroid hormone transporters—Functions and clinical implications. Nat Rev Endocrinol 11:406–417.

Bianco AC, Salvatore D, Gereben B, berry MJ, Larsen PR. 2002. Biochemistry, cellular and molecular biology, and physiological roles of the iodothyronine selenodeiodinases. Endocr Rev 23:38–89.

Billon N, Jolicoeur C, Tokumoto Y, Vennström B, Raff M. 2002. Normal timing of oligodendrocyte development depends on thyroid hormone receptor alpha 1 (TRalpha1). EMBO J 21:6452–6460.

Boelen A, Mikita J, Boiziau C, Chassande O, Fliers E, Petry KG. 2009. Type 3 deiodinase expression in inflammatory spinal cord lesions in rat experimental autoimmune encephalomyelitis. Thyroid 19:1401–1406.

Boelen A, Kwakkel J, Fliers E. 2011. Beyond low plasma T3: Local thyroid hormone metabolism during inflammation and infection. Endocr Rev 32:670–693.

Boulanger JJ, Messier C. 2014. From precursors to myelinating oligodendrocytes: Contribution of intrinsic and extrinsic factors to white matter plasticity in the adult brain. Neuroscience 269:343–366.

Boyd A, Zhang H, Williams A. 2013. Insufficient OPC migration into demyelinated lesions is a cause of poor remyelination in MS and mouse models. Acta Neuropathol 125:841–859.

Calzà L, Giardino L, Pozza M, Bettelli C, Micera A, Aloe L. 1998. Proliferation and phenotype regulation in the subventricular zone during experimental allergic encephalomyelitis: In vivo evidence of a role for nerve growth factor. Proc Natl Acad Sci U S A 95:3209–3214.

Calzà L, Fernández M, Giuliani A, Aloe L, Giardino L. 2002. Thyroid hormone activates oligodendrocyte precursors and increases a myelin-forming protein and NGF content in the spinal cord during experimental allergic encephalomyelitis. Proc Natl Acad Sci USA 99:3258–3263.

Calzà L, Fernandez M, Giardino L. 2015. Role of the thyroid system in myelination and neural connectivity. Comp Physiol 5:1405–1421

Casaccia-Bonnefil P, Liu A. 2003. Relationship between cell cycle molecules and onset of oligodendrocyte differentiation. J Neurosci Res 72:1–11.

Castelo-Branco G, Stridh P, Guerreiro-Cacais AO, Adzemovic MZ, Falcão AM, Marta M, Berglund R, Gillett A, Hamza KH, Lassmann H, Hermanson O, Jagodic M. 2014. Acute treatment with valproic acid and l-thyroxine ameliorates clinical signs of experimental autoimmune encephalomyelitis and prevents brain pathology in DA rats. Neurobiol Dis 71:220–233.

Chen Y, Balasubramaniyan V, Peng J, Hurlock EC, Tallquist M, Li J, Lu QR. 2007. Isolation and culture of rat and mouse oligodendrocyte precursor cells. Nat Protoc 2:1044–1051.

Chew LJ, King WC, Kennedy A, Gallo V. 2005. Interferon-gamma inhibits cell cycle exit in differentiating oligodendrocyte progenitor cells. Glia 52:127–143.

Courtin F, Zrouri H, Lamirand A, Li WW, Mercier G, Schumacher M, Goascogne CL, Pierre M. 2005. Thyroid hormone deiodinases in the central and peripheral nervous system. Thyroid 15:931–942.

Dell'Acqua ML, Lorenzini L, D'Intino G, Sivilia S, Pasqualetti P, Panetta V, Paradisi M, Filippi MM, Baiguera C, Pizzi M, Giardino L, Rossini PM, Calzà L. 2012. Functional and molecular evidence of myelin- and neuroprotection by thyroid hormone administration in experimental allergic encephalomyelitis. Neuropathol Appl Neurobiol 38:454–470.

Dentice M, Marsili A, Zavacki A, Larsen PR, Salvatore D. 2013. The deiodinases and the control of intracellular thyroid hormone signaling during cellular differentiation. Biochim Biophys Acta 1830:3937–3945.

Denver RJ, Williamson KE. 2009. Identification of a thyroid hormone response element in the mouse Kruppel-like factor 9 gene to explain its postnatal expression in the brain. Endocrinology 150:3935–3943.

de Vries EM, Fliers E, Boelen A. 2015. The molecular basis of the non-thyroidal illness syndrome. J Endocrinol 225:R67–81.

D'Intino G, Lorenzini L, Fernández M, Taglioni A, Perretta G, Del Vecchio G, Villoslada P, Giardino L, Calzà L. 2011. Triiodothyronine administration ameliorates the demyelination/remyelination ratio in a non-human primate model of multiple sclerosis by correcting tissue hypothyroidism. J Neuroendocrinol 23:778–790.

Docter R, Krenning EP, de Jong M, Hennemann G. 1993. The sick euthyroid syndrome: Changes in thyroid hormone serum parameters and hormone metabolism. Clin Endocrinol (Oxf) 39:499–518.

Dugas JC, Ibrahim A, Barres BA. 2012. The T3-induced gene KLF9 regulates oligodendrocyte differentiation and myelin regeneration. Mol Cell Neurosci 50:45–57.

Durand B, Raff M. 2000. A cell-intrinsic timer that operates during oligodendrocyte development. Bioessays 22:64–71.

Elitt CM and Rosenberg PA. 2014. The challenge of understanding cerebral white matter injury in the premature infant. Neuroscience 276:216–238.

Falahati S, Breu M, Waickman AT, Phillips AW, Arauz EJ, Snyder S, Porambo M, Goeral K, Comi AM, Wilson MA, Johnston MV, Fatemi A. 2013. Ischemia-induced neuroinflammation is associated with disrupted development of oligodendrocyte progenitors in a model of periventricular leukomalacia. Dev Neurosci 35:182–196.

Fancy SP, Chan JR, Baranzini SE, Franklin RJ, Rowitch DH. 2011. Myelin regeneration: A recapitulation of development? Annu Rev Neurosci 34:21–43.

Fernández M, Pirondi S, Manservigi M, Giardino L, Calza L. 2004a. Thyroid hormone participates in the regulation of neural stem cells and oligodendrocyte precursor cells in the central nervous system of adult rat. Eur J Neurosci 20:2059–2070

Fernández M, Giuliani A, Pirondi S, D'Intino G, Giardino L, Aloe L, Levi-Montalcini R, Calzà L. 2004b. Thyroid hormone administration enhances remyelination in chronic demyelinating inflammatory disease. Proc Natl Acad Sci USA 101:16363–16368.

Fernández M, Paradisi M, Del Vecchio G, Giardino L, Calzà L. 2009. Thyroid hormone induces glial lineage of primary neurospheres derived from non-pathological and pathological rat brain: Implications for remyelination-enhancing therapies. Int J Dev Neurosci 27:769–778.

Franco PG, Silvestroff L, Soto EF, Pasquini JM. 2008. Thyroid hormones promote differentiation of oligodendrocyte progenitor cells and improve remyelination after cuprizone-induced demyelination. Exp Neurol 212:458–467.

Franklin RJM, Hinks GL. 1999. Understanding CNS remyelination: Clues from developmental and regeneration biology. J Neurosci Res 58:207–213.

St Germain DL, Galton VA, Hernandez A. 2009. Minireview: Defining the roles of the iodothyronine deiodinases: Current concepts and challenges. Endocrinology 150:1097–1107.

Goodin DS. 2014. The epidemiology of multiple sclerosis: Insights to disease pathogenesis. Handb Clin Neurol 122:231–266.

Harsan LA, Steibel J, Zaremba A, Agin A, Sapin R, Poulet P, Guignard B, Parizel N, Grucker D, Boehm N, Miller RH, Ghandour MS. 2008. Recovery from chronic demyelination by thyroid hormone therapy: Myelinogenesis induction and assessment by diffusion tensor magnetic resonance imaging. J Neurosci 28:14189–14201.

Huang MP, Rodgers KA, O'Mara R, Mehta M, Abuzahra HS, Tannenbaum AD, Persons K, Holick MF, Safer JD. 2011. The thyroid hormone degrading type 3 deiodinase is the primary deiodinase active in murine epidermis. Thyroid 21:1263–1268.

Hung PL, Huang CC, Huang HM, Tu DG, Chang YC. 2013. Thyroxin treatment protects against white matter injury in the immature brain via brain-derived neurotrophic factor. Stroke 44:2275–2283.

Jo S, Kalló I, Bardóczi Z, Arrojo e Drigo R, Zeöld A, Liposits Z, Oliva A, Lemmon VP, Bixby JL, Gereben B, Bianco AC. 2012. Neuronal hypoxia induces Hsp40-mediated nuclear import of type 3 deiodinase as an adaptive mechanism to reduce cellular metabolism. I. Neurosci 32:8491–8500.

Kang SM, Cho MS, Seo H, Yoon CJ, Oh SK, Choi YM, Kim DW. 2007. Efficient induction of oligodendrocytes from human embryonic stem cells. Stem Cells 25:419–424.

Kang Z, Wang C, Zepp J, Wu L, Sun K, Zhao J, Chandrasekharan U, DiCorleto PE, Trapp BD, Ransohoff RM, Li X. 2013. Act1 mediates IL-17-induced EAE pathogenesis selectively in NG2+ glial cells. Nat Neurosci 16:1401–1408.

Kremer D, Aktas O, Hartung HP, Küry P. 2011. The complex world of oligodendroglial differentiation inhibitors. Ann Neurol 69:602–618.

Kuhlmann T, Miron V, Cui Q, Wegner C, Antel J, Brück W. 2008. Differentiation block of oligodendroglial progenitor cells as a cause for remyelination failure in chronic multiple sclerosis. Brain 131:1749–1758.

Lassmann H, van Horssen J, Mahad D. 2012. Progressive multiple sclerosis: Pathology and pathogenesis. Nat Rev Neurol 8:647–656.

Lee JY, Kim MJ, Stanley EG, Elefanty AG, Petratos S. 2015. Monocarboxylate transporter 8 is expressed on oligodendrocyte progenitors derived from human embryonic stem cells. Int J Dev Neurosci 47:69

Li WW, Le Goascogne C, Ramaugé M, Schumacher M, Pierre M, Courtin F. 2001. Induction of type 3 iodothyronine deiodinase by nerve injury in the rat peripheral nervous system. Endocrinol 142:5190–5197.

Liu C, Li Y, Yu J, Feng L, Hou S, Liu Y, Guo M, Xie Y, Meng J, Zhang H, Xiao B, Ma C. 2013. Targeting the shift from M1 to M2 macrophages in experimental autoimmune encephalomyelitis mice treated with fasudil. PLoS One 8: e54841–54854.

López-Espíndola D, Morales-Bastos C, Grijota-Martínez C, Liao XH, Lev D, Sugo E, Verge CF, Refetoff S, Bernal J, Guadaño-Ferraz A. 2014. Mutations of the thyroid hormone transporter MCT8 cause prenatal brain damage and persistent hypomyelination. J Clin Endocrinol Metab 99:E2799–2804.

Marziali LN, Garcia CI, Pasquini JM. 2015. Transferrin and thyroid hormone converge in the control of myelinogenesis. Exp Neurol 265:129–141.

Meijer DH, Kane MF, Mehta S, Liu H, Harrington E, Taylor CM, Stiles CD, Rowitch DH. 2012. Separated at birth? The functional and molecular divergence of OLIG1 and OLIG2. Nat Rev Neurosci 13:819–831.

Miller RH, Mi S. 2007. Dissecting demyelination. Nat Neurosci 10:1351–1354.

Moog NK, Entringer S, Heim C, Wadhwa PD, Kathmann N, Buss C. 2015. Influence of maternal thyroid hormones during gestation on fetal brain development. Neuroscience. doi: 10.1016/j.neuroscience.2015.09.070. Epub ahead of print

Morte B, Bernal J. 2014. Thyroid hormone action: Astrocyte-neuron communication. Front Endocrinol 5:82–87.

Nait-Oumesmar B, Picard-Riera N, Kerninon C, Decker L, Seilhean D, Höglinger GU, Hirsch EC, Reynolds R, Baron-Van Evercooren A. 2007. Activation of the subventricular zone in multiple sclerosis: Evidence for early glial progenitors. Proc Natl Acad Sci U S A 104:4694–4699.

Picard-Riera N, Decker L, Delarasse C, Goude K, Nait-Oumesmar B, Liblau R, Pham-Dinh D, Baron-Van Evercooren A. 2002. Experimental autoimmune encephalomyelitis mobilizes neural progenitors from the subventricular zone to undergo oligodendrogenesis in adult mice. Proc Natl Acad Sci USA 99:13211–13216.

Piccio L, Buonsanti C, Mariani M, Cella M, Gilfillan S, Cross AH, Colonna M, Panina-Bordignon P. 2007. Blockade of TREM-2 exacerbates experimental autoimmune encephalomyelitis. Eur J Immunol 37:1290–1301.

Pluchino S, Muzio L, Imitola J, Deleidi M, Alfaro-Cervello C, Salani G, Porcheri C, Brambilla E, Cavasinni F, Bergamaschi A, Garcia-Verdugo JM, Comi G, Khoury SJ, Martino G. 2008. Persistent inflammation alters the function of the endogenous brain stem cell compartment. Brain 131:2564–2578.

Raff M. 2006. The mystery of intracellular developmental programmes and timers. Biochem Soc Trans 34:663–670.

Robinson AP, Rodgers JM, Goings GE, Miller SD. 2014. Characterization of oligodendroglial populations in mouse demyelinating disease using flow cytometry: Clues for MS pathogenesis. PLoS One 9:e107649–107663.

Rodgers JM, Miller SD. 2012. Cytokine control of inflammation and repair in the pathology of multiple sclerosis. Yale J Biol Med 85:447–468.

Rodgers JM, Robinson AP, Miller SD. 2013. Strategies for protecting oligodendrocytes and enhancing remyelination in multiple sclerosis. Discov Med 16:53–63.

Schang AL, Van Steenwinckel J, Chevenne D, Alkmark M, Hagberg H, Gressens P, Fleiss B. 2014. Failure of thyroid hormone treatment to prevent inflammation-induced white matter injury in the immature brain. Brain Behav Immun 37:95–102.

Schwartz CE, May MM, Carpenter NJ, Rogers RC, Martin J, Bialer MG, Ward J, Sanabria J, Marsa S, Lewis JA, Echeverri R, Lubs HA, Voeller K, Simensen RJ, Stevenson RE. 2005. Allan-Herndon-Dudley syndrome and the monocarboxylate transporter 8 (MCT8) gene. Am J Hum Genet 77:41–53.

Silvestroff L, Bartucci S, Pasquini J, Franco P. 2012. Cuprizone-induced demyelination in the rat cerebral cortex and thyroid hormone effects on cortical remyelination. Exp Neurol 235:357–367.

Strait KA, Carlson DJ, Schwartz HL, Oppenheimer JH. 1997. Transient stimulation of myelin basic protein gene expression in differentiating cultured oligodendrocytes: A model for 3,5,3′-triiodothyronine-induced brain development. Endocrinology 138:635–641.

Su Z, Yuan Y, Chen J, Zhu Y, Qiu Y, Zhu F, Huang A, He C. 2011. Reactive astrocytes inhibit the survival and differentiation of oligodendrocyte precursor cells by secreted TNF-α. J Neurotrauma 28:1089–1100.

Tanner DC, Cherry JD, Mayer-Pröschel M. 2011. Oligodendrocyte progenitors reversibly exit the cell cycle and give rise to astrocytes in response to interferon-γ. J Neurosci 31:6235–6246.

Tepavcevic V, Lazarini F, Alfaro-Cervello C, Kerninon C, Yoshikawa K, Garcia-Verdugo JM, Lledo PM, Nait-Oumesmar B, Baron-Van Evercooren A. 2011. Inflammation-induced subventricular zone dysfunction leads to olfactory deficits in a targeted mouse model of multiple sclerosis. J Clin Invest 121:4722–4734.

Trotter J, Karram K, Nishiyama A. 2010. NG2 cells: Properties, progeny and origin. Brain Res Rev 63:72–82.

van Tilborg E, Heijnen CJ, Benders MJ, van Bel F, Fleiss B, Gressens P, Nijboer CH. 2016. Impaired oligodendrocyte maturation in preterm infants: Potential therapeutic targets. Prog Neurobiol 136:28–49.

Vose LR, Vinukonda G, Jo S, Miry O, Diamond D, Korumilli R, Arshad A, Zia MT, Hu F, Kayton RJ, La Gamma EF, Bansal R, Bianco AC, Ballabh P. 2013. Treatment with thyroxine restores myelination and clinical recovery after intraventricular hemorrhage. J Neurosci 33:17232–17246.

Watzlawik J, Warrington AE, Rodriguez M. 2010. Importance of oligodendrocyte protection, BBB breakdown and inflammation for remyelination. Expert Rev Neurother 10:441–457.

Whittemore SR, Morassutti DJ, Walters WM, Liu RH, Magnuson DS. 1999. Mitogen and substrate differentially affect the lineage restriction of adult rat subventricular zone neural precursor cell populations. Experimental Cell Research 252:75–95.

Zhang J, Zhang ZG, Li Y, Ding X, Shang X, Lu M, Elias SB, Chopp M. 2015a. Fingolimod treatment promotes proliferation and differentiation of oligodendrocyte progenitor cells in mice with experimental autoimmune encephalomyelitis. Neurobiol Dis 76:57–66.

Zhang M, Ma Z, Qin H, Yao Z. 2015b. Thyroid Hormone Potentially Benefits Multiple Sclerosis via Facilitating Remyelination. Mol Neurobiol. DOI: 10.1007/s12035-015-9375-z. Epub ahead of print

Zhu X, Zuo H, Maher BJ, Serwanski DR, LoTurco JJ, Lu QR, Nishiyama A. 2012. Olig2-dependent developmental fate switch of NG2 cells. Development 139:2299–2307.

5. CONCLUSIONS AND PERSPECTIVES

The different nature of foetal OPCs, involved in developmental myelination, and adult OPCs, involved in myelin dynamics, could reflect a different response of the two cells to demyelinating insults.

We demonstrated that foetal and adult NSCs-derived OPCs show similar role of RXRγ in T3-mediated differentiation and the same response to inflammation-mediated differentiation block. However, the two systems show different response to T3-mediated differentiation induction in physiological conditions, mediated by differentially expressed NRs, and to PARP inhibition, selectively lethal for foetal OPCs. Moreover, the two systems show a totally different response to OGD-induced cell death, with OPCs/OLs selective vulnerability only in foetal cultures.

Further studies will focus on the role of RXRγ in the T3-mediated differentiation induction, with a focus on TRs/RXRγ dimerization and genes target identification. Moreover deiodinases and glutamate involvement in foetal-selective OGD-induced cell death will be investigated.

The understating of molecular machinery underlying differences in physiological differentiation and different response to demyelinating insults in foetal and adult OPCs, will open the way to new strategies focused on the developing of differential therapies in foetal and adult demyelinating diseases.

6. REFERENCES

Albert M, Antel J, Brück W, Stadelmann C. Extensive cortical remyelination in patients with chronic multilple sclerosis. Brain Pathol, 2007. 17: 129-138.

Alhenius H and Kokaia Z. Isolation and generation of neurosphere cultures from embryonic and adult mouse brain. Methods Mol Biol, 2010; 633: 241-252.

Alvarez-Builla and Garcia-Verdugo. Neurogenesis in adult subventricular zone. J Neurosci, 2002. 22: 629-634.

Back SA, Han BH, Luo NL, Chricton CA, Xanthoudakis S, Tam J, Arvin KL and Holtzman DM. Selective vulnerability of late oligodendrocyte progenitors to hypoxia-ischemia. J Neurosci, 2002. 22: 455-463.

Baldassarro VA, Dolci LS, Mangano C, Giardino L, Gualandi C, Focarete ML and Calzà L. In Vitro Testing of Biomaterials for Neural Repair: Focus on Cellular Systems and High-Content Analysis. Biores Open Access, 2016. 5: 201-211.

Baldassarro VA, Marchesini A, Giardino L and Calzà L. PARP activity and inhibition in fetal and adult oligodendrocyte precursor cells: Effect on cell survival and differentiation. Stem Cell Res, 2017a. 22: 54-60.

Baldassarro VA, Marchesini A, Giardino L and Calzà L. Vulnerability of primary neurons derived from Tg2576 Alzheimer mice to oxygen and glucose deprivation: role of intraneuronal amyloid-β accumulation and astrocytes. Dis Model Mech, 2017b. 10: 671-678.

Baldassarro VA, Marchesini A, Facchinetti F, Villetti G, Calzà L, Giardino L. Cell death in pure-neuronal and neuron-astrocyte mixed primary culture subjected to oxygen-glucose deprivation: The contribution of poly(ADP-ribose) polymerases and caspases. Microchem J, 2018, 136:215-222

Baldassarro VA, Krezel W, Giardino L and Calzà L. Nuclear receptors and foetal vs. adult oligodendrocyte precursor cells differentiation. Unpublished - A

Baldassarro VA, Marchesini A, Giardino L and Calzà L. Foetal and adult oligodendrocyte precursor cells are differentially vulnerable to inflammation and oxygen-glucose deprivation. Unpublished - B

Barateiro A and Fernandes A. Temporal oligodendrocyte lineage progression: in vitro models of proliferation, differentiation and myelination. Biochim Biophys Acta, 2014. 1843: 1917-1929.

Baxi EG, Schott JT, Fairchild AN, Kirby LA, Karani R, Uapinyoying P, et al. A selective thyroid hormone β receptor agonist enhances human and rodent oligodendrocyte differentiation. Glia, 2014; 62: 1513–1529.

Bengtsson SL, Nagy Z, Skare S, Forsman L, Forssberg H and Ulle´n F. Extensive piano practicing has regionally specific effects on white matter development. Nat. Neurosci. 2005; 8: 1148–1150.

Bercury KK and Macklin WB. Dynamics and Mechanisms of CNS myelination. Developmental Cell. 2015; 32: 447-458.

Berger R, Jensen A, Hossmann KA and Paschen W. Effect of mild hypothermia during and after transient in vitro ischemia on metabolic disturbances in hippocampal slices at different stages of development. Brain Res Dev Brain Res, 1998. 105: 67-77.

Bernal J, Guadaño-Ferraz A, Morte B. Thyroid hormone transporters - Functions and clinical implications. Nat Rev Endocrinol. 2015; 11: 406–417.

Bhatt A, Fan LW and Pang Y. Strategies for myelin regeneration: lessons learned from development. Neural Regen Res, 2014. 9: 1347-1350.

Bianco AC, Salvatore D, Gereben B, berry MJ, Larsen PR. Biochemistry, cellular and molecular biology, and physiological roles of the iodothyronine selenodeiodinases. Endocr Rev. 2002; 23: 38–89.

Billon N, Tokumoto Y, Forrest D and Raff M. Role of thyroid hormone receptors in timing oligodendrocyte differentiation. Dev Biol, 2001. 235: 110-120.

Billon N, Jolicoeur C, Tokumoto Y, Vennstr€om B, Raff M. Normal timing of oligodendrocyte development depends on thyroid hormone receptor alpha 1 (TRalpha1). EMBO J. 2002; 21: 6452–6460.

Boelen A, Kwakkel J, Fliers E. Beyond low plasma T3: Local thyroid hormone metabolism during inflammation and infection. *Endocr Rev* 32: 670-693, 2011.

Borjini N, Fernández M, Giardino L and Calzà L. Cytokine and chemokine alterations in tissue, CSF, and plasma in early presymptomatic phase of experimental allergic encephalomyelitis (EAE), in a rat model of multiple sclerosis. J Neuroinflammation, 2016. 13: 291.

Boyd A, Zhang H and Williams A. Insufficient OPC migration into demyeli- nated lesions is a cause of poor remyelination in MS and mouse models. Acta Neuropathol, 2013. 125: 841–859.

Bradl M and Lassmann H. Oligodendrocytes: biology and pathology. Acta Neuropathol. 2010; 119: 37-53.

Brousse B, Magalon K, Durbec P and Cyre M. Region and dynamic specificities of adult neural stem cells and oligodendrocyte precursors in myelin regeneration in the mouse brain. Biol Open, 2015. 4: 980-992.

Buntnix M, Vanderlocht J, Hellings N, Vandenabeele F, Lambrichts I, Raus J, Ameloot M, Stinissen P, Steels P. Characterization of three human oligodendroglial cell lines as a

model to study oligodendrocyte injury: morphology and oligodendrocyte-specific gene expression. J Neurocytol, 2003. 32: 25-38.

Butts BD, Houde C and Mehmet H. Maturation-dependent sensitivity of oligodendrocyte lineage cells to apoptosis: implications for normal development and disease. Cell Death Diff, 2008. 15: 1178-1186

Cai Q, Ma T, Li C, Tian Y and Li H. Catalpol Protects Pre-Myelinating Oligodendrocytes against Ischemia-induced Oxidative Injury through ERK1/2 Signaling Pathway. Int J Biol Sci, 2016. 12: 1415-1426.

Calzà L, Fernandez M, Giuliani A, D'Intino G, Pirondi S, Sivilia S, Paradisi M, Desordi N and Giardino L. Thyroid hormone and remyelination in adult central nervous system: A lesson from an inflammatory-demyelinating disease. Brain Res Brain Res Rev, 2005. 48: 339-346.

Calzà L, Fernandez M, Giardino L. Cellular approaches to central nervous system remyelination stimulation: Thyroid hormone to pro- mote myelin repair via endogenous stem and precursor cells. J Mol Endocrinol, 2010. 44: 13-23.

Calzà L, Fernandez M, Giardino L. Role of the thyroid system in myelination and neural connectivity. Comp Physiol. 2015; 5:1405–1421

Calzà L, Baldassarro VA, Fernandez M, Giuliani A, Lorenzini L and Giardino L. Thyroid hormone and the white matter of the central nervous system: from development to repair. Vit and Horm, 2017. In press.

Casaccia-Bonnefil P and Liu A. Relationship between cell cycle molecules and onset of oligodendrocyte differentiation. Journal of Neuroscience Research, 2003. 72: 1–11.

Castelo-Branco G, Stridh P, Guerreiro-Cacais AO, Adzemovic MZ, Falcão AM, Marta M, Berglund R, Gillett A, Hamza KH, Lassmann H, Hermanson O, Jagodic M. Acute treatment with valproic acid and l-thyroxine ameliorates clinical signs of experimental

autoimmune encephalomyelitis and prevents brain pathology in DA rats. Neurobiol Dis, 2014. 71: 220-233.

Chen Y, Balasubramaniyan V, Peng J, Hurlock EC, Tallquist M, Li J, Lu QR. Isolation and culture of rat and mouse oligodendrocyte precursor cells. Nat Protoc, 2007. 2: 1044-1051.

Chew LJ, King WC, Kennedy A andGallo V. Interferon-gamma inhibits cell cycle exit in differentiating oligodendrocyte progenitor cells. Glia, 2005. 52: 127–143.

Choe Y, Huynh T and Pleasure S. Migration Migration of Oligodendrocyte Progenitor Cells Is Controlled by Transforming Growth Factor Family Proteins during Corticogenesis. J Neurosci, 2014. 34: 14973-14983.

Chojnacki A, Kelly JJ, Hader W, Weiss S. Distinctions between fetal and adult human platelet-derived growth factor-responsive neural precursors. Ann Neurol, 2008. 64: 127-142.

Crawford AH, Chambers C and Franklin RJ. Remyelination: The true regeneration of the central nervous system. Journal of Comparative Pathology, 2013. 149: 242–254.

Cui QL, D'Abate L, Fang J, Leong SY, Ludwin S, Kennedy TE, Antel J, Almazan G. Human fetal oligodendrocyte progenitor cells from different gestational stages exhibit substantially different potential to myelinate. Stem Cells Dev, 2012. 21: 1831-1837.

Dawson MR, Polito A, Levine JM and Reynolds R. Therapeutic applications of PARP inhibitors: anticancer therapy and beyond. Mol Aspects Med, 2003. 34: 1217-1256.

De Groot LJ. The non-thyroidal illness syndrome. 2015

Dell'Acqua ML, Lorenzini L, D'Intino G, Sivilia S, Pasqualetti P, Panetta V, Paradisi M, Filippi MM, Baiguera C, Pizzi M, Giardino L, Rossini PM, Calzà L. Functional and molecular evidence of myelin- and neuroprotection by thyroid hormone administration

in experimental allergic encephalomyelitis. Neuropathol Appl Neurobiol, 2012. 38: 454-470.

Del Vecchio G1, Giuliani A, Fernandez M, Mesirca P, Bersani F, Pinto R, Ardoino L, Lovisolo GA, Giardino L, Calzà L. Effect of radiofrequency electromagnetic field exposure on in vitro models of neurodegenerative disease. Bioelectromagnetics, 2009. 30: 564-572.

Deng W, Rosenberg PA, Volpe JJ and Jensen FE. Calcium-permeable AMPAkainate receptors mediate toxicity and preconditioning by oxygen-glucose deprivation in oligodendrocyte precursors. PNAS, 2003. 100: 6801-6806.

Deng W, Yue Q, Rosenberg PA, Volpe JJ and Jensen FE. Oligodendrocyte excitotoxicity determined by local glutamate accumulation and mitochondrial function. J Neurochem, 2006. 98: 213-222.

Dentice M, Marsili A, Zavacki A, Larsen PR and Salvatore D. The deiodinases and the control of intracellular thyroid hormone signaling during cellular differentiation. Biochim Biophys Acta, 2013. 1830: 3937–3945.

Dendrou CA, Fugger L and Friese MA. Immunopathology of multiple sclerosis. Nat Rev Immunol, 2015. 15: 545-558.

de Vries EM, Fliers E and Boelen, A. The molecular basis of the non-thyroidal ill- ness syndrome. Journal of Endocrinology, 2015. 225: R67–R81.

Dimou L and Gallo V. NG2-glia and their functions in the central nervous system. Glia, 2015. 63: 1429-1451.

Dincman TA, Beare JE, Ohri SS and Whittemore SR. Isolation of cortical mouse oligodendrocyte precursor cells. J Neurosci Methods, 2012. 209: 219-226. Triiodothyronine administration ameliorates the demyelination/remyelination ratio in a

non-human primate model of multiple sclerosis by correcting tissue hypothyroidism. J Neuroendocrinol, 2011. 23: 778-790.

D'Intino G, Lorenzini L, Fernandez M, Taglioni A, Perretta G, Del Vecchio G, Villoslada P, Giardino L, Calzà L.

Dugas JC, Ibrahim A and Barres BA. The T3-induced gene KLF9 regulates oligodendrocyte differentiation and myelin regeneration. Mol Cell Neurosci, 2012. 50: 45–57.

Durand B and Raff M. A cell-intrinsic timer that operates during oligodendrocyte development. Bioessays, 2000. 22: 64–71.

Dumitrescu AM and Refetoff S. The syndromes of reduced sensitivity to thyroid hormone. Biochim Biophys Acta, 2013. 1830: 3987-4003.

El Waly B, Macchi M, Cayre M and Durbec P. Oligodendrogenesis in the normal and pathological central nervous system. Front. Neurosci, 2014. 8: 145

Fancy SPJ, Chan JR, Baranzini SE, Franklin JM and Rowitch DH. Myelin regulation: a recapitulation of development? Annu Rev Neurosci, 2011. 34: 21-43.

Falahati S, Breu M, Waickman AT, Phillips AW, Arauz EJ, Snyder S, Porambo M, Goeral K, Comi AM, Wilson MA, Johnston MV and Fatemi A. Ischemia- induced neuroinflammation is associated with disrupted development of oli- godendrocyte progenitors in a model of periventricular leukomalacia. Dev Neurosci, 2013. 35: 182–196.

Fernandez M, Pirondi S, Antonelli T, Ferraro L, Giardino L and Calzà L. Role of c-Fos protein on glutamate toxicity in primary neural hippocampal cells. J Neurosci Res, 2005. 82: 115-125.

Fernández M, Baldassarro VA, Sivilia S, Giardino L and Calzà L. Inflammation severely alters thyroid hormone signaling in the central nervous system during experimental

allergic encephalomyelitis in rat: Direct impact on OPCs differentiation failure. Glia, 2016. 64: 1573-1589.

Franklin RJ, Bayley SA, Milner R, Ffrench-Constant C and Blakemore WF. Differentiation of the O-2A progenitor cell line CG-4 into oligodendrocytes and astrocytes following transplantation into glia-deficient areas of CNS white matter. Glia, 1995. 13: 39-44.

Franklin RJM and Ffrench-Constant C. RemyelinationintheCNS:frombiologyto therapy. Nat. Rev. Neurosci, 2008. 9, 839–855

Franklin RJM and Hinks GL. Understanding CNS remyelination: Clues from developmental and regeneration biology. J Neurosci Res, 1999 58:207–213.

Fuentealba LC, Obernier K and Alvarez-Buylla A. Adult neural stem cells bridge their niche. Cell Stem Cell, 2012 10: 698-708.

Fukushima S, Nishikawa K, Furube E, Muneoka S, Ono K, Takebayashi H and Miyata S. Oligodendrogenesis in the fornix of adult mouse brain; the effect of LPS-induced inflammatory stimulation. Brain Res, 2015. 1627: 52-69.

Gao FB and Raff M. Cell size control and a cell-intrinsic maturation program in proliferating oligodendrocyte precursor cells. J Cell Biol, 1997. 138: 1367-1377.

Gao FB, Apperly J and Raff M. Cell-intrinsic timers and thyroid hormone regulate the probability of cell -cycle withdrawal and differentiation of oligodendrocyte precursor cells. Dev Biol. 1998. 197: 54-66.

Glass CK and Ogawa S. Combinatorial roles of nuclear receptors in inflammation and immunity. Nat Rev Immunol, 2006. 6: 44-55.

Glass CK and Saijo K. Nuclear receptor transrepression pathways that regulate inflammation in macrophages and T cells. Nat Rev Immunol, 2010. 10: 365-376.

Goldberg MP and Choi DW. Combined oxygen and glucose deprivation in cortical cell culture: calcium-dependent and calcium-independent mechanisms of neuronal injury. J Neurosci, 1993. 13: 3510-3524.

Goldman SA and Kuypers NJ. How to make an oligodendrocyte. Development, 2015. 142: 3983-3995.

Gonzales KA and Ng HH. Driving pluripotency and reprogramming: nuclear receptors at the helm. Semin Cell Dev Biol, 2013. 24: 670-678.

Gonzalez-Perez O and Alvarez-Buylla A. Oligodendrogenesis in the subventricular zone and the role of epidermal growth factor. Brain Res Rev, 2011. 67: 147-156.

Goodin DS. The epidemiology of multiple sclerosis: Insights to disease pathogenesis. Handb Clin Neurol, 2014. 122: 231–266.

Gudi V, Moharregh-Khiabani D, Skripuletz T, Koutsoudaki PN, Kotsiari A, Skuljec J, Trebst C, Stangel M. Regional differences between grey and white matter in cuprizone induced demyelination. Brain Res, 2009. 1283: 127-138.

Hlatky L, Sachs RK, Alpen EL. Joint oxygen-glucose deprivation as the cause of necrosis in a tumor analog. J Cell Physiol, 1988. 134: 167-178.

Holsberger DR, Jirawatnotai S, Kiyokawa H, Cooke PS. Thyroid hormone regulates the cell cycle inhibitor p27Kip1 in postnatal murine Sertoli cells. Endocrinology, 2003. 144: 3732-3738.

Huang W and Glass CK. Nuclear receptors and inflammation control: molecular mechanisms and pathophysiological relevance. Arterioscler Thromb Vasc Biol, 2010 30: 1542-1549.

Huang MP, Rodgers KA, O'Mara R, Mehta M, Abuzahra HS, Tannenbaum AD, Persons K, Holick MF and Safer JD. The thyroid hormone degrading type 3 deiodinase is the primary deiodinase active in murine epidermis. Thyroid, 2011 21:1263–1268.

Hughes EG, Kang SH, Fukaya M and Bergles DE. Oligodendrocyte progenitors balance growth with self-repulsion to achieve homeostasis in the adult brain. Nat Neurosci. 2013. 16: 668–676.

Ibarrola N and Rodriguez-Pe˜na A. Hypothyroidism coordinately and transiently affects myelin protein gene expression in most rat brain regions during postnatal development. Brain Res, 1997. 752: 285-293.

Jablonska B, Scafidi J, Aguirre A, Vaccarino F, Nguyen V, Borok E, Horvath TL, Rowitch DH, Gallo V. Oligodendrocyte regeneration after neonatal hypoxia requires FoxO1-mediated p27Kip1 expression. J Neurosci, 2012. 32: 14775-14793.

Jakovcevski I, Filipovic R, Mo Z, Rakic S and Zecevic N. Oligodendrocyte development and the onset of myelination in the human foetal brain. Frontiers in Neuroanatomy, 2009. 3: 1-15.

Jensen NA, Smith GM, Garvey JS, Shine HD, Hood L. Cyclic AMP has a differentiative effect on an immortalized oligodendrocyte cell line. J Neurosci Res, 1993. 35: 288-296.

Jo S, Kalloò I, Bardóczi Z, Arrojo e Drigo R, Zeo˙ld A, Liposits Z, Oliva A, Lemmon VP, Bixby JL, Gereben B and Bianco AC. Neuronal hypoxia induces Hsp40-mediated nuclear import of type 3 deiodinase as an adaptive mechanism to reduce cellular metabolism. J Neurosci, 2012. 32: 8491-8500.

Kanakasabai S, Pestereva E, Chearwae W, Gupta SK, Ansari S and Bright JJ. PPARg agonists promote oligodendrocyte differentiation of neural stem cells by modulating stemness and differentiation genes. PlosONE, 2012. 7: e50500.

Kang SM, Cho MS, Seo H, Yoon CJ, Oh SK, Choi YM and Kim DW. Effi- cient induction of oligodendrocytes from human embryonic stem cells. Stem Cells, 2007. 25:419–424.

Kang Z, Wang C, Zepp J, Wu L, Sun K, Zhao J, Chandrasekharan U, DiCorleto PE, Trapp BD, Ransohoff RM, Li X. Act1 mediates IL-17-induced EAE pathogenesis selectively in NG2+ glial cells. Nat Neurosci, 2013. 16: 1401-1408.

Káradóttir R and Attwell D. Neurotransmitter receptors in the life and death of oligodendrocytes. Neuroscience, 2007. 145: 1426-1438.

Káradóttir R, Cavelier P, Bergersen HL and Attwell D. NMDA receptors are expressed in oligodendrocytes and activated in ischaemia. Nature, 2005. 438: 1162-1166.

Karram K, Chatterjee N and Trotter J. NG2-expressing cells in the nervous system: role of the proteoglycan in migration and glial-neuron interaction. J Anat, 2005. 207: 735-744.

Kessaris N, Fogarty M, Iannarelli P, Grist M, Wegner M and Richardson WD. Competing waves of oligodendrocytes in the forebrain and postnatal elimination of an embryonic lineage. Nat. Neurosci, 2006. 9:173–79.

Kipp M, van der Star B, Vogel DY, Puentes F, van der Valk P, Baker D and Amor S. Experimental in vivo and in vitro models of multiple sclerosis: EAE and beyond. Mult Scler Relat Disord, 2012. 1: 15-28.

Ko HL and Ren EC. Functional aspects of PARP1 in DNA repair and transcription. Biomolecules, 2012. 2: 524-548.

Kojetin DJ, Matta-Camacho E, Hughes TS, Srinivasan S, Nwachukwu JC, Cavett V, Nowak J, Chalmers MJ, Marciano DP, Kamenecka TM, Shulman AI, Rance M, Griffin PR, Bruning JB and Nettles KW. Structural mechanism for signal transduction in RXR nuclear receptor heterodimers. Nat Commun, 2015. 6: 8013.

Kolodziejczyk K, Saab AS, Nave KA, Attwell D. Why do oligodendrocyte lineage cells express glutamate receptors? F1000 Biol Rep, 2010. 2: 57.

Krezel W, Dupé V, Mark M, Dierich A, Kastner P, Chambon P. RXR gamma null mice are apparently normal and compound RXR alpha +/-/RXR beta -/-/RXR gamma -/- mutant mice are viable. Proc Natl Acad Sci USA, 1996. 93: 9010-9094.

Kuhlmann T, Miron V, Cui Q, Wegner C, Antel J and Bruck W. Differentiation block of oligodendroglial progenitor cells as a cause for remyelination failure in chronic multiple sclerosis, Brain, 2008. 131: 1749–1758.

Kurinczuk JJ, White-Koning M, Badawi N. Epidemiology of neonatal encephalopathy and hypoxic-ischaemic encephalopathy. Early Hum Dev, 2010. 86: 329-338.

Kwakkel J, Wiersinga WM, Boelen A. Interleukin-1beta modulates endogenous thyroid hormone receptor alpha gene transcription in liver cells. J Endocrinol, 2007. 194: 257-265.

La Gamma EF and Paneth N. Clinical importance of hypothyroxinemia in the preterm infant and a discussion of treatment concerns. Curr Opin Pediatr, 2012. 24: 172-180.

Lassmann H, van Horssen J and Mahad D. Progressive multiple sclerosis: Pathology and pathogenesis. Nat Rev Neurol, 2012. 8: 647–656.

Lee S, Chong SY, Tuck SJ, Corey JM, Chan JR. A rapid and reproducible assay for modeling myelination by oligodendrocytes using engineered nanofibers. Nat Protoc, 2013. 8: 771-782.

Lee JY, Kim MJ, Stanley EG, Elefanty AG and Petratos S. Monocarboxylate transporter 8 is expressed on oligodendrocyte progenitors derived from human embryonic stem cells. Int J Dev Neurosci, 2015. 47: 69.

Lee JY and Petratos S. Thyroid hormone signaling in oligodendrocytes: From extracellular transport to intracellular signal. Molecular Neurobiology, 2016. 53: 6568–6583.

Lee S and Privalsky ML. Heterodimers of retinoic acid receptors and thyroid hormone receptors display unique combinatorial regulatory properties. Mol Endocrinol, 2005. 19: 863-878.

Leong SY, Rao VT, Bin JM, Gris P, Sangaralingam M, Kennedy TE and Antel JP. Heterogeneity of oligodendrocyte progenitor cells in adult human brain. Ann Clin Transl Neurol, 2014. 1: 272-283.

Li WW, Le Goascogne C, Ramaugé M, Schumacher M, Pierre M and Courtin F. Induction of type 3 iodothyronine deiodinase by nerve injury in the rat peripheral nervous system. Endocrinol, 2001. 142: 5190–5197.

Li J, Ramenaden ER, Peng J, Koito H, Volpe JJ and Rosenberg PA. Tumor necrosis factor alpha mediates lipopolysaccharide-induced microglial toxicity to developing oligodendrocytes when astrocytes are present. J Neurosci, 2009. 28: 5321-5330.

Liao H and Mani DS. Advances in oligoprotection. Neurosci Med, 2011. 2: 2.

Lin T, Xiang Z, Cui L, Stallcup W and Reeves SA. New mouse oligodendrocyte precursor (mOP) cells for studies on oligodendrocyte maturation and function. J Neurosci Methods, 2006. 157: 187-194.

Liu C, Li Y, Yu J, Feng L, Hou S, Liu Y, Guo M, Xie Y, Meng J, Zhang H, Xiao B, Ma C. Targeting the shift from M1 to M2 macrophages in experi- mental autoimmune encephalomyelitis mice treated with fasudil. PLoS One, 2013. 8: e54841–54854.

Lu Y, Yang Y, Wang Z, Wang C, Du Q, Wang Q and Luan Z. Isolation and culture of human oligodendrocyte precursor cells from neurospheres. Brain Res Bull, 2015. 118: 17-24.

Malik IA, Baumgartner BG, Naz N, Sheikh N, Moriconi F, Ramadori G. Changes in gene expression of DOR and other thyroid hormone receptors in rat liver during acute-phase response. Cell Tissue Res, 2010. 342: 261-272.

Maruvada P, Dimitrieva NI, East-Palmer J and Yen PM. Cell cycle-dependent expression of thyroid hormone receptor-beta is a mechanism for variable hormone sensitivity. Molecular Biology of the Cell, 2004. 15: 1895-1903.

Matute C, Torre I, Pe´rez-Cerda´ F, Pe´rez-Samart´ın A, Alberdi E, Etxebarria E, Arranz AM, Ravid R, Rod´ıguez-Antigu¨edad A, Sa´nchez-Go´mez M, Domercq M (2007) P2X(7) receptor blockade prevents ATP excitotoxicity in oligodendrocytes and ameliorates experimental autoimmune encephalomyelitis. J Neurosci, 2007. 27: 9525–9533.

McIver SR, Muccigrosso M, Gonzales ER, Lee JM, Roberts MS, Sands MS and Goldberg MP. Oligodendrocyte degeneration and recovery after focal cere- bral ischemia. Neuroscience, 2010. 169: 1364–1375.

Mekhail M, Almazan G and Tabrizian M. Oligodendrocyte-protection and remyeli- nation post-spinal cord injuries: A review. Progress in Neurobiology, 2012. 96, 322–339.

Menn B, Garcia-Verdugo JM, Yaschine C, Gonzalez-Perez O, Rowitch D and Alvarez-Buylla A. Origin of oligodendrocytes in the subventricular zone of the adult brain. The Journal of Neuroscience, 2006. 26: 7907–7918.

Merrill JE. In Vitro and In Vivo Pharmacological Models to Assess Demyelination and Remyelination. Neuropsychopharmacology, 2009. 34: 55-73.

Michalski JP and Kothary R. Oligodendrocytes in a nutshell. Frontiers in Cellular Neuroscience, 2015. 9: 1-11.

Miller RH and Mi S. Dissecting demyelination. Nat Neursci, 2007. 10: 1351-1354.

Miron VE, Kuhlmann T and Antel JP. CElls of the oligodendrocglial lineage, myelination, and remyelination. Biochimica et Biophysica Acta, 2011. 1812: 184-193.

Mohácsik P, Zeöld A, Bianco AC and Gereben B. Thyroid hormone and the neuroglia: both source and target. J Thyroid Res, 2011. 2011: 215718.

Morte B and Bernal J. Thyroid hormone action: Astrocyte-neuron communication. Front Endocrinol, 2014. 5: 82–87.

Mucida D, Park Y, Kim G, Turovskaya O, Scott I, Kronenberg M, and Cheroutre H. Reciprocal TH17 and regulatory T cell differentiation mediated by retinoic acid. Science, 2007. 317: 256–260.

Myers SA, Bankston AN, Burke DA, Ohri SS and Whittemore SR. Does the preclinical evidence for functional remyelination following myelinating cell engraft- ment into the injured spinal cord support progression to clinical trials?. Experimental Neurology, 2016. 283: 560–572.

Pantoni L, Sarti C, Alafuzoff I, Jellinger K, Munoz DG, Ogata J and Palumbo V. Postmortem examination of vascular lesions in cognitive impair- ment: a survey among neuropathological services. Stroke, 2006. 37: 1005–1009.

Pascual G and Glass CK. Nuclear receptors versus inflammation: mechanisms of transrepression. Trends Endocrinol Metab, 2006. 17: 321-327.

Patel JR and Klein RS. Mediators of oligodendrocyte differentiation during remyelination. FEBS Lett, 2011. 585: 3730-3737.

Plane JM, Grossenbacher SK, Deng W. PARP-1 deletion promotes subventricular zone neural stem cells toward a glial fate. J. Neurosci. Res. 2012, 90.

Pluchino S, Muzio L, Imitola J, Deleidi M, Alfaro-Cervello C, Salani G, Porcheri C, Brambilla E, Cavasinni F, Bergamaschi A, Garcia-Verdugo JM, Comi G, Khoury SJ and Martino G. Persistent inflammation alters the function of the endogenous brain stem cell compartment. Brain, 2008. 131: 2564-2578.

Polito A and Reynolds R. NG2-expressing cells as oligodendrocyte progenitors in the normal and demyelinated adult central nervous system. J Anat, 2005. 207: 707-716.

Power J, Mayer-Pröschel M, Smith J, Noble M. Oligodendrocyte precursor cells from different brain regions express divergent properties consistent with the differing time courses of myelination in these regions. Dev Biol, 2002. 245: 362-375.

Pringproa K, Kumnok J, Ulrich R, Baumgärtner W, Wewetzer K. In vitro characterization of a murine oligodendrocyte precursor cell line (BO-1) following spontaneous immortalization. Int J Dev Neurosci, 2008. 26: 283-291.

Puzianowska-Kuznicka M, Pietrzak M, Turowska O and Nauman A. Thyroid hormones and their receptors in the regulation of cell proliferation. Acta Biochim Pol, 2006. 53: 641-650.

Raff M. The mystery of intracellular developmental programmes and timers. Biochem Soc Trans, 2006. 34: 663–670.

Richter-Landsberg C, Heinrich M. OLN-93: a new permanent oligodendroglia cell line derived from primary rat brain glial cultures. J Neurosci Res, 1996. 45: 161-173.

Rio Hortega DP. Histogenesis y evolucion normal; exodo y distribucion regional de la microglia. Memor. Real. Soc. Esp. Hist. Nat, 1921 11, 213–268.

Robertson WF. On a new method of obtaining a black reaction in certain tissue-elements of the central nervous system (platinum method) Scott Med Surg J. 1899; 4: 23–30.

Rocha-Ferreira E and Hristova M. Plasticity in the neonatal brain following hypoxic-ischemic injury. Neural Plast, 2016. 2016: 4901014.

Rodgers JM, Robinson AP and Miller SD. Strategies for protecting oligo- dendrocytes and enhancing remyelination in multiple sclerosis. Discov Med, 2013. 16: 55-63.

Sanchez-Gomez 2003

Saijo K, Crotti A and Glass CK. Nuclear receptors, inflammation, and neurodegenerative diseases. Adv Immunol, 2010. 106: 21-59.

Schang AL, Van Steenwinckel J, Chevenne D, Alkmark M, Hagberg H, Gressens P and Fleiss B. Failure of thyroid hormone treatment to prevent inflammation-induced white matter injury in the immature brain. Brain Behav Immun, 2014. 37: 95–102.

Schlegel AA, Rudelson JJ, and Tse PU. White matter structure changes as adults learn a second language. J. Cogn. Neurosci, 2012. 24: 1664–1670.

Schoonover CM, Seibel MM, Jolson DM, Stack MJ, Rahman RJ, Jones SA, Mariash CN and Anderson GW. Thyroid hormone regulates oligodendrocyte accumulation in developing rat brain white matter tracts. Endocrinology, 2004. 145: 5013–5020.

Sozmen EG, Rosenzweig S, Llorente IL, DiTullio DJ, Machnicki M, Vinters HV, Havton LA, Giger Rj, Hinman JD and Carmichael ST. Nogo receptor blockade overcomes remyelination failure after white matter stroke and stimulates functional recovery in aged mice. Proceedings of the National Academy of Sciences of the United States of America, 2016. 113: E8453–E8462.

Stergiopoulos A and Politis PK. The role of nuclear receptors in controlling the fine balance between proliferation and differentiation of neural stem cells. Arch Biochem Biophys, 2013. 534: 27-37.

Su Z, Yuan Y, Chen J, Zhu Y, Qiu Y, Zhu F, Huang A and He C. Reactive astrocytes inhibit the survival and differentiation of oligodendrocyte precursor cells by secreted TNF-a. J Neurotrauma, 2011. 28: 1089–1100.

Tanner DC, Cherry JD and Mayer-Pro€schel M. Oligodendrocyte progenitors reversibly exit the cell cycle and give rise to astrocytes in response to interferon-c. J Neurosci, 2011. 31: 6235–6246.

Tekkök SB and Goldberg MP. AMPA/Kainate Receptor Activation Mediates Hypoxic Oligodendrocyte Death and Axonal Injury in Cerebral White Matter. J Neurosci, 2001. 21: 4237-4248.

Tognatta and Miller 2016

Tokumoto Y, Tamaki S, Kabe Y, Takubo K and Suematsu M. Quiescence of adult oligodendrocyte precursor cells requires thyroid hormone and hypoia to activate Runx1. Sci Rep, 2017. 7: 1019.

Trotter J, Karram K and Nishiyama A. NG2 cells: Properties, progeny and origin. Brain Res Rev, 2010. 63: 72–82.

Urbán N and Guillemot F. Neurogenesis in the embryonic and adult brain: same regulators, different roles. Front Cell Neurosci, 2014. 8: 396.

Yao SY, Ljunggren-Rose A, Chandramohan N, Whetsell WO Jr and Sriram S. In vitro and in vivo induction and activation of nNOS by LPS in oligodendrocytes. J Neuroimmunol, 2010. 229: 146-156.

Yao S, Pandey P, Ljunggren-Rose A, Sriram S. LPS mediated injury to oligodendrocytes is mediated by the activation of nNOS: relevance to human demyelinating disease. Nitric Oxide, 2010. 22: 197-204.

Yeung MS, Zdunek S, Bergmann O, Bernard S, Salehpour M, Alkass K, Perl S, Tisdale J, Possnert G, Brundin L, et al. Dynamics of oligodendrocyte generation and myelination in the human brain. Cell, 2014. 159: 766–774.

Wang L, Zhang X, Farrar WL, Yang X. Transcriptional crosstalk between nuclear receptors and cytokine signal transduction pathways in immunity. Cell Mol Immunol, 2004. 1: 416-424.

Wang Z, Colognato H and Ffrench-Constant C. Contrasting effects of mitogenic growth factors on myelination in neuron-oligodendrocyte co-cultures. Glia, 2007. 55: 537-545.

Warner MH and Beckett GJ. Mechanisms behind the non-thyroidal illness syndrome: an update. J Endocrinol, 2010. 205: 1-13.

Windrem MS, Nunes MC, Rashbaum WK, Schwartz TH, Goodman RA, McKhann G 2nd, Roy NS, Goldman SA. Fetal and adult human oligodendrocyte progenitor cell isolates myelinate the congenitally dysmyelinated brain. Nat Med, 2004. 10: 93-97.

Wolswijk G and Noble M, Identification of an adult-specific glial progenitor cell. Development, 1989. 105: 387-400.

Wolswijk G, Riddle PN and Noble M. Coexistence of perinatal and adult forms of a glial progenitor cell during development of the rat optic nerve. Development, 1990. 109: 691-698.

Wolswijk G, Riddle PN and Noble M. Platelet-derived growth factor is mitogenic for O-2Aadult progenitor cells. Glia, 1991. 4: 495-503.

Viganò F, Möbius W, Götz M and Dimou L. Transplantation reveals regional differences in oligodendrocyte differentiation in the adult brain. Nat Neursoci, 2013. 16: 1370-1372.

Viganò F and Dimou L. The heterogeneous nature of NG2-glia. Brain Res, 2016. 1638: 129-137.

Zhang Y, Luo X, Wu D and Xu Y. ROR nuclear receptors: structures, related diseases and drug discovery. Acta Pharmacologica Sinica, 2015. 36: 71-87.

Zhang Y, Dépond M, He L, Foudi A, Kwarteng EO, Lauret E, Plo I, Desterke C, Dessen P, Fujii N, Opolon P, Herault O, Solary E, Vainchenker W, Joulin V, Louache F and Wittner M. CXCR4/CXCL12 axis counteracts hematopoietic stem cell exhaustion through selective protection against oxidative stress. Sci Rep, 2016. 6: 37827.

Zhuang S, Bao L, Linhananta A and Liu W. Molecular modeling revealed that ligand dissociation from thyroid hormone receptors is affected by receptor heterodimerization. J Mol Graph Model, 2013. 44: 155-160.

Zuchero JB and Barres BA. Intrinsic and extrinsic control of oligodendrocyte development. Curr Opin Neurobiol, 2013. 23: 914-920.